University of Alberta

Mass Spectrometry for Polymer Characterization

by

Rui Chen

A thesis submitted to the Faculty of Graduate Studies and Research in partial fulfillment of the requirements for the degree of Doctor of Philosophy

Department of Chemistry

Edmonton, Alberta

Spring, 2002

National Library of Canada
Acquisitions and Bibliographic Services
395 Wellington Street
Ottawa ON K1A 0N4
Canada

Bibliothèque nationale du Canada
Acquisitions et services bibliographiques
395, rue Wellington
Ottawa ON K1A 0N4
Canada

Your file Votre référence

Our file Notre référence

The author has granted a non-exclusive licence allowing the National Library of Canada to reproduce, loan, distribute or sell copies of this thesis in microform, paper or electronic formats.

The author retains ownership of the copyright in this thesis. Neither the thesis nor substantial extracts from it may be printed or otherwise reproduced without the author's permission.

L'auteur a accordé une licence non exclusive permettant à la Bibliothèque nationale du Canada de reproduire, prêter, distribuer ou vendre des copies de cette thèse sous la forme de microfiche/film, de reproduction sur papier ou sur format électronique.

L'auteur conserve la propriété du droit d'auteur qui protège cette thèse. Ni la thèse ni des extraits substantiels de celle-ci ne doivent être imprimés ou autrement reproduits sans son autorisation.

0-612-68553-5

Canada

University of Alberta

Library Release Form

Name of Author: Rui Chen

Title of Thesis: Mass Spectrometry for Polymer Characterization

Degree: Doctor of Philosophy

Year this Degree Granted: 2002

Permission is hereby granted to the University of Alberta Library to reproduce single copies of this thesis and to lend or sell such copies for private, scholarly or scientific research purposes only.

The author reserves all other publication and other rights in association with the copyright in the thesis, and except as herein before provided, neither the thesis nor any substantial portion thereof may be printed or otherwise reproduced in any material form whatever without the author's prior written permission.

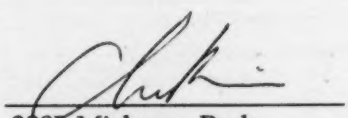

329J, Michener Park
Edmonton, AB, Canada, T6H 4M5

April 12, 2002

University of Alberta

Faculty of Graduate Studies and Research

The undersigned certify that they have read, and recommend to the Faculty of Graduate Studies and Research for acceptance, a thesis entitled Mass Spectrometry for Polymer Characterization submitted by Rui Chen in partial fulfillment of the requirements for the degree of Doctor of Philosophy.

Dr. Liang Li
Professor of Chemistry

Dr. Charles A. Lucy
Professor of Chemistry

Dr. Mark T. McDermott
Associate Professor of Chemistry

Dr. Rik R. Tykwinski
Assistant Professor of Chemistry

Dr. Phillip Y.K. Choi
Associate Professor of
Chemical and Material Engineering

Dr. J. Jonathan Amster
Professor of Chemistry
University of Georgia

April 12, 2002

To my dearest parents, my wife and my brother

Abstract

Mass spectrometry (MS) has become increasingly important for polymer characterization. This thesis describes my research efforts on developing enabling MS methods for polymer structural and composition analysis.

Polyethylene (PE) is one of most challenging polymers to be analyzed by MS. A study on the reactions of atomic transition-metal ions with long-chain alkanes, the oligomers of PE, by laser desorption ionization (LDI) post-source decay is described. It is found that many transition metal ions can form adduct ions with long chain alkanes in LDI. However, the thermal energies possessed by these large alkanes can lead to somewhat unusual reactivity and cause fragmentation. With the groundwork laid, a further study on the ionization behavior of several PE samples is then presented. It is demonstrated that low molecular mass PE can be analyzed by conventional MALDI MS, but a rational design of improved sample preparation conditions is still needed to reduce or eliminate fragmentation for PE analysis.

Many synthetic polymers do not readily fragment under the low energy collision-induced dissociation (CID) condition. A robust and routine method to generate low energy CID mass spectra of polyglycols in an ESI ion trap MS was developed. From the resulting MS/MS spectra, a wealth of structural information can be obtained. The utility of the method was examined by such applications as copolymer sequencing and structural analysis of fatty acid methyl ester ethoxylates. The described method offers the possibility of studying polymer structures by conventional low energy CID tandem MS.

Copolymer composition determination by MALDI MS represents one important research area in polymer MS. It is demonstrated that experimental conditions, such as the type of solvents and matrices, could significantly alter the outcome of composition computation based on the commonly employed "composition estimate" approach. Through a statistical comparison, it is shown that average molecular mass, on the other hand, is considerably less affected by such experimental conditions. It is further demonstrated that average molecular mass can be a much more reliable and reproducible parameter for copolymer composition determination.

Acknowledgements

I would like to thank my supervisor, Dr. Liang Li, for his guidance, encouragement, and most of all, his faith in me. His vision, dedication and enthusiasm have been and will continue to be a great inspiration for me.

I thank my committee members, Drs. Charles A. Lucy, Mark T. McDermott, Rik R. Tykwinski, Phillip Y.K. Choi, and I. Jonathan Amster, for their wonderful suggestions and constructive criticisms to my thesis.

My thanks also go to my collaborators. Without many insightful discussions with them, my research could have been much more difficult. In particular, I wish to acknowledge the following individuals: John Green and William Dianis from Dow Chemical Co., Amy Tseng, Mary Uhing and James Svarz from Nalco Chemical Co., and William Wallace and Charlie Guttman from NIST.

I am grateful for the scholarships and awards I have received from the Department of Chemistry, the University of Alberta, and the Killam Trust Fund. Their recognition of my humble work means so much for me personally.

It has been a fun journey for the past four and half years, largely owing to the group of talented people I have been privileged to work with. I owe a debt of gratitude to Mr. Alan Doucette, Mr. Dave Craft, Mr. Chris McDonald, Dr. Bernd Keller, Dr. Talat Yalcin, Dr. Zhengping Wang, Mrs. Jing Zheng, Mrs. Nancy Zhang, Mrs. Lidan Tao, Mrs. Hongying Zhong and Ms. Xinlei Yu. Special thanks go to Mrs. Nancy Zhang, Ms. Xinlei Yu and Dr. Talat Yalcin for participating in some of my research projects.

My deepest gratitude goes to my parents, my wife and my brother for their endless and unconditional love. They are my world…

Table of Contents

Chapter 1 1

Introduction to Polymer Characterization by Mass Spectrometry

1.1 Introduction 1

1.2 Mass Spectrometry 5

1.2.1 MALDI Time-of-flight (TOF) MS 6

1.2.2 ESI Ion Trap (IT) MS 12

1.2.3 Tandem MS for Polymer Characterization 17

1.3 Conclusions 20

1.4 Literatures Cited 21

Chapter 2 27

Reactions of Atomic Transition-Metal Ions with Long-Chain Alkanes

2.1 Introduction 28

2.2 Experimental 29

2.2.1 Materials and Reagents 29

2.2.2 LDI and PSD 30

2.3 Results and Discussion 31

2.4 Summary 48

2.5 Literatures Cited 49

Chapter 3 52

Laser Desorption Ionization and MALDI Time-of-Flight Mass Spectrometry for Low Molecular Mass Polyethylene Analysis

3.1 Introduction 53

3.2 Experimental 55

3.2.1 Chemicals and Reagents 55

3.2.2 LDI and MALDI Sample Preparation 55
3.2.3 Instrumentation 56
3.3 Results and Discussion 56
3.3.1 LDI MS of PE in Linear and Reflectron TOF 56
3.3.2 The Origin(s) of the Low Mass Peaks Present in LDI Spectra of PE 61
3.3.3 Copper Cationization 65
3.3.4 MALDI MS of PE 67
3.3.5 Molecular Mass Calculation 68
3.4 Summary 73
3.5 Literatures Cited 74

Chapter 4 76
Application of an Integrated MALDI-TOF, ESI MS and MS/MS Approach to Characterizing Complex Polyols
4.1 Introduction 77
4.2 Experimental 78
4.2.1 Materials and Reagents 78
4.2.2 Instrumentation 79
4.3 Results and Discussion 80
4.3.1 Characterization of EO/PO Copolymers 80
4.3.2 Analysis of Polyol Mixture 84
4.4 Summary 91
4.5 Literature Cited 92

Chapter 5 96
Characterization of Polyglycol Ethers by Low Energy Tandem MS in an ESI Ion Trap Mass Spectrometer

5.1 Introduction 96
5.2 Experimental 99
5.2.1 Materials and Reagents 99
5.2.2 Sample Preparation 100
5.2.3 H/D Exchange 100
5.2.4 ESI MS and MS/MS 100
5.3 Results and Discussion 101
5.3.1 Low Energy CID of PEG Methyl Ether with Commonly Used Cations 101
5.3.2 Low Energy CID of PEG Methyl Ether with Transition Metal Ions 107
5.3.3 Ionization/Fragmentation of PEG by Co^{2+} in ESI MS and MS/MS 112
5.3.4 Ionization/Fragmentation of PEG Methyl Ether by Ag^{+}: A H/D Exchange Approach 117
5.3.5 Applications of Ag^{+} Cationization: Fragmentation of Multiply Charged Adduct Ions from Polyglycols with Medium Molecular Mass 125
5.3.6 Copolymer analysis by ESI MS/MS 130
5.3.6.1 Introduction 130
5.3.6.2 Copolymer Differentiation: Block *vs.* Random 131
5.3.6.3 Sequencing of EO/PO Copolymers: A Model System 136
5.4 Summary 141
5.5 Literatures Cited 142

Chapter 6 148

Characterization of Poly(Ethylene Glycol) Esters Using Low Energy Collision-Induced Dissociation in Electrospray Ionization Mass Spectrometry

6.1 Introduction 149

6.2 Experimental 150

6.2.1 Materials and Reagents 150

6.2.2 ESI MS and MS/MS 151

6.3 Results and Discussion 152

6.3.1 Differentiation of PEG Ethers and PEG Esters by ESI MS/MS 152

6.3.2 End Group Elucidation for PEG Dibenzoate and Related Issues 154

6.3.3 Fatty Acid Methyl Ester Ethoxylates (FAMEE) 170

6.4 Summary 176

6.5 Literatures Cited 177

Chapter 7 183

Composition Analysis of Ethylene Oxide/Propylene Oxide Copolymer by MALDI MS

7.1 Introduction 186

7.2 Experimental 188

7.2.1 Materials and Reagents 188

7.2.2 MALDI-TOF MS 189

7.3 Results and Discussion 189

7.3.1 Effects of MALDI Experimental Conditions on Quantitative Composition Analysis of Ethylene Oxide/Propylene Oxide Copolymer 189

7.3.2 A Statistical View: Compositional Estimate *vs.* Average Molecular Mass 199
7.3.3 EO/PO Determination by Average Molecular Mass Measured by MALDI MS 206
7.4 Summary 209
7.5 Literatures Cited 211
7.6 Appendix: Program "PeakPick" for Copolymer Mass Assignment 215

Chapter 8 221
Conclusions and Future Work

List of Tables

Table 2.1 Product distributions of reactions of Ni^+ with small alkanes and $C_{28}H_{58}$. 43

Table 3.1 Molecular mass calculation from MALDI MS for PE 1000. 72

Table 4.1 Traditional analytical testing results of the EO/PO Copolymers. 80

Table 7.1 Comparison of composition results from NMR and feed ratio. 184

Table 7.2 Assignment of major peaks shown in Figure 7.1B. 191

Table 7.3 Relative peak ratios among the ^{12}C peaks from different clusters obtained by using different matrices. 194

Table 7.4 Solvent effect on EO/PO and Mn calculation. 203

Table 7.5 Analyte/Matrix (A/M) ratio effect on EO/PO and Mn calculation. 204

Table 7.6 Matrix effect on EO/PO and Mn calculation. 204

List of Figures

Figure 1.1 Schematic illustration of the principle of MALDI.....6

Figure 1.2 Schematic of a linear TOF mass spectrometer.....8

Figure 1.3 Principle of the electrospray ionization process.....13

Figure 1.4 Schematic of a quadrupole ion trap mass spectrometer.....14

Figure 1.5 Schematic of a reflectron (ion mirror) TOF mass spectrometer. Vs is the voltage applied on the repeller, and V_R represents the voltages applied on the ion mirrors.....17

Figure 2.1 Laser desorption ionization mass spectra of $C_{28}H_{58}$ obtained by using different metals. The metal-alkane adduct ions are labeled as M and their fragment ions are labeled as F. The Ag cluster ions are labeled as C. All other peaks are mainly from impurities.....32

Figure 2.2 Laser desorption ionization mass spectra of $C_{36}H_{74}$ obtained by using different metals. The metal-alkane adduct ions are labeled as M and their fragment ions are labeled as F. The Ag cluster ions are labeled as C. All other peaks are mainly from impurities.....33

Figure 2.3 Expanded mass spectra showing the molecular ion regions of metal ion $C_{28}H_{58}$ (A) and $C_{36}H_{74}$ (B) adducts. The dehydrogenation products are labeled as "$-H_2$" or "$-2H_2$".....34

Figure 2.4 Post-source decay mass spectra of metal-ion $C_{28}H_{58}$ adducts.....36

Figure 2.5 Post-source decay mass spectra of metal-ion $C_{36}H_{74}$ adducts.....37

Figure 2.6 Expanded PSD spectrum of $Ni(C_{28}H_{58})^+$ showing the dealkylation fragment ions.....41

Figure 2.7 Normalized PSD spectra of $Fe(C_{28}H_{58})^+$ and $Fe(C_{36}H_{74})^+$.....47

Figure 3.1 LDI mass spectra of (A) PE1100, (B) PE2100, and (C) PE4250.. These samples were from American Polymer Standards Corporation.....57

Figure 3.2 LDI mass spectra of (A) PE500, (B) PE1000, and (C) PE2000. These samples were from Polymer Laboratories Inc. 58

Figure 3.3 Expanded LDI spectrum of PE1000 from Figure 3.2B. 62

Figure 3.4 LDI mass spectra of PE1150 obtained at two different laser power settings in the Applied Biosystems LDI TOF mass spectrometer: (A) laser power index 2400 and (B) laser power index 2500. The peaks labeled as C are from the silver cluster ions. 63

Figure 3.5 LDI mass spectra of a long chain alkane, $C_{94}H_{190}$, obtained at two different laser power settings in the Applied Biosystems LDI TOF mass spectrometer: (A) laser power index 2150 and (B) laser power index 2450. The peaks labeled as C are from the silver cluster ions. 64

Figure 3.6 LDI spectra of PE500 and PE1000 obtained by using copper cationization. 66

Figure 3.7 MALDI mass spectra of PE1000 obtained by using silver cationization with (A) dithranol, (B) *trans,trans*-1,4-diphenyl-1,3-butadiene, (C) *all-trans* retinoic acid, and (D) no matrix. LI is the laser power index. 68

Figure 3.8 An exponential curve fitting of the data obtained using RA as the matrix of sample PE1100. The label ♦ represents the original data points and the solid line is the calculated curve. 70

Figure 3.9 A column-chart representation of the data from Figure 3.7C. (A) before and (B) after correction. 71

Figure 4.1 MALDI-TOFMS mass spectra of four batches of EO/PO polymers. 82

Figure 4.2 Expanded MALDI-TOF mass spectra from Figure 4.1. 83

Figure 4.3 ESI mass spectra of Sample E obtained by (A) without the addition of NaCl, (B) with the addition of NaCl and (C) with the addition of $AgNO_3$. 86

Figure 4.4 (A) ESI mass spectra of Samples E and F obtained with the addition of NaCl. (B) Expanded ESI mass spectra. 89

Figure 4.5 MS/MS spectra of selected oligomer ions at (A) m/z 445, and (B) m/z 471. 90

Figure 5.1 ESI mass spectra of PEG methyl ether obtained using different cations for ionization: (A) H^+, (B) NH_4^+, (C) Na^+, and (D) Li^+. 102

Figure 5.2 ESI MS/MS spectra of PEG methyl ether 11-mer with different cations: (A) H^+, (B) NH_4^+, and (C) Li^+. 104

Figure 5.3 ESI mass spectra of PEG methyl ether obtained using sodium ion and different transition metal ions for ionization: (A) Na^+, (B) Zn^{2+}, (C) Co^{2+}, (D) Ni^{2+}, and (E) Ag^+. 108

Figure 5.4 ESI MS/MS spectra of PEG methyl ether 12-mer with different transition metal ions: (A) Zn^{2+}, (B) Co^{2+}, (C) Ni^{2+}, and (D) Ag^{+}. 111

Figure 5.5 ESI mass spectra of (A) PEG (hydroxyl terminated), (B) PEG methyl ether, and (C) PEG dimethyl ether obtained using 0.015 M $Co(NO_3)_2$. 113

Figure 5.6 ESI mass spectra of PEG dimethyl ether obtained by using 0.015M (A) $Co(NO_3)_2$, (B) $CoCl_2$, and (C) $CoBr_2$. Peaks labeled as P are from ion pair metal complex, S are from sodium attachment, and F are from in-source fragmentation. 115

Figure 5.7 ESI MS/MS spectra of (A) $[CH_3O\text{-}EO_{10}\text{-}CH_3]CoNO_3^{+}$, (B) $[CH_3O\text{-}EO_{10}\text{-}CH_3]CoCl^{+}$, and (C) $[CH_3O\text{-}EO_{10}\text{-}CH_3]CoBr^{+}$. In the figure, $\alpha=CH_4$. 116

Figure 5.8 (A) ESI MS/MS spectra of argentinated PEG methyl ether 12-mer with and without D exchange. (B) Expanded spectra from (A). 120

Figure 5.9 (A) ESI mass spectrum of PPG 2000 obtained using Ag^{+} as the cationization reagent. (B) ESI MS/MS spectrum of the doubly charged ion at m/z=1248.0. (C) ESI MS/MS spectrum of the triply charged ion at m/z=926.7. 126

Figure 5.10 ESI mass spectrum of PEG 3350 obtained using Ag^{+} as the cationization reagent. 127

Figure 5.11 ESI MS/MS spectra of PEG 3350 with Ag^{+} as the cationization reagent: (A) from +3 ion at m/z=1746, (B) from +4 ion at m/z=927, and (C) from +5 ion at m/z=727. 129

Figure 5.12 (A) ESI mass spectrum of a tri-block copolymer obtained using Li^+ as cationization reagent. (B) Expanded spectrum of (A) showing a repeat pattern of peaks. 132

Figure 5.13 (A) ESI mass spectrum of a random copolymer obtained using Li^+ as cationization reagent. (B) Expanded spectrum of (A) showing a repeat pattern of peaks. 133

Figure 5.14 ESI MS/MS spectra of (A) block and (B) random EO/PO copolymers obtained using Li^+ as the cationization reagent. 135

Figure 5.15 ESI MS spectrum of block copolymer TPM from Dow Chemical Canada obtained using Li^+ as the cationization reagent. 136

Figure 5.16 ESI MS/MS spectrum of one lithiated TPM oligomer. 137

Figure 5.17 ESI MS/MS spectrum of the same oligomer shown in Figure# obtained by using Co^{2+} as the cationization reagent. Peaks labeled as α (A) are the product ions from the cleavages initiated from EO end and β (B) are from the PO end. 140

Figure 6.1 ESI mass spectra of PEGs obtained using Li^+ for ionization: (A) PEG-ME, and (B) PEG-MOL. 153

Figure 6.2 ESI MS/MS spectra of PEGs with Li^+: (A) PEG-ME, and (B) PEG-MOL. 153

Figure 6.3 ESI mass spectra of PEG-DBZ obtained using different cations for ionization: (A) Na^+, (B) Li^+, (C) NH_4^+, (D) Ag^+, (E) Co^{2+}, and (F) Cu^{2+}. 156

Figure 6.4 (A) ESI MS/MS spectrum of PEG-DBZ pentamer with Na^+ at m/z=469.2. (B) ESI MS^3 spectrum of the product ions at m/z=347.2 from Figure 6.4 (A). 157

Figure 6.5 (A) ESI MS/MS spectrum of PEG-DBZ pentamer with Li^+ at m/z=453.3. (B) ESI MS^3 spectrum of the product ions at m/z=331.3 from Figure 6.5 (A). 159

Figure 6.6 (A) ESI MS/MS spectrum of PEG-DBZ pentamer with Ag^+ at m/z=553.2. (B) ESI MS^3 spectrum of the product ions at m/z=431.1 from Figure 6.6 (A). 160

Figure 6.7 (A) ESI MS/MS spectrum of PEG-DBZ pentamer with NH_4^+ at m/z=465.2. (B) ESI MS^3 spectrum of the product ions at m/z=149 from Figure 6.7 (A). (C) ESI MS^4 spectrum of the product ions at m/z=105 from Figure 6.7 (B). 165

Figure 6.8 (A) ESI MS/MS spectrum of PEG-DBZ quadrimer at m/z=465.8 obtained using $Cu(NO_3)_2$. (B) ESI MS/MS spectrum of PEG-DBZ quadrimer at m/z=496.0 obtained using $CoCl_2$. 166

Figure 6.9 Schematic illustration of the MS-based protocol for PEG ester characterization. 169

Figure 6.10 (A) ESI mass spectrum of PEG-MOL obtained using NH_4^+ under normal operation mode. (B) ESI mass spectrum of PEG-MOL obtained using NH_4^+ with in-source fragmentation. (C) ESI MS/MS spectrum of PEG-MOL pentamer at m/z=520.2 with NH_4^+. (D) Fragmentation spectrum of product ions at m/z=309.1 from both Figure 6.10 (B) and (C). 171

Figure 6.11 (A) ESI mass spectrum of PEG-DS obtained using Li^+ as the cationization reagent. The peaks labeled with ▲, *, and ● indicate they are from different product series. (B) ESI MS/MS spectrum of ions at m/z=953 with Li^+. (C) ESI MS/MS spectrum of ions at m/z=941 with Li^+. (D) ESI MS/MS spectrum of ions at m/z=969 with Li^+. In Figures (B), (C), and (D), P denotes the parent ions of each spectrum. 173

Figure 6.12 Fragmentation spectra of product ions at (A) m/z=311, and (B) m/z=283. In both cases, product ions were generated by in-source fragmentation of PEG-DS with NH_4^+. 175

Figure 7.1 (A) MALDI-TOF mass spectrum and (B) expanded spectrum of an EO/PO copolymer. *All-trans* retinoic acid was used as the matrix. 190

Figure 7.2 Expanded MALDI-TOF mass spectra obtained by using different matrices: (A) low mass and (B) high mass region of the copolymer distribution. The copolymer sample was mixed with 0.1 M matrix/THF solution in 1:10 volume ratio. The laser power used was at the desorption/ionization threshold (LI = ~1750). 193

Figure 7.3 Expanded MALDI-TOF mass spectra obtained by using different solvents: (A) low mass and (B) high mass region of the copolymer distribution. *All-trans* retinoic acid was used as the matrix. The copolymer sample was mixed with 0.1 M matrix solution in different solvents in 1:15 volume ratio. The laser power used was at the desorption/ionization threshold (LI = ~1750). 196

Figure 7.4 Expanded MALDI-TOF mass spectra obtained by using different analyte concentrations: (A) low mass and (B) high mass region of the copolymer distribution. *All-trans* retinoic acid was used as the matrix. The number shown refers to the volume ratio of the copolymer sample and 0.1 M

matrix/THF solution. The laser power used was at the desorption/ionization threshold (LI = ~1750). 197

Figure 7.5 Expanded MALDI-TOF mass spectra obtained by using different laser power: (A) low mass and (B) high mass region of the copolymer distribution. *All-trans* retinoic acid was used as the matrix. The copolymer sample was mixed with 0.1 M matrix/THF solution in a volume ratio of 1:100. 198

Figure 7.6 MALDI mass spectra of four standards and one unknown sample. All samples were dissolved in THF and RA was used as the matrix. Analyte/Matrix=1:10 (v/v). 200

Figure 7.7 Flow chart of computer *C* program "PeakPick". 202

Figure 7.8 Calibration curves. (A) From the Mn data vs. wt% EO determined by the feed ratio and the error bar shows the standard deviation, and (B) from the NMR data vs. wt% EO determined by the feed ratio. 207

List of Schemes

Scheme 5.1 Nomenclature of the fragment ions. 105

Scheme 5.2 Fragmentation pathway for the formation of A_{ME} ions using Co^{2+}. 109

Scheme 5.3 Fragmentation pathway for the formation of A_H ions using Co^{2+}. 110

Scheme 5.4 Fragmentation pathway for the formation of B_H ions using Co^{2+}. 112

Scheme 5.5 Fragmentation pathways for the formation of A series ions using Ag^+. 121

Scheme 5.6 Fragmentation pathways for the formation of B series ions using Ag^+. 122

Scheme 5.7 Formation of two types of A_{MEII} ions using Ag^+. 124

Scheme 5.8 Partial fragmentation pathway for lithiated CH_3O-PO_3-EO_7-H oligomer. 138

Scheme 6.1 Abbreviations and chemical structures of the PEGs used in this study. 151

Scheme 6.2 Proposed fragmentation pathways for PEG-DBZ with different metal ions. 161

Scheme 6.3 Schematic illustration of the formation of the ions at m/z=149 in the case of using Ag^+ as the cationization reagent. 162

Chapter 1. Introduction to Polymer Characterization by Mass Spectrometry

1.1 Introduction

Polymers are large molecules made up of simple repeat units. They are widely used in our daily life as plastics, fibers, and coatings, to name a few applications. Recent years have witnessed a number of important advances in polymer applications. Examples include aerospace applications, metal replacement, nonflammable materials, conducting materials, and bio-medical applications [1].

Most synthetic polymers can have molecular masses ranging from several thousand up to several million Daltons. It is noted here that in this thesis, a polymer is any material composed of repeating monomeric molecules. Much of the data presented in this thesis are the experimental results of relatively low molecular mass polymers (M_n<5000 Da), which would otherwise be categorized as oligomers. The distinction between polymer and oligomer is obscured, for the reason that much of the focus of my research has been on the structural aspects of polymers, rather than on the determination of their molecular masses.

One feature that distinguishes polymers from other typical organic compounds is their heterogeneity. This heterogeneity could derive from several aspects of polymer structures. Most polymers exhibit molar-mass distribution and functionality distribution (i.e., one polymer possesses several types of end groups). For random copolymers, there is, in addition, a chemical composition distribution. For block copolymers, there are additional sequence and block-length distributions. For commercial polymers, the matter

is further complicated by the existence of polymer additives, such as anti-oxidants and plasticizers. Characterization of polymers has been, and still remains a challenging task.

In principle, conventional characterization methods for organic compounds, such as infrared (IR) spectroscopy, ultraviolet/visible (UV/vis) spectroscopy, and nuclear magnetic resonance (NMR) spectroscopy, can be easily adapted for characterizing polymers, despite the complexity of polymer samples. However, one common problem associated with these classical methods is that they are "averaging" methods, meaning that they measure average properties at the expense of losing individual compositional details that are intrinsic to polymers. In most cases, they do not differentiate between unique oligomers present in a sample, nor do they distinguish impurities and/or additives.

Of primary interest in polymer characterization is estimation of molecular mass and its distribution. There are several techniques that are widely used for this purpose [2]. The direct methods include osmometry and light scattering (LS). The technique of osmometry is limited to polymers with masses below 10,000 Da, and fails to differentiate polymers with a narrow distribution from those with a wide distribution. The LS method is error-prone because of dust interference. Furthermore, this technique cannot be applied to copolymers. Indirect methods include gel permeation chromatography (GPC) or size-exclusion chromatography (SEC) and intrinsic viscosity measurements. These methods require calibration. A lack of narrowly distributed standards is the most commonly encountered problem for GPC. Therefore, one usually must resort to the use of secondary standards such as polystyrene (PS), which introduces further problems in this method. This is especially true for the mass determination of non-linear polymers and copolymers, because the hydrodynamic volume of the polymer under investigation

could be significantly different from that of secondary standards. The intrinsic viscosity method suffers from a lack of Mark-Houwink-Sakurada constants essential for mass determination for many polymeric systems. One additional drawback is that this method only yields viscosity average molecular mass.

Overcoming the problems possessed by these conventional methods, and providing a complementary, rapid, and accurate method, has been the driving force for pursuing mass spectrometric method development for polymer characterization. The endeavor, however, has been hampered for decades by the nonvolatile nature of polymers. Any material to be analyzed by mass spectrometry (MS) must first be transferred into the gas phase by means of vaporization and/or desorption. Therefore, traditional polymer mass spectrometry methods, including gas chromatography (GC)/MS, pyrolysis GC/MS, and direct pyrolysis/MS, would either involve a degradation step (in pyrolysis GC/MS and direct pyrolysis/MS) or only apply to the analysis of volatile components and low molecular mass oligomeric materials (GC/MS). Detailed reviews on these topics can be found in references 2 and 3.

The advent of soft ionization techniques, including electrospray ionization (ESI) and matrix-assisted laser desorption/ionization (MALDI), in the late 1980's marked the beginning of a new era for polymer MS. Poly(ethylene glycol) (PEG) with molecular mass up to 5 million Da, and PS with molecular mass up to 1.5 million Da, have been detected by ESI [4] and MALDI [5], respectively. In general, the mass spectra of polymers generated by MALDI and ESI yields a wealth of information for polymer properties such as repeat unit, end group, and molecular mass of the polymer. Moreover, they do so in a discrete manner. Oligomers are essentially mass resolved by mass

analyzers if resolution permits. This will allow a direct assessment of an individual polymer chain property. More MALDI and ESI applications in polymer characterization will be reviewed along with the introduction of these techniques in the later sections of this chapter.

The main objective of the research presented in this thesis has been to develop enabling MS methods for polymer structure and composition characterization. Of particular interest are the following three areas: 1) To achieve a better understanding of gas phase reactions between atomic transition metals with long chain alkyl, leading to MALDI-MS method development for polyethylene (PE) analysis (Chapters 2 and 3). PE is considered by many the most challenging polymer to be analyzed by MS due to its lack of heteroatoms or double bonds. 2) To develop structural characterization strategies based on ESI tandem mass spectrometry (MS^n). Much of my research effort has been dedicated to this area (Chapters 4, 5 and 6). 3) To investigate the experimental effect on the commonly used MS approach for copolymer composition computation, and to provide an alternative, and more robust method for this purpose (Chapter 7). Understanding how spectra can be affected by the experimental conditions is the first and foremost step in developing a mass spectrometric approach for compositional quantification.

The research presented covers three major research areas in polymer MS, namely, molecular mass determination, structural elucidation, and copolymer composition analysis. Aside from scientific curiosity, developing analytical methodologies that can be used for real world sample analysis has always been a major thrust. Many results presented in this thesis are either direct real-world applications or have an implication to these applications.

In this chapter, fundamentals of the two MS techniques heavily used in my research, MALDI time-of-flight (TOF) MS and ESI ion trap (IT) MS, will be briefly described. Advances in polymer MS/MS will also be reviewed.

1.2 Mass Spectrometry

Mass spectrometric analyses involve the formation of gas phase ions and measurement of the mass-to-charge (m/z) ratio of these ions [6]. Depending on the ionization method used, the analyte molecules are first converted to gas-phase molecular ions, quasi-molecular ions, or fragments. The mass analyzer separates these ions according to their m/z ratio. The ion current from the mass-separated ions is then detected by a suitable detector, and displayed in a mass spectrum in the form of ion abundance *vs.* m/z. The choice of method for the ionization of a compound depends upon the nature of the sample under investigation and the information required. For ionization of volatile materials, electron ionization (EI) and chemical ionization (CI) are often used. In polymer MS, these techniques are limited to analyzing monomers and low molecular mass oligomers, or coupled with degradation methods such as pyrolysis. For ionization of nonvolatile materials, such as most polymeric systems, fast atom bombardment (FAB), secondary ion mass spectrometry (SIMS), and MALDI can be used. As well, analyte solutions can be converted to gas phase ions by means of thermospray ionization (TSI) and ESI. MALDI and ESI, often referred to as "soft ionization" techniques, usually generate intact quasi-molecular ions of polymers under investigation, and are therefore well suited for molecular mass determination and composition analysis. When fragmentation information is desirable, "hard" ionization techniques or tandem mass spectrometry can be chosen.

1.2.1 MALDI Time-of-Flight (TOF) MS

The advent of MALDI by two research groups [7-10] in 1987-1988 has had tremendous impact on MS analysis of biopolymers such as proteins and peptides [11]. It has been recognized that this technique is amendable to synthetic polymer analysis as well. It was demonstrated in one of the very first publications on MALDI [10] that polyethylene glycol (PEG) with a molecular mass up to 25 kDa can be analyzed despite the intrinsic complexity of the polymers. The following discussion will be restricted to polymer analysis with MALDI.

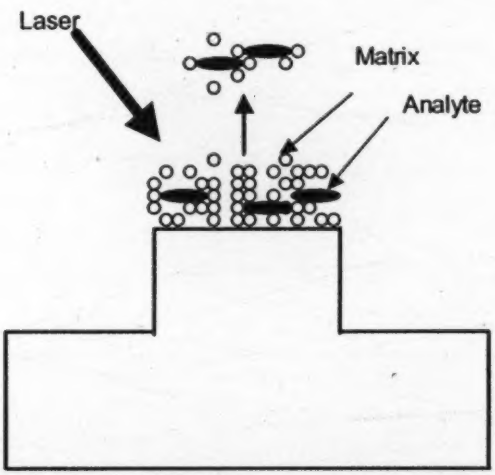

Figure 1.1. Schematic illustration of the principle of MALDI.

Figure 1.1 demonstrates the principle of this technique. A polymer sample is dissolved in the appropriate solvents and usually mixed with a proper matrix solution to achieve a molar ratio of analyte to matrix <1:100. A solution of cationization reagent, usually a metal salt, is also added. About 1 μL of the resulting mixture is then deposited onto a MALDI sample target. After solvent evaporation, the analyte and matrix form co-crystals on the target. Recently, it has been shown that electrospraying sample onto a

MALDI target can control the evaporation process to obtain an improved sample/matrix mixing [12]. Normally, an ultraviolet (UV) laser beam (337 nm) of a short pulse (~3 ns duration) and a power of ~10^6 W/cm^2 is used to irradiate the sample target. Upon irradiation, a large amount of energy is absorbed efficiently by the chromophoric matrix molecules. The matrix is desorbed, ionized and dissociated. This process breaks down the crystalline structure of the matrix and changes it into a super-compressed gas. As the gas expand rapidly, it transports entrapped analyte molecules (or molecular ions) into the gas phase.

The ionization mechanism of MALDI has always been a source of debate [13-14]. Of particular importance for polymer ionization in MALDI is the ion-molecule reactions in the gas phase. It was shown that Na^+ could be well solvated in the gas phase by PEG oligomers [15], suggesting a gas-phase cation "capture". Dorgruel *et al.* [16] showed that in poly(methyl methacrylate) (PMMA) analysis, use of pure matrix salts as matrix does not give analyte signal. Whereas adding such salts into the matrix enhances analyte-sodium signal, meaning that the adduct is not pre-formed in the condensed phase. For PS, a sample preparation using immiscible solvents to exclude pre-formation of PS-metal complexes in solution still generates a strong PS-metal adduct signal, indicating a gas phase reaction mechanism [17]. However, this gas phase ion-molecule reaction by no means should be considered as the only polymer ionization mechanism. Investigation of polymer ionization in MALDI remains an active research area.

For polymer MALDI MS, the matrix mainly performs the following two important functions: (1) it absorbs photon energy from the laser pulse and transfers it into excitation energy of the solid system, and (2) it serves as a "solvent" for the analyte,

isolating the polymer molecules from each other, and thereby greatly reduces intermolecular interactions. An ideal matrix should have high adsorption at the chosen laser emission wavelength, good stability, low vapor pressure, reasonable solubility in solvents that can dissolve the analyte, and good miscibility with the analyte in the solid phase. Although some empirical guidelines in choosing suitable matrices for polymer MALDI MS have been suggested [3], to date, it is still essentially a process of trial and error.

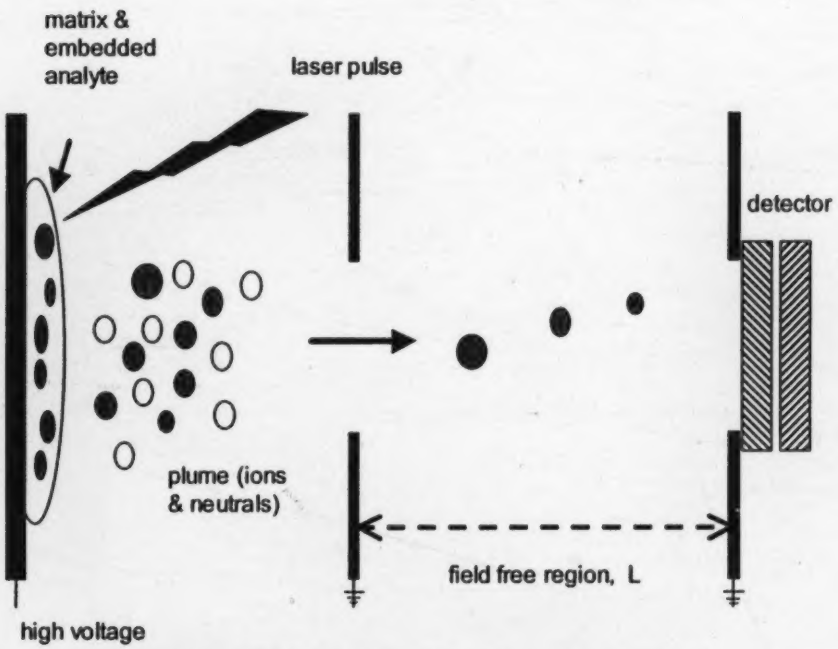

Figure 1.2. Schematic of a linear TOF mass spectrometer.

Many types of mass spectrometers can be coupled with MALDI. These include time-of-flight (TOF), Fourier Transform Ion Cyclotron Resonance (FT-ICR), quadrupole ion trap (IT), and magnetic sector. Amongst these, TOF is most commonly used because its pulsed ion detection mode matches well with the pulsed ionization process of MALDI.

In addition, TOF has a high duty cycle (i.e., the ratio of the ions detected to the ions generated), high ion transmission, and multi-channel detection, making it a desirable mass analyzer for high sensitivity MALDI analysis. Above all, the theoretically unlimited mass detection range of TOF makes it particularly attractive for polymer MALDI MS. It has been demonstrated that with a MALDI linear TOF mass spectrometer, PS with molecular mass up to 1.5 million Da can be detected [5].

Figure 1.2 shows the basic principle of a linear TOF analyzer. For m/z separation by a TOF analyzer, the ions generated in the ion source are accelerated by a high potential V to acquire kinetic energy in the keV range. Then, the ions traverse through a field free drift tube with a length L, typically 0.5-2 m. The time taken by the ions to reach the detector, t, is measured. The equations to describe the basic principle, with the approximation that no ions possess initial kinetic energy, are listed below (Equations 1.1-1.3). The flight time, t, depends upon the velocity, v, and therefore, depends upon m/z as well.

$$ZeV = \frac{1}{2}mv^2 \qquad \textbf{Equation 1.1}$$

$$t = L/v \qquad \textbf{Equation 1.2}$$

$$v = \left(\frac{2ZeV}{m}\right)^{0.5} \Rightarrow t = \left(\frac{m}{Z}\right)^{0.5} \frac{L}{(2eV)^{0.5}} \qquad \textbf{Equation 1.3}$$

in which e is the unit of elementary charge, m is the mass of the ion, Z is the charge state, v is the linear velocity, and L is the flight path length.

A linear TOF analyzer often suffers from poor mass resolution (<300). The initial kinetic energy, spatial and temporal distributions of the ions all contribute to the velocity

spread of ions of the same mass. Their effects on degradation in resolution, however, can be significantly minimized by time-lag focusing and/or use of a reflectron [18-19].

Time-lag focusing [18] introduces a delay time between ion formation and acceleration. The time lag (hundreds of ns to several μs) causes ions with the same mass drifting away from (or toward) the detector to acquire a higher (or lower) kinetic energy compensation, so they can reach the detector at the same time. The reflectron is an ion mirror with an electric field that retards and reflects the ions. The ions of higher kinetic energy penetrate deeper into the reflectron and take a longer time to return. With properly arranged geometry and voltages, they will reach the detector at the same time as those ions of identical mass but lower initial kinetic energy, which spend less time inside the reflectron. A reflectron instrument equipped with a time-lag focusing ion source can offer mass resolution (full width at half maximum, FWHM) of 10,000-20,000 [19]. Moreover, such instrumental configuration provides a significant improvement in mass measurement accuracy. Mass accuracy of better than 50 ppm can be routinely achieved for ions below 5000 Da. In addition, it permits tandem mass spectrometry studies, which will be described in Chapter 1.2.3.

There are a variety of MALDI MS applications for synthetic polymer characterization, including end group determination, copolymer composition analysis, and molecular mass measurement. Some types of polymeric materials analyzed include PEG, PMMA, PS, polyesters, nylons, and functional polyols [2,3,19].

For end group determination by MALDI MS, the general approach is to acquire an oligomer-resolved mass spectrum, thereby allowing the derivation of residual mass by subtracting the mass of repeat units. For example, it is demonstrated that using time-lag

focusing, the end groups in PEG with mass 15,000 Da can be revealed with mass accuracy 80 ppm or better [20]. PMMAs with a variety of end groups have also been studied [21]. Using a FTICR analyzer, the mass accuracy for the end group of a PMMA with molecular mass 6000 Da can be as high as 23.6 mmu (milli-mass unit) [22]. It must be realized that without other chemistry information, the mass spectra alone cannot identify the chemical structure of the end groups.

To date, most of the published work done by MALDI MS has been for homopolymers. There has been relatively little work done on copolymers. The copolymer spectra generated by MALDI are often too complex to conclusively identify the chemical linkages. A more detailed account for copolymer analysis by MALDI can be found in Chapter 7.

The most persistent theme for polymer MALDI MS is probably molecular mass measurement. There is a great body of work published in this area [2,3,19]. MALDI is generally considered an accurate average mass measurement method for polymers with polydispersity less than 1.2 [23], providing that a good sample preparation protocol is followed to generate the spectra. The National Institute of Standard and Technology (NIST) has recently conducted a round-robin experiment among 18 laboratories to investigate the accuracy of MALDI MS for polymer mass measurement [24]. The low uncertainty in the molecular mass results shows good reproducibility from lab to lab. However, great care has to be taken when calculating the molecular mass and comparing data obtained from more traditional methods such as GPC. For example, Schriemer *et al.* [25] described an important correction factor for signal intensity because most mass spectra data are collected linear in time instead of in mass. Jackson *et al.* [26] showed

that comparing M_p (mass of the most probable peak) values from mass spectrum and GPC can be misleading. A better way for fair comparison is to use M_n and M_w, which are defined as below, where M_i, n_i are the mass and the molar number of the i^{th} chain, respectively.

$$Mn = \frac{\sum n_i M_i}{\sum n_i} \qquad \textbf{Equation 1.4}$$

$$Mw = \frac{\sum n_i M_i^2}{\sum n_i M_i} \qquad \textbf{Equation 1.5}$$

There are potentially a number of experimental parameters that can affect the appearance of a mass spectrum, and hence M_n and M_w results. Many of these parameters can be controlled [5, 25]. For example, the type of solvent used in MALDI sample preparation can influence the mass spectral data [5, 16, 27-29]. But so long as the use of non-solvents in sample preparation is avoided, reproducible mass spectra and reliable M_n and M_w can be obtained [28]. As for the mass measurement of polymers with polydispersity greater than 1.2, the problem can be alleviated, to a certain extent, by using GPC to fractionate samples prior to MALDI analysis. One example is the work done by Montaudo and co-workers [30]. A polydispersed poly(dimethylsiloxane) with molecular mass ranging from 3,300 Da to 300,000 Da was analyzed with success. This GPC/MS combination should be useful for condensation polymer and copolymer analysis.

1.2.2 ESI Ion Trap (IT) MS

ESI is an atmospheric pressure ionization technique applicable to a wide range of compounds in solution. Modern ESI originates from the work done by Dole and co-workers [31] in the late 1960s, involving spraying dilute solutions of macromolecules

through a syringe held at high potential into a gas-filled chamber for mass spectrometric analysis. This technique was revived and successfully coupled to a mass spectrometer in the mid-1980's by Fenn and co-workers [4,32,33]. Although synthetic polymers were among the focus of early research in ESI, ESI has gained most of its popularity in the analysis of biomolecules such as protein and peptide [34,35].

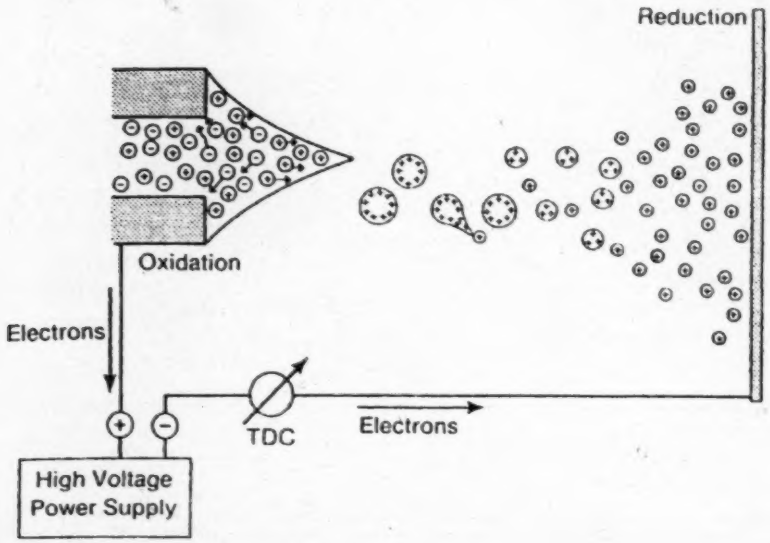

Figure 1.3. Principle of the electrospray ionization process.

In ESI, a dilute solution of the analyte is injected at a constant flow through a small diameter capillary or needle tip held at high voltage (0.5-5 kV) relative to a counter electrode. As the solution passes through the needle, the accumulation of excess charge due to high potential creates a Taylor cone at the exit. The solution is sprayed from the exit, and the solvent begins to evaporate, creating an aerosol of highly charged droplets. Charged droplets shrink due to evaporation in a sheath of dry nitrogen gas at moderate temperature. As the droplets shrink, coulombic repulsion forces become sufficient to overcome the surface tension, and the charged droplets disintegrate into fine droplets.

The shrinking and disintegrating process repeats until it produces droplets so small that the electric field at the liquid surface becomes high enough to enable the solute ions "escape" from the liquid phase to the gas phase (ion-evaporation) to become detectable [36]. A schematic illustration is shown in Figure 1.3. A high flow rate of coaxial gas can be used to assist the process of aerosol formation. This technique has been referred to as ion spray [37]. Compared to electrospray, where only electrical forces are used for nebulization, droplets in ion spray are formed by a combination of electric field and sheath gas, thereby enabling a stable spray from 100% water to 100% organic modifier even for high flow rate analysis (1-2 mL/min). This feature greatly facilitates the direct coupling of conventional liquid chromatography (LC) to ESI MS.

Since ESI generates ions continuously, it is often coupled to a scanning mass analyzer such as a quadrupole (Q) or a quadrupole ion trap (IT). The operation of both Q and IT is based upon the motion of ions in an oscillating electric field. Only the quadrupole IT is discussed in the following.

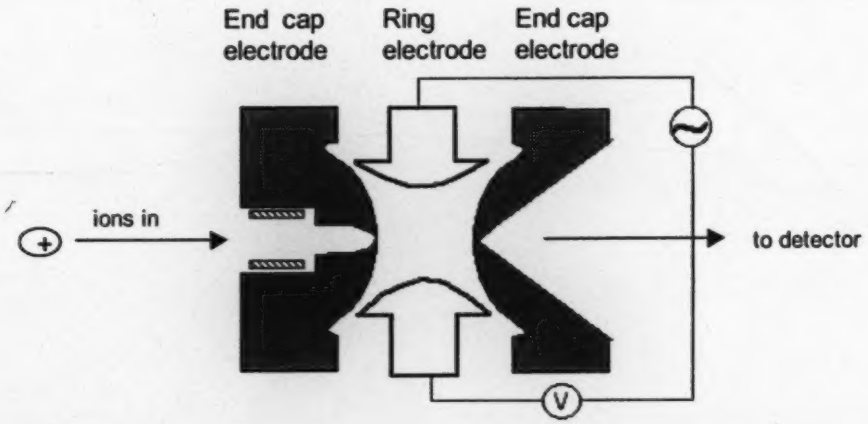

Figure 1.4. Schematic of a quadrupole ion trap mass spectrometer.

A quadrupole ion trap comprises of two end cap electrodes and a ring electrode, as shown in Figure 1.4. A hyperbolic electric field is created inside the chamber by the potentials applied on the electrodes. Externally generated ions are injected into the trap. With a proper setting of radio frequency (RF) voltage on the ring electrode, ions within a certain mass range follow a stable trajectory in the hyperbolic field, and are thereby trapped. Upon collision with the bath gas (usually helium), the ions are focused into the center due to the loss of translational energy. These ions can be ejected out of the trap by using an ion selective instability operation mode or a resonance ejection mode, and detected by an external electron multiplier. In resonance ejection, a supplementary RF voltage with a frequency that is lower than that of the main RF voltage applied to the ring is applied between the end-cap electrodes at a much smaller amplitude. By scanning the amplitude of the main RF, ions of different m/z are sequentially brought into resonance with the supplementary RF signal. These ions pick up translational energy and are then ejected at a much lower RF voltage than would normally be required. An analogous technique of resonant excitation provides the basis for MS/MS operation with ion trap [6].

Despite the great success of ESI in bio-molecule analysis, it has proven difficult for polymer analysis. Compared to the wide range of polymers analyzed by MALDI, only a limited number of synthetic polymers have been analyzed by ESI with success. There are two major factors limiting ESI for polymer applications. The first is the additional charges on the detected ions. The increased charge decreases the m/z and enables the detection of high mass species. It was found that up to 23 sodium ions could be deposited on the large PEG oligomers, which could significantly extend the mass

range of conventional mass analyzer [38]. PEG with molecular mass up to 5 million Da was detected by ESI MS [4]. However, the higher charge is not a single charge state, but a distribution of charge states. When this distribution is superimposed upon the oligomer distribution inherent to polymers, the resulting spectrum becomes extremely complex, even for polymers with moderate molecular mass. It usually requires a high-resolution mass analyzer to resolve the oligomer peaks. For example, with a Fourier Transform (FT) analyzer, the spectra of PEGs with molecular mass up to 23 kDa were deconvoluted and assigned [39]. The second limiting factor is the limited solubility of most polymers in ESI amendable solvents such as water and methanol. It is shown that an *N,N*-dimethylformamide (DMF) /tetrahydrofuran (THF) solvent system could be used in ESI at elevated cone potential to analyze PEG [40] and PS [41,42] with certain success. But this is far from becoming a routine practice.

Molecular mass measurement of a polymer by ESI MS should be performed with great caution. Operational parameters such as cone voltage [43] and accumulation time [44] were found to have great impact on the outcome. Solvent polarity was also shown to affect the observed distribution [45].

ESI MS is found most successful in analyzing low molecular mass surfactants [46-49] where the charge state can be controlled to a single charge or a few charges. One unique advantage of ESI MS lies in the ease with which it can couple with separation techniques. The analysis of low molecular mass PEG by GPC/ESI MS has been demonstrated [46]. ESI was also coupled with reverse-phase liquid chromatography (RPLC) for surfactant analysis in environmental water samples [47]. With a GPC-ESI-

FTMS configuration, a copolymer composed of two monomers of same mass was separated, and the oligomers were identified [48].

1.2.3 Tandem MS for Polymer Characterization.

In principle, polymer structural information can be obtained by using tandem MS where the oligomer ion of interest is selected for dissociation via techniques such as collision-induced dissociation (CID) [51] and fragment ions are analyzed in a second stage of MS. Multiple stages of MS or MS^n are possible using IT and FTMS instruments. Two techniques, namely, post source decay (PSD) and CID, are most commonly used in polymer tandem MS.

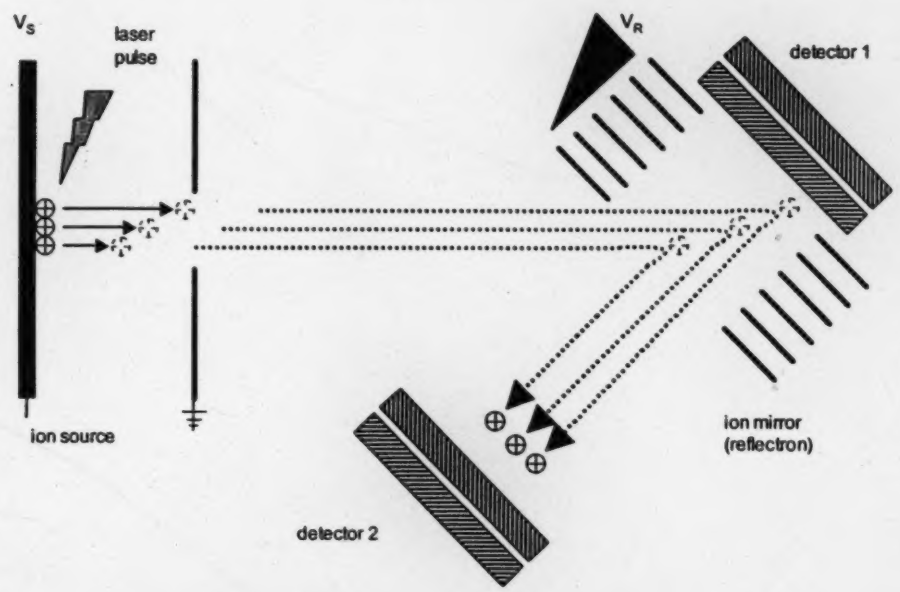

Figure 1.5. Schematic of a reflectron (ion mirror) TOF mass spectrometer. Vs is the voltage applied on the repeller, V_R represents the voltages applied on the ion mirrors.

MALDI of neutral sample molecules can result in the formation of molecular ions (or quasi-molecular ions) with a wide range of internal energies. Consequently, a number of molecular ions (or quasi-molecular ions) can undergo one or more dissociation processes. If dissociation takes place at a sufficiently high rate that it almost entirely occurs within the source region, this dissociation is called in-source decay (ISD). In general, this is not a desired process for structural elucidation due to the lack of control in fragmentation and the inability to mass select of the precursor ions. If, dissociation takes place during the ion transit between ion source and detector, these fragment ions are called metastable ions. In practice, metastable ions often refer to those ions resulting from the unimolecular dissociation process [6].

In a linear TOF MS, metastable ions cannot be separated. This is because an ion resulting from a fragmentation in the flight tube continues with approximately the same velocity as the precursor ion and therefore strikes the detector at the same time as the precursor ion. In a reflectron instrument (Figure 1.5), however, the neutral product will not be reflected in the ion mirror. The time of arrival of the neutral fragment at detector 1 identifies the precursor ion, and the charged fragment is reflected and detected by detector 2. Measurement of the arrival time of the fragment ion correlated to a specific precursor ion defines the routes for unimolecular fragmentation of this ion.

Despite a large number of applications in peptide analysis, the literature of polymer MALDI PSD is scarce. The main reason is that the low internal energy gained via MALDI is usually not sufficient for polymer chain fragmentation. Nonetheless, this technique has been successfully used to analyze poly(propylene glycol) (PPG) [51], PMMA [52], polyisobutylene [53], PEG [53,54], and polyurethanes [55]. The general

applicability of this technique and the quality of the fragment ion spectra for structural analysis remains to be determined.

In contrast to PSD, dissociation may be caused deliberately by ion-neutral or ion-molecule collisions. In this process, a fraction of the kinetic energy of a moving ion is converted to internal energy through collision with background gas molecules. Since CID has a relatively high cross section, it can be much more efficient than unimolecular dissociation [6]. Depending on the collisional energy, CID can be classified as high energy (keV) or low energy (<100 eV). They differ in interaction time of the ions and background gas, and therefore the excitation modes available to the ions. Depending upon the energy requirement, high energy CID generally promotes direct bond cleavages, whereas low energy CID favors rearrangements [6].

CID combined with chemical ionization, field desorption, secondary ion, or fast atom bombardment has been used to analyze short chain oligomers [56-72]. While ESI and MALDI tandem MS have been widely used for biomolecular structural analysis, their use in polymer structural analysis is presently limited in scope [43, 52, 73-82]. Many polymers require the use of high energy CID that can only be accomplished in limited types of instruments such as a sector/time-of-flight mass spectrometer, because they do not readily fragment under low energy CID [73-76, 81]. Unfortunately this type of instrument is not accessible to most researchers for routine analysis. More details on this subject can be found in Chapters 5 and 6. It is clear that a robust and readily adaptable method for generating low energy CID spectra of polymeric materials would open the door for many polymer researchers to characterize their polymers by MS/MS.

1.3 Conclusions

Mass spectrometry, especially MALDI and ESI, has been developed to provide a significant amount of information of polymer structure and average molecular mass. MS is now recognized as an important characterization method for polymers, complementary to traditional methods such as IR, NMR, and GPC. However, due to the complexity inherent to polymers, there are still many challenges to be met. In particular, MS/MS application on polymeric systems seems to lag behind its counterpart in bio-systems. A continuous effort into these research areas is of fundamental and practical importance.

1.4 Literatures Cited

1. Stevens, M. P. *Polymer Chemistry*, Oxford University Press, New York, **1999**.
2. Montaudo, G.; Lattimer, R. P. *Mass Spectrometry of Polymers*, CRC Press LLC, New York, **2002**.
3. Hantom, S. D. *Chem. Rev.* **2001**, 101, 527.
4. Nohmi, T.; Fenn, J. B. *J. Am. Chem. Soc.* **1992**, 114, 3241.
5. Schriemer, D. C.; Li, L. *Anal. Chem.* **1996**, 68, 2721.
6. Chapman, J. R. *Practical Organic Mass Spectrometry*, John Wiley & Sons, West Sussex, England, **1994**.
7. Karas, M.; Bachmann, D.; Bahr, Y.; Hillenkamp, F. *Int. J. Mass Spectrom. Ion Proc.* **1987**, 78, 53.
8. Karas, M.; Hillenkamp, F. *Anal. Chem.* **1988**, 60, 2299.
9. Tanaka, K.; Ido, Y.; Akita, S. *Proceedings of the Second Japan-China joint Symposium on Mass Spectrometry*, Matsuda, H.; Liang, X. T. Eds, Bando Press, Osaka, Japan, **1987**, 185.
10. Tanaka, K.; Waki, H.; Ido, Y.; Akita, S.; Yoshida, Y.; Yoshida, T. *Rapid Commun. Mass Spectrom.* **1988**, 2, 151.
11. Hillenkamp, F.; Karas, M.; Beavis, R. C.; Chait, B. T. *Anal. Chem.* **1981**, 63, 1193A.
12. Hensel, R. R.; King, R. C.; Owens, K. G. *Rapid Commun. Mass Spectrom.* **1997**, 11, 1785.
13. Karas, M.; Bahr, U.; Giebmann, U. *Mass Spectrom. Rev.* **1991**, 10, 335.
14. Zenobi, R.; Knochenmuss, R. *Mass Spectrom. Rev.* **1998**, 17, 337.

15. von Helden, G.; Wyttenbach, T.; Bowers, M. T. *Science* **1993**, 4, 93.

16. Dorgruel, D.; Nelson, R. W.; Williams, P. *Rapid Commun. Mass Spectrom.* **1996**, 10, 801.

17. Lehmann, E.; Knochenmuss, R.; Zenobi, R. *Rapid Commun. Mass Spectrom.* **1997**, 11, 1483.

18. Cotter, R. J. *Time-of-Flight Mass Spectrometry, ACS Professional Reference Books,* Washington, DC, **1997**.

19. Nielen, M. W. F. *Mass Spectrom. Rev.* **1999**, 18, 309.

20. Whittal, R. M.; Schriemer, D. C.; Li, L. *Anal. Chem.* **1997**, 69, 2734.

21. Maloney, D. R.; Hunt, K. H.; Lloyd, P. M.; Muir, A. V. G.; Richards, S. N.; Derrick, P. J.; Haddleton, D. M. *J. Chem. Soc. Chem. Commun.* **1995**, 561.

22. Easterling, M. L.; Mize, T. H.; Amster, I. J. *Int. J. Mass Spectrom. Ion Proc.* **1997**, 160/170, 387.

23. Montaudo, G.; Montaudo, M. S.; Puglisi, C.; Samperi, F. *Rapid Commun. Mass Spectrom.* **1995**, 9, 453.

24. Guttman, C. M.; Wetzel, S. J.; Blair, W. R.; Fanconi, B. M. Girard, J. E.; Goldschmidt, R. J.; Wallace, W. E.; Vander Hart, D. L. *Anal. Chem.* **2001**, 73, 1252.

25. Schriemer, D. C.; Li, L. *Anal. Chem.* **1996**, 69, 4176.

26. Jackson, C.; Larsen, B.; McEwen, C. *Anal. Chem.* **1996**, 68, 1303.

27. Chen, H. R.; Guo, B. C. *Anal. Chem.* **1997**, 69, 4399.

28. Yalcin, T.; Dai, Y. Q.; Li, L. *J. Am. Soc. Mass Spectrom.* **1998**, 9, 1303.

29. Hanton, S. D.; Cornelio Clark, P. A.; Owens, K. G. *J Am. Soc. Mass Spectrom.* **1999**, 10, 104.

30. Montaudo, M. S.; Puglisi, C.; Samperi, F. Montaudo, G. *Rapid Commun. Mass Spectrom.* **1998**, 12, 519.

31. Dole, M. *J. Chem. Phys.* **1968**, 49, 2240.

32. Yamashita, M.; Fenn, J. B. *J. Phys. Chem.* **1984**, 88, 4671.

33. Whitehouse, C. M.; Dreyer R. N.; Yamashita, M.; B. Fenn, J. B. *Anal. Chem.* **1985**, 57, 675.

34. Dass, C. *Principles and Practices of Biological Mass Spectrometry*, John Wiley & Sons, New York, **2001**.

35. Cole, R. B. *Electrospray Ionization Mass Spectrometry*, John Wiley & Sons, New York, **1997**.

36. Kebarle, P.; Tang. L. *Anal. Chem.* **1993**, 65, 972A.

37. Bruins, A. P.; Covey, T. R.; Henion, D. *Anal. Chem.* **1987**, 59, 2642.

38. Wong, S. F.; Meng, C. K.; Fenn, J. B. *J. Phys. Chem.* **1988**, 92, 546.

39. O'Connor, P. B.; McLafferty, F. *J. Am. Chem. Soc.* **1995**, 117, 12826.

40. Saf, R.; Mirtl, C.; Hummel, K. *Tetrahedron Lett.* **1994**, 35, 6654.

41. Jasieczek, C. B.; Buzy, A.; Haddleton, D. M.; Jennings, K. R. *Rapid Commun. Mass Spectrom.* **1996**, 10, 509.

42. Deery, M. J.; Jennings, K. R.; Jasieczek, C. B.; Haddleton, D. M.; Jackson, A. T.; Yates, H. T.; Scrivens, J. H. *Rapid Commun. Mass Spectrom.* **1997**, 11, 57.

43. Hunt, S. M.; Sheil, M. M.; Belov, M.; Derrick, P. J. *Anal. Chem.* **1998**, 70, 1812.

44. Maziarz, E. P.; Baker, G. A.; Lorenz, S. A.; Wood, T. D. *J. Am. Soc. Mass Spectrom.* **1999**, 10, 1298.

45. Latourte, L.; Blais, J. –C.; Tabet, J. –C. *Anal. Chem.* **1997**, 69, 2742.

46. Prokai, L.; Simonsick, Jr. W.J. *Rapid Commun. Mass Spectrom.* **1993**, 7, 854.

47. Crescenzi, C.; Di Corcia, A.; Samperi, R.; Marcomini, A. *Anal. Chem.* **1995**, 67, 1797.

48. Ogura, I.; DuVal, D. L.; Kawakami, S.; Miyajima, K. *J. Am. Oil Chem. Soc.* **1996**, 73, 137.

49. Castillo, M.; Alonso, M. C.; Riu, J.; Barcelo, D. *Environ. Sci. Technol.* **1999**, 33, 1300.

50. Aeserud, D. J.; Prokai, L.; Simonsick, Jr. W. J. *Anal. Chem.* **1999**, 71, 4793.

51. Mowart, I. A.; Donovan, R. J.; Maier, R. J. *Rapid Commun. Mass Spectrom.* **1997**, 11, 89.

52. Scrivens, J. H.; Jackson, A. T.; Yates, H. T.; Green, M. R.; Crutchley G.; Brown, J.; Bateman, R. H.; Bowers, M. T.; Gidden, J. *Int. J. Mass Spectrom. Ion Proc.* **1997**, 165, 363.

53. Varney, J. E.; Derrick, P. J.; Szilagyi, Z.; Vekey, K. *Proc. 45th ASMS Conf. Mass Spectrom. Allied Topics*, Palm Springs, CA. **1997**, p317.

54. Kowalski, P.; Guttman, C.; Wallace, W. *Proc. 46th ASMS Conf. Mass Spectrom. Allied Topics*, Orlando, FL. **1998**, p1060.

55. Puapaiboon, U.; Taylor, R. T.; Jai-nhuknan, J. *Rapid Commun. Mass Spectrom.* **1999**, 13, 516.

56. Busch, K. L.; Glish, G.L.; McLuckey, S.A. *Mass Spectrometry/Mass Spectrometry*, VCH Publishers: New York, **1988**.

57. Tou, J. C.; Zakett, D.; Caldecourt, V. J. *Tandem Mass Spectrometry*, McLafferty, F. W. Ed., Wiley, New York, **1984**.

58. Lyon, P. A.; Stebbings, W. L.; Crow, F. W.; Tomer, K. B.; Lippstreu, D. L.; Gross, M. L. *Anal. Chem.* **1984**, 56, 8.

59. Lyon, P. A.; Crow, F. W.; Tomer, K.B.; Gross, M. L. *Anal. Chem.* **1984**, *56*, 2278.

60. Catlow, D. A.; Johnson, M.; Monaghan, J. J.; Porter, C.; Scrivens, J. H. *J. Chromatogr.* **1985**, 328, 167.

61. Craig, A. G.; Derrick, P. J. *J. Chem. Soc., Chem. Commun.* **1985**, 891.

62. Craig, A. G.; Derrick, P. J. *J. Am. Chem. Soc.* **1985**, 107, 6707.

63. Ballistreri, A.; Garozzo, D.; Giuffrida, M.; Montaudo, G.; Filippi, A.; Guaita, C.; Manaresi, P.; Pilati, F. *Macromolecules* **1987**, 20, 1029.

64. Kiplinger, J. P.; Bursey, M. M. *Org. Mass Spectrom.* **1988**, 23, 342.

65. Lattimer, R. P.; Munster, H.; Budzikiewicz, H. *Int. J. Mass Spectrom. Ion Proc.* **1989**, 90, 119.

66. Ventura, F.; Fraisse, D.; Caixach, J.; Rivera, J. *Anal. Chem.* **1991**, 63, 2095.

67. Maleknia, S.; Liou, C. C.; Brodbelt, J. *Org. Mass Spectrom.* **1991**, 26, 997.

68. Kalinoski, H. T.; Hargiss, L. O. *J. Am. Soc. Mass Spectrom.* **1992**, 3, 150.

69. Lattimer, R. P. *J. Am. Soc. Mass Spectrom.* **1992**, 3, 225.

70. Lattimer, R. P. *Int. J. Mass Spectrom. Ion Proc.* **1992**, 116, 24.

71. Lattimer, R. P. *J. Am. Soc. Mass Spectrom.* **1994**, 5, 1072.

72. Selby, T. L.; Wesdemiotis, C.; Lattimer, R. P. *J. Am. Soc. Mass Spectrom.* **1994**, 5, 1081.

73. Jackson, A. T.; Yates, H. T.; Scrivens, J. H.; Critchley, G.; Brown, J.; Green, M. R.; Bateman, R. H. *Rapid Commun. Mass Spectrom.* **1996**, 10, 1668.

74. Jackson, A. T.; Yates, H. T.; MacDonald, W. A.; Scrivens, J. H.; Critchley, G.; Brown, J.; Deery, M. J.; Jennings, K. R.; Brookes, C. *J. Am. Soc. Mass Spectrom.* **1997**, 8, 132.

75. Bottrill, A. R.; Giannakopulos, A. E.; Waterson, C.; Haddleton, D. M.; Lee, K. S.; Derrick, P. J. *Anal. Chem.* **1999**, 71, 3637.

76. Pastor, S. J.; Wilkins, C. L. *Int. J. Mass Spectrom. Ion Proc.* **1998**, 175, 81.

77. Hunt, S. M.; Binns, M. S.; Sheil, M. M. *J. Appl. Polym. Sci.* **1995**, 56, 1589.

78. McEwen, C. N.; Simonsick, W. J., Jr.; Larsen, B. S.; Ute, K.; Hatada, K. *J. Am. Soc. Mass Spectrom.* **1995**, 6, 906.

79. Mahon, A.; Kemp, T. J.; Buzy, A.; Jennings, K. R. *Polymer*, **1996**, *37*, 531.

80. Yalcin, T.; Gabryelski, W.; Li, L. *Proceedings of the 46th ASMS Conference on Mass Spectrometry and Allied Topics*, Orlando, FL, **1998**, p1054.

81. Yalcin, T.; Gabryelski, W.; Li, L. *Anal. Chem.* **2000**, 72, 3847.

82. Adamus, G.; Kowalczuk, M. *Rapid Commun. Mass Spectrom.* **2000**, 14, 195.

Chapter 2. Reactions of Atomic Transition-Metal Ions with Long-Chain Alkanes

Understanding metal ion interactions with long chain alkanes is not only of fundamental importance in the areas of organometallic chemistry, surface chemistry and catalysis, but also has significant implication in mass spectrometric method development for the analysis of polyethylene. Polyethylene represents one of the most challenging classes of polymers to be analyzed by mass spectrometry. In this chapter, reactions of several transition-metal ions including Cr^+, Mn^+, Fe^+, Co^+, Ni^+, Cu^+ and Ag^+ with long chain alkanes, $C_{28}H_{58}$ and $C_{36}H_{74}$, are reported. A metal powder and the nonvolatile alkane are co-deposited onto a sample target of a laser desorption/ionization (LDI) time-of-flight (TOF) mass spectrometer. The metal ions generated by LDI react with the vaporized alkane during desorption. It is found that all of these metal ions can form adducts with the long-chain alkanes. Fe^+, Co^+ and Ni^+ produce in-source fragment ions resulting from dehydrogenation and dealkylation of the adduct ions. The post-source decay (PSD) spectra of the metal-alkane adduct ions are recorded. It is shown that PSD of Ag^+ alkane adduct ions produces bare metal ions only, suggesting weak binding between this metal ion and alkane. The PSD spectra of the Fe^+, Co^+ and Ni^+ alkane adduct ions display extensive fragmentation. Fragment ions are also observed in the PSD spectra of Cr^+, Mn^+ and Cu^+ alkane adduct ions. The high reactivity of Fe^+, Co^+ and Ni^+ is consistent with that observed in small alkane systems.

A form of this chapter is published as:
R. Chen, and L. Li, "Reactions of atomic transition-metal ions with long-chain alkanes", *J. Am. Soc. Mass Spectrom.* **2001**, 12, 367-375.

The unusually high reactivity of Cr^+, Mn^+ and Cu^+ is rationalized by a reaction scheme where a long-chain alkane first forms a complex with a metal ion via ion/induced dipole interactions. If sufficient internal energy is gained during the complex formation, metal ions can insert into C-H and C-C bonds of the alkane, followed by fragmentation. The thermal energy of the neutral alkane is believed to be the main source of the internal energy acquired in the complex. Finally, the implication on mass spectrometric method development for polyethylene analysis is discussed.

2.1 Introduction

There are a great number of studies on gas phase reactions of alkanes with atomic transition-metal ions [1-4]. Understanding these reactions is of fundamental importance in the areas of organometallic chemistry, surface chemistry, and catalysis [1-4]. Primary tools used for these studies include ion cyclotron resonance (ICR) or Fourier transform ICR mass spectrometry (MS) [5-10], ion-beam MS [1,11-12], and conventional tandem MS [13-16]. Metal ions are often generated by surface ionization [1], laser desorption/ionization [17], fast atom bombardment of metals [18], or electron impact of organometallic compounds [4]. Under well-defined conditions, extensive information on reaction pathways, energetics and kinetics of many alkane-metal systems as well as intrinsic properties of metal ions have been obtained. However, all these studies have been focused on the interactions of transition-metal ions with small, gaseous alkanes.

In this chapter, an investigation of reactions of transition-metal ions with long-chain, nonvolatile alkanes by using laser desorption/ionization (LDI) time-of-flight mass spectrometry is described. Besides the fundamental importance, studies of intrinsic interaction properties between long-chain alkanes and transition-metal ions should be

particularly valuable for mass spectrometric method development in analyzing hydrocarbons such as polyethylene. Transition-metal ions have been increasingly used as a means of ionizing polymeric materials for mass spectrometric characterization of polymers [19]. Selection of a proper metal ion is critical for the success of polymer analysis by MS. For example, Ag^+ is now commonly used to ionize polystyrene and it allows the ionization of high molecular mass polystyrene with molecular weights up to 1.5 million Da [20]. On the other hand, Cu^+, as opposed to Ag^+, has been shown to provide efficient ionization of high molecular mass polybutadiene and polyisoprenes [21]. At present, polyethylene represents perhaps the most challenging polymer for MS analysis. Thus, studies of interactions between long-chain alkanes and transition-metal ions should benefit the development of MS methods for polyethylene analysis. A better understanding of reactivity of transition-metal ions will also assist in interpretation of mass spectra of polymeric materials.

It is shown in this work that all transition metal ions studied can form adduct ions with long chain alkanes in LDI. It is also demonstrated that thermal energies possessed by these large alkanes can lead to somewhat unusual reactivity with metal ions such as Cr^+, Mn^+ and Cu^+. A number of common products from the fragmentation of metal-ion long-chain alkane complexes are detected.

2.2 Experimental

2.2.1 Materials and Reagents. The two alkanes studied in this work, octacosane ($C_{28}H_{58}$) and hexatriacontane ($C_{36}H_{74}$), were purchased from Aldrich Chemical Co. (Milwaukee, WI). The purities of the alkanes were checked by gas chromatography/MS and no detectable impurities were found in electron impact ionization spectra. The high purity

(>98%) metal powders, Cr, Mn, Fe, Co, Ni, Cu and Ag, were obtained from Aldrich or Fisher (Mississauga, Ontario) and used as received. Chlorobenzene and isopropyl alcohol (HPLC grade) were obtained from Sigma (Milwaukee, WI).

2.2.2 LDI and PSD. Laser desorption/ionization was carried out in an Applied Biosystems Voyager laser desorption/ionization time-of-flight (TOF) mass spectrometer (Framingham, MA). The metal powders were first suspended in isopropyl alcohol and then transferred onto the LDI sample target. One μl of alkane solution at a concentration of 5 mg/ml in chlorobenzene was deposited on top of the metal powders on the sample target and dried in the air. Metal powders and alkanes were desorbed by a 337-nm laser beam from a pulsed nitrogen laser. Ions generated in the source were extracted into the flight tube after 100 ns delay. Precursor ions can be selected with an ion gate in the instrument.

The post-source decay (PSD) products of the selected ions, mainly from metastable dissociation processes [22], were detected by the second lag of the reflectron TOF. All spectra were the results of signal averaging of between 100 and 200 shots and calibrated internally using the distinctive metal ions or their clusters. All data were reprocessed using the Igor Pro Software package (WaveMetrics, Lake Oswego, OR) and no background subtraction was performed.

2.3 Results and Discussion

Figures 2.1 and 2.2 show the LDI mass spectra of $C_{28}H_{58}$ and $C_{36}H_{74}$ obtained by using different transition-metal ions as the ionization reagent. The analyte peaks, labeled as M and F, are from the molecular ions and fragment ions, respectively. The Ag cluster ions are labeled as C. Other unlabeled peaks are from impurities. These impurity peaks can be readily distinguished from the actual analyte peaks during the process of LDI spectral recording. The concomitant appearance of the analyte peaks with appropriate relative intensities is an indication that they are from the same chemical origins. Fragment ion spectra are very reproducible, whereas the relative intensities between the impurity peaks and analyte peaks vary widely from shot to shot and location to location on the same spot. The impurity peaks were found in blanks, indicating that they are from the metal powders, solvents and/or containers used for sample preparation. These impurities might be present in a trace amount; but their ionization efficiencies can be much higher than alkanes, resulting in a relatively high background.

Figures 2.1 and 2.2 display some salient features for the two alkanes. In all cases, metal-ion/alkane adducts are observed as the base peaks in the spectra. Note that the term 'adduct' used here does not reflect the true nature of interaction. In addition, dehydrogenation products are detected. Figure 2.3 displays the expanded mass spectra in the molecular ion regions of the metal ion adducts. The isotope distributions match very well with the calculated distributions (not shown). In the case of Fe^+, the base peak is the dehydrogenation product resulting from loss of two H_2 from the adduct ion. As seen from Figures 2.1 and 2.2, in-source fragmentation products from loss of alkyl groups from the adduct ions are observed for Fe^+, Co^+ and Ni^+. Very weak signals of these fragment ions are also detected for Cu^+.

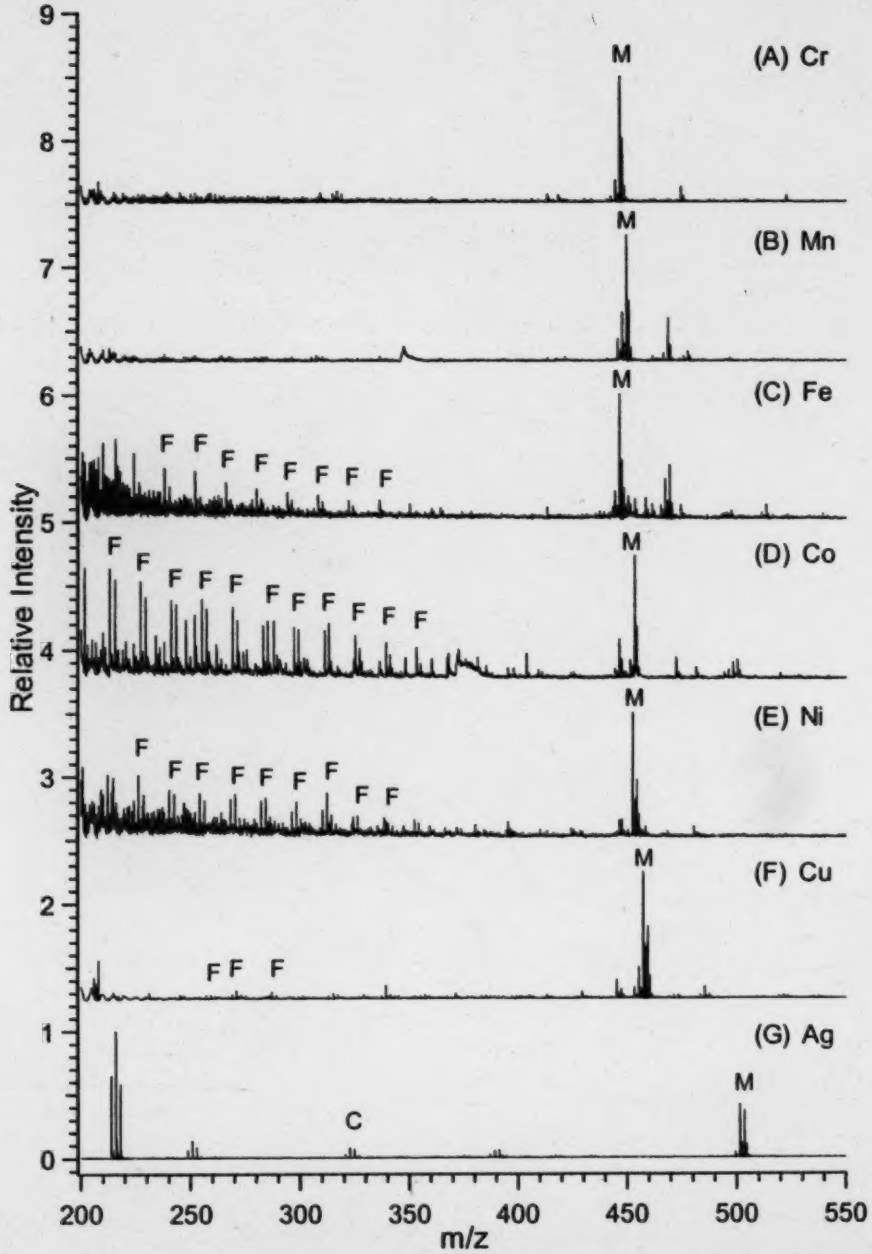

Figure 2.1. Laser desorption ionization mass spectra of $C_{28}H_{58}$ obtained by using different metals. The metal-alkane adduct ions are labeled as M and their fragment ions are labeled as F. The Ag cluster ions are labeled as C. All other peaks are mainly from impurities.

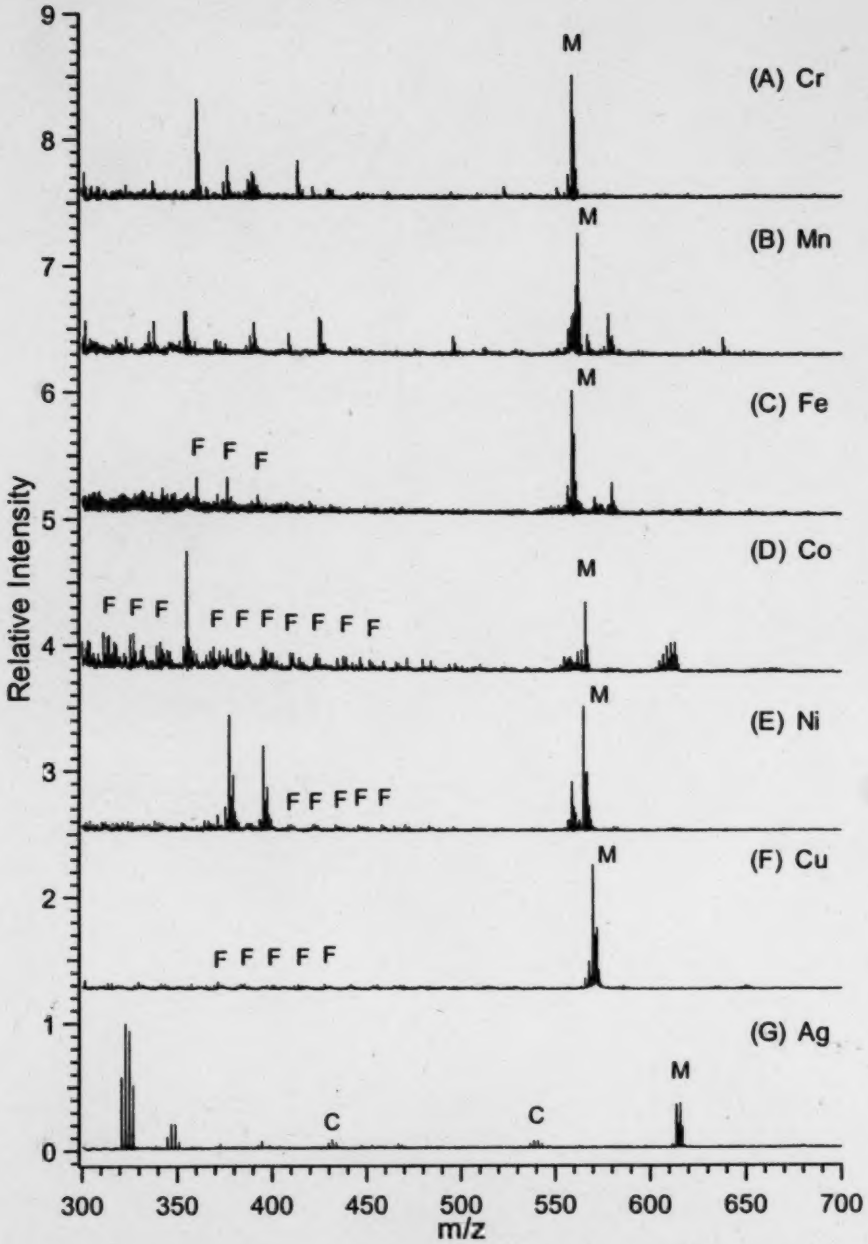

Figure 2.2. Laser desorption ionization mass spectra of $C_{36}H_{74}$ obtained by using different metals. The metal-alkane adduct ions are labeled as M and their fragment ions are labeled as F. The Ag cluster ions are labeled as C. All other peaks are mainly from impurities.

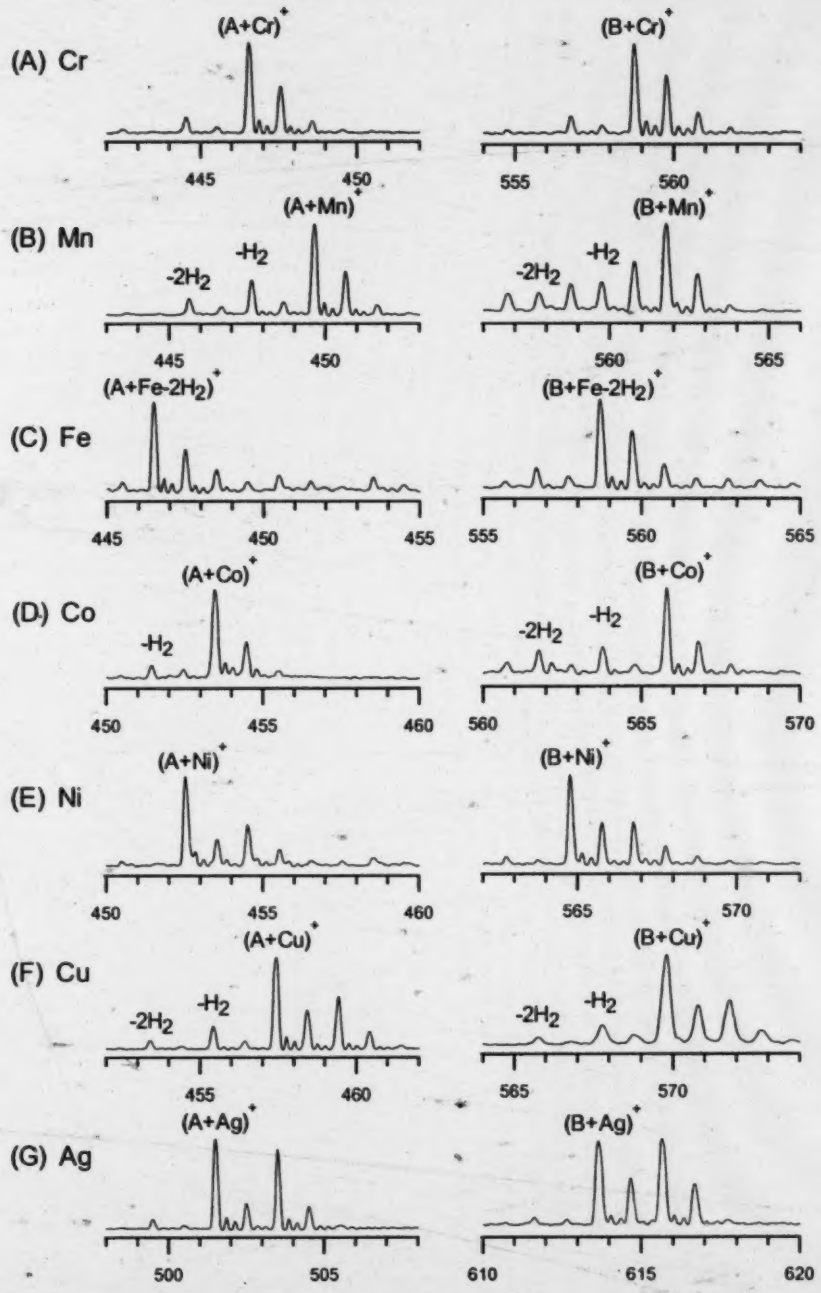

Figure 2.3. Expanded mass spectra showing the molecular ion regions of metal ion $C_{28}H_{58}$ (A) and $C_{36}H_{74}$ (B) adducts. The dehydrogenation products are labeled as "$-H_2$" or "$-2H_2$".

Figures 2.4 and 2.5 show the PSD mass spectra of the metal-alkane adduct ions. For Fe^+, Co^+ and Ni^+ alkane adducts, dealkylation products are dominant in the PSD spectra. No bare metal ions from Fe, Co and Ni are observed. In the case of Cu^+, very weak peaks at m/z 63 and 65 may be assigned to Cu^+, as shown in the inserts of Figures 2.4F and 2.5F. For Cr^+ and Mn^+, dealkylation products along with bare metal ions are observed in their PSD spectra. The occurrence of these fragment ions is independent of the laser power used. However, their intensities generally increase as laser power increases. The post source decay of the Ag^+-alkane complex produces exclusively Ag^+.

As the metal ion interacts with the alkane, several possible intermediates can be produced. One is the weakly and non-covalently bound adduct ion, which can readily dissociate back to the reactants. Another possible intermediate is a metal-ion insertion product. The metal ion can insert into a C-H or C-C bond of the alkane via an oxidative addition mechanism [1]. If the internal energy of this intermediate product is not very high, it can survive the entire duration of flight to be detected as the intact metal-alkane ion. Products with high internal energy will undergo fragmentation, via processes such as dehydrogenation or dealkylation. For unreactive metal ions such as Cu^+ and Ag^+ where direct metal ion insertion to alkanes is not possible, an intermediate involving a three-center two-electron bond between the metal ion and C-H or C-C has been proposed for small alkanes [23-25]. In this case, fragmentation takes place via heterolytic cleavage with electron donation from C-H or C-C bond into the empty *s* orbital of the metal ion.

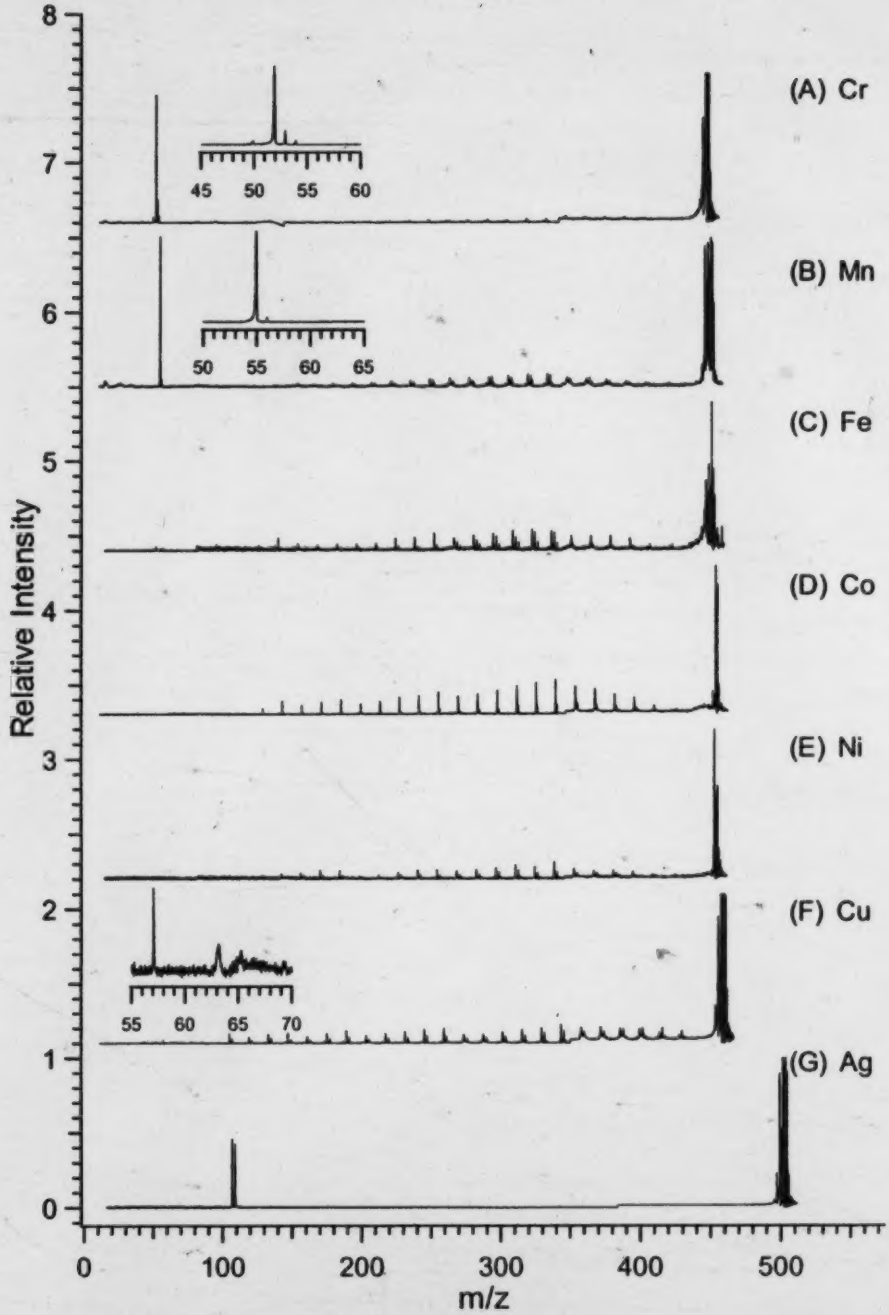

Figure 2.4. Post-source decay mass spectra of metal-ion $C_{28}H_{58}$ adducts.

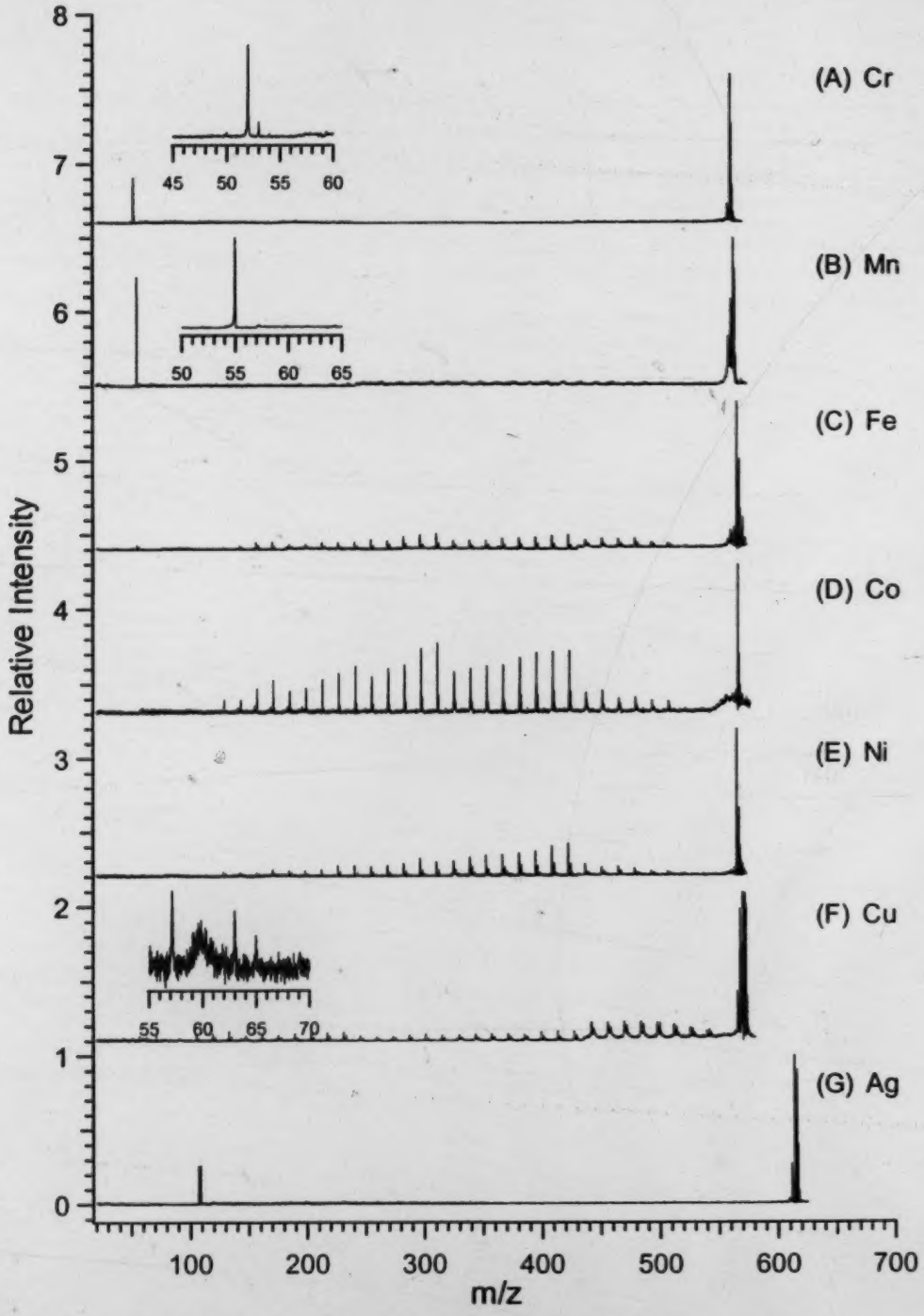

Figure 2.5. Post-source decay mass spectra of metal-ion $C_{36}H_{74}$ adducts.

The reactivity observed in this study for the reactive metal ions of Fe^+, Co^+ and Ni^+ can be explained by considering the modified oxidative addition mechanism. The actual reaction mechanism involved in metal ion alkane interactions is still a subject of on-going theoretical and experimental investigation [26-32]. The traditional mechanism stated that metal ion insertion, followed by β-H or β-carbon migration, results in subsequent loss of H_2 and short-chain alkanes [1]. Earlier reports on this mechanism assumed the CH or CC insertion by the metal ion as the rate-limiting step. Recent work suggests that the highest energy barrier lies in the formation of multicenter transition states (MCTSs) [26-32]. MCTSs are formed after the metal ion insertion and before the H_2 or short-chain alkane elimination. If it is assumed that there are MCTSs formed in the interaction of a long chain alkane and a metal ion, it is unclear whether the formation of MCTSs is the rate-limiting step. Unlike a short chain alkane, intramolecular interactions near or away from the metal ion insertion site are expected to occur for a long chain alkane system. One can speculate that any such interactions could affect the energetics of MCTSs. Nevertheless, the rationale presented in this work will adhere to the simple oxidative addition mechanism to provide a qualitative description of the reaction process involved in the long-chain alkane metal ion interactions. In the following discussion, the similarity and differences observed in reactivity and reaction products between those reported with short-chain alkane systems and that from this study of long-chain alkanes are addressed.

Studies of the reaction dynamics of alkane and transition metal ions have generated a considerable amount of interest [29-32]. The experimental setup used in this study provides some information about the reaction products at different time scales. For the Fe^+, Co^+ and Ni^+ complexes, by operating the instrument in a DC extraction mode,

fragment ions with similar intensities as those with delayed extraction (delay time = 100 ns) were observed. This result suggests that these fragment ions are formed by fast dissociation of the alkane-metal ion during the ionization process. The lack of any bare metal ions in the PSD spectra of these adducts indicates that during the time frame of metastable ion dissociation (i.e., tens of microseconds), dehydrogenation and dealkylation are the major fragmentation pathways.

Weisshaar and coworkers have used a combination of delayed extraction and application of a retarding field in the flight tube to probe the ion-molecule reaction dynamics in the time scale up to 25 μs [30]. In their work, supersonic jet-cooled alkanes such as C_3H_8 or n-C_4H_{10} interacted with a packet of Ni^+ produced by laser-induced resonant two-photon ionization in a field free region of the TOF mass spectrometer. Of particular interest, they found that dissociation of Ni^+-butane or Ni^+-propane complexes occurs promptly (< 1 μs) as well as over a long range of time scales (0.5 to 25 μs) and fragment product ratios are similar at all times [30,32]. In the current reflectron PSD experiments, the time limit for PSD in the first lag of the reflectron is about 32 μs for $Ni(C_{28}H_{58})^+$ and 36 μs for $Ni(C_{36}H_{74})^+$. The results shown here, albeit obtained under different conditions from those of Weisshaar and coworkers, indicate that fragmentation also occurs at a long range of time scales for much larger alkane metal ion complexes.

Considering a large degree of freedom associated with a long-chain alkane metal ion complex, the observation of fragment ions at long time scales raises the question as to whether statistical theory is applicable to the fragmentation of such a large complex. There are a number of examples in the literature related to the fragmentation of other types of high mass ions. For example, thermal induced fragmentation of peptide and protein ions in the interface region of an electrospray ionization mass spectrometer is

commonly observed [33,34]. Photodissociation of proteins can be observed in TOF even though the energy deposited in the molecule is low (i.e., one photon absorption from a 193-nm laser beam) [35]. It has been noted that the basic assumption of statistical theory may not hold for large molecules [35,36]. In this work, as proposed below, the complexes of long chain alkanes and metal ions may have much smaller degrees of freedom. Thus the internal energy required to fragment the complex could be much less than that predicted by statistical theory. It is noted that, unlike small alkane systems where theoretical calculations such as those based on density functional theory have been successfully carried out [31], quantitative description of reaction energetics and dynamics of large systems remains formidably challenging at present.

The types of reaction products from Fe^+, Co^+, or Ni^+ interaction with long-chain alkanes are similar in conventional spectra and PSD spectra. It has been shown that exothermic reactions of Fe^+, Co^+ and Ni^+ with linear alkanes up to heptane produce ions with the molecular formula $M(C_nH_{2n})^+$ [37]. The same types of ionic products are obtained in this work, as illustrated in an expanded, representative PSD spectrum shown in Figure 2.6 obtained from Ni(alkane)$^+$. However, the loss of CH_4 from M(alkane)$^+$, observed in some small alkane systems (usually weak signals), is not found for the long-chain alkanes. The first dealkylation product in the series is the loss of C_2H_6. This is consistent with the notion that metal insertion into the terminal C-CH_3 bond is the least preferred reaction [37]. Unlike Co^+ and Ni^+ where a very small percentage of dehydrogenation products are observed, Fe(alkadiene)$^+$ is a dominant peak in the Fe^+ mass spectrum (see Figure 2.3C). This might be attributed to the larger excess energy retained on the Fe(alkene)$^+$ product after the initial metal insertion reaction. It has been noted that the insertion process is most exothermic for Fe^+, compared to Co^+ and Ni^+ [37].

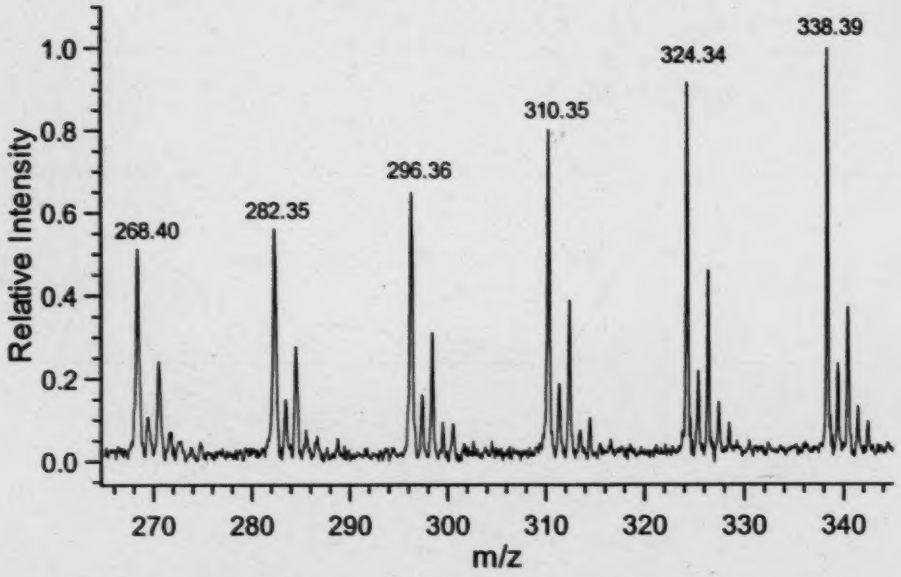

Figure 2.6. Expanded PSD spectrum of $Ni(C_{28}H_{58})^+$ showing the dealkylation fragment ions.

It is worth commenting on the ratios of the products from alkane elimination and H_2 elimination. Table 2.1 lists the branching fractions of $Ni(C_{28}H_{58})^+$ calculated from the source fragmentation spectrum (i.e., Figure 2.1E up to m/z ~200) along with those reported in the literature for short chain alkanes. Table 2.1 shows that alkane elimination is strongly favored for the long chain alkane over H_2 elimination. In addition, among the alkane elimination products, there is a strong propensity for the loss of larger alkanes. This is the case for all three metal ions, as shown in Figure 2.1C-E. Studies of small alkane metal ion reactions suggest that alkane elimination occurs via CC insertion, whereas H_2 elimination occurs via CH insertion. If this holds for the larger alkanes, then the results here show that attacking CC bonds is strongly favored over CH bonds for

larger alkane systems. However, whether the CC bond insertion is equally probable or more selective across the long chain cannot be readily inferred from the results shown here. The product distribution that favors the low mass fragment ions does not necessarily result from the selective CC insertion. The larger fragment ions initially produced by equally likely insertion into any CC bond may possess sufficient internal energy to further dissociate, resulting in a mass spectrum mainly composed of low mass fragment ions. The PSD spectra do show a product distribution containing many higher mass fragment ions. They are from the alkane-metal complex with lower energy than those undergoing fragmentation in the source region.

Unlike Fe^+, Co^+, and Ni^+, Cr^+, Mn^+ and Cu^+ are known to be unreactive toward linear alkanes (e.g., n-butane) or they do not exothermically react to form any other products besides adduct complexes [1]. Non-reactivity is attributed to the stability associated with ground states in half-filled or filled shells of these metal ions [1]. It is noted that direct metal-ion insertion into a C-H or C-C bond has a relatively high energy-barrier. For example, insertion of Ag^+ into the C-C bond of C_2H_6 to form CH_3-Ag^+-CH_3 requires ~1.9 eV activation energy [25,38]. Insertion of Cu^+ into C-H and C-C bonds is endothermic by ~1.7 and 1.2 eV, respectively [23]. Thus the observation of fragment ions in the present work from these otherwise unreactive transition-metal ions indicates that a substantial amount of excess energy was present in the intermediate. When the excess energy exceeds the energy barrier required for dehydrogenation or dealkylation, fragment ions are produced.

Table 2.1. Product distributions of the reactions of Ni^+ with small alkanes[a] and $C_{28}H_{58}$.

Alkane	C_3H_8	C_4H_{10}	C_5H_{12}	C_6H_{14}	C_7H_{16}	$C_{28}H_{58}$
$-H_2$	0.20	0.24	0.29	0.48	0.33	
$-CH_4$	0.80	0.17	0.04			
$-C_2H_6$		0.59	0.49	0.27	0.14	
$-C_3H_8$			0.16	0.17	0.22	
$-C_4H_{10}$				0.05	0.21	0.020
$-C_5H_{12}$					0.09	0.032
$-C_6H_{14}$						0.026
$-C_7H_{16}$						0.043
$-C_8H_{18}$						0.047
$-C_9H_{20}$						0.049
$-C_{10}H_{22}$						0.064
$-C_{11}H_{24}$						0.061
$-C_{12}H_{26}$						0.083
$-C_{13}H_{28}$						0.087
$-C_{14}H_{30}$						0.10
$-C_{15}H_{32}$						0.11
$-C_{16}H_{34}$						0.14
$-C_{17}H_{36}$						0.14

[a]From [37].

There are two possible sources of this excess energy. One is from excited metal ions that react with the alkane. However, the excitation or promotion energy of these

metal ions is quite high: 1.53 eV for Cr^+ from a 3d to 4s orbital, 6.83 eV for Mn^+, and 2.72 eV for Cu^+ [39,40]. Under the conditions used for the production of metals ions by desorption of metal powders with a 337-nm laser beam, significant numbers of excited metal ions are unlikely. This notion is consistent with those noted in ICR experiments where LDI has been commonly used for metal ion production [41].

A likely source of excess energy is from the initial thermal energy of the neutral alkane. For short-chain alkanes the average rotational and vibrational energies are very small and have no significant effect on thermodynamics of the metal-alkane interaction. For example, Chen and Armentrout calculated that, at 305 K, the average internal energy of CH_4 is 0.039 eV from the rotational energy contribution plus 0.0005 eV from the vibrational energy contribution [42]. However, for long-chain alkanes having high number of oscillators, the average thermal energy can be quite high, particularly in cases where heating (as in LD) is involved to vaporize the samples. According to the calculation schemes presented by Drahos and Vekey [43], the average thermal energy of octacosane ($C_{28}H_{58}$, bp 278°C/15 mm) is estimated to be 1.02 eV at 300 K, 2.74 eV at 500 K and 9.52 eV at 1000 K. For hexatriacontane ($C_{36}H_{74}$, bp 265°C/1 mm), the thermal energy is calculated to be 1.31 eV at 300 K, 3.53 eV at 500 K and 12.24 eV at 1000 K. The temperatures of the gas phase molecules generated by LD are unknown, but are expected to be well above room temperature [44]. Thus, the gas-phase long chain alkane can have a substantial amount of thermal energy as the neutral reactant.

The following scenario is proposed for the reaction of an otherwise unreactive metal ion with a long chain alkane. The long chain alkane initially interacts with the metal ion via long-range electrostatic interactions. For a large, polarizable alkane, both long-range electrostatic and short-range non-covalent interactions with the metal ion are

expected to occur [45]. The metal ion bound to a C-C or C-H bond can still interact with the remaining part of the alkane molecule via long-range interactions to form a more compact complex. The short- and long-range interactions in the complex will restrict the motions of many oscillators in the molecule, which reduces the number of rotational and vibrational energy relaxation channels. As a result, a significant portion of the original thermal energy from the alkane can convert into the excess energy required for metal ion insertion to a C-C or C-H bond. Subsequent fragmentation can occur if the metal ion inserted complex still possesses a sufficient amount of internal energy.

The reactivity differences observed among Cr^+, Mn^+, Cu^+ as well as Ag^+ could be attributed to the different amount of excess energy generated in forming the complex. In the case of Ag^+, the interaction between this metal ion and alkane is weak. Most of the species are in the form of van der Waals adduct ions that readily dissociate during the ion extraction and in the field free flight region, as evidenced by strong Ag^+ signals observed in the PSD spectrum. Only a small amount of dehydrogenation product is generated, likely from metal insertion into the C-H bond. It is noted that in the studies of small, branched alkanes with Ag^+, dehydrogenation product was not observed, although a number of other products were detected via the heterolytic cleavage mechanism [25]. Ionic products of alkane, alkene or alkadiene without metal ion attached are not observed in the long-chain alkane reactions. In studying small alkanes, the excess energy is usually from a collision-induced process, not the thermal energy of the reactant as in the case of the present study. Thus a greater amount of internal energy may be placed in the long chain alkane-metal ion complex. The chain length difference may also influence the reaction mechanism(s) and energy exit channels.

By examining the product distributions of the Cr^+, Mn^+ and Cu^+ interactions with the long-chain alkanes (see Figures 2.4 and 2.5), it is clear that dehydrogenation product signals are much more intense than those of dealkylation products. Thus the observation of dehydrogenation products in the case of Ag^+ is not surprising. If more energy could be placed to the Ag^+-alkane complex, dealkylation products are expected.

Among the four otherwise inactive transition-metal ions, Cu^+ displays the highest reactivity. The PSD spectrum of Cu^+-alkane shows the most intense dealkylation products and the least amount of bare metal ion, compared to Cr^+, Mn^+ and Ag^+. This is likely due to greater binding ability of Cu^+ to the alkane [41] to form a relatively more compact complex, resulting in a larger excess energy. This larger excess energy, in combination with a smaller energy barrier for Cu^+ insertion into the C-H or C-C bond (1.2 eV for Cu^+ insertion into C-C vs., for example, 1.9 eV for Ag^+ insertion into C-C), yields the dominant metal insertion complex. Subsequent dealkylation results in more stable $Cu(alkene)^+$, compared to $Ag(alkene)^+$ [46-48].

The reactivity of Cr^+ and Mn^+ appears to lie in-between Ag^+ and Cu^+. Dealkylation becomes noticeable in the PSD spectrum only at higher laser power. In addition, a very intense Cr^+ or Mn^+ signal is observed, suggesting that most of the Cr^+-alkane or Mn^+-alkane complex are in the form of van der Waals adduct ions. At lower laser power, the intensity of fragment ions is reduced. This is likely due to the reduction of the temperature or the initial thermal energy of the alkane vaporized by LD, hence the reduction of the excess energy placed on the intermediate.

It is worth noting that under similar conditions $C_{36}H_{74}$ appears to fragment more readily than $C_{28}H_{58}$. Figure 2.7 shows the PSD spectra of the two alkanes reacting with Fe^+. These two spectra are normalized to the precursor ions. It is clear from Figure 2.7

that more intense dealkylation products with $C_{36}H_{74}$ are observed. This result may be explained by considering the higher initial thermal energy of $C_{36}H_{74}$ than that of $C_{28}H_{58}$.

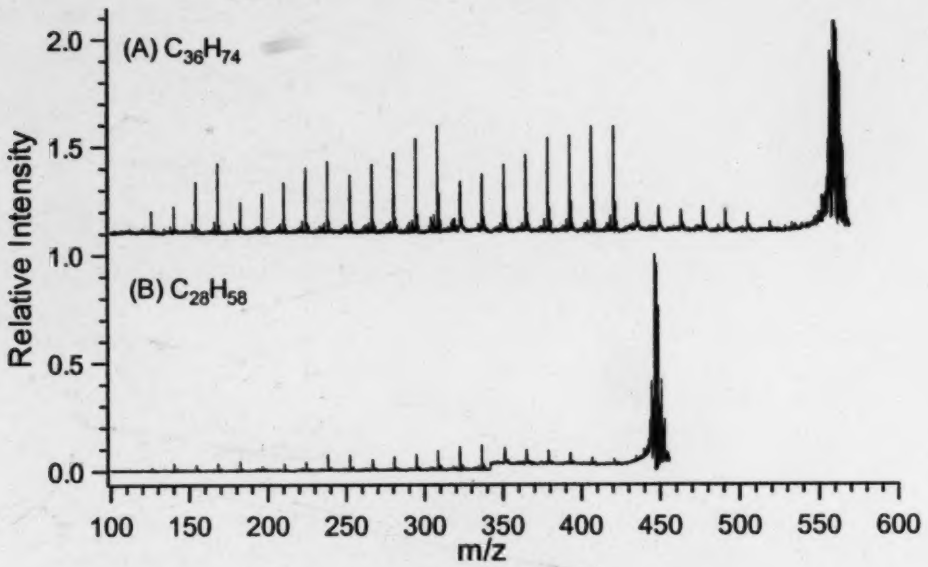

Figure 2.7. Normalized PSD spectra of $Fe(C_{28}H_{58})^+$ and $Fe(C_{36}H_{74})^+$.

Finally, it is interesting to note that the LDI technique reported here can produce metal ion clusters. In particular, very intense cluster ions are formed in the case of Ag (see Figures 2.1G and 2.2G). There are no metal cluster-alkane adduct ions detected. This type of adduct ions was observed when fast atom bombardment was used as the ionization source for studying metal ion interactions with isobutane [18]. However, it has been noted that the high reactivity of Cu^+ and its clusters was likely due to the excited metal ions formed in FAB [41].

2.4 Summary

In summary, it is demonstrated that laser desorption ionization time-of-flight mass spectrometry can be used to study transition-metal ion interactions with relatively long-chain alkanes. The observed product distribution as well as the reactivity of Cr^+, Mn^+, Cu^+ and Ag^+ is different from those with small alkane systems. The difference is attributed to the large initial thermal energy of a more polarizable long-chain alkane that can be converted into excess energy when a more rigid metal-ion alkane complex is formed. The results shown here suggest that all transition-metal ions studied in this work can potentially be useful as the cationization reagent for polyethylene analysis. The LDI spectra of long chain alkanes obtained by using silver ion display the least amount of fragmentation and thus the silver ion is perhaps the most suitable transition-metal ion for molecular mass analysis of polyethylene. Finally, the fragmentation patterns of long chain alkanes studied in this work should be very useful in interpreting LDI spectra of polyethylene. Some preliminary work from this laboratory on LDI and matrix-assisted laser desorption/ionization of low molecular mass polyethylenes (up to MW 4000) by using silver ion as cationization reagent and dithanol or *all-trans* retinoic acid as matrix has been presented at conferences [49]. A detailed description of the method along with the interpretation of the obtained mass spectra under different experimental conditions will be described in the next chapter.

2.5 Literatures Cited

1. Armentrout, P. B.; Beauchamp, J.L. *Acc. Chem. Res.* **1989**, 22, 315.
2. Russell, D. H. Ed. *Gas Phase Inorganic Chemistry,* Plenum: New York, **1989**.
3. Marks, T. J., Ed. *Bonding Energetics in Organometallic Compounds, ACS Symposium Series 428*, American Chemical Society: Washington, DC, **1990**.
4. Eller, K.; Schwarz, H. *Chem. Rev.* **1991**, 91, 1121.
5. Foster, M. S.; Beauchamp, J. L. *J. Am. Chem. Soc.* **1971**, 93, 4924.
6. Allison, J.; Freas, R. B.; Ridge, D. P. *J. Am. Chem. Soc.* **1979**, 101, 1332.
7. Freas, R. B.; Ridge, D. P. *J. Am. Chem. Soc.* **1980**, 102, 7129-7131.
8. Marshall, A. G. *Acc. Chem. Res.* **1985**, 18, 316.
9. Laude, D. A., Jr.; Johlman, C. L.; Brown, R. S.; Weil, D. A.; Wilkins, C. L. *Mass Spectrom. Rev.* **1986**, 5, 107.
10. Freiser, B. S. *Techniques for the Study of Ion-Molecule Reactions*; Farrar, J.M., Saunders, W.H., Jr., Eds. Wiley-Interscience: New York, **1988**; p.61.
11. Hodges, R. V.; Armentrout, P. B.; Beauchamp, J. L. *Int. J. Mass Spectrom. Ion Phys.* **1979**, 29, 375.
12. Ervin, K. M.; Armentrout, P. B. *J. Chem. Phys.* **1985**, 83, 166.
13. McLafferty, F. W. Ed. *Tandem Mass Spectrometry,* Wiley: New York, **1983**.
14. Hanratty, M. A.; Beauchamp, J. L.; Illies, A. J.; Bowers, M. T. *J. Am. Chem. Soc.* **1985**, 107, 1788.
15. Schulze, C.; Schwarz, H.; Peake, D. A.; Gross, M. L. *J. Am. Chem. Soc.* **1987**, 109, 2368.
16. Mestdagh, H.; Morin, N.; Rolando, C. *Tetrahedron Lett.* **1986**, 27, 33.

17. Cody, R. B.; Burnier, R. C.; Reents, W. D., Jr.; Carlin, T. J.; McCrery, D. A.; Lengel, R. K.; Freiser, B. S. *Int. J. Mass Spectrom. Ion Phys.* **1980**, 33, 37.

18. Freas, R. B.; Campana, J. E. *J. Am. Chem. Soc.* **1985**, 107, 6202.

19. Kahr, M. S.; Wilkins, C. L. *J. Am. Soc. Mass Spectrom.* **1993**, 4, 453.

20. Schriemer, D. C.; Li, L. *Anal. Chem.* **1996**, 68, 2721.

21. Yalcin, T.; Schriemer, D. C.; Li, L. *J. Am. Soc. Mass Spectrom.* **1997**, 8, 1220.

22. Spengler, B. *J. Mass Spectrom.* **1997**, 32, 1019.

23. Georgiadis, R.; Fisher, E. R.; Armentrout, P. B. *J. Am. Chem. Soc.* **1989**, 111, 4251.

24. Fisher, E. R.; Armentrout, P. B. *J. Phys. Chem.* **1990**, 94, 1674.

25. Chen, Y. M.; Armentrout, P. B. *J. Phys. Chem.* **1995**, 99, 11424.

26. Holthausen, M. C.; Fiedler, A.; Schwarz, H.; Koch, W. *J. Phys. Chem.* **1996**, 100, 6236.

27. Holthausen, M. C.; Koch, W. *J. Am. Chem. Soc.* **1996**, 118, 9932.

28. Holthausen, M. C.; Koch, W. *Helv. Chim. Acta* **1996**, 79, 1939.

29. Noll, R. J.; Weisshaar, J. C. *J. Am. Chem. Soc.* **1994**, 116, 10288.

30. Noll, R. J.; Yi, S. S.; Weissharr, J. C. *J. Phys. Chem. A* **1998**, 102, 386.

31. Yi, S. S.; Bloomberg, M. R. A.; Siegbahn, P. E. M.; Weissharr, J. C. *J. Phys. Chem. A* **1998**, 102, 395.

32. Bloomberg, M.; Yi, S. S.; Noll, R. J.; Weisshaar, J. C. *J. Phys. Chem. A* **1999**, 103, 7254.

33. Rockwood, A. L; Busman, M.; Udseth, H. R.; Smith, R. D. *Rapid Commum. Mass Spectrom.* **1991**, 5, 582.

34. Busman, M.; Rockwood, A. L.; Smith, R. D. *J. Phys. Chem.* **1992**, 96, 2397.

35. Gimon-Kinsel, M. E.; Kinsel, G. R.; Edmondson, R. D.; Russell, D. H. *J. Am. Soc. Mass Spectrom.* **1995**, 6, 578.

36. Schlag, E. W.; Levine, R. D. *Chem. Phys. Lett.* **1989**, 163, 523.

37. Halle, L. F.; Armentrout, P. B.; Beauchamp, J. L. *Organometallics* **1982**, 1, 963.

38. Rosi, M.; Bauschlicher, C. W., Jr.; Langhoff, S. R.; Partridge, H. *J. Phys. Chem.* **1990**, 94, 8656.

39. Armentrout, P. B.; Halle, L. F.; Beauchamp, J. L. *J. Am. Chem. Soc.* **1981**, 103, 6501.

40. Levin R. D.; Lias, S. G. *Ionization Potential and Appearance Potential Measurements, 1971-1981*; National Bureau of Standards: Washington, DC, **1982**.

41. Peake, D. A.; Gross, M. L. *J. Am. Chem. Soc.* **1987**, 109, 600.

42. Chen, Y. M.; Armentrout, P. B. *J. Phys. Chem.* **1995**, 99, 10775.

43. Drahos, L.; Vekey, K. *J. Am. Soc. Mass Spectrom.* **1999**, 10, 323.

44. Zenobi, R.; Hahn, J. H.; Zare, R. N. *Chem. Phys. Lett.* **1988**, 150, 361.

45. Hankinson, D. J.; Allison, J. *J. Phys. Chem.* **1987**, 91, 5307.

46. Jones, R. W.; Staley, R. H. *J. Am. Chem. Soc.* **1982**, 104, 2296.

47. Deng, H. T.; Kebarle, P. *J. Am. Chem. Soc.* **1998**, 120, 2925.

48. Deng, H. T.; Kebarle, P. *J. Phys. Chem. A* **1998**, 102, 571.

49. (a) Li, L. *Proceedings of the 46th ASMS Conference on Mass Spectrometry;* Orlando, FL, May 31-June 4, **1998**; paper 1184. (b) Li, L. presented at the European Polymer Federation Workshop on Mass Spectrometry of Polymers; Catania, Italy, December 1-3, **1999**; paper 3.

Chapter 3. Laser Desorption Ionization and MALDI Time-of-Flight Mass Spectrometry for Low Molecular Mass Polyethylene Analysis

Polyethylene (PE)'s inert nature and difficulty to dissolve in conventional solvents at room temperature present special problems for sample preparation and ionization in mass spectrometric analysis. A study of the ionization behavior of several polyethylene samples with molecular masses up to 4000 Da in laser desorption/ionization (LDI) time-of-flight mass spectrometers equipped with a 337-nm laser beam is presented in this chapter. It is demonstrated unequivocally that silver or copper ion attachment to saturated polyethylene can occur in the gas phase during the UV LDI process. In LDI spectra of polyethylene with molecular masses above ~1000 Da, low mass ions corresponding to metal-alkene structures are observed in addition to the principal distribution. By interrogating a well-characterized polyethylene sample and a long chain alkane, $C_{94}H_{190}$, these low mass ions are determined to be the fragmentation products of the intact metal-polyethylene adduct ions. It is further illustrated that fragmentation can be reduced by adding matrix molecules to the sample preparation.

A form of this chapter is published as:
R. Chen, T. Yalcin, W. Wallace, C. Guttman and L. Li, "Laser desorption ionization and MALDI time-of-flight mass spectrometry for low molecular mass polyethylene analysis", *J. Am. Soc. Mass Spectrom.* **2001**, 12, 1186-1192.

3.1 Introduction

With the advances in ionization techniques such as matrix-assisted laser desorption/ionization (MALDI) and electrospray ionization (ESI), mass spectrometry (MS) has become a very important tool for polymer characterization [1,2]. In particular, MALDI can be used to analyze many different types of polymers including relatively non-polar polymers such as polybutadienes and polyisoprenes [3]. At present, the most challenging task in polymer MS is perhaps the analysis of polyethylene (PE). Polyethylene is inert and contains no heteroatom or double bond for possible proton or metal ion attachment, presenting a special problem for ionization. However, PE is one of the most important commodity polymers and a detailed PE characterization is of significance for the optimization of polymerization chemistry, for new catalyst development, in polymer processing, as well as for quality control in manufacturing [4]. Since PE characterization by traditional polymer characterization methods such as gel permeation chromatography (GPC) and nuclear magnetic resonance (NMR) can be quite involved, there is a strong interest in using alternative methods that can provide rapid and accurate information on polymer structure, average molecular mass and molecular mass distributions.

There are only a few reports on the mass spectrometric analysis of PE. Field desorption ionization MS has been used for generating intact molecular ions from paraffin wax and low molecular mass PE samples such as PE700 and PE1000 [4-8]. PE spectra from secondary ion mass spectrometry mainly consist of fragment ions [9]. Cody and co-workers have reported that direct laser desorption ionization (LDI) of hard wax (unsaturated long-chain hydrocarbons) generated weak signals; but electron impact ionization of the desorbed neutrals produced good results [10]. Weidner and co-workers

have reported the analysis of waxes by IR and UV laser desorption [11]. Kahr and Wilkins presented the first report on detection of PE with M_n and M_w up to 2300 Da by laser desorption ionization in Fourier Transform (FT) MS [12]. In their work, silver salts were mixed with PE and the sample was desorbed and ionized with a 10.6 μm laser beam from a CO_2 laser. In the past few years, data on PE analysis using conventional MALDI time-of-flight (TOF) mass spectrometers equipped with a 337-nm laser beam carried out in this lab have been presented at several conferences [13]. Recently, a study of metal ion interaction with long chain alkanes – oligomers of PE, is also presented, and it is illustrated that a number of transition metal ions can form adduct ions with alkanes using LDI with a 337-nm laser beam [14].

In this chapter, a study of the ionization behavior of several PE samples is reported, with the objective that these results will stimulate further research activities in both method development and fundamental study of the LDI process related to PE analysis. This work is focused on using conventional MALDI-TOF-MS for PE analysis, since such instruments are widely available and being used for polymer characterization. Low molecular mass PE samples from several sources are examined and their spectra are presented as raw data (i.e., no baseline correction and smoothing) to serve as reference spectra for future spectral comparison.

3.2 Experimental

3.2.1 Chemicals and Reagents. Pyrene, perlene, anthracene, 9-nitroanthracene, *all-trans* retinoic acid (RA), dithranol (DH), 2,5-dihydroxybenzoic acid, and *trans, trans*-1,4-diphenyl-1,3-butadiene (DPBT) were purchased from Aldrich Chemical Co (Milwaukee, WI). Chlorobenzene, methanol, tetrahydrofuran (THF), silver nitrate, copper powder, and cobalt powder were from Fisher (Mississauga, Ontario). Polyethylenes with varying molecular masses were from American Polymer Standards Corp., Polymer Laboratories Inc., and Scientific Polymer Products. All chemicals were used without purification.

3.2.2 LDI and MALDI Sample Preparation. For PE500 and PE1000, samples were dissolved in chlorobenzene at 5 mg/ml at ambient temperature. For samples with molecular masses above 2000 Da, heating was required to achieve the desired concentration (5 mg/ml). Matrices were dissolved in THF to a concentration of 0.1 M. Silver nitrate was dissolved in methanol to make a saturated solution.

Sample deposition was done in the following manner. One microliter of matrix solution was first transferred onto the stainless steel sample target to form the first layer. About 0.2 μl of silver nitrate solution was then put onto the spot as the second layer. Finally, 1 μl of sample solution was deposited on top of the second layer. In the case of laser desorption experiment, the formation of the matrix layer was omitted. For the copper cationization experiment, the copper powder was first suspended in isopropyl alcohol and then transferred onto the sample target as the first layer. Sample solution was directly deposited onto the copper powder and air-dried.

3.2.3 Instrumentation. The LDI and MALDI experiments were done in two instruments. The linear time-lag focusing MALDI time-of-flight mass spectrometer was constructed at the University of Alberta and it has been described in detail elsewhere [15]. The Applied Biosystems Voyager laser desorption/ionization time-of-flight (TOF) mass spectrometer (Framingham, MA) equipped with a reflectron was also used. Both instruments employ a 337-nm photon beam from a pulsed nitrogen laser to generate ions. All spectra were the results of signal averaging of between 100 and 200 shots and calibrated using a peptide mixture. Data processing was done with the IGOR Pro software package (WaveMetrics Inc., Lake Oswego, OR). The spectra presented in this chapter were from raw data with no baseline correction and no signal smoothing.

3.3 Results and Discussion

3.3.1 LDI MS of PE in Linear and Reflectron TOF.

Figure 3.1 shows the LDI mass spectra of three PE samples from American Polymer Standards Corporation. These spectra were obtained in a linear TOF mass spectrometer. In all cases, the mass difference between two adjacent peaks from the main distribution is 28 Da, corresponding to the mass of the repeat unit of $-CH_2CH_2-$. From the masses and peak intensities of the main distribution after the removal of low mass ion contributions (see section 3.3.5), M_n and M_w are found to be 1010 Da and 1103 Da, respectively, for PE1100 (see Figure 3.1A) with a polydispersity (PD) of 1.095. The GPC molecular mass data provided by the supplier are M_n 1050 Da, M_w 1150 Da and PD 1.095. For this particular sample, the LDI molecular mass results match nicely with those of GPC.

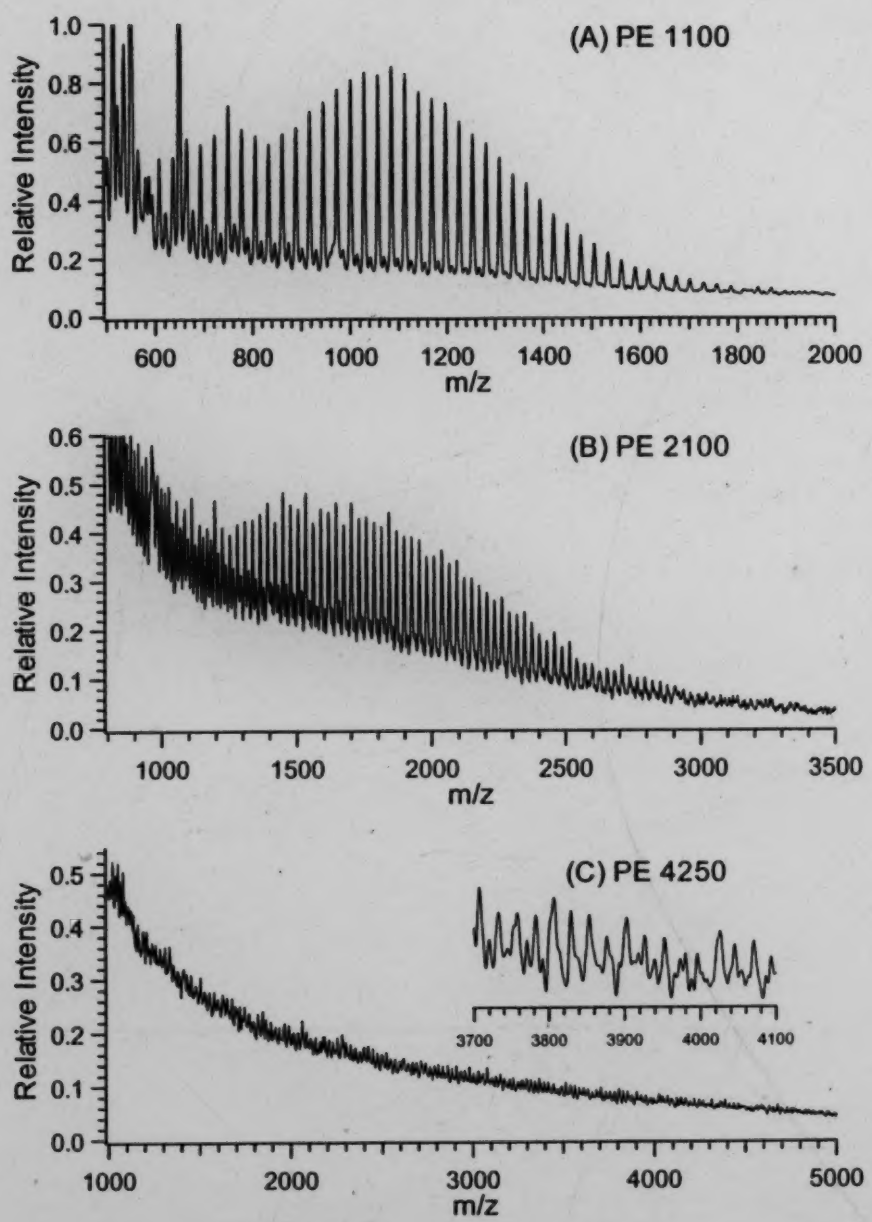

Figure 3.1. LDI mass spectra of (A) PE1100, (B) PE2100, and (C) PE4250. These samples were from American Polymer Standards Corporation.

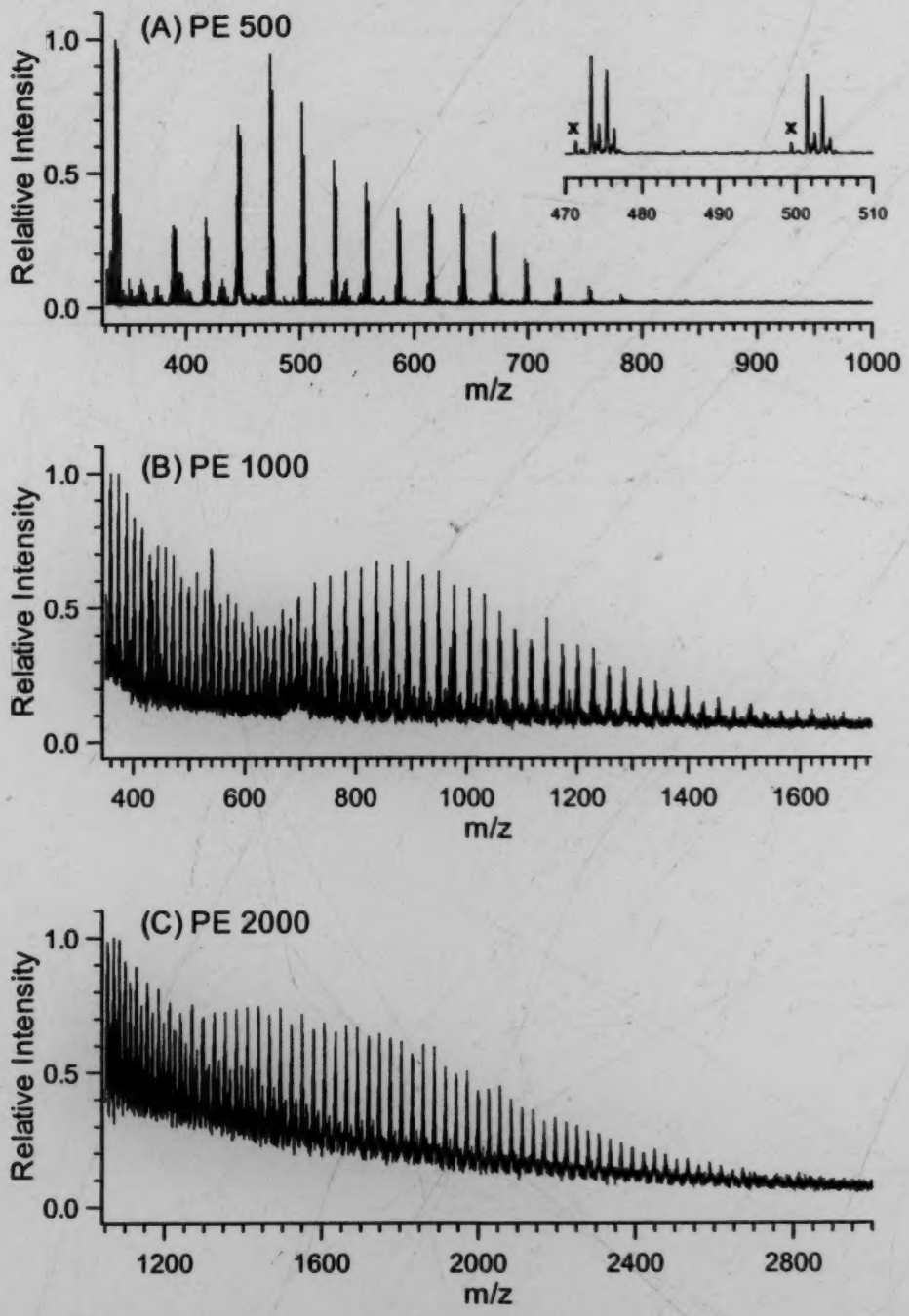

Figure 3.2. LDI mass spectra of (A) PE500, (B) PE1000, and (C) PE2000. These samples were from Polymer Laboratories Inc.

The main distribution of PE2100 (Figure 3.1B) spans from m/z ~1000 to ~3000. From this distribution, M_n and M_w are calculated to be 1815 Da and 2021 Da, respectively, with PD 1.113. The GPC data are M_n 1900 Da, M_w 2150 Da and PD 1.132. Again, in this case, the LDI results are consistent with those of GPC. However, in the LDI spectrum of PE2100, there are a considerable number of low mass peaks with mass difference of 14 Da between adjacent peaks. The origin of these peaks can be from the fragment ions of PE oligomers or from the impurities present in the sample.

The LDI spectrum shown in Figure 3.1C is particularly interesting. The GPC data supplied by the supplier indicate that this sample has a polydispersity of 1.435 with M_n 2300 Da and M_w 3300 Da. Weak signals from PE are observed and the spectrum shows a characteristic shape that resembles the MALDI mass spectra of many polydisperse polymers. The correct average molecular mass information cannot be obtained from the LDI spectrum for this PE sample. Note that the expanded spectrum shown in the inset of Figure 3.1C illustrates there are PE peaks at m/z above 4000.

The spectra shown in Figure 3.1 can be reproducibly obtained with relative standard deviations of less than 2% for the molecular mass data from replicate experiments. However, the spectral resolution is low, even with the time-lag focusing linear TOF instrument, which readily provides isotope resolution for MALDI of molecules with molecule masses below 2000 Da. The degradation of resolution is likely related to the energetics of the ions produced by LDI. These ions may not be spatially distributed in the ion extraction region with well-defined velocity profiles, as is the case for MALDI ions. Time-lag focusing for reducing the time spread of ions of identical masses is only effective if they are distributed in the flight axis in a coherent manner [15-

17]. It is envisioned that further investigation of ion energetics from LDI of PE should be able to provide useful information on the dynamics of ion formation and expansion, which has an implication in extending the technique to analyzing higher molecular mass PE samples.

Using the reflectron TOF combined with time-lag focusing, relatively high resolution mass spectra of PE can be obtained. Figure 3.2 shows the LDI mass spectra of three samples from Polymer Laboratories, Inc. Isotope resolution is obtained in all cases. The inset of Figure 3.2A shows the correct isotope distribution of a silver attached PE oligomer ion. The masses of the major peaks correspond to $[alkane+Ag]^+$. Minor peaks with masses matched with silver attached alkene are also observed (see peaks labeled as X). These ions with similar molecular mass distribution as that of $[alkane+Ag]^+$ may be from a trace amount of mono-alkene (i.e., one double bond) present in the sample. Radical polymerization of PE can produce a small amount of these by-products [18]. Instead of the more facile process of hydrogen extraction to terminate the chain reaction that will result in the main product of alkanes, loss of hydrogen in the radical chain can occur and will result in mono-alkenes and, to a much less extent, cyclic alkanes. It is noted that the relative intensity between the alkane and peak X in the LDI spectra does not reflect the relative amount of these two components in a PE sample. This is due to the likely difference in overall analytical efficiencies of the two components. In the case of silver-alkene adducts, alkene is more readily ionized by silver ion attachment via d-π interaction, while only weak static interaction is involved in the alkane and silver adduct ion formation. Another source for peak X is from the dehydrogenation of $[alkane+Ag]^+$

in LDI, which has been previously observed in LDI of long-chain alkanes with silver cationization [14, 19].

3.3.2 The Origin(s) of the Low Mass Peaks Present in LDI Spectra of PE.

As in the linear TOF LDI analysis of PE1100, PE2100 and PE4250 (Figure 3.1), the PE1000 and PE2000 spectra shown in Figure 3.2B and C display many low mass peaks in addition to the principal distribution. Figure 3.3 shows the expanded LDI spectra of PE1000. The peaks labeled as "P" are mainly from $[alkane+Ag]^+$. The peaks labeled as "S" have masses corresponding to $[mono\text{-}alkene+Ag]^+$. The silver isotope ($Ag^{109}$) peak of the mono-alkene silver adduct ion (i.e., $[mono\text{-}alkene+Ag^{109}]^+$) overlaps with that of $[alkane+Ag]^+$. Many other peaks from ions with masses 2 or 4 Da less than that of $[alkene+Ag]^+$ (i.e., di-alkene and tri-alkene) are also detected. In addition, the mass difference among the adjacent peaks from $[mono\text{-}alkene+Ag]^+$ is 14 Da. As Figure 3.3 shows, the intensity of peak P decreases at the lower mass tail of the principal distribution while peak S starts to become more dominant peak in the spectra. As the masses further decrease, peak P will be mainly from the silver isotope (Ag^{109}) peak of peak S (see, for example, the peak cluster in m/z 550-560). It is noted that the spectral patterns of the low mass ions are the same for PE1000 and PE2000.

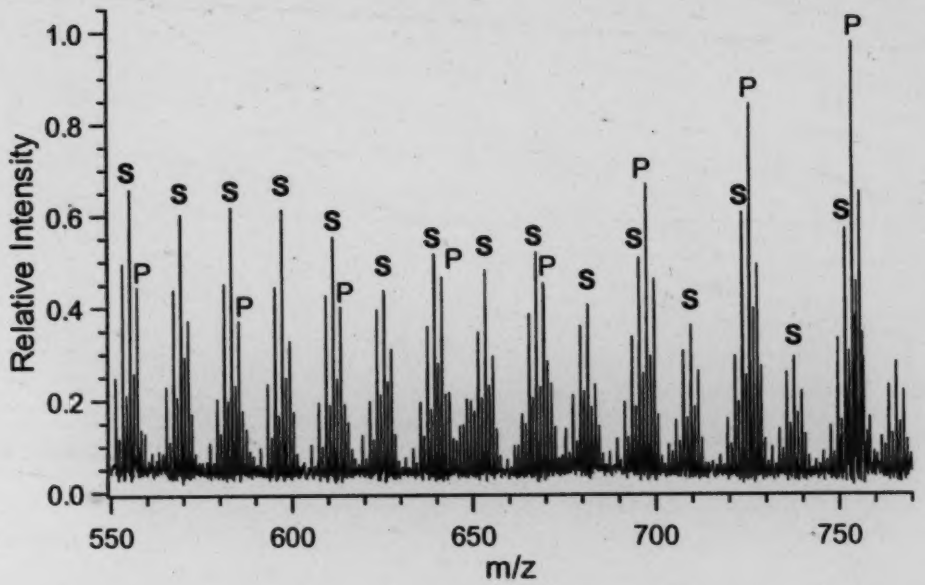

Figure 3.3. Expanded LDI spectrum of PE1000 from Figure 3.2 B. The peaks labeled as "P" are mainly from [alkane+Ag]$^+$. The peaks labeled as "S" have masses corresponding to [mono-alkene+Ag]$^+$.

To determine the origin(s) of these low mass peaks, a PE1150 sample was investigated in detail. The material from Scientific Polymer Products is an anionically polymerized polybutadiene of low polydispersity that has been saturated to form a polyethylene. Figure 3.4 shows the LDI spectra of this sample. The peaks labeled as C are from the silver cluster ions. The pattern of the low mass peaks from this sample matches with those in PE1000 and PE2000 (Figure 3.2). This sample was carefully examined by using FT-IR and GPC. IR data suggests that there are only 0.04 C=C bonds per 100 C-C bonds (i.e., 0.04% unsaturation). Thus the sample contains a very small amount of alkenes. The GPC chromatogram shows a very symmetric peak with no visible tailing at the low molecular mass region, which indicates that no appreciable amount of low molecule mass species are present in the sample. However, in the spectra

shown in Figure 3.4, high intensities of low mass ions are detected, which suggest these peaks are from the fragment ions. One may still argue that these are from the impurities that are present in trace amounts, but favorably ionized.

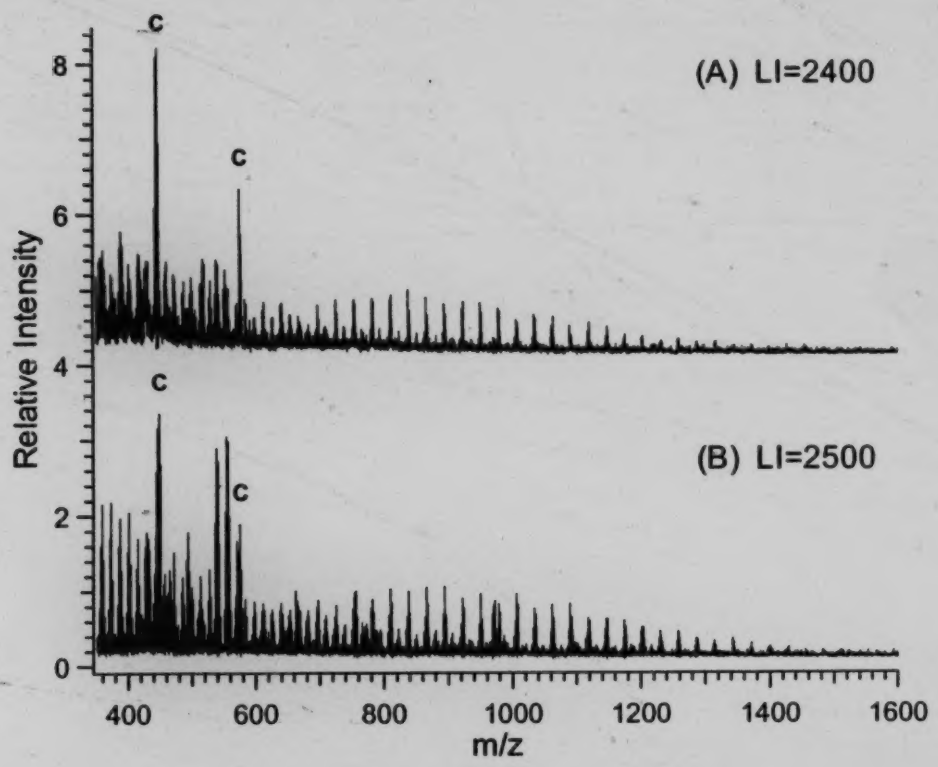

Figure 3.4. LDI mass spectra of PE1150 obtained at two different laser power settings in the Applied Biosystems LDI TOF mass spectrometer: (A) laser power index 2400 and (B) laser power index 2500. The peaks labeled as C are from the silver cluster ions.

Strong evidence to support the argument of these low mass ions being fragment ions is given by the analysis of a long-chain alkane, $C_{94}H_{190}$ [20]. The LDI spectra of this alkane using silver cationization are shown in Figure 3.5. At a lower laser power, fragment ions are still observed as shown in Figure 3.5A. With the increase of laser power, more intense and extensive fragment ions are observed (see Figure 3.5B). The

types of fragment ions match with those in PE samples. Moreover, for the PE samples, a similar trend of laser power dependence is observed. This is demonstrated in Figure 3.4 for the PE1150 sample. In PE samples, the intensities of the fragment ions should be from the sum of all fragment ions produced by individual oligomer ions.

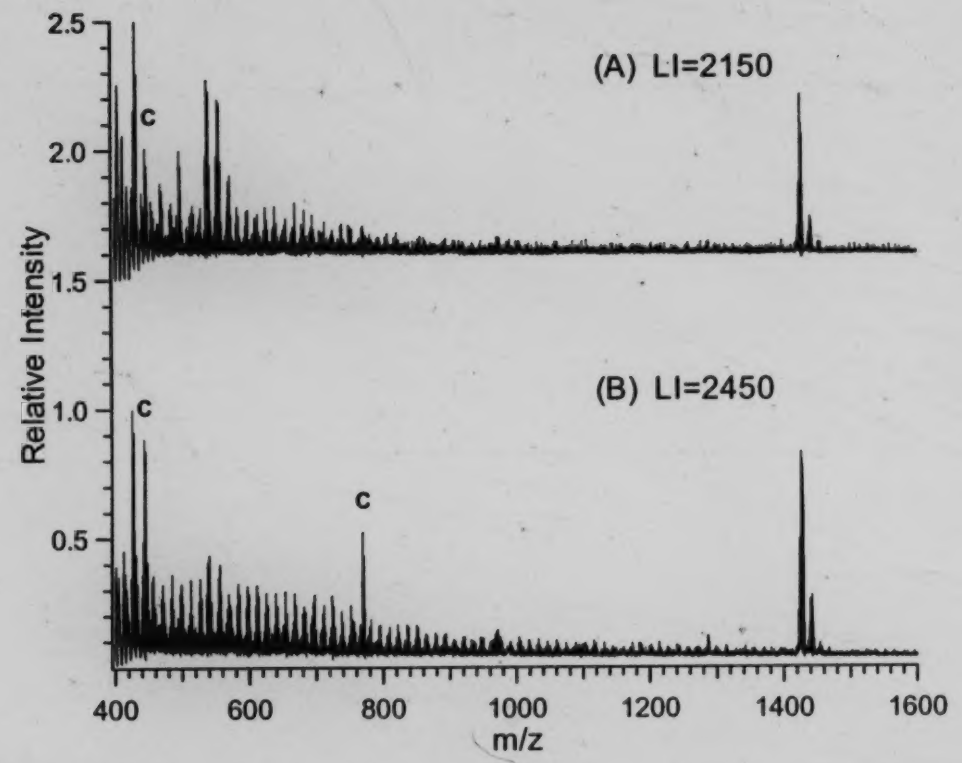

Figure 3.5. LDI mass spectra of a long chain alkane, $C_{94}H_{190}$, obtained at two different laser power settings in the Applied Biosystems LDI TOF mass spectrometer: (A) laser power index 2150 and (B) laser power index 2450. The peaks labeled as C are from the silver cluster ions.

In Chapter 2 it is shown that several transition metal ions can form adduct ions with long chain alkanes [13]. Silver adduct ions are most stable and no fragment ions

were detected from LDI of $C_{28}H_{58}$ and $C_{36}H_{74}$ with silver cationization. Other metal ions give different degrees of fragmentation with these two alkanes. Figure 3.5 shows that, for very long chain alkanes, fragmentation can occur even with silver cationization.

3.3.3 Copper Cationization.

It is not surprising that other transition metal ions can form adduct ions with polyethylene. Figure 3.6 shows the LDI mass spectra of PE500 and PE1000 obtained by using copper as the cationization reagent. The quality of the spectrum shown in Figure 3.6A for PE500 is comparable to that of Figure 3.1A obtained by silver cationization. Thus copper cationization appears to be also effective for this sample. However, when Figure 3.6B is compared to Figure 3.2B, it can be seen that copper cationization is not as effective as silver cationization for analyzing PE1000. With copper cationization, the signal to noise ratio for the principal distribution is not as high as in the case of silver cationization. This is true for other higher molecular mass PE samples being examined (data not shown). It can be concluded that, with the sample preparation protocol used in this work, silver cationization generally provides better results than copper cationization for PE analysis.

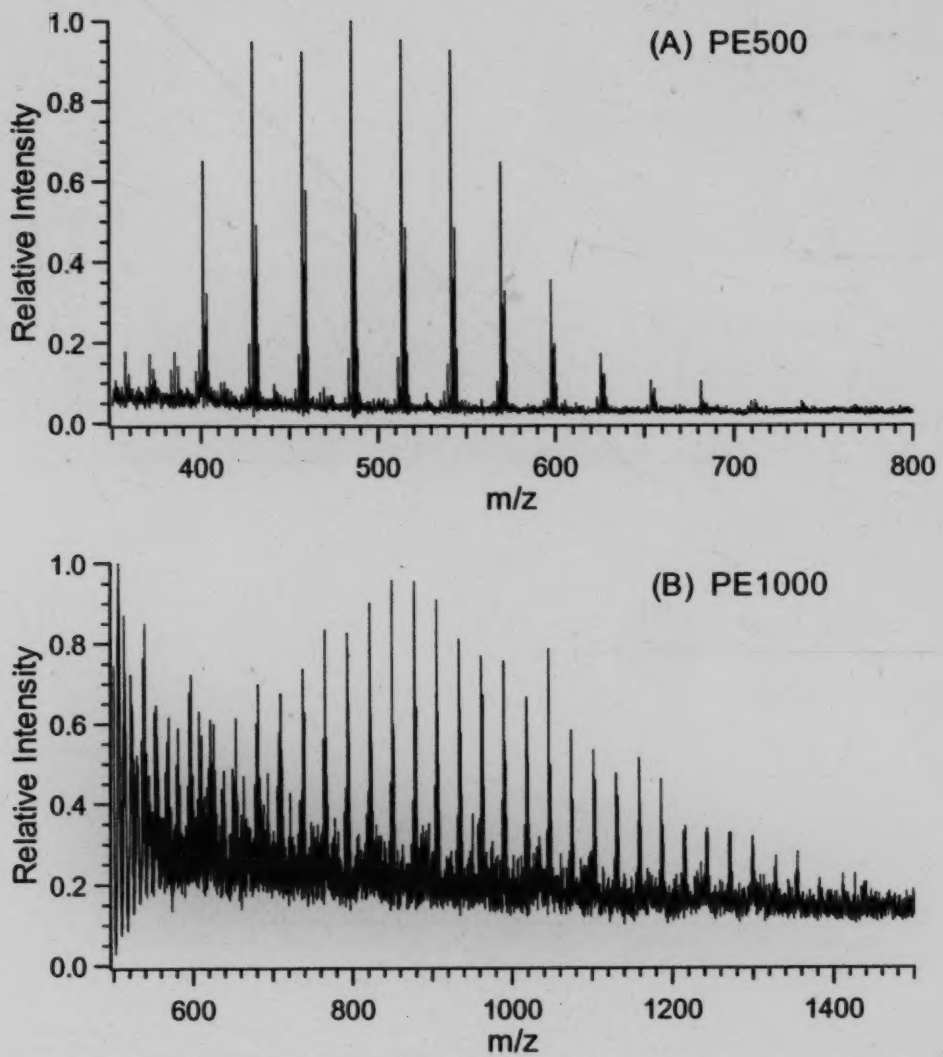

Figure 3.6. LDI spectra of PE500 and PE1000 obtained by using copper cationization.

3.3.4 MALDI MS of PE.

Now that the low mass ions in LDI spectra of PE have been identified as from the fragment ions, a series of experiments using matrices in the sample preparation were carried out to examine whether MALDI can reduce the fragmentation. Many known polymer MALDI matrices have been tested and these include pyrene, perlene, anthracene, 9-nitroanthracene, *all-trans* retinoic acid (RA), dithranol (DH), 2,5-dihydroxybenzoic acid, *trans,trans*-1,4-diphenyl-1,3-butadiene (DPBT), and cobalt powder. Among which, RA, DPBT and DH were found to be useful to enhance signal intensities and/or reduce fragmentation. This is demonstrated in Figure 3.7 for PE1100. For clarity, the LDI spectrum shown in Figure 3.2B is reproduced here as Figure 3.7D. The use of a matrix reduces the laser threshold required for LDI in all three cases. Comparison of Figure 3.7A with Figure 3.7D shows that the use of dithranol enhances the overall S/N ratios, but does not change the relative intensities between the principal distribution and the fragment ions. The use of DPBT decreases the intensities of the fragment ion peaks relative to the principal distribution (Figure 3.7B). However, the intensities of high mass oligomers in the principal distribution are also reduced. In the case of *all-trans* retinoic acid (Figure 3.7C), good signal to noise ratios are obtained and only small reduction in relative intensity between the fragment ions and the oligomer ions is noted.

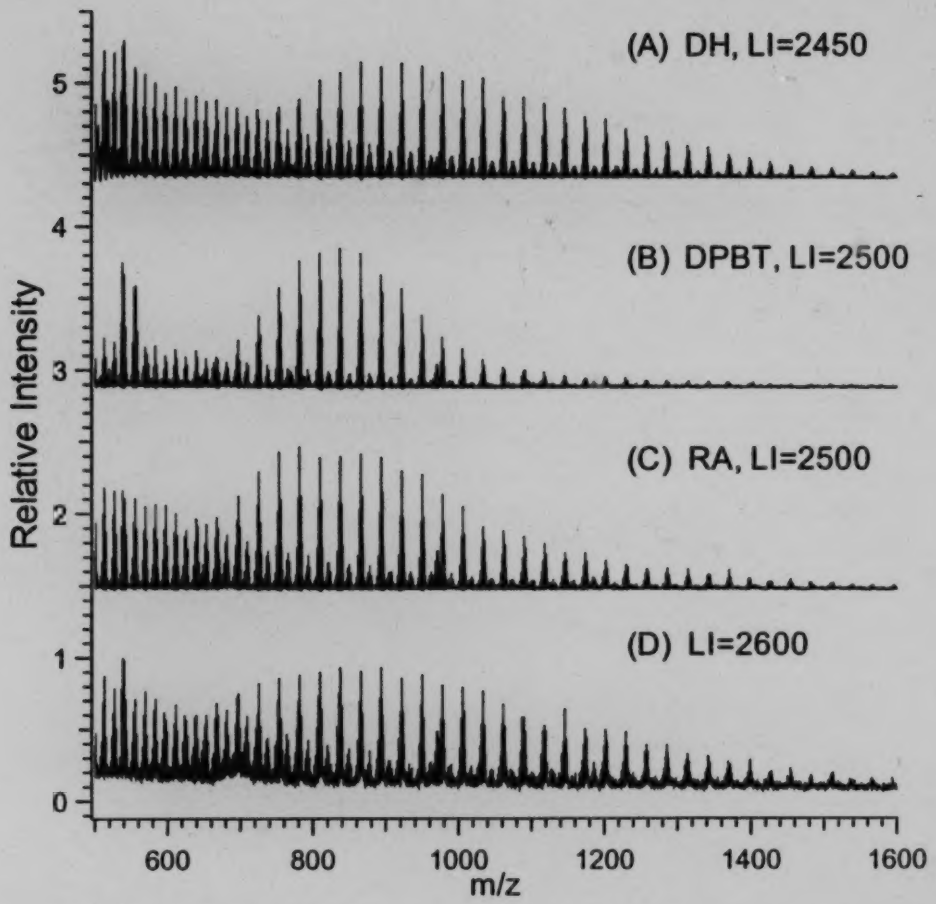

Figure 3.7. MALDI mass spectra of PE1000 obtained by using silver cationization with (A) dithranol, (B) *trans,trans*-1,4-diphenyl-1,3-butadiene, (C) *all-trans* retinoic acid, and (D) no matrix. LI is the laser power index.

3.3.5 Molecular Mass Calculation.

As shown in Figure 3.7, the type of matrix can affect the shape of the principal distribution. The reason for this variation is unknown. It is likely that matrix molecules play a role in both sample preparation and ionization. For average molecular mass determination, changes in oligomer peak distribution should affect the M_n and M_w data.

However, the presence of fragment ion peaks at the low mass region that overlap with the low mass tail of the principal distribution complicates the M_n and M_w calculation. Fortunately, with the exception of the high polydispersity sample (Figure 3.1C), all other samples give Gaussian-like principal distributions. In addition, as Figure 3.3 shows, the PE oligomer peaks can be readily distinguished from the fragment ions or mono-alkene/silver ions. At the high mass tail of the principal distribution, peak P is from [alkane+Ag^{107}]$^+$. The heights of these peaks can be used for average mass calculation. At the low mass tail, peak P is no longer just from [alkane+Ag^{107}]$^+$. The fragment ion, [mono-alkene+Ag^{109}]$^+$, contributes to the intensity of this peak. This fragment ion contribution to the total ion intensity of peak P can be calculated from a curve fitted to the intensities of peaks arising from the alkenes only. In Figure 3.3, the peak S cluster ions between two adjacent P peaks are from the alkene ions only. It is found that the intensities of these S peaks can fit an exponential function.

Figures 3.8 and 3.9 exemplify the described curve fitting, peak intensity correction, and subsequent molecular mass calculation, using the data from Figure 3.7C. The data points in Figure 3.8 (labeled as ♦) are exclusively from [mono-alkene+Ag^{109}]$^+$ (i.e. peak S cluster ions between two adjacent P peaks), and fit with an exponential equation with a correlation coefficient R^2=0.9845. The equation provided therein is then used to calculate the [mono-alkene+Ag^{109}]$^+$ contribution to the P series in the low mass tail. Figure 3.9 is a column-chart representation of the original data and the corrected data after the subtraction of [mono-alkene+Ag^{109}]$^+$ contribution. As can be seen, the low mass region peak intensities are substantially lowered, and a Gaussian-like distribution is restored after the correction (Figure 3.9B). The data obtained in Figure 3.9B is

considered to be the true representation of PE-Ag^+ ion intensity, and therefore used for the molecular mass calculation using Equations 3.1-3.3. All these can be readily accomplished using a Microsoft Excel program, and the results are listed in Table 3.1.

$$M_n = \frac{\sum n_i M_i}{\sum n_i} \qquad \textbf{Equation 3.1}$$

$$M_w = \frac{\sum n_i M_i^2}{\sum n_i M_i} \qquad \textbf{Equation 3.2}$$

$$PD = \frac{M_w}{M_n} \qquad \textbf{Equation 3.3}$$

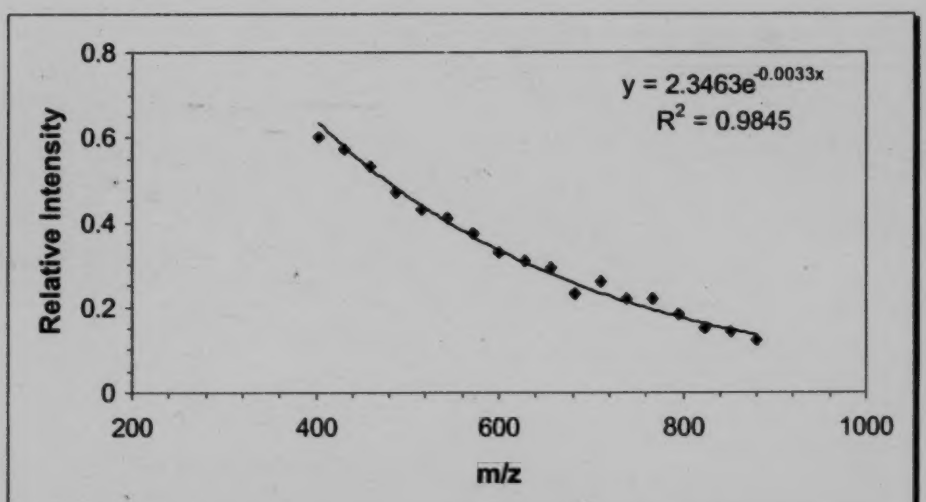

Figure 3.8. An exponential curve fitting of the data obtained using RA as the matrix of sample PE1100. The label ♦ represents the original data points and the solid line is the calculated curve.

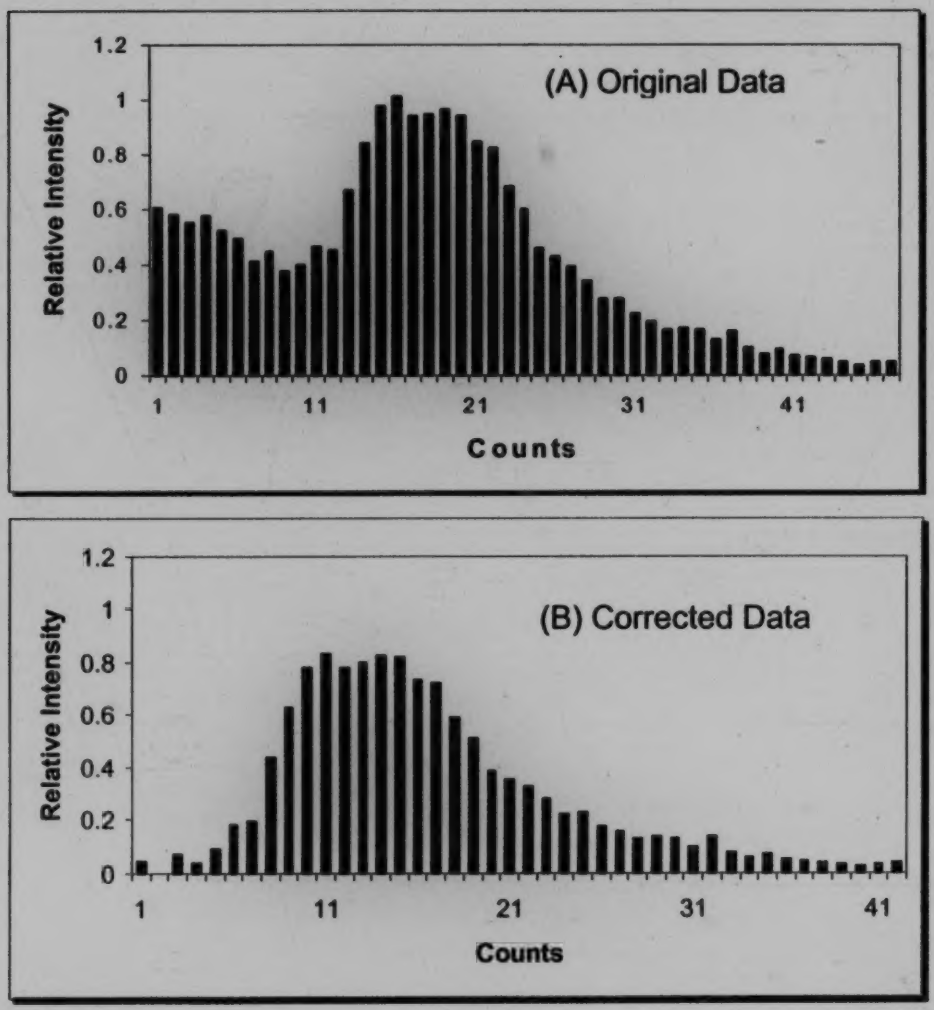

Figure 3.9. A column-chart representation of the data from Figure 3.7C: (A) before and (B) after correction.

The results listed in Table 3.1 clearly indicate that matrix can influence the outcome of the LDI experiment. The relative standard deviation among the average masses obtained using different matrices is about 8%, well exceeding the generally acceptable criterion (5%) for molecular mass determination by MALDI. More work is

needed to find an optimal matrix and sample preparation method for MALDI analysis of PE.

Table 3.1. Molecular mass calculation from MALDI MS for PE 1000.

Matrix	Mn (Da)	Mw (Da)	PD	Ref.
Dithranol	1031	1064	1.031	Fig. 3.7A
DPBT	876	894	1.021	Fig. 3.7B
RA	934	979	1.048	Fig. 3.7C
None	1016	1066	1.049	Fig. 3.7D
RSD%	7.5	8.2		

Finally, it is worth commenting on the difference observed in the data presented here and that reported by Kahr and Wilkins [12]. Specifically, in their work, a CO_2 laser beam was used for desorption/ionization in FTMS. In their spectra, very few fragment ions were observed. The data presented herein clearly demonstrate that LDI of low molecular mass PE can also be done in a TOF mass spectrometer using a 337 nm laser for desorption/ionization. However, fragment ions are observed even with the use of matrices that are shown to be very effective for other types of polymers. Whether the mass analyzer (FTMS vs. TOF) plays any role in determining the outcome of a LDI spectrum of PE is unknown. Nor is it clear about the effects of laser wavelengths on the extent of fragmentation in LDI of polyethylene, since a direct comparison using the same experimental conditions has not been made. Based on the current knowledge of the mechanisms of LDI and MALDI using UV and IR laser [21-25], it is difficult to predict whether IR irradiation is better than UV for desorption ionization of PE or *vice versa*. In

LDI and MALDI of many other molecules, similar results can be obtained from UV and IR laser desorption [24,25].

3.4 Summary

In summary, it is shown that LDI mass spectra of low molecular mass polyethylene with narrow polydispersity can be obtained in conventional time-of-flight mass spectrometers equipped with a nitrogen laser. The method is not suitable for molecular mass analysis of polyethylene with broad polydispersity. Low mass ions detected in LDI of polyethylene with molecular masses above ~1000 Da are unequivocally shown to be mainly from the fragment ions of the PE-metal adduct ions. While addition of commonly used polymer matrices such as RA and dithranol to the sample preparation assists in enhancing signal intensity and/or reducing the extent of fragmentation, fragmentation cannot be totally eliminated with the current sample preparation method in a conventional MALDI-TOF mass spectrometer equipped with a nitrogen laser. Fragmentation is likely a major obstacle that needs to be overcome in order to extend the LDI or MALDI method to analyzing higher molecular mass polyethylene. A rational design of improved sample preparation conditions that would significantly reduce or eliminate fragmentation requires a better understanding of the LDI process related to polyethylene analysis.

3.5 Literatures Cited

1. Hanton, S. D. *Chem. Rev.* **2001**, 101, 527.
2. Nielen, M. W. F. *Mass Spectrom. Rev.* **1999**, 18, 309.
3. Yalcin, T.; Schriemer, D. C.; Li, L. *J. Am. Soc. Mass Spectrom.* **1997**, 8, 1220.
4. Evans, W. J.; DeCoster D. M.; Greaves, J. *Macromolecules,* **1995**, 28, 7929.
5. Beckey, H. D. *Principles of Field Ionization and Field Desorption Mass Spectrometry*, Pergamon Press: New York, **1977**.
6. Lattimer, R. P.; Schulten, H. -R. *Int. J. Mass Spectrom. Ion Phys.* **1983**, 52, 105.
7. Lattimer, R. P.; Harris, R. E.; Ross, D. B.; Diem, H. E. *Rubber Chem. Technol.* **1984**, 57, 1013.
8. Lattimer, R. P.; Harris, R. E.; Rhee, C.K.; Schulten, H. -R. *Anal. Chem.* **1986**, 58, 3188.
9. Walzak, M. J.; McIntyre, N. S.; Prater, T.; Kaberline, S.; Graham, B.A. *Anal. Chem.* **1999**, 71, 1428.
10. Cody, R. B.; Bjarnason, A.; Weil, D. A. *Lasers and Mass Spectrometry*, Lubman, D. M. Ed. Oxford University Press: New York, **1990**; p316.
11. Weidner, S.; Kuhn, G.; Friedrich, J. *Rapid Commun. Mass Spectrom.* **1998**, 12, 1373.
12. Kahr, M. S.; Wilkins, C. L. *J. Am. Soc. Mass Spectrom.* **1993**, 4, 452.
13. (a) Li, L. "*Instrumental and Analytical Method Development of MALDI MS for Polymer Analysis*", presented at the 46th ASMS Conference on Mass Spectrometry, May 31-June 4, **1998**, Orlando, FL.; paper 1184. (b) Li, L. "*Investigation of Analytical Capabilities and Limitations of MALDI-TOF Mass*

Spectrometry for Polymer Analysis", presented at the European Polymer Federation Workshop on Mass Spectrometry of Polymers, December 1-3, **1999**, Catania, Italy; paper 3. (c) Li, L. "*Mass Spectrometry for Polymer Characterization*", presented at the 219th ACS National Meeting in San Francisco, March 26-30, **2000**, paper 17.

14. Chen, R.; Li, L. *J. Am. Soc. Mass Spectrom.* **2001**, 12, 367.
15. Whittal, R. M.; Li, L. *Anal. Chem.* **1995**, 67, 1950.
16. Whittal, R. M.; Russon, L. M.; Weinberger, S. R.; Li, L. *Anal. Chem.* **1997**, 69, 2147.
17. Whittal, R. M.; Li, L. *American Laboratory*, **1997**, 28, 30.
18. Brown, W. H.; Foote, C. S. *Organic Chemistry*, 3rd ed.; Harcourt: Orlando, **2001**; Chap XIV, p965.
19. Evans, W.; DeCoster, D. M.; Greaves, J. J. *J. Am. Soc. Mass Spectrom.* **1996**, 7, 1070.
20. Khoury, F.; Fanconi, B.; Barnes, J. D.; Bolz, L. H. *J. Chem. Phys.* **1973**, 59, 5849.
21. Cotter, R.J.; Tabel, J. -C. *Anal. Chem.* **1984**, 56, 1662.
22. Linder, B.; Seydel, V. *Anal. Chem.* **1985**, 57, 895.
23. Karas, M.; Bachman, D.; Hillenkamp, F. *Anal. Chem.* **1985**, 57, 2935.
24. Zenobi, R.; Knochenmuss, R. *Mass Spectrom. Rev.* **1998**, 17, 337.
25. Cotter, R. J. *Time-of-Flight Mass Spectrometry*, American Chemical Society: Washington DC, **1997**; Chapter 6, p113.

Chapter 4. Application of an Integrated MALDI-TOF, ESI MS and MS/MS Approach to Characterizing Complex Polyols

Polyols are used in a wide range of industrial applications including surfactants and precursors for grafted polymers. Characterization of polyols is of significance in correlating compositions and structures with their properties. In this chapter, it is illustrated by two real world examples where traditional analytical methods including GPC and NMR failed to reveal compositional differences, but the combination of MALDI-TOF, ESI MS and MS/MS can produce compositional information required for problem solving. The first example involves failure analysis of four ethylene oxide and propylene oxide (EO/PO) copolymer products. The results from the MS analysis unequivocally demonstrate that one of the samples has a small variation in copolymer composition, leading to its abnormal activity. The second example is in the area of deformulation of complex polyol mixtures. Two samples displaying similar properties and activities are found to be two different polyol blends. One of the samples is a more cost-effective product. These examples demonstrate that MALDI, ESI MS and MS/MS should be seriously considered as an integrated component of an overall polyol characterization program in product failure analysis and de-formulation.

A form of this chapter is published as:
R. Chen, A. M. Tseng, M. Uhing, and L. Li, "Application of an integrated matrix-assisted laser desorption/ionization time-of-flight, electrospray ionization mass spectrometry and tandem mass spectrometry approach to characterizing complex polyol mixtures" *J. Am. Soc. Mass Spectrom.* **2001**, 12, 55-60.

4.1 Introduction

Surfactants such as alkyl polyethers, polyethylene glycol (PEG)-esters and ethylene oxide (EO)/propylene oxide (PO) copolymers are commonly used in industrial defoaming and antifoaming applications. These defoamers and antifoam products are often chemically very complex, with effectiveness and activity depending on their water dispersibility, hydrophilic lipophilic balance (HLB), microstructure, and overall polymer composition. Complete characterization of these materials can be very challenging. Traditional analytical techniques, such as IR, NMR, gel permeation chromatography (GPC) and GC/MS, can provide some structural and compositional information including the determination of functional groups, average number of moles of ethoxylation and average molecular weights of the polymeric materials. However, analytical data obtained from these methods may not be sufficient for problem solving or deformulation for complex polyol samples.

Mass spectrometry, particularly matrix-assisted laser desorption/ionization (MALDI) and electrospray ionization (ESI) MS, can be used to analyze polyol samples with relative ease. Polyols are widely used as a model system for MALDI and ESI mass spectrometric method development [1-24].

MALDI or ESI MS has been demonstrated to be useful in analyzing targeted polyol products [25,26], monitoring polymer synthesis [27-32], characterizing thermal degradation behaviors [33,34], qualitative and quantitative analysis of polyol surfactants in environmental samples or consumer products [35-42]. In the polymer industry, product failure analysis and deformulation of complex polymer mixtures represent two of the major analytical challenges. The failure of a batch of product from a product line may be caused by a number of variables including contamination or deviation from proper

processing during manufacturing. In many cases, fast turnaround time for analyses can make the difference between shipping the product or shutting down the manufacturing lines. Product deformulation consists of separating an unknown product into its constituent components and then identifying each of these components. Direct laser desorption ionization Fourier Transform MS has been used to analyze different known formulations of polyols [43]. To date, there is no literature report of ESI or MALDI applications in the areas of product failure analysis and deformulation.

The objective of the work presented in this chapter is to illustrate two real world examples that have greatly benefited from the utility of mass spectrometric methods based on MALDI, ESI and MS/MS. It is demonstrated that MALDI and ESI MS are complementary to each other in analyzing complex polyol samples, and both techniques should be considered in a polyol analysis program. In conjunction with traditional analytical methods, they can accomplish a more thorough characterization of low molecular weight polyols and their mixtures. Since characterization of functional polyols is such an important activity in industry, the considerations on several technical and data interpretation issues brought about by this work should be useful for others tackling similar real world samples.

4.2 Experimental

4.2.1 Materials and Reagents. *All*-trans-retinoic acid and dithranol were purchased from Aldrich Chemical Co. (Milwaukee, WI). Tetrahydrofuran (THF) and acetonitrile (glass distilled HPLC grade) were purchased from EM Science (Gibbstown, NJ). HPLC grade methanol and ethanol were obtained from Sigma (Milwaukee, WI). Sodium

chloride and silver nitrate were from Fisher (Mississauga, Ontario). Distilled water was from a Milli-Q UV plus ultra-pure system (Millipore, Mississauga, ON). Polyols and polyol mixtures were from Nalco Chemical (Naperville, Illinois). All reagents and samples were used without further purification.

4.2.2 Instrumentation. Gel permeation chromatography (GPC) analysis was performed with μStyragel columns with THF mobile phase. Weight average molecular weight (Mw) and polydispersity of the polymers were determined using polystyrene standards (Polysciences, Warrington, PA). ^{13}C NMR spectra of the polymers were obtained with a Varian Unitylnova 300 spectrometer. Weight percentages of EO and hydroxyl equivalents were determined from the NMR data. IR spectra were obtained using a Nicolet 710 FTIR Spectrometer. GC-MS analysis was performed on a HP 5973 MSD System or on an Extrel 400 GC/LC/MS system. Sample inorganic contents were determined by ICP analysis using a Thermo Jarrell Ash ICP 9000 system. All these were conducted at the Nalco Chemical Company, Naperville, IL.

MALDI-TOFMS spectra were obtained using a home-built time-lag focusing linear TOF mass spectrometer at the University of Alberta [44]. Two matrices were used, 0.1 M dithranol and 0.15 M *trans,trans*-1,4-retinoic acid in THF. All spectra were the results of signal averaging from 100 to 200 laser shots. The instrument was calibrated externally using a peptide mixture containing bradykinin and insulin chain B.

ESI MS^n experiments were carried out on an Agilent/Bruker Esquire-LC Ion Trap LC/MS^n system. Samples were diluted by methanol/water mixture (volume ratio 1:1) with addition of salt solutions to appropriate concentrations, and infused into the

electrospray interface by a syringe pump (Cole-Parmer Instrument Co., IL) at a flow rate of 10 μl/min.

All data were reprocessed using the Igor Pro Software package (WaveMetrics, Lake Oswego, OR) and no background subtraction was performed.

4.3 Results and Discussion

4.3.1 Characterization of EO/PO Copolymers.

Table 4.1. Traditional Analytical Testing Results of the EO/PO Copolymers

Test method	Sample A	Sample B	Sample C	Sample D
Water Dispersibility	Settles out	Settles out	Stable dispersion	Settles out
ID by NMR, IR	EO/PO	EO/PO	EO/PO	EO/PO
wt.% EO	9.2	9.0	9.5	8.9
Hydroxyl Equivalent	990	990	1060	1050
Mw (Da) from GPC	2200	2200	2400	2400
Polydispersity	1.1	1.1	1.1	1.1
ICP Analysis	39 ppm Ca^{2+}	37 ppm Ca^{2+}	860 ppm K^{+}	44 ppm Ca^{2+}
Sp. Gravity @15.6 °C	1.013	1.013	1.012	1.014

EO/PO copolymers are used as surfactants in various products. Four copolymer samples with similar bulk properties in this study were obtained from various suppliers. The results obtained from traditional analysis, including IR, NMR, GPC, and ICP, are summarized in Table 4.1. Molecular masses of all four samples range between 2200-2400 with narrow polydispersity (Mw/Mn = 1.1) from GPC. NMR also shows similar EO/PO ratios for all samples. Despite the similarity in properties measured by the traditional methods, Sample C shows different activity, water dispersibility and stability. This indicates that there are possible structural or compositional differences among these samples. The high K^+ content in Sample C detected by ICP is not the cause of the activity differences, since the presence or absence of K^+ does not affect the polyol activity.

Figure 4.1 shows the MALDI-TOF MS spectra of the four polyols. There are four main distributions in each spectrum, representing different PO and EO compositions. All peaks are from PO/EO copolymers initiated with the CH_2=CH-CH_2O- group. The general formula confirmed by NMR and IR (see Table 4.1) is as follows:

$$CH_2=CH\text{-}CH_2O\text{-}[CH_2\text{-}CH(CH_3)\text{-}O]_n\text{-}[CH_2\text{-}CH_2\text{-}O]_m\text{-}H$$

Noting that all peaks are Na^+ adduct peaks, copolymer masses can therefore be calculated using the equation:

$$M = 44.05m + 58.08(n+1) + 23.03 \text{ (average mass)} \qquad \textbf{Equation 4.1}$$

where n and m correspond to the PO and EO numbers in the structural formula, respectively. The calculation indicates that the major distributions (i.e., masses from ~1300 to 3000) of four copolymers are composed of 10 to 13 units of EO and 14 to 42 units of PO. From the analysis, it can be postulated that these EO/PO copolymers were

likely produced by first polymerizing EO to form predominately four EO homopolymers with the number of repeating units ranging from 10 to 13. These species were then copolymerized with PO to form the copolymers. Differences in the distribution of EO oligomers can lead to the differences in the relative amounts of the four distributions present in the final samples (see below).

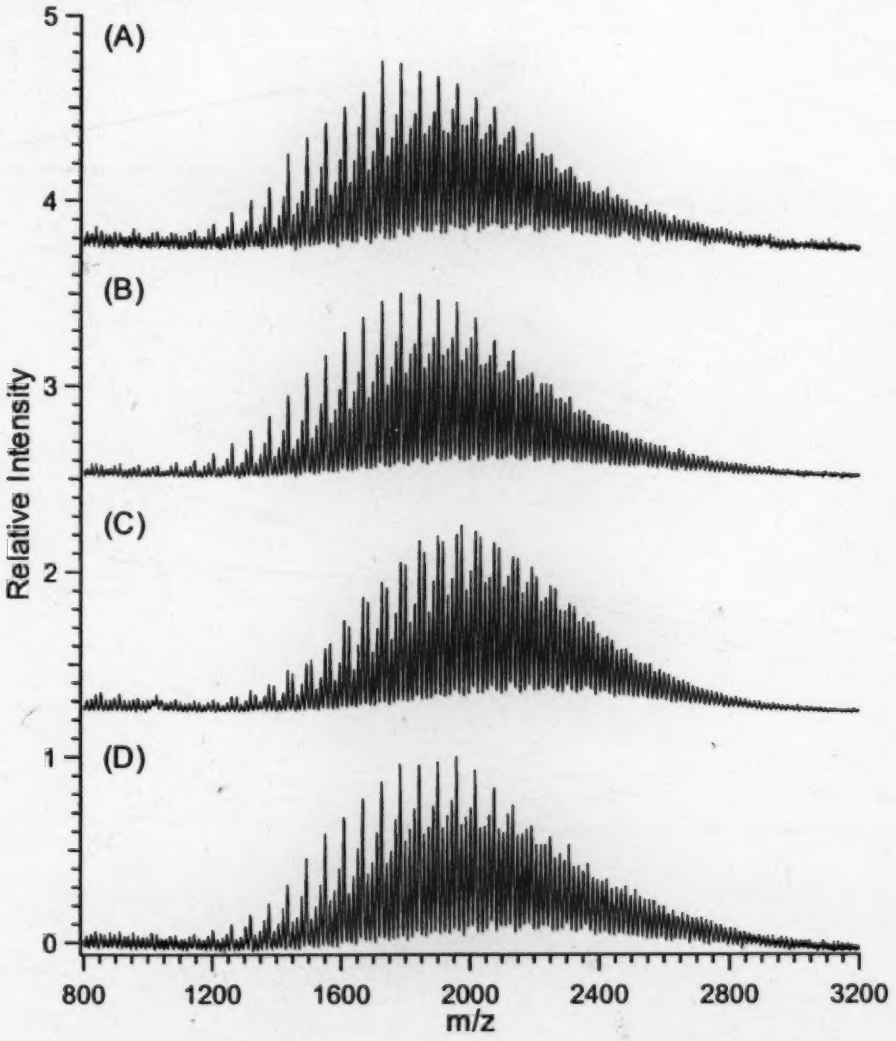

Figure 4.1. MALDI TOF mass spectra of four batches of EO/PO polymers.

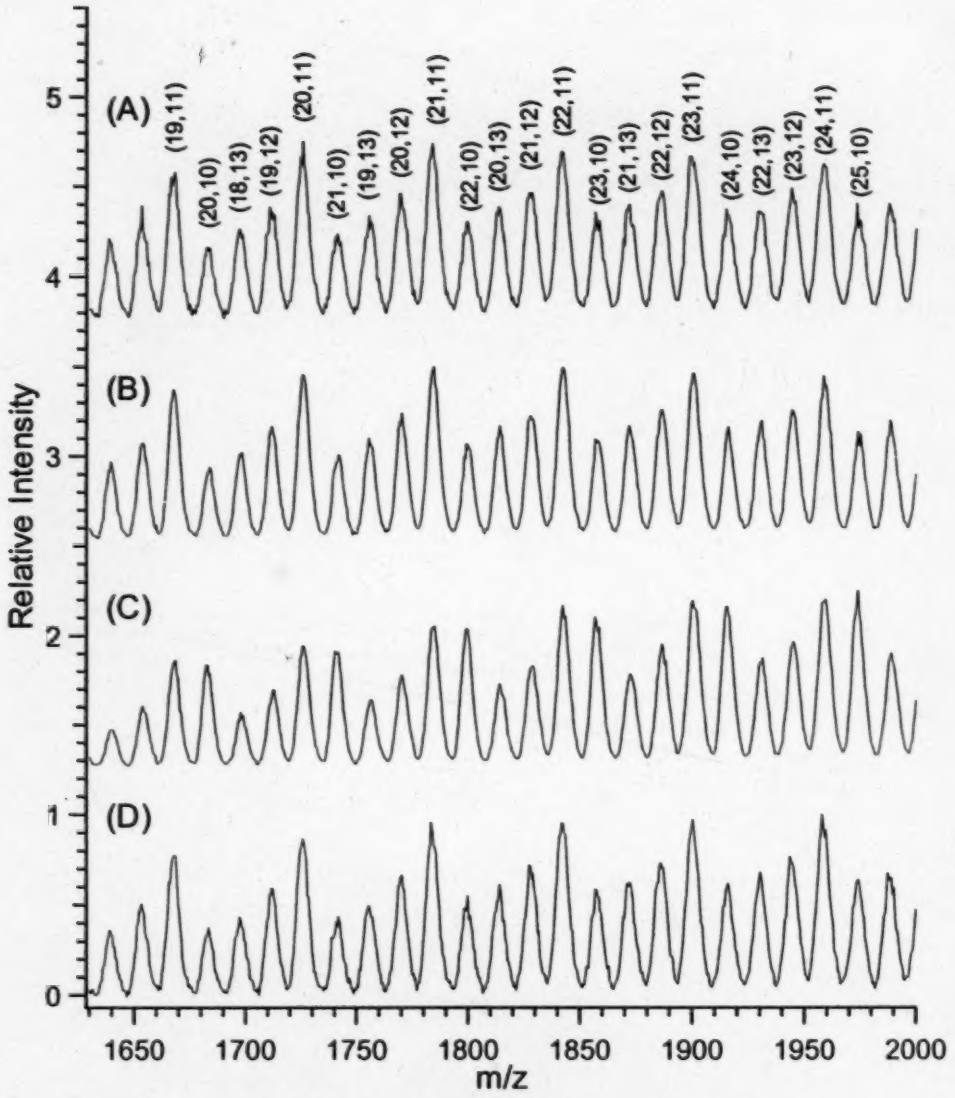

Figure 4.2. Expanded MALDI TOF mass spectra from Figure 4.1.

Figure 4.2 shows an expanded plot of the mass spectral region from m/z 1660 to 1980 for all four samples. The molar number of EO in the four distributions in these four samples ranges from 10 to 13, with PO repeating units ranging from 19 to 25 (see m, n values corresponding to each peak shown in Figure 4.2). The relative amounts of the

four adjacent distributions (between every 58 mass units) are the same for Samples A, B and D, but clearly different for sample C. For example, the intensity of the mass peak labeled as (20 PO, 10 EO) in sample C is about twice as that of the other three samples. MALDI-TOF MS results reveal that the composition of sample C is slightly different from those of the others, suggesting key differences in copolymer production, perhaps, are due to process variations that result in a higher 10 EO content in sample C. This small compositional variation could not be detected by traditional analytical techniques, but causes significant differences in the polymer's water dispersibility and activity. While MALDI-TOF is not quantitative in compositional analysis, this example clearly demonstrates that it is a very useful technique to detect subtle variations among similar samples.

It should be noted that the spectra shown in Figure 4.2 were obtained with a linear time-of-flight mass spectrometer. With a reflectron time-of-flight instrument, isotopic resolution should be expected, which would provide more information on the copolymer composition.

4.3.2 Analysis of Polyol Mixture.

Surface-active agents such as alkoxylated materials are generally formulated as mixtures of low molecular weight components to obtain desired activity and effectiveness in certain applications. Positive identification/differentiation of these materials is of importance for batch-to-batch quality control, deformulation of unknown products, and optimizing cost/performance ratio.

Two defoamers used in this study, Samples E and F, are nominally the same product and display similar activity. However, the bulk appearance of these two

materials is quite different, brownish vs. reddish in color. Examination of these two samples using traditional analytical techniques found no differences. Both samples are suspected to be EO/PO block copolymers. NMR analysis indicates that both samples contain about 53 weight % EO and tall oil fatty acid (i.e., C-18 monounsaturated fatty acid). GPC determines that the average molecular mass of both samples is about 350. No useful MALDI results were obtained. Problems with MALDI analysis of low molecular mass polyols include the overlapping of the analyte and matrix peaks, severe signal suppression by abundant matrix and possible sample loss under high vacuum prior to desorption/ionization. For these two samples, MALDI spectra display only matrix background peaks. ESI MS is therefore applied for this application. With the use of solvents such as water and methanol, ESI should produce mass spectra free of matrix peaks commonly found in MALDI. In addition, unlike MALDI, solution phase separation techniques can be readily combined with ESI [5]. Compared to traditional MS methods such as chemical ionization (CI) MS, higher molecular mass polyols can be analyzed by ESI MS [20]. ESI MS and MS/MS can also provide an alternative means of analyzing low mass polyols, as shown below.

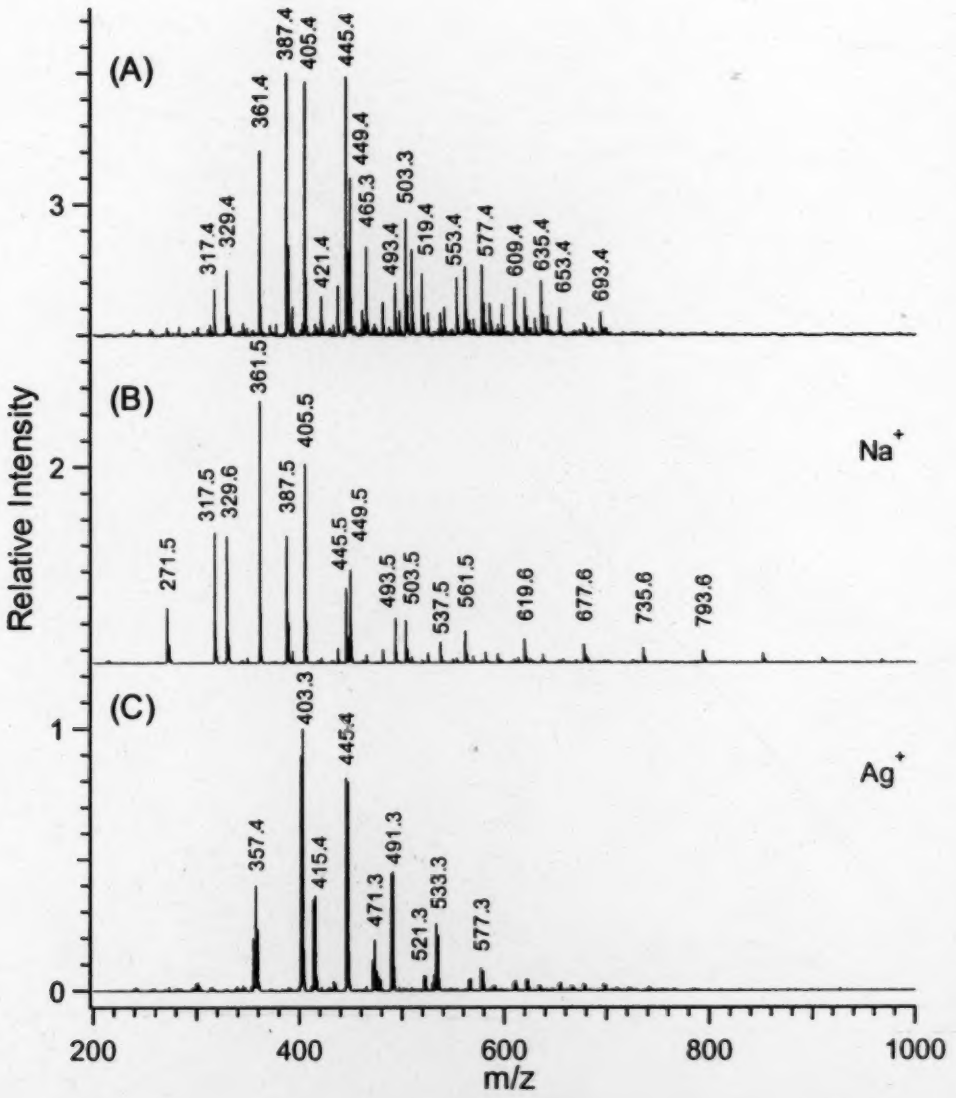

Figure 4.3. ESI mass spectra of Sample E obtained by (A) without the addition of NaCl, (B) with the addition of NaCl, and (C) with the addition of $AgNO_3$.

Figure 4.3 shows the ESI MS spectra of Sample E with different sample treatments. Figure 4.3A is the most complex spectrum among three and contains more peaks than the other two. Several series of EO and PO are shown. After the addition of NaCl, a much cleaner spectrum with higher S/N ratio is generated (see Figure 4.3B). Moreover, a PO oligomer distribution in the mass region of 600-1000 Da, which is not found in Figure 4.3A, can be seen. The presence of high salt contents in the original sample can account for the observation. Sodium and potassium salts are the most common contaminants. They possibly originate from the manufacture process or sample preparation process. A comparison between Figure 4.3A and Figure 4.3B reveals that several pairs of peaks 16 amu apart (i.e., m/z 405 and 421, 493 and 509, etc.) have the same chemical origins, but different metal ions, namely, Na^+ vs. K^+, attached. Failure to realize this will over-count the species present and lead to incorrect compositional information. The results from the addition of silver salt (Figure 4.3C) confirm the above interpretation. In order to comprehensively recognize all the species in an unknown industrial sample, it is our experience that addition of at least two types of cation is necessary. This practice has been commonly used in polymer mass spectrometry such as ESI analysis of other types of polymers [22,45].

Figure 4.4A shows the ESI MS spectra of Samples E and F obtained by adding the same amount of Na^+. Both samples are mainly composed of one PO (m/z=271.4, 329.4, 387.4 etc.) and one EO (m/z=317.5, 361.5, 405.5 etc.) in the mass region of 200-500 Da, but slightly differ in the relative abundance. The most probable peaks (M*p*) appear at m/z=361.5, which is in agreement with the GPC results. It also clearly shows that neither sample is EO/PO copolymer. An EO/PO copolymer should display a unique

distribution pattern derived from a combination of certain numbers of EO and PO. Both samples appear to be mixtures of EO and PO. On the other hand, the major disparity between the two samples lies in the mass region of 500-1000 Da (see Figure 4.4B). Sample E displays one PO distribution labeled as P in Figure 4B, while Sample F has three EO distributions with similar intensities labeled as E1, E2 and E3.

To positively identify the major components of both samples, MS/MS experiments were performed. Unfortunately, sodiated or potassiated polyols of these samples do not fragment under the low energy collision-induced dissociation (CID). This finding is consistent with those reported by others on different polyols and using ionization techniques other than ESI [46,47]. However, it was found that silver cationization in ESI can be used as a general method of producing high-quality low energy CID spectra for many different functional polyols. The signal-to-noise ratio and information content in the MS/MS spectra of polyol-silver adduct ions are often better than those of protonated species. This method was applied to these two samples. Figure 4.5 shows representative MS/MS spectra. Oligomer ions at m/z=445.2 (see Figure 4.3C) were selected from major EO distribution and oligomer ions at m/z=471.2 were from the major PO distribution. Consecutive losses of 44 u or 58 u are found in the MS/MS spectra. It is clear that two oligomer ions with the nominally same m/z's from Samples E and F display almost identical fragmentation patterns, indicating that they are from the same species. The observed fragmentation patterns also indicate that the end-groups are likely attached to the repeating units via ether or hydroxyl bonds, not ester bonds. More detailed research will be described in Chapters 5 and 6. While the MS/MS results suggest that these two samples contain common components, unambiguous structural

identification of these components is not possible. Nevertheless, for this particular application, the results from ESI MS and MS/MS are sufficient to conclude that Samples E and F have different formulations with the same major components. It turns out that sample F is much more cost effective than Sample E.

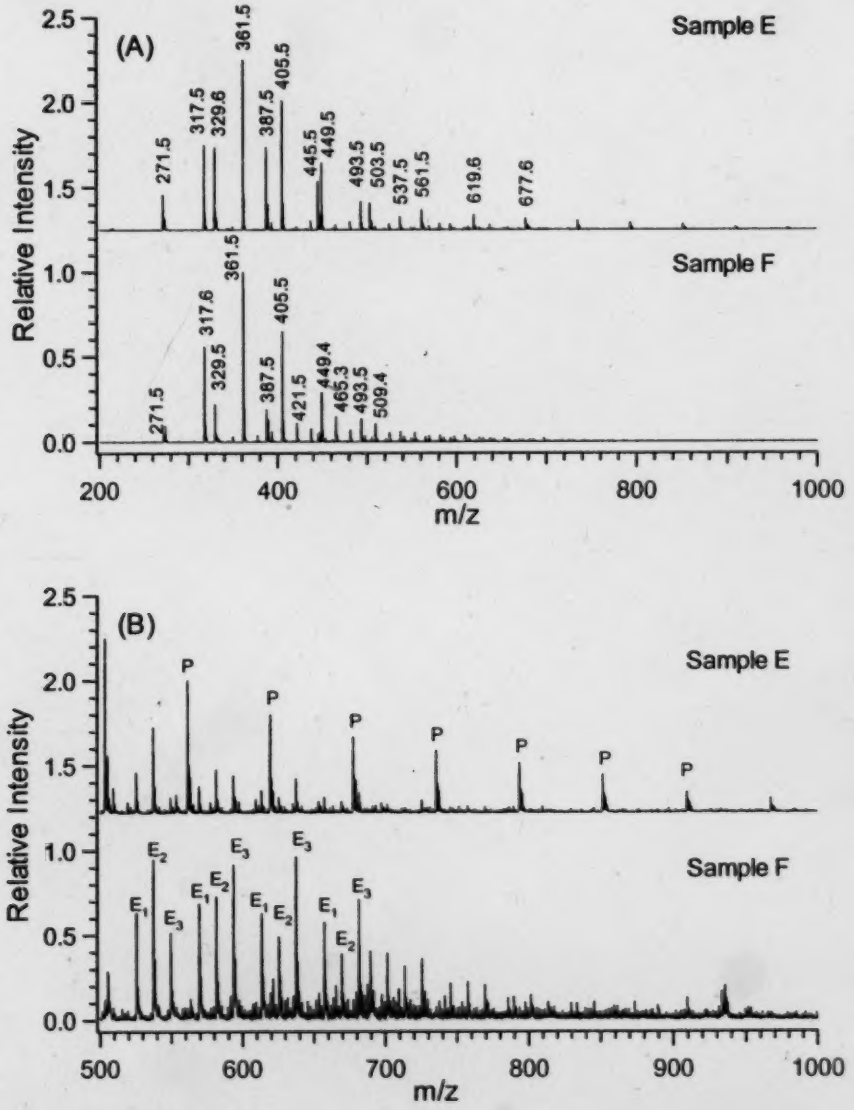

Figure 4.4. (A) ESI mass spectra of Samples E and F obtained with the addition of NaCl. (B) Expanded ESI mass spectra.

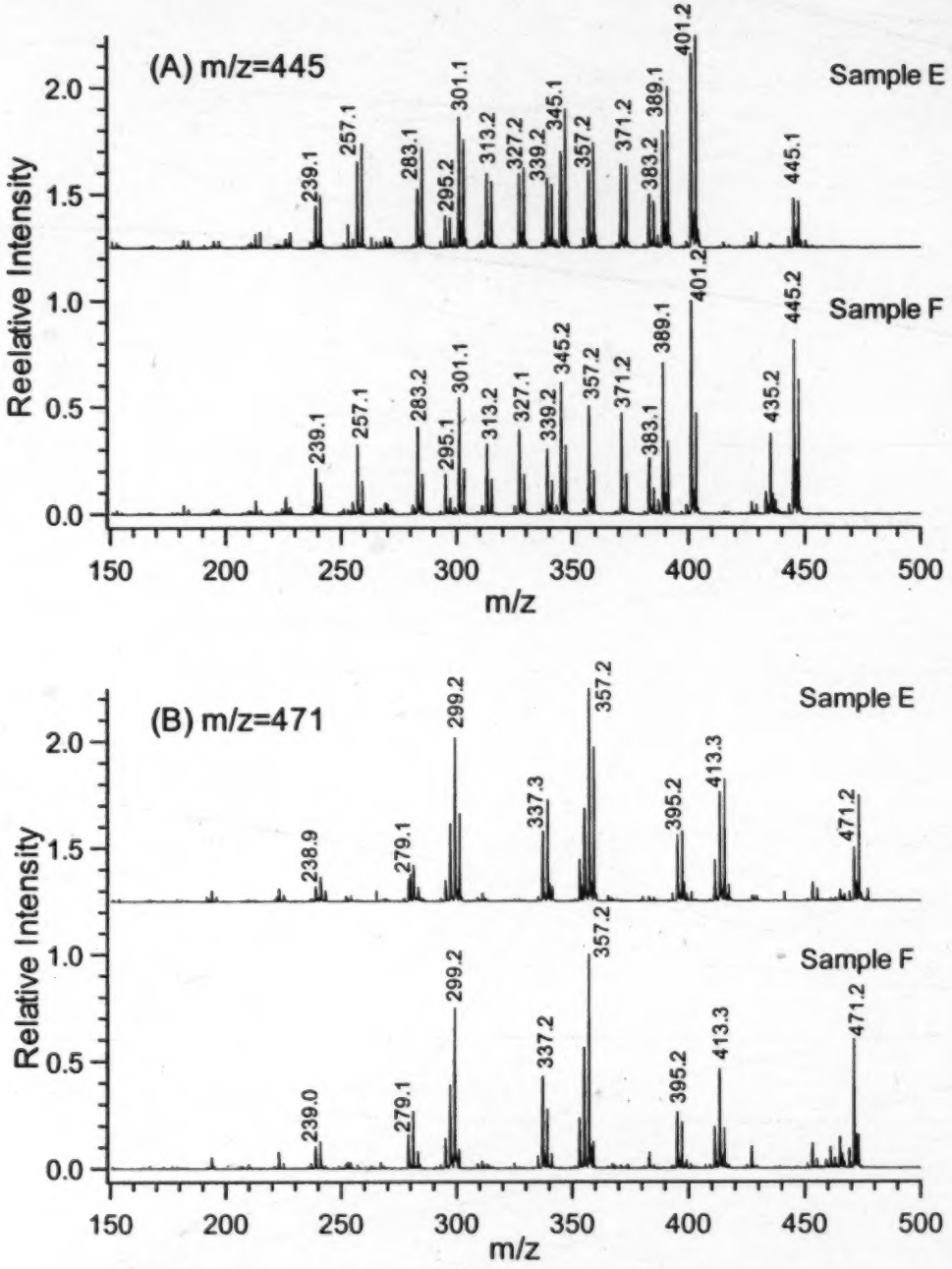

Figure 4.5. MS/MS spectra of selected oligomer ions at (A) m/z 445, and (B) m/z 471.

It should be pointed out that regarding the relative amount of the individual polymers in the mixture, neither ESI spectra nor MALDI TOF spectra could provide such information. The overall analytical efficiency including ionization efficiency and ion suppression effect can be quite varied for different polyols.

4.4 Summary

In summary, it is illustrated that the techniques of MALDI-TOF, ESI MS and MS/MS have their unique roles in characterizing low molecular weight polyols and their mixtures. The combination of these techniques can be very useful for solving real world problems in polyol chemistry. The applications also demonstrated the demand for further method development in the area of structural characterization of polyols by ESI MS/MS, which will be described in the next two chapters.

4.5 Literature Cited

1. Bahr, U.; Deppe, A.; Karas, M.; Hillenkamp, F.; Giessman, U. *Anal. Chem.* **1992**, 64, 2866.
2. Danis, P. O.; Karr, D. E.; Mayer, F.; Holle, A.; Watson, C. H. *Org. Mass Spectrom.* **1992**, 27, 843.
3. Danis, P. O.; Karr, D. E. *Org. Mass Spectrom.* **1993**, 28, 923.
4. Juhasz, P.; Costello, C. E. *Rapid Commun. Mass Spectrom.* **1993**, 7, 343.
5. Prokai, L.; Simonsick, Jr. W. J. *Rapid Commun. Mass Spectrom.* **1993**, 7, 853.
6. Montaudo, G.; Montaudo, M. S.; Puglisi, C.; Samperi, F. *Macromolecules* **1995**, 28, 4562.
7. Dey, M.; Castoro, J. A.; Wilkins, C. L. *Anal. Chem.* **1995**, 67, 1575.
8. Blais, J. C.; Tessier, M.; Bolbach, G.; Remaud, B.; Rozes, L.; Guittard, J.; Brunot, A.; Marechal, E.; Talet, J. C. *Int. J. Mass Spectrom. Ion Proc.* **1995**, 144, 131.
9. Weidner, S.; Kuhn, G.; Just, U. *Rapid Commun. Mass Spectrom.* **1995**, 9, 697.
10. Jackson, A. T.; Yates, H. T.; Scrivens, J. H.; Critchley, G.; Brown, J.; Green, M. R.; Bateman, R. H. *Rapid Commun. Mass Spectrom.* **1996**, 10, 1668.
11. Fei, X.; Murray, K. K. *Anal. Chem.* **1996**, 68, 3555.
12. Whittal, R. M.; Schriemer, D. C.; Li, L. *Anal. Chem.* **1997**, 69, 2734.
13. O'Connor, P. B.; Duursma, M. C.; van Rooij, G. J.; Heeren, R. M. A.; Boon, J. J. *Anal. Chem.* **1997**, 69, 2751.
14. Hensel, R. R.; King, R. C.; Owens, K. G. *Rapid Commun. Mass Spectrom.* **1997**, 11, 1785.

15. Parees, D. M.; Hanton, S. D.; Cornelio Clark, P.A.; Willcox, D. A. *J. Am. Soc. Mass Spectrom.* **1998**, 9, 282.

16. Pastor, S. J.; Wilkins, C. L. *Int. J. Mass Spectrom. Ion Proc.* **1998**, 175, 81.

17. Pasch, H. *Phys. Chem. Chem. Phys.* **1999**, 1, 3879.

18. Rashidzadeh, H.; Wang, Y.; Guo, B. C. *Rapid Commun. Mass Spectrom.* **2000**, 14, 439.

19. Wong, S. F.; Meng, C. K.; Fenn, J. B. *J. Phys. Chem.* **1988**, 92, 546.

20. Takashi, N.; Fenn, J. B. *J. Am. Chem. Soc.* **1992**, 114, 3241.

21. O'Connor, P. B.; McLafferty, F. W. *J. Am. Chem. Soc.* **1995**, 117, 12826.

22. Hunt, S. M.; Sheil, M. M.; Belov, M.; Derrick, P. J. *Anal. Chem.* **1998**, 70, 1812.

23. Maziarz, E. P.; Baker, G. A.; Lorenz, S. A.; Wood, T. D. *J. Am. Soc. Mass Spectrom.* **1999**, 10, 1298.

24. Guo, X. H.; Fokkens, R. H.; Peeters, H. J. W.; Nibbering, N. M. M.; de Koster, C. G. *Rapid Commun. Mass Spectrom.* **1999**, 13, 2223.

25. Whittal, R. M.; Li, L.; Lee, S.; Winnik, M. A. *Macromol. Rapid Commun.* **1996**, 17, 59.

26. Lee, S.; Winnik, M. A.; Whittal, R. M.; Li, L. *Macromolecules* **1996**, 29, 3060.

27. Watson, E.; Shah, B.; DePrince, R.; Hendren, R. W.; Nelson, R. *BioTechnique* **1994**, 16, 278.

28. Weidner, S.; Kuhn, G. *Rapid Commun. Mass Spectrom.* **1996**, 10, 942.

29. Bullock, J.; Chowdhury, S.; Johnston, D. *Anal. Chem.* **1996**, 68, 3258.

30. Barry, J. P.; Carton, W. J.; Pesci, K. M.; Anselmo, R. T.; Radtke, D. R.; Evans, J. V. *Rapid Commun. Mass Spectrom.* **1997**, 11, 437.

31. Sauvagnat, B.; Enjalbal, C.; Lamaty, F.; Lazaro, R.; Martinez, J.; Aubagnac, J. -L. *Rapid Commun. Mass Spectrom.* **1998**, 12, 1034.

32. Enjalbal, C.; Sauvagnat, B.; Lamaty, F.; Lazaro, R.; Martinez, J.; Mouchet, P.; Roux, F.; Aubagnac, J. -L. *Rapid Commun. Mass Spectrom.* **1999**, 13, 1775.

33. Barton, Z.; Kemp, T. J.; Buzy, A.; Jennings, K. R. *Polymer* **1995**, 36, 4927.

34. Lattimer, R. P. *Proceedings of the 47th ASMS Conference on Mass Spectrometry and Allied Topics*, **1999**, June 13-17, Dallas, TX. Paper 175.

35. Sherrard, K. B.; Marrlott, P. J.; McCormick, M. J.; Colton, R.; Smith, G. *Anal. Chem.* **1994**, 66, 3394.

36. Crescenzi, C.; Di Corcia, A.; Samperi, R.; Marcomini, A. *Anal. Chem.* **1995**, 67, 1797.

37. Ogura, I.; DuVal, D.L.; Kawakami, S.; Miyajima, K. *J. Am. Oil Chem. Soc.* **1996**, 73, 137.

38. Cumme, G. A.; Blume, E.; Bublitz, R.; Hoppe, H.; Horn, A. *J. Chromatogr. A.* **1997**, 791, 245.

39. Crowther, M. W.; O'Connell, T. R.; Carter, S. P. *J. Am. Oil Chem. Soc.* **1998**, 75, 1867.

40. Van Rooij, G. J.; Duursma, M. C.; de Koster, C. G.; Heeren, R. M. A.; Boon, J. J.; Wijnand Schuyl, P. J.; van der Hage, E. R. E. *Anal. Chem.* **1998**, 70, 843.

41. Willetts, M.; Clench, M. R.; Greenwood, R.; Mills, G.; Carolan, V. *Rapid Commun. Mass Spectrom.* **1999**, 13, 251.

42. Castillo, M.; Alonso, M. C.; Riu, J.; Barcelo, D. *Environ. Sci. Technol.* **1999**, 33, 1300.

43. Nuwaysir, L. M.; Wilkins, C. L.; Simonsick, Jr., W. J. *J. Am. Soc. Mass Spectrom.* **1990**, 1, 66.

44. Whittal, R. M.; Li, L. *Anal. Chem.* **1995**, 67, 1950.

45. Mahon, A.; Kemp, T. J.; Buzy, A.; Jennings, K. R. *Polymer* **1996**, 37, 531.

46. Selby, T. L.; Wesdemiotis, C.; Lattimer, R. P. *J. Am. Soc. Mass Spectrom.* **1994**, 5, 1081.

47. Lattimer, R. P. *J. Am. Soc. Mass Spectrom.* **1992**, 3, 225.

Chapter 5. Characterization of Polyglycol Ethers by Low Energy Tandem MS in an ESI Ion Trap Mass Spectrometer

5.1. Introduction

Mass spectrometry (MS) has become an increasingly important tool for polymer analysis. In principle, structural information can be obtained by using tandem MS (or MS/MS) where the oligomer ion of interest is selected for dissociation via techniques such as collision-induced dissociation (CID) [1]. Tandem MS combined with chemical ionization, field desorption, secondary ion, or fast atom bombardment has been used to analyze short chain oligomers [2-17]. With the development of electrospray ionization (ESI) and matrix-assisted laser desorption ionization (MALDI), MS became readily amenable to high molecular mass polymer analysis. While ESI and MALDI tandem MS have been widely used for bimolecular structural analysis, their use in polymer structural analysis is presently limited in scope [18-29]. One major reason is that many industrially important polymers do not readily fragment under the low energy CID condition [18-21,28]. These polymers require the use of high energy CID that can only be done in special instruments such as a sector/time-of-flight mass spectrometer [18-21,28]. Unfortunately this type of instrument is not accessible to most researchers for routine analyses.

A form of this chapter is published as:
R. Chen, and L. Li, "Lithium and transition metal ions enable low energy collision-induced dissociation of polyglycols in electrospray ionization mass spectrometry" *J. Am. Soc. Mass Spectrom.* **2001**,12, 832-839.

MALDI in-source or post-source decay can generate fragment ions for certain polymers [18,30-33]; but the general applicability of the technique and quality of the fragment ion spectra for structural analysis remain to be determined. On the other hand, there are a host of ESI mass spectrometers with different instrumental configurations that can provide low energy CID capability. It is clear that a robust and readily adaptable method for generating low energy CID spectra of polymeric materials would open the door for many polymer researchers to characterize their polymers by MS/MS.

High energy CID of polyglycols in combination with secondary ion or FAB [17] and MALDI [18] has been investigated. Of interest, it has been shown [17] that all alkali adduct ions of PEG can fragment by high energy CID; but the Li^+ adduct ion gives somewhat enhanced fragment ion signals, compared to Na^+ or K^+ adducts. Under the low energy CID condition, the Na^+ or K^+ PEG adduct ions do not fragment in conventional tandem mass spectrometers [17,21]. There is one report showing the fragmentation of $[PEG+Na]^+$ in MALDI FTMS using sustained off-resonance irradiation CID [22]. Lattimer has shown that lithiated polyglycol ions generated by FAB can undergo efficient low energy CID to produce structural information rich MS/MS spectra for low mass oligomers ($m/z < 500$) [14].

There are a number of reports of ESI MS studies of polyglycols [36-54]. In general, sodiated or potassiated PEG adducts formed by ESI do not dissociate in the interface region [36-54]. In contrast, protonated PEG fragments so easily that in-source fragmentation cannot be avoided [21]. Moreover, protonation is generally not very efficient compared to alkali adduct ion formation. Thus protonated PEG signals are either absent or weak in the mass spectrum of PEG, even with strong acidification of

sample solutions. This is particularly true for many real world samples where the concentration of alkali ions is high. Even with extensive sample clean-up, the residual alkali ions can still suppress the protonation of PEG. In short, functional polyglycols are currently viewed as a class of polymer that is not readily amendable to ESI low energy CID for structural characterization.

In this chapter, a robust and routine method of generating low energy CID mass spectra of polyglycol ethers in an ESI ion trap mass spectrometer is described. Based on the work by Lattimer *et al.* on FAB CID MS studies of polyglycols [14], it is demonstrated that lithiated polyglycols formed by ESI can be readily fragmented with low energy CID and, with ESI, it is also demonstrated the possibility of generating fragment ions for oligomers with masses around 3100. In addition, it is found that polyglycol adduct ions with transition metal ions can also be readily fragmented in a manner from which wealthy structural information can be obtained.

The protocol was further examined by the analysis of copolymers. It is shown that based on the MS/MS spectra generated by using Li^+ and/or Co^{2+}, not only structurally similar co-polyols with different monomer structures can be readily differentiated, but also the complete sequence of a block co-polyol with short chain length can be obtained. This method complements the existing MS approaches for copolymer sequence/composition analysis.

5.2 Experimental

5.2.1 Materials and Reagents. In the experiments, poly(ethylene glycol) (hydroxyl terminated) (PEGDH, average M_n *ca.* 600, 3350), poly(ethylene glycol) methyl ether (PEGME, average M_n *ca.* 550), poly(ethylene glycol) dimethyl ether (PEGDM, average M_n *ca.* 500), poly(ethylene glycol) butyl ether, poly(propylene oxide) (hydroxyl terminated), and poly(propylene oxide) butyl ether, with average molecular masses ranging from 300 to 4000 Da, were studied. Unless otherwise indicated, all samples were purchased from Aldrich Chemical Co. (Milwaukee, WI) and analyzed without purification.

For copolymer study, ethylene oxide terminated poly(propylene oxide) (average Mn *ca.* 1100, molar ratio EO:PO=0.15:1) and poly(ethylene oxide-*ran*-propylene oxide) monobutyl ether (average Mn ca. 970) were purchased from Polyscience Inc. (Warrington, PA) and Aldrich Chemical Co. (Milwaukee, WI), respectively, and analyzed without purification.

The model block copolymer, TPM, was a gift from Dow Chemical Canada. It was synthesized in the following manner. A Dowanol (commercial name) was reacted with KOH, and the mixture was then ethoxylated in a N_2 protected autoclave at 110 °C with pressure 60 psig. The general formula of this copolymer is as the following:

$$CH_3O\text{-}PO_3\text{-}EO_n\text{-}H$$

Phosphoric acid stock solution, ammonium acetate, sodium chloride, lithium chloride, silver nitrate, cobalt chloride, cobalt nitrate, cobalt bromide, nickel nitrate and zinc chloride were obtained from various commercial sources and used as received. Methanol-d_4 and deuterium oxide (D_2O) were purchased from Cambridge Isotope Lab.

Inc. (Andover, MA). HPLC grade methanol was obtained from Sigma (Milwaukee, WI). Distilled water was from a Milli-Q UV plus ultra-pure system (Millipore, Mississauga, ON).

5.2.2 Sample Preparation. In general, phosphoric acid solution was diluted and all salts were dissolved in water/methanol mixture (1:1 v/v) at a concentration of 0.1 M. The analyte solution was prepared by mixing analyte stock solution, 10% (v/v) cationization solution and appropriate amount of water/methanol mixture (volume ratio 1:1 for PEG and 1:3 for PPG and copolymers) to make a final analyte concentration of about 100 μM. Any variations from the above general procedure are indicated in the corresponding sections.

5.2.3 H/D Exchange. PEG methyl ether and silver nitrate were dissolved in the mixture of methanol-d_4 and deuterium oxide (volume ratio 1:1) and mixed to make final concentrations 100 μM and 10 mM, respectively.

5.2.4 ESI MS and MS/MS. All MS experiments were carried out in a Bruker/Agilent Esquire-LC Ion Trap LC/MS^n system. Sample solution was infused into the electrospray interface by a syringe pump (Cole-Parmer Instrument Co., IL) at a flow rate of 10 μl/min. The potentials between needle and capillary, capillary and skimmer 1, were 4.5 KV and 50 V, respectively. The capillary temperature was kept at 300 °C. Mass spectra were acquired over the range of m/z 15-2200. All data were reprocessed using the Igor Pro Software package (WaveMetrics, Lake Oswego, OR) without background subtraction.

5.3 Results and Discussion

5.3.1 Low Energy CID of PEG Methyl Ether with Commonly Used Cations.

Figure 5.1 shows the ESI spectra of PEG methyl ether (average M_n *ca.* 550 Da) obtained using different cationization reagents. Despite great effort to minimize in-source fragmentation by lowering the voltage differences between source and skimmer, and improving signal-to-noise (S/N) ratio by adjusting solvent conditions, protonation of PEG generates the most complex and noisy spectrum (see Figure 5.1A). Protonated species (M as labeled in Figure 5.1A), sodiated species (S), and some in-source fragments (F) are identified. In the NH_4^+ case, ammoniated, protonated, sodiated species, and fragment ions are observed (see Figure 1B); but the in-source fragmentation is less severe compared to the protonation experiment. The ESI mass spectra of Na^+, K^+, and Cs^+ adduct ions are almost the same and Figure 5.1C displays the spectrum obtained from the sodium cationization of PEG. For all other polyglycols studied by ESI in this work, alkali ions provide efficient cationization with no in-source fragmentation.

Figure 5.1D shows the ESI mass spectrum obtained using lithium ions as the cationization reagent. It is interesting to note that the intensities of the minor components in the low mass region (<500 Da) are somewhat enhanced in the Li^+ case. This finding is similar to what was observed in MALDI analysis of low mass polyglycols using Li^+ as the cationization reagent [55]. Cationization of PEG and other polyglycols by alkali metal ions including Li^+, Na^+, K^+, and Cs^+ has been extensively studied using MALDI to produce the adduct ions [55-57]. The observation of more intense low mass oligomers generated using Li^+ compared to Na^+ in MALDI was attributed to the fact that the lowest energy conformer of $[PEG+Li]^+$ requires less oxygen atoms than for $[PEG+Na]^+$ [57].

The same explanation may be applied to this ESI work. This observation should have implication in polymer molecular mass analysis.

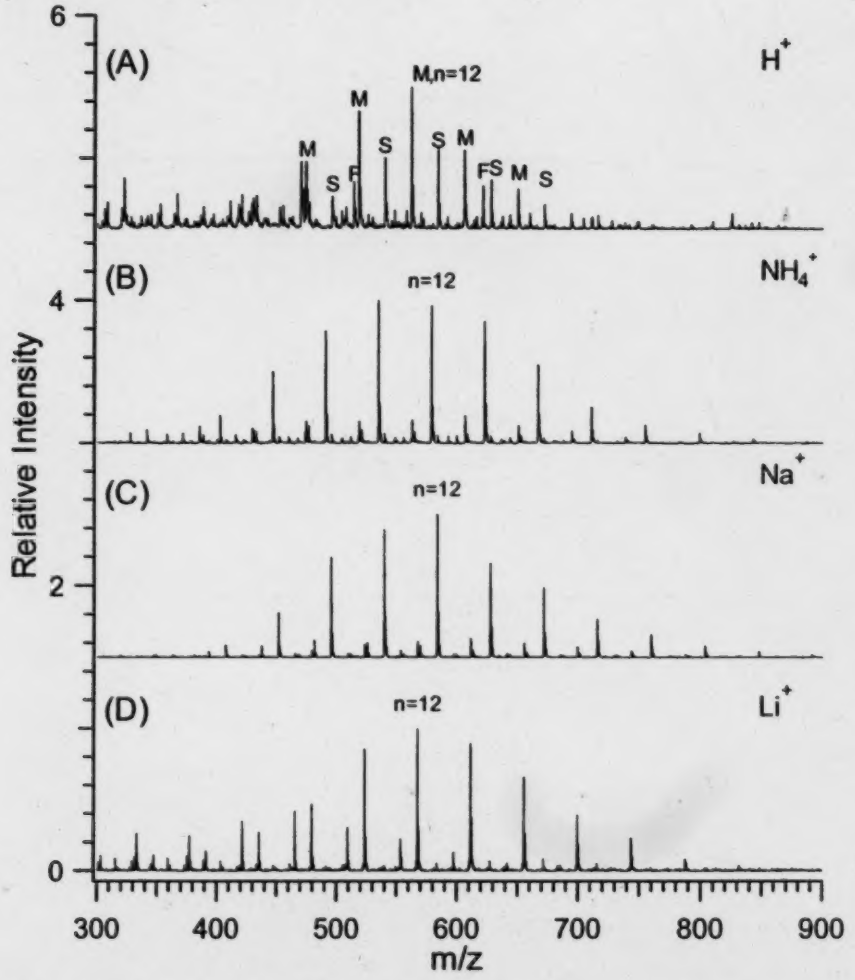

Figure 5.1. ESI mass spectra of PEG methyl ether obtained using different cations for ionization: (A) H^+, (B) NH_4^+, (C) Na^+, and (D) Li^+. In (A), peaks labeled as S are from sodium attachment, M from protonation, and F from fragmentation. The *n* denotes the number of the repeating units of the most intense peak.

In practice, Na^+ is the most common contaminant in PEG analysis. Na^+ can be brought into a sample from polymer initiators, solvents, and/or containers used for

sample preparation. It is not surprising that most of the PEG spectra obtained by ESI and MALDI are sodiated peaks, even if no cationization reagent is purposely added to the sample. For molecular mass analysis where ion fragmentation must be avoided, Na^+ serves the purpose of generating reproducible mass spectra of PEGs. Unfortunately, these easily formed $[PEG+Na]^+$ ions fail to produce fragment ions under low energy CID in the ion trap mass spectrometer. The K^+ and Cs^+ adduct ions do not fragment either.

As shown in Figure 5.1D, Li^+ can provide efficient ionization of polyglycols to produce intact oligomer ions. Moreover, ESI generated Li^+ adduct ions can be readily fragmented using low energy CID, as illustrated in Figure 5.2C. This observation is entirely consistent with what Lattimer has reported in the FAB low energy CID experiment [14]. Compared to other alkali metal ions, Li^+ was found to enhance the fragmentation of polyglycols [14] as well as a variety of other compounds [58-60]. While the ESI-generated ions generally possess far less internal energy (i.e., cooler ions) than those produced by FAB or MALDI [61], this work suggests that the energy gained through CID is sufficient to fragment the lithiated ESI ions.

Figure 5.2 shows the ESI MS/MS spectra of the PEG 11-mer produced using three different cationization reagents. While protonation is not an effective way of generating MS spectra, $[PEG+H]^+$ ions, if present, can be fragmented as shown in Figure 5.2A. This is not surprising in light of the fact that in-source fragmentation can be readily observed in protonated PEG species. Since the signal intensity in the MS spectrum of $[PEG+H]^+$ is low, the MS/MS spectrum of $[11\text{-mer}+H]^+$ shown in Figure 5.2A also displays a low S/N ratio.

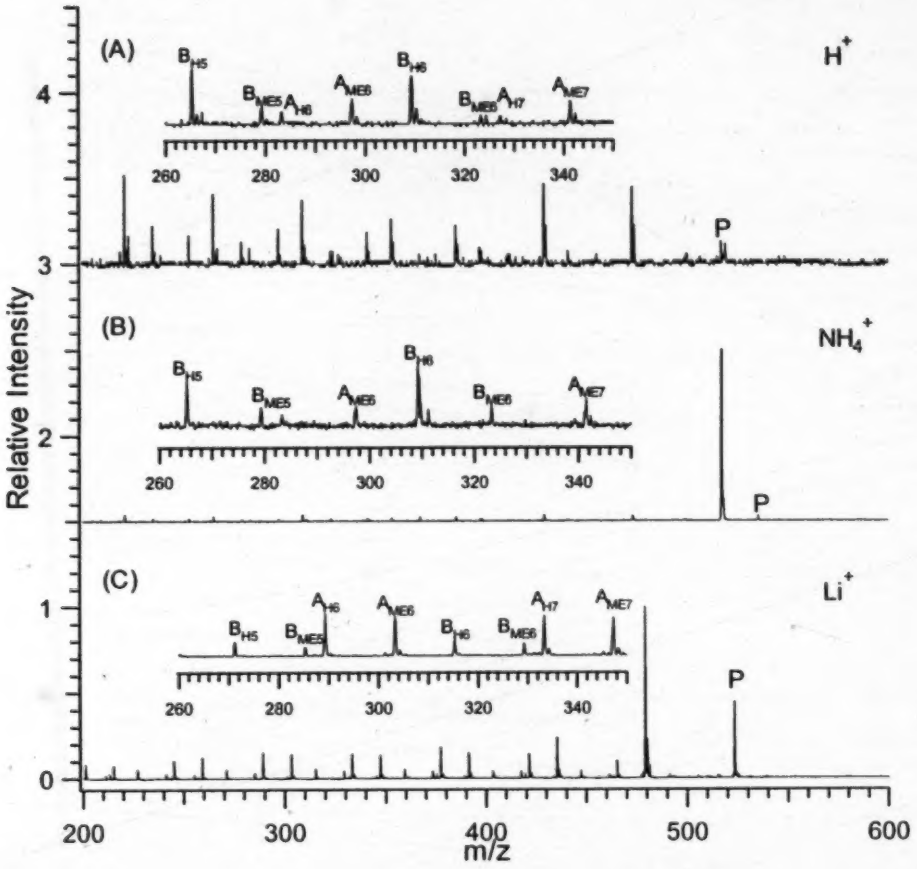

Figure 5.2. ESI MS/MS spectra of PEG methyl ether 11-mer with different cations: (A) H^+, (B) NH_4^+, and (C) Li^+. The peak annotations are according to Scheme 5.1.

In the case of NH_4^+ cationization (see Figure 5.2B), the most dominant peak in the MS/MS spectrum is the protonated 11-mer as a result of the loss of NH_3 (-17 Da) from the molecular ion peak. Some weak fragment peaks from subsequent fragmentation of $[11\text{-mer}+H]^+$ are also observed (see the inset of Figure 5.2B). Compared to panels A and B in Figure 5.2, the CID spectrum of $[11\text{-mer}+Li]^+$ (Figure 5.2C) shows a higher S/N ratio. This is also true for other polyglycols studied in this work. The fragment ions

observed correspond to backbone chain cleavage and can be readily assigned to the polyglycol structures. Scheme 5.1 shows the fragmentation pattern of a singly charged oligomer (trimer) ionized by a cationization reagent R. The nomenclature for the fragment ions is consistent with that reported [14,17]. To differentiate fragment ions containing different end groups, α and ω are used to represent ions containing α and ω end group, respectively. The number in the label denotes the n^{th} repeat unit from the end group α or ω. The **A** series ions have been proposed to be generated by a charge-induced fragmentation mechanism, where the **B** and **C** series ions are thought to be formed via charge-remote fragmentation [14,17]. For PEG methyl ether, α is hydrogen (H) and ω is the methyl group (ME). Some of the fragment ions shown in Figure 5.2 are labeled according to Scheme 5.1.

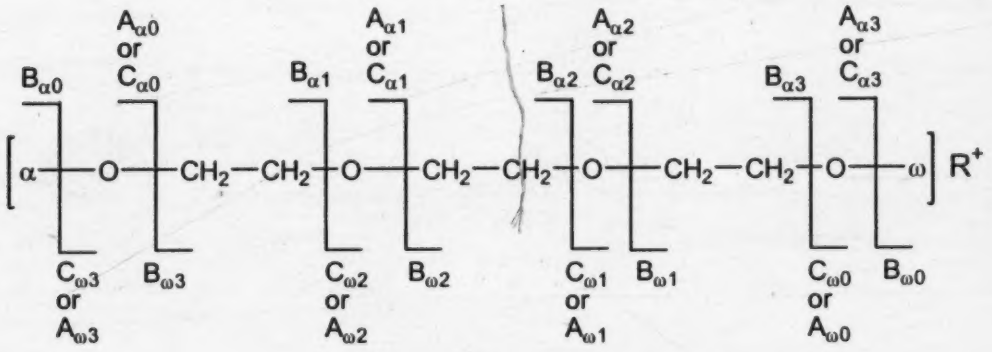

Scheme 5.1. Nomenclature of the fragment ions.

As Figure 5.2 shows, the fragment ions from protonated or lithiated precursor ions are distributed throughout the entire mass range. This observation is somewhat different from what was found in FAB MS/MS. In FAB, the MS/MS spectrum of the lithiated PEG decamer ion showed intense fragment ions throughout the entire mass range,

whereas the fragment spectrum from the protonated decamer ion showed only low mass fragment ions [14]. The difference observed in ESI MS/MS and FAB MS/MS is likely due to the difference in energetics for the precursor ions generated by the two modes of ionization. FAB generates ions with higher internal energy, compared to ESI [61]. Protonated species are more labile than the lithiated ions and the additional energy gained via CID in FAB can cause a greater extent of fragmentation for the protonated ions, resulting in predominately low mass fragment ions in FAB MS/MS of $[decamer+H]^+$. Figure 5.2A or 5.2B also shows that the $\mathbf{B_H}$ series ions are relatively more intense in the MS/MS spectra of protonated 11-mer, compared to the $\mathbf{B_{ME}}$ and **A** series ions. This is likely due to the readiness of protonation of the hydroxyl end group. As a consequence, charge-remote fragmentation from the hydroxyl end is favored. For the fragmentation of lithiated 11-mer ions (see Figure 5.2C), the $\mathbf{A_H}$ and $\mathbf{A_{ME}}$ series ions show similar peak intensity and both are stronger than the **B** series ions. Charge-induced fragmentation is clearly favored and peak intensities of both **A** and **B** series ions are not affected by the end group structure. This observation is not surprising considering that, unlike protonation, the lithium ion forms a complex with multiple oxygen atoms in the ethylene oxide chains. Note that FAB MS/MS of lithiated species also showed more intense **A** series ions generated by the facile charge-induced fragmentation [14].

The ability of lithiated polyglycol ions to dissociate under low energy CID is related to the binding strength between the metal ion and polyglycol chain [14,59]. The binding between Li^+ and the polymer chain is stronger than that between the other alkali metal ions and the polymer chain [14]. Thus, the internal energy gained via CID, in the case of lithiated oligomer ions, is channeled towards the polymer chain, causing polymer

dissociation. In contrast, for the other alkali metal ions, dissociation of the interactions between the metal ion and polymer chain is the energy release channel. It is clear that any metal ions bound strongly to the polymer chain would potentially cause fragmentation of the polymer chain, provided that a sufficient amount of energy is given to the adduct ion. This is indeed the case for the polyglycol complex formed by using divalent transition metal ions as the cationization reagents in ESI, as described in section 5.3.2.

5.3.2 Low Energy CID of PEG Methyl Ether with Transition Metal Ions.

Figure 5.3 shows the ESI mass spectra of PEG methyl ether obtained using transition metal ions for ionization. Panels B, C, and D in Figure 5.3 show the spectra obtained with Zn^{2+}, Co^{2+}, and Ni^{2+}, respectively. The oligomer peaks labeled as M are from $[oligomer+metal-H]^{+}$. Apparently, in the current case, because of the readily replaceable proton at the hydroxyl site, the divalent metal ion reacts with the oligomer to form the singly charged species with the loss of a proton. However, as will be described in the section 5.3.3, ionization of PEG by divalent transition metal ions strongly depends on PEG structure, and involved counter ion as well. More than one type of singly charged ion involving the metal ions can co-exist in the ESI spectrum, and data interpretation should be exercised with great caution.

The sodiated ESI spectrum is shown in Figure 5.3A for comparison. Despite the use of a large amount of salts, the ESI spectra from Zn^{2+}, Co^{2+}, and Ni^{2+} still display peaks from sodiated species with varied relative intensity (labeled as S in Figure 5.3). This observation suggests that these metal ions do not ionize the polyglycol as efficiently

as the alkali metal ions. However, their adduct ions can be readily fragmented under low energy CID, as shown in panels A, B, and C in Figure 5.4. By replacing a proton, the divalent metal ion forms a strong bond with the polymer chain and the energy gained by CID causes chain fragmentation.

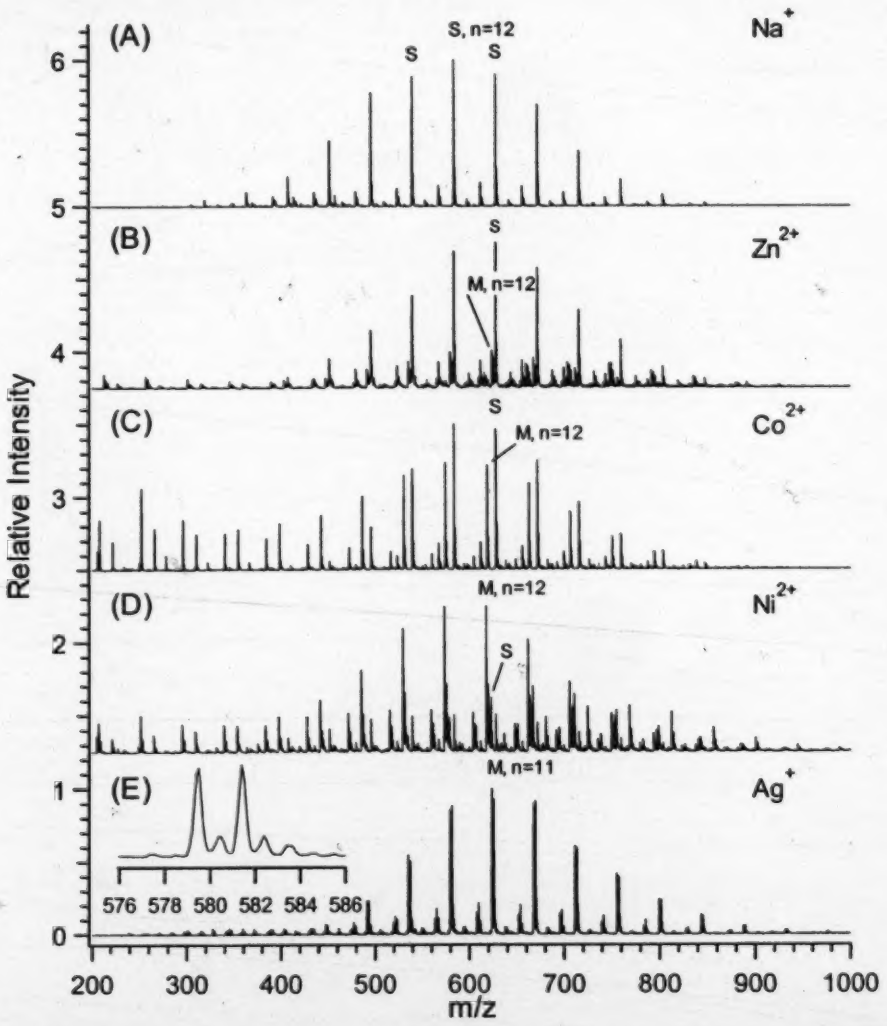

Figure 5.3. ESI mass spectra of PEG methyl ether obtained using sodium ion and different transition metal ions for ionization: (A) Na^+, (B) Zn^{2+}, (C) Co^{2+}, (D) Ni^{2+}, and (E) Ag^+. The peaks labeled as S are from sodium attachment, M from corresponding cation interaction. The *n* denotes the number of the repeating units of the most intense peak.

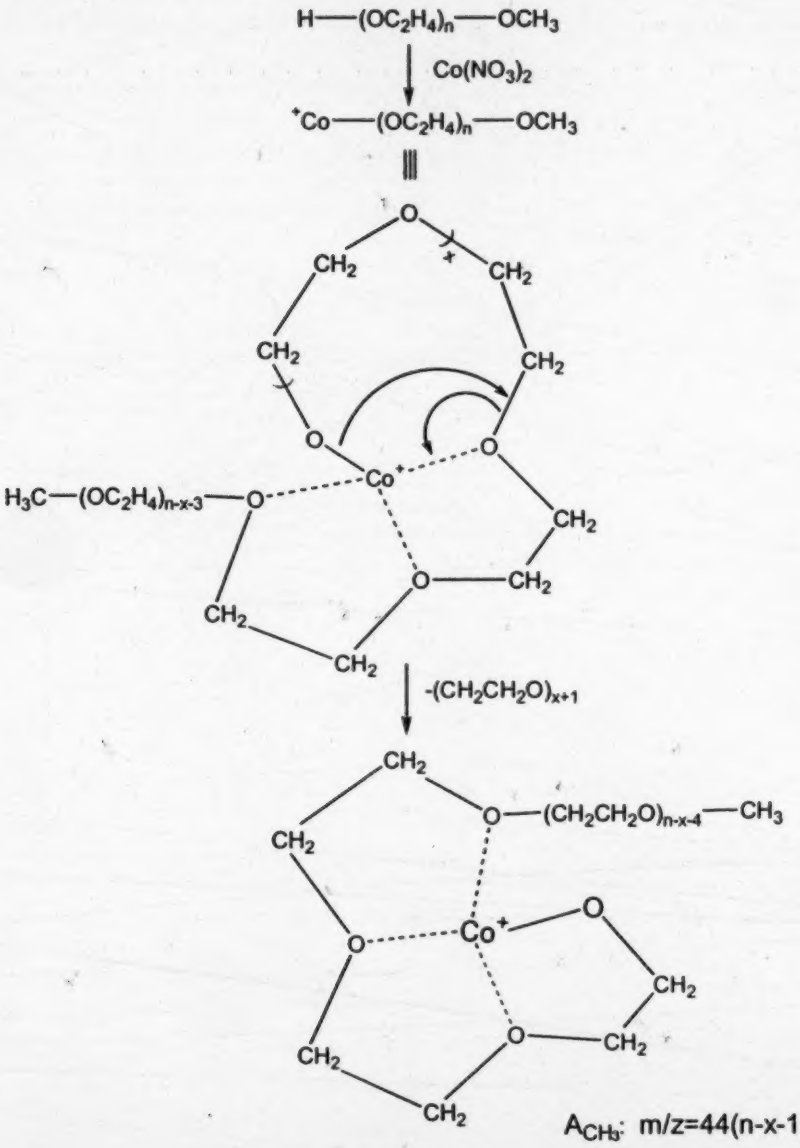

Scheme 5.2. Fragmentation pathway for the formation of A_{ME} ions using Co^{2+}.

The insets in Figure 5.4 show the expanded spectra with peaks labeled according to Scheme 5.1. The **A** series ions containing the methyl end group are likely formed via charge-induced dissociation. This is illustrated in Scheme 5.2 using the ionization

reagent Co^{2+} as an example. The metal ion is proposed to form a tetrahedral complex with the internal chains of ethylene oxide, which induces the loss of ethylene oxide group(s). Such complex can be easily formed owing to the facility with which PEG chain folds itself. The **A** and **B** series ions containing the hydrogen end group are likely formed via charge-remote dissociation, as shown in Schemes 5.3 and 5.4. The **B** series ions containing the methyl end group are not observed. This finding supports the argument that charge-remote dissociation is responsible for generating the **B** series ions. The divalent metal ion is covalently bound to the hydroxyl end and thus charge-remote dissociation can only initiate from this site.

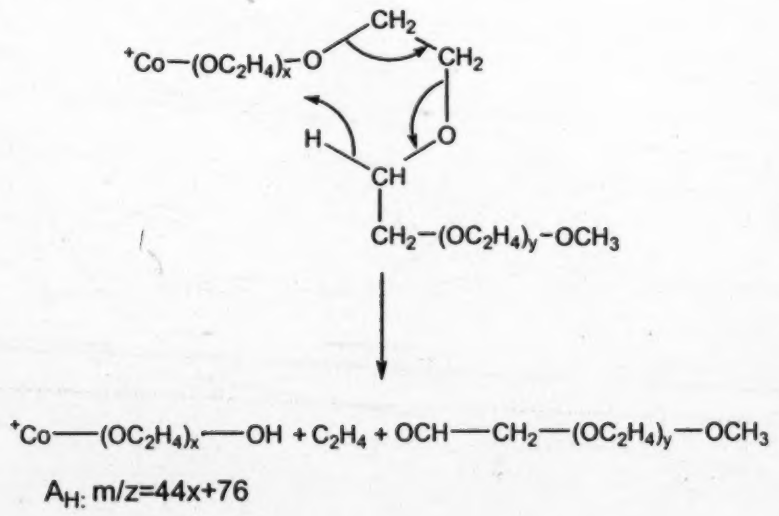

Scheme 5.3. Fragmentation pathway for the formation of A_H ions using Co^{2+}.

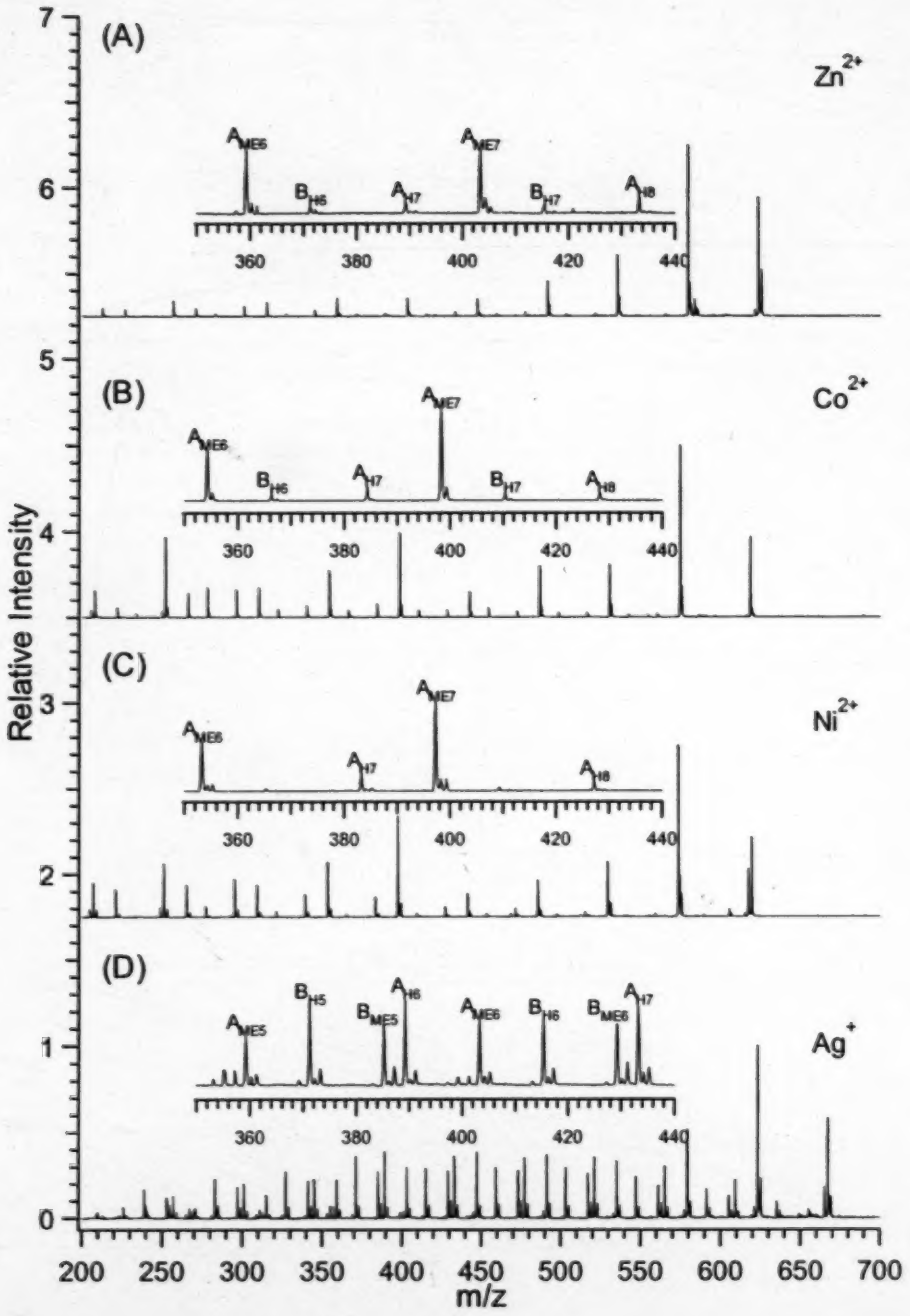

Figure 5.4. ESI MS/MS spectra of PEG methyl ether 12-mer with different transition metal ions: (A) Zn^{2+}, (B) Co^{2+}, (C) Ni^{2+}, and (D) Ag^{+}. The peak annotations are according to Scheme 5.1.

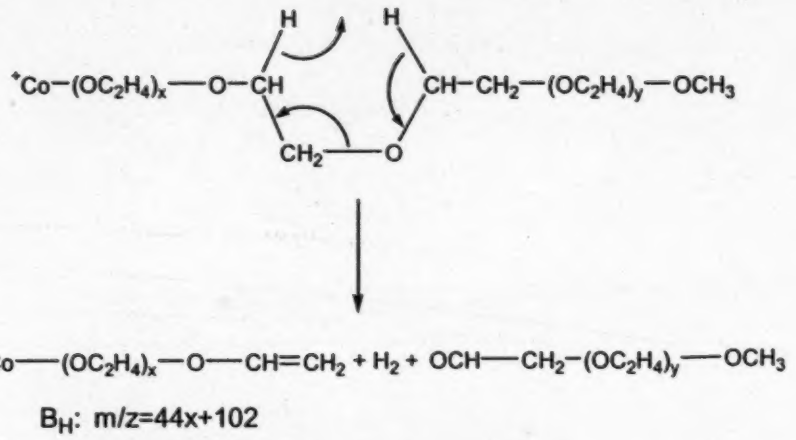

Scheme 5.4. Fragmentation pathway for the formation of B_H ions using Co^{2+}.

5.3.3 Ionization/Fragmentation of PEG by Co^{2+} in ESI MS and MS/MS.

Transition metal ions are being increasingly used in polymer MS, especially for apolar polymers, by both MALDI and ESI. For example, cationization of polystyrene was investigated using silver, zinc, copper, cobalt, and palladium by means of MALDI and ESI [62]. It was found that silver, copper, and palladium yielded efficient cationization of polystyrene oligomers, and it was argued that the cationization occurred by gas phase ion-molecule reactions rather than pre-formed ions from the condensed phase. On the other hand, many transition metal complexes exist as charged species in solution [63]. In the case of PEG, considering that oxygen atoms are present in every repeat unit, and the ease with which PEG chain can fold itself, one would expect a great amount of PEG metal ion complexes formed in the solution. ESI is an excellent tool for studying such complexes, due to its ability to transfer pre-formed ions with their structures intact and often with their charge retained. Note that, a slightly higher Co^{2+} concentration of 0.015 M was used to obtain the spectra presented in this section.

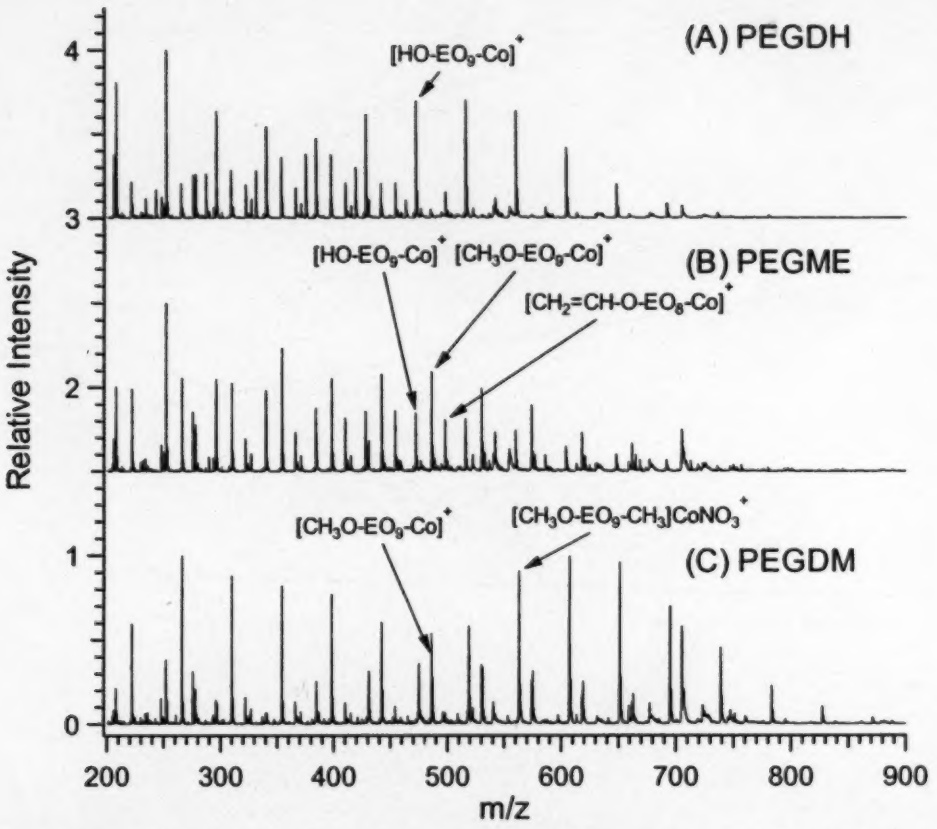

Figure 5.5. ESI mass spectra of (A) PEG (hydroxyl terminated), (B) PEG methyl ether, and (C) PEG dimethyl ether obtained using 0.015 M $Co(NO_3)_2$.

Figure 5.5 shows the ESI mass spectra of three PEGs with different end groups using Co^{2+} as the cationization reagent. In PEGDH and PEGME, there is at least one mobile proton present in the end group moiety. As anticipated, the main peaks in Figure 5.5A result from the replacement of one proton in the end group by a Co^{2+}. The peaks at low mass region are the results of in-source fragmentation in a much similar manner as those depicted in scheme 5.3 and 5.4. For PEG methyl ether (Figure 5.5B), in addition to the main distribution with representative structure $[CH_3O\text{-}EO_n\text{-}Co]^+$, fragment series $\mathbf{A_H}$

(with structure $[HO\text{-}EO_n\text{-}Co]^+$, Scheme 5.3) and $\mathbf{B_H}$ (with structure $[CH_2{=}CH\text{-}O\text{-}EO_n\text{-}Co]^+$, Scheme 5.4) are also abundant.

In the case of PEG dimethyl ether (Figure 5.5C), where no mobile proton is available, the PEGs are ionized by forming the ion pairs involving the PEG-Co^{2+} complex in combination with the counterion NO_3^-. This ion pair formation was also observed in other transition metal-ligand systems [63,64]. In all cases, no doubly charged ions were found. Even for PEG dimethyl ether, in which Co^{2+} being coordinated by 4 or 6 EO units seems quite feasible. This is possibly due to the lower desolvation energy of a singly charged ion pair metal complex compared with a doubly charged species. During the ESI process, a singly charged species is much more likely to desorb from a charged droplet than a multiply charged ion. These comparative results indicate, for low molecular mass PEG, cationization is not necessarily a simple matter involving only cations and repeat units. Depending on the PEG structure, end group and counter ion could engage in this process as well.

Since ionization of PEG dimethyl ether by Co^{2+} is associated with a counter ion, a series of experiments using different cobalt salts were carried out to examine whether counter ions have any effect on the ionization. Figure 5.6 displays ESI mass spectra of PEG dimethyl ether obtained using three different cobalt salts. Judged by the intensity ratio between P (resulting from ion pair metal complex) and S (resulting from Na^+ attachment, Na^+ is from impurity), the ionization efficiency decreases in the order $Co(NO_3)_2 > CoCl_2 > CoBr_2$. No sodium attachment peak was found in the case of using $Co(NO_3)_2$. The exact reason for such difference is not known. It is noted, however, that

both $CoCl^+$ and $CoBr^+$, but not $CoNO_3^+$, were observed. The stable existence of cobalt in such forms might prevent further coordination with PEG that requires more energy.

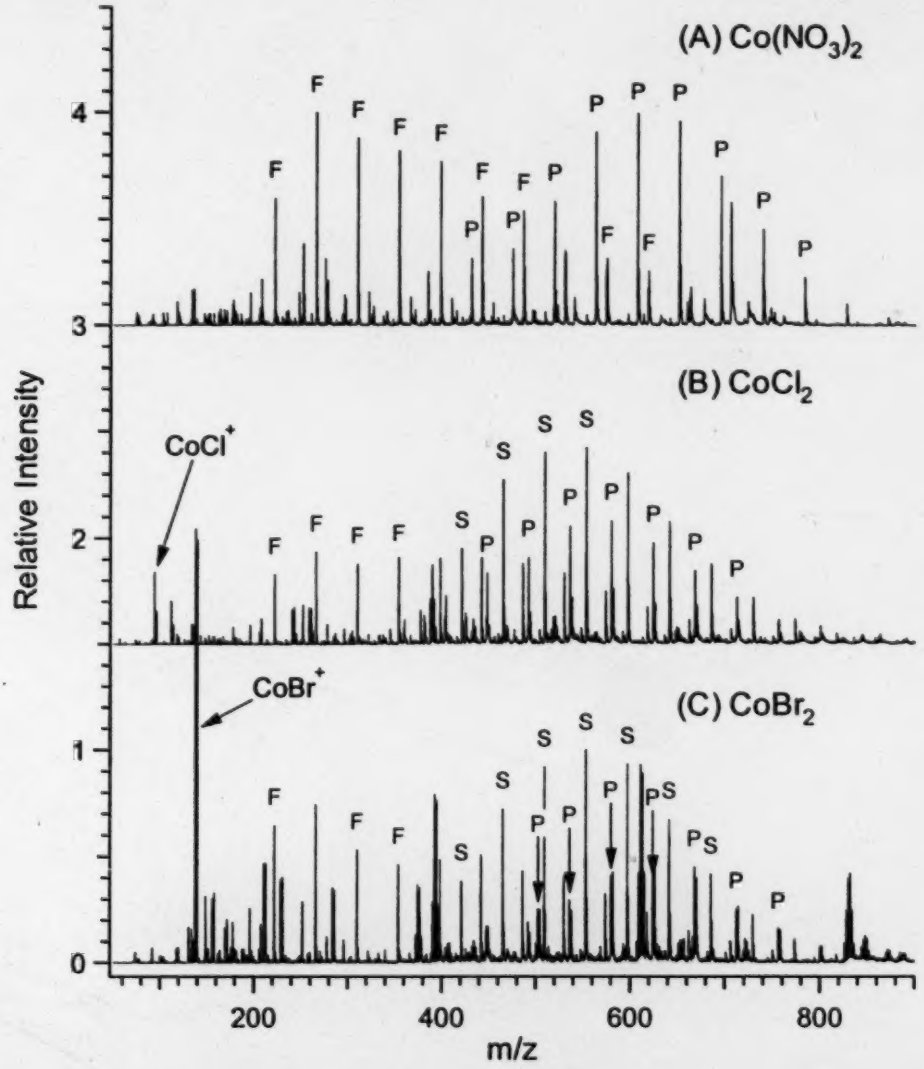

Figure 5.6. ESI mass spectra of PEG dimethyl ether obtained by using 0.015M (A) $Co(NO_3)_2$, (B) $CoCl_2$, and (C) $CoBr_2$. Peaks labeled as P are from ion pair metal complex, S are from sodium attachment, and F are from in-source fragmentation.

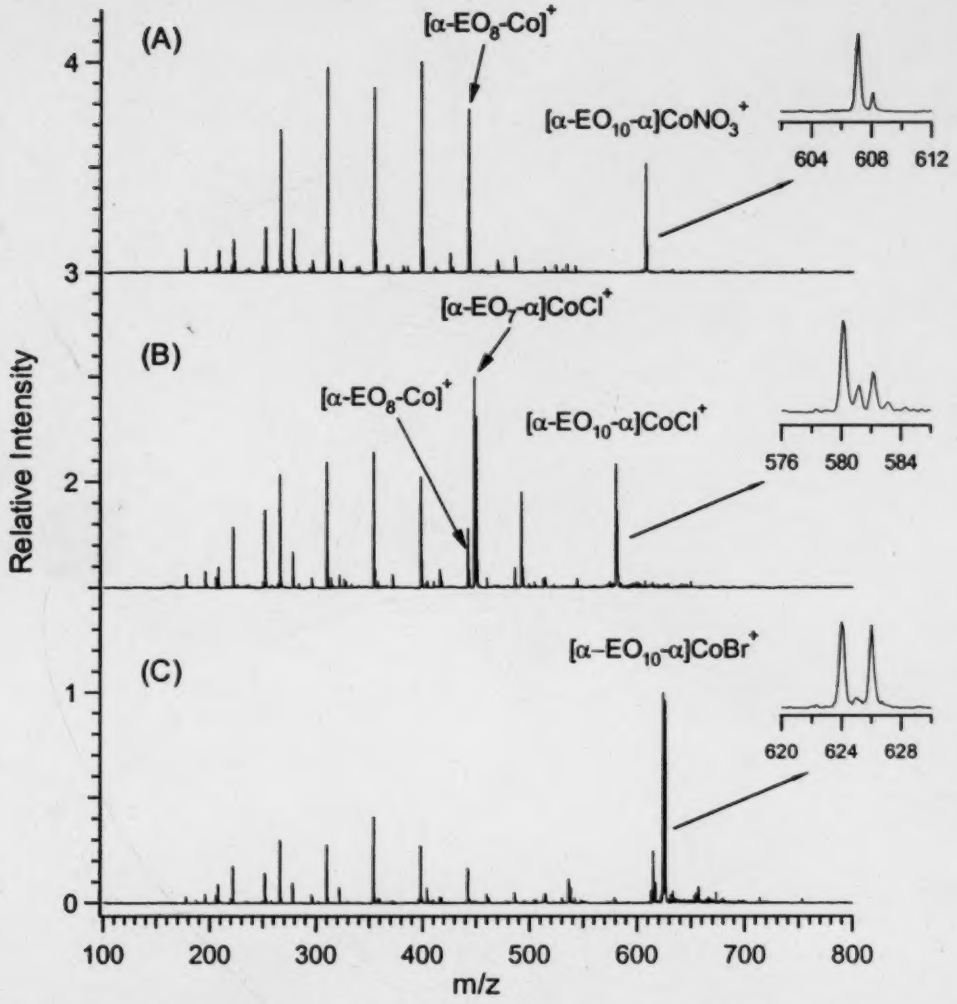

Figure 5.7. ESI MS/MS spectra of (A) $[CH_3O\text{-}EO_{10}\text{-}CH_3]CoNO_3^+$, (B) $[CH_3O\text{-}EO_{10}\text{-}CH_3]CoCl^+$, and (C) $[CH_3O\text{-}EO_{10}\text{-}CH_3]CoBr^+$. In the figure, α=$CH_3$.

Further MS/MS on ion pair metal complexes with the general formula $[PCoX]^+$, where P represents PEG and X represents counter ion, displays rather different fragmentation behavior, as shown in Figure 5.7. Common products (below m/z 450 Da) with the structure $[CH_3O\text{-}EO_n\text{-}Co]^+$ are observed in all cases. However, the predominant product ion in the case of using $CoCl_2$ corresponds to a direct loss of 3 EO units with

counter ion moiety intact. Among all, the ions generated by using $CoBr_2$ produce the least abundant product ions, indicating a somewhat enhanced stability of the parent ion.

In summary, it is demonstrated that when using divalent transition metal ions such as Co^{2+} for ionization of low molecular mass PEG, in addition to repeat units and cations, end group and counter ion influence the fragmentation process as well, depending on the PEG structure. Counter ions can significantly affect ionization efficiency and subsequent fragmentation, and therefore should be considered as an integral part when selecting cationization reagent.

5.3.4 Ionization/Fragmentation of PEG Methyl Ether by Ag^+: A H/D Exchange Approach.

Another transition metal ion that we have investigated for ESI of polyglycols is the silver ion. Ag^+ is known to be capable of ionizing non-polar polymers such as polystyrene in both ESI [62,65] and MALDI [62] due to possible binding between Ag^+ and phenyl rings. To date, there is no report on the use of Ag^+ for ionization of polyglycols. To gauge the efficiency of silver cationization for PEG in ESI, a control experiment was conducted in which the same molar amounts of Na^+, Ag^+, and H^+ were added to the PEG methyl ether sample. Sodiated and silver-ion attached peaks were detected while protonated species were completely suppressed. The intensity ratios between the Ag^+- and Na^+-adduct peaks vary from 1-3%. This result suggests that it should be possible to produce ESI spectra composed of predominately Ag^+-PEG adduct ions by adjusting the silver ion concentration. For all polyglycol samples listed in the Experimental and several real world samples [Chapter 3], oligomer distributions with silver cationization can be consistently obtained. In contrast, most of these samples

produce few or no protonated species, even in very acidic solvents for ESI. These results demonstrate that, besides alkali ions, silver cationization is also very effective for generating ESI spectra of polyglycols.

One unique feature of using Ag^+ cationization for generating ESI mass spectra is the distinct isotope pattern associated with the silver adduct ion. Any singly charged silver attached oligomer ion displays two peaks that are 2 mass units apart with similar intensities. This is shown in the inset of Figure 5.3E. The isotope pattern greatly facilitates the peak assignment in the ESI mass spectrum. With alkali metal ions, it is often necessary to use different metal ions for ionization and observe of the mass shifts to confirm peak assignment. This is particularly true for distinguishing peaks of the minor components in a sample from those resulting from different metal ions or proton attached to the principal polymer distribution. In the PEG methyl ether example, by examining the spectrum shown in Figure 5.3E, the minor peaks displaying the characteristic isotope peaks must be from impurities present in the sample.

The silver-attached adduct ions can be dissociated very efficiently under the low energy CID condition; yet they are sufficiently stable to survive the interface region. Figure 5.4D shows the fragment ion spectrum of the argentinated 11-mer. Compared to the MS/MS spectrum from the lithiated adduct ion (Figure 5.2C), a larger number of fragment ions with greater intensities are observed in Figure 5.4D. In addition, an MS/MS experiment can be readily conducted in a manner that the mass window of the parent ion is varied to include Ag^{107} isotope only, Ag^{109} isotope only, or both of them, respectively. Any silver ion attached fragments display the isotope patterns, thereby

facilitating the interpretation of fragment ions (e.g., any internal fragment ions with no silver ion attached will not show the isotope pattern).

The fragment ions observed in Figure 5.4D are from the cleavage of polyglycol chains with two different end groups (-OH and -OMe). Peak assignment is shown in the inset of Figure 5.4D according to Scheme 1. However, compared to the fragmentation of lithiated adduct ions (see Figure 5.2C) and divalent transition metal ion adduct ions (see Figure 5.4A, B, and C), fragmentation of argentinated 11-mer generates a much different spectrum with much more intense **B** series ions.

To account for the rather peculiar fragmentation behavior of PEG-Ag^+ adduct ions, a proton/deuteron (H/D) exchange experiment was conducted. The underlying principle is that with D replacing H at the hydroxyl site in PEG methyl ether, any fragment ions with mass shift would retain the hydroxyl end group moiety, and those without mass shift should result from a pathway where the hydroxyl end group moiety is lost as neutral. Largely owing to the conjugate acidic nature of the hydroxyl proton in the PEG methyl ether structure, such a H/D exchange can be easily accomplished by dissolving the sample and salts into deuterated solvents. The similar practice has been reported in the fragmentation mechanism study using FAB MS/MS [15, 16].

Figure 5.8 shows the ESI MS/MS spectra of sample PEG methyl ether with and without D replacement. Inheriting the same nomenclature in Scheme 1, it is found that all corresponding hydroxyl end group containing fragment ion pairs (i.e. $\mathbf{A_H}$, $\mathbf{B_H}$ *vs.* $\mathbf{A_D}$, $\mathbf{B_D}$) have 1 Da mass difference (see figure 5.8B). Accordingly, all $\mathbf{A_{ME}}$ and $\mathbf{B_{ME}}$ pairs have identical masses, with the exception of $\mathbf{A_{ME11}}$. In addition, no $\mathbf{B_{ME11}}$ ions were observed.

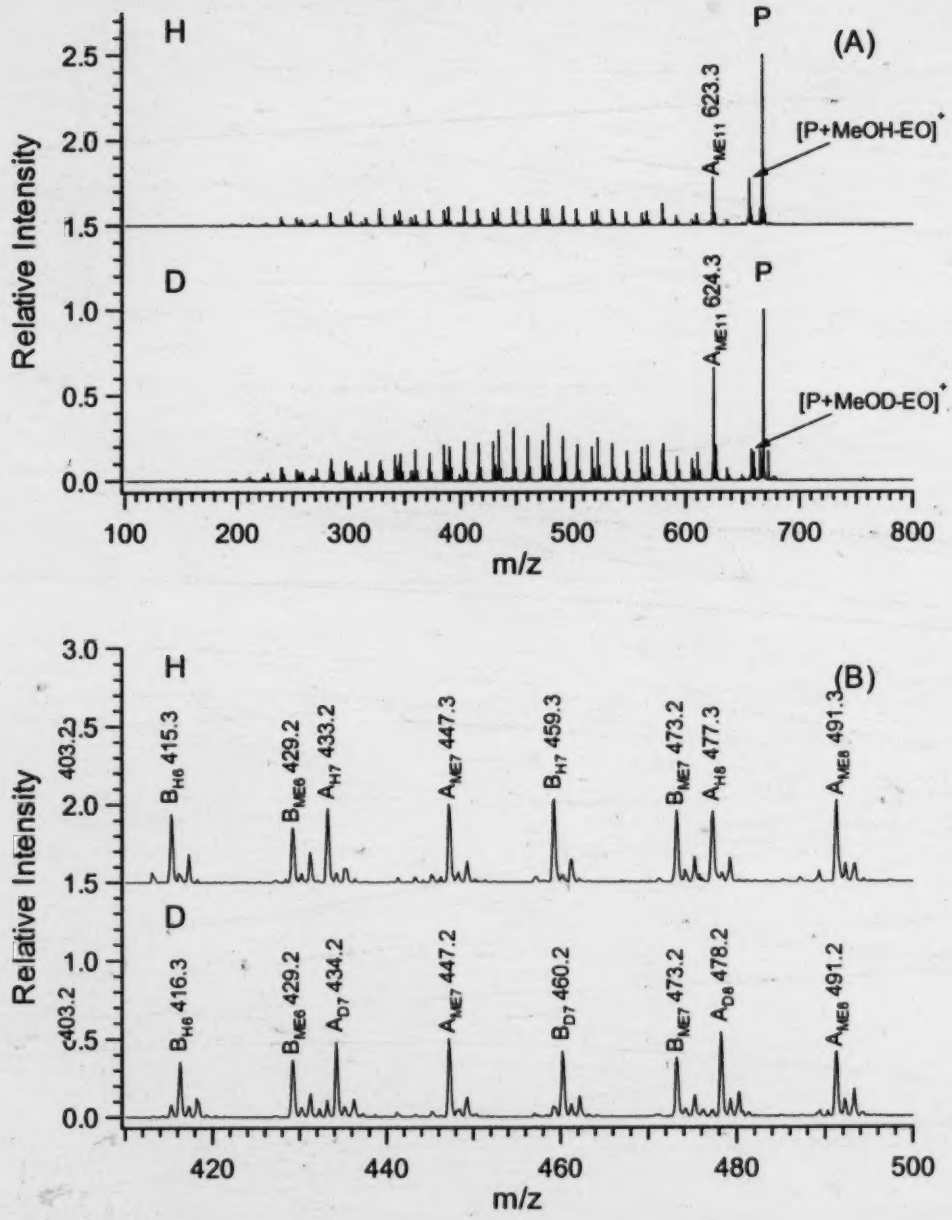

Figure 5.8. (A) ESI MS/MS spectra of argentinated PEG methyl ether 12-mer with and without D exchange. (B) Expanded spectra from (A). The peak annotations are according to Scheme 5.1.

The following fragmentation pathways (Scheme 5 and 6), much similar to those proposed by Lattimer [10, 14-17] for the fragmentation of lithiated PEGs, are seemingly able to offer a satisfactory interpretation of all the observations. All mass calculations are based on ^{107}Ag isotope. It is noted that the presentation of the argentinated PEG structure does not indicate the true position of the Ag^+, nor does it imply any charge-remote fragmentation nature.

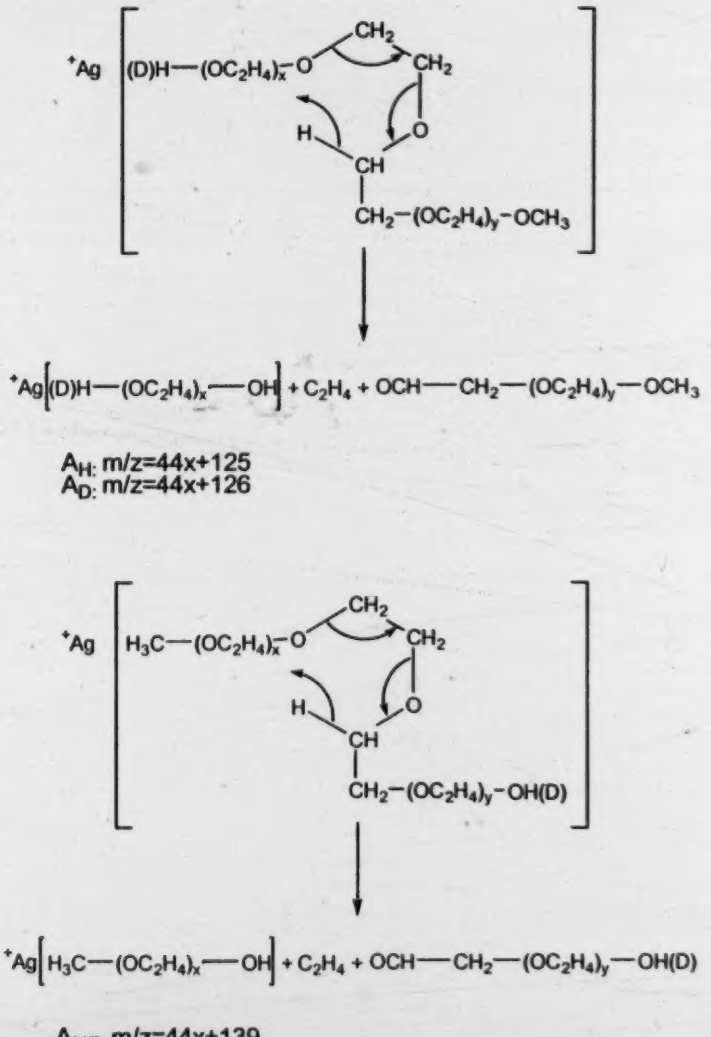

Scheme 5.5. Fragmentation pathways for the formation of A series ions using Ag^+.

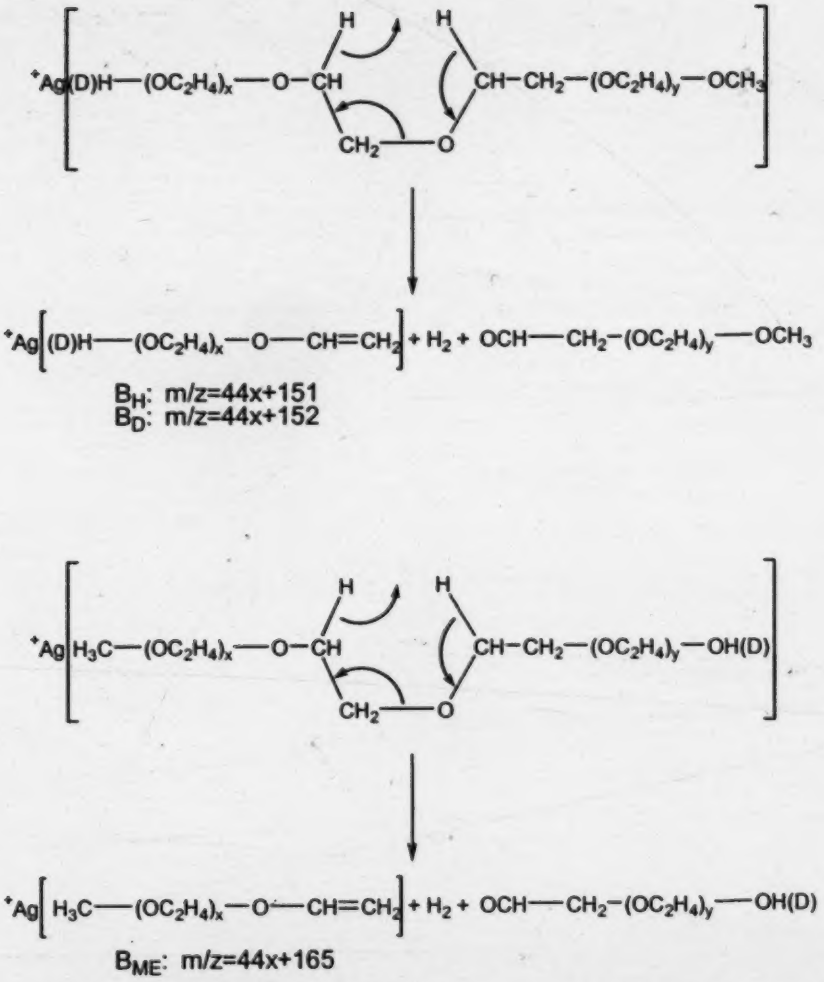

Scheme 5.6. Fragmentation pathways for the formation of B series ions using Ag^+.

The fragmentation difference between using Ag^+ and using divalent transition metal ions, such as Co^{2+}, Ni^{2+}, and Zn^{2+} employed in this study, lies in the ionization mechanism. In the previous section, it is shown that divalent transition metal ions ionize PEG methyl ether by forming a covalent bond. These metal ions are immobilized in the structure throughout the entire fragmentation process. Consequently, the probability of charge-initiated fragmentation is greatly reduced, as evidenced in the lack of $\mathbf{B_{ME}}$ ions in

Figure 5.4A, B, and C. Furthermore, the charge-remote fragmentation is also restricted, as the charge inductive effect will weaken as the distance increases. This explains the weak signal intensities of the $\mathbf{A_H}$ and $\mathbf{B_H}$ series ions distant from the charge site, but somewhat enhanced signal close to the charge site.

In the case of Ag^+, since ionization essentially takes place by attachment, there is no steric restriction for Ag^+ to access any oxygen atoms in the chain structure. Therefore, all series of ions possess similar intensities. The higher signal intensities in the middle of the spectrum are likely due to the formation of a more geometrically favorable intermediate, with two non-involving branches ($-(CH_2CH_2O)_x-$ and $-(CH_2CH_2O)_y-$ parts in Scheme 5.5 and 5.6) having equal or similar chain length.

Both Li^+ and Ag^+ have similar ionization mechanism; yet, the resulting MS/MS spectra are fairly different. The most perceptible difference is that Ag^+ adducts generate much more intense **B** ions. This is likely due to the formation of more stable **B** ions by silver attachment. For the B ion with a structure of $Ag[CH_2{=}CH\text{-}(OCH_2CH_2)_y\text{-}OH$ or $CH_3]^+$ (see Scheme 6), the silver ion can interact with the double bond via $d\text{-}\pi$ interaction to form a strong binding. In the case of lithium, only electrostatic interactions between the metal ion and the oxygen atoms occur.

The fragmentation pathway shown in Scheme 5.5 can also account for the 1 Da mass difference of the two types of $\mathbf{A_{ME11}}$ ions, with and without D replacement, by an extension of Scheme 5.5 to the hydroxyl end, as shown in Scheme 7. But the similar extension cannot be applied to Scheme 5.6. As a consequence, there are no $\mathbf{B_{ME11}}$ ions observed.

Poly(ethylene glycol) butyl ether (M_n ~1000) and poly(propylene glycol) butyl ether (M_n ~1100) were also examined by using silver ion as the cationization reagent. The ionization and fragmentation behavior of these two samples is similar to that of PEG methyl ether. In the MS/MS spectra (data not shown), the dominant fragment peaks are from the **A** and **B** series ions, as in the case of PEG methyl ether. No obvious steric hindrance effect on fragmentation from the butyl group is observed.

It is realized, however, that a thorough fragmentation mechanism determination would require a more scrutinized approach. It is difficult to pinpoint the origins of the observed product ions within current experimental frame. Nonetheless, the above discussion clearly indicates that H/D exchange in conjunction with MS/MS can serve as an effective means for fragmentation study, providing such isotope exchange could take place readily. Moreover, the ionization/fragmentation of PEGs by Ag^+ should have great implications in PEG structural elucidation. Some examples will be given in section 5.3.5.

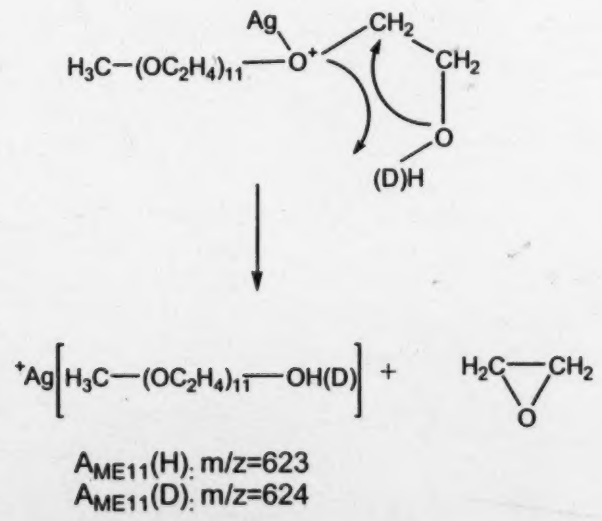

Scheme 5.7. Formation of two types of A_{ME11} ions using Ag^+.

5.3.5 Applications of Ag^+ Cationization: Fragmentation of Multiply Charged Adduct Ions from Polyglycols with Medium Molecular Mass.

One important attribute of ESI is the ability to generate multiply charged ions, which are found to be more readily dissociated compared to the singly charged ions [37]. Thus ESI tandem MS can potentially be very useful for determining structures of higher mass polymers that are not amendable to FAB or even MALDI MS/MS. Figure 5.9 illustrates the ESI mass spectrum of PPG using Ag^+ as the cationization reagent. There are two distributions. Judged by mass spacing, the lower m/z range (600-1000) is mainly composed of triply charged species while the higher m/z range (1000-1500) consists of mainly doubly charged species. No singly charged species were detected. The relative intensities between two charge states could be greatly affected by varying the instrumental parameters, such as the cone voltage and the trap drive in the ion trap mass spectrometer. Figure 5.9B shows the MS/MS spectrum of the doubly charged ions with m/z 1248.0. Two types of product ions can be identified: one with a series of doubly charged product ions (m/z lower than the parent ion, extending to m/z ~700); and a second with peaks outside the m/z region 700-1200 are clearly from singly charged product ions separated by 58 units. Structure information can be obtained by analyzing the low mass, singly charged products. Some of the peaks corresponding to the **A** series ions of PPG are labeled in Figure 5.9B. Figure 5.9C is the MS/MS spectrum of a triply charged ion at m/z=926.7. It bears a similar pattern to that of the doubly charged species, except that triply charged products are also found mixed with the doubly charged fragment ion products.

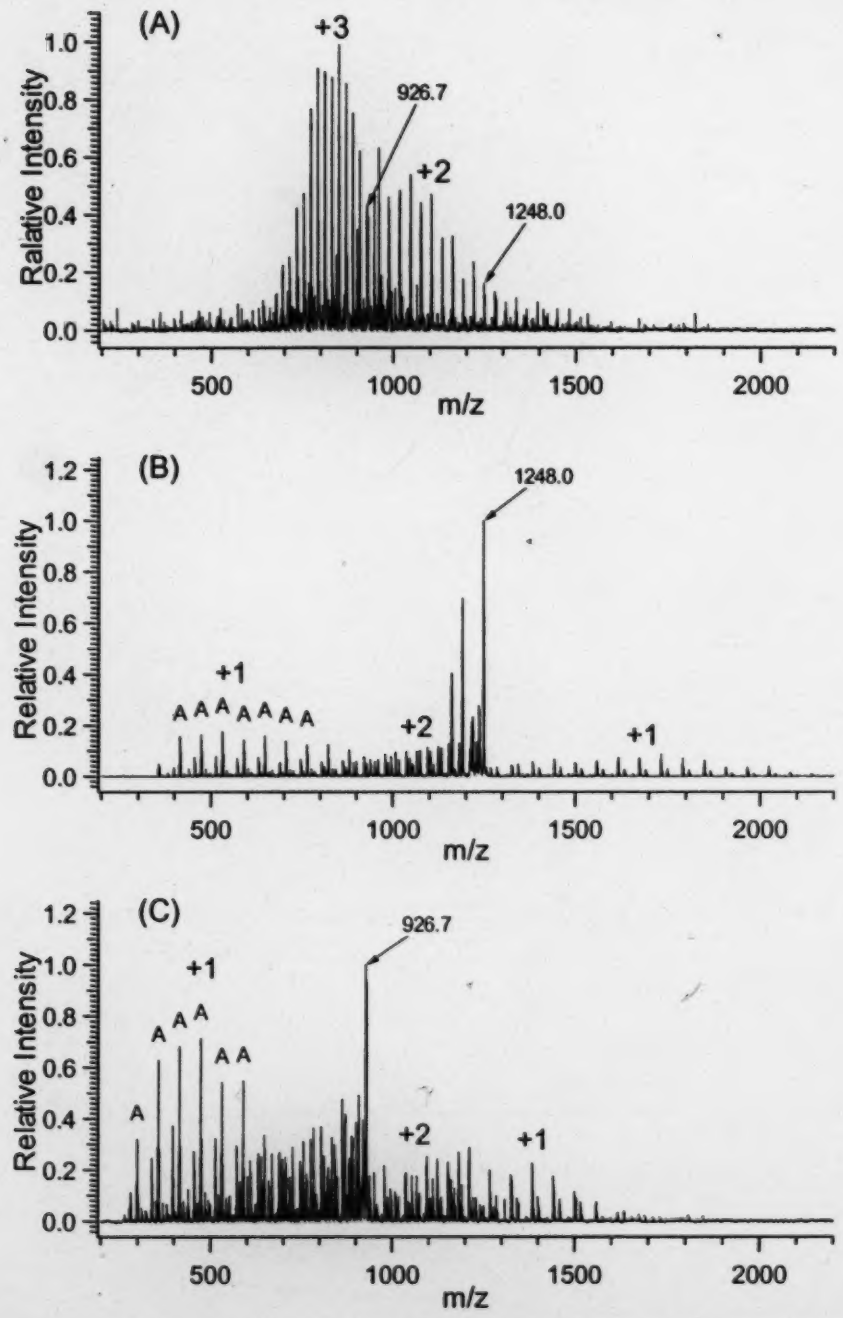

Figure 5.9. **(A) ESI mass spectrum of PPG 2000 obtained using Ag^+ as the cationization reagent. (B) ESI MS/MS spectrum of the doubly charged ion at m/z=1248.0. (C) ESI MS/MS spectrum of the triply charged ion at m/z=926.7.**

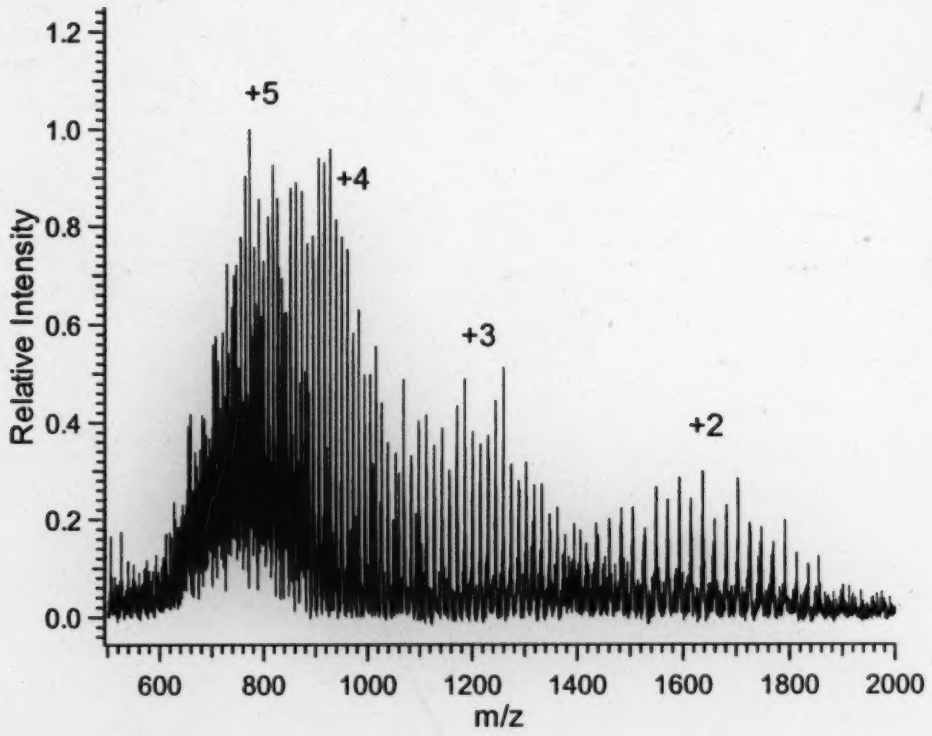

Figure 5.10. ESI mass spectrum of PEG 3350 obtained using Ag^+ as the cationization reagent.

Figures 5.10 and 5.11 show examples of using silver ion as cationization reagent for generating MS and MS/MS spectra of polyglycols with masses around 3000. Figure 5.10 is the MS spectrum of PEG 3350 displaying oligomer peaks with multiple charges from +2 to +5. Figure 5.11A shows the fragment spectrum of the triply charged ion at m/z~1171. Many charge stripping products and multiply charged fragment ion products are observed. The peak at m/z 1746 is likely due to an artifact associated with the ion trap instrument (i.e., leakage of ions during isolation and dissociation). Figure 5.11B shows the MS/MS spectrum from a +4 ion at m/z 927, displaying many fragment ions. Some of the peaks from the A and B series ions are labeled. Figure 5.11C shows the

fragment ion spectrum of the +5 ion at m/z 727. Extensive fragment ions resulting from the polymer chain dissociation are observed. Again, the peak at m/z 1230 in Figure 5.11B, and the peak at m/z 905 in Figure 5.13C are likely the leaked ions from the intact oligomer ions. For the +5 ion at m/z 727, there are five silver ions attached to the oligomer. Thus the oligomer mass is about 3100 Da. Further attempts to produce fragment ion spectra of polyglycols with molecular weights above 4000 have failed to give any meaningful results. It is found that the ESI spectra for the higher mass polyglycols are very complex. Isolation of a single oligomer ion is difficult with the current ion trap instrument. Further investigation should focus on how experimental parameters affect the mass range assessable for MS/MS.

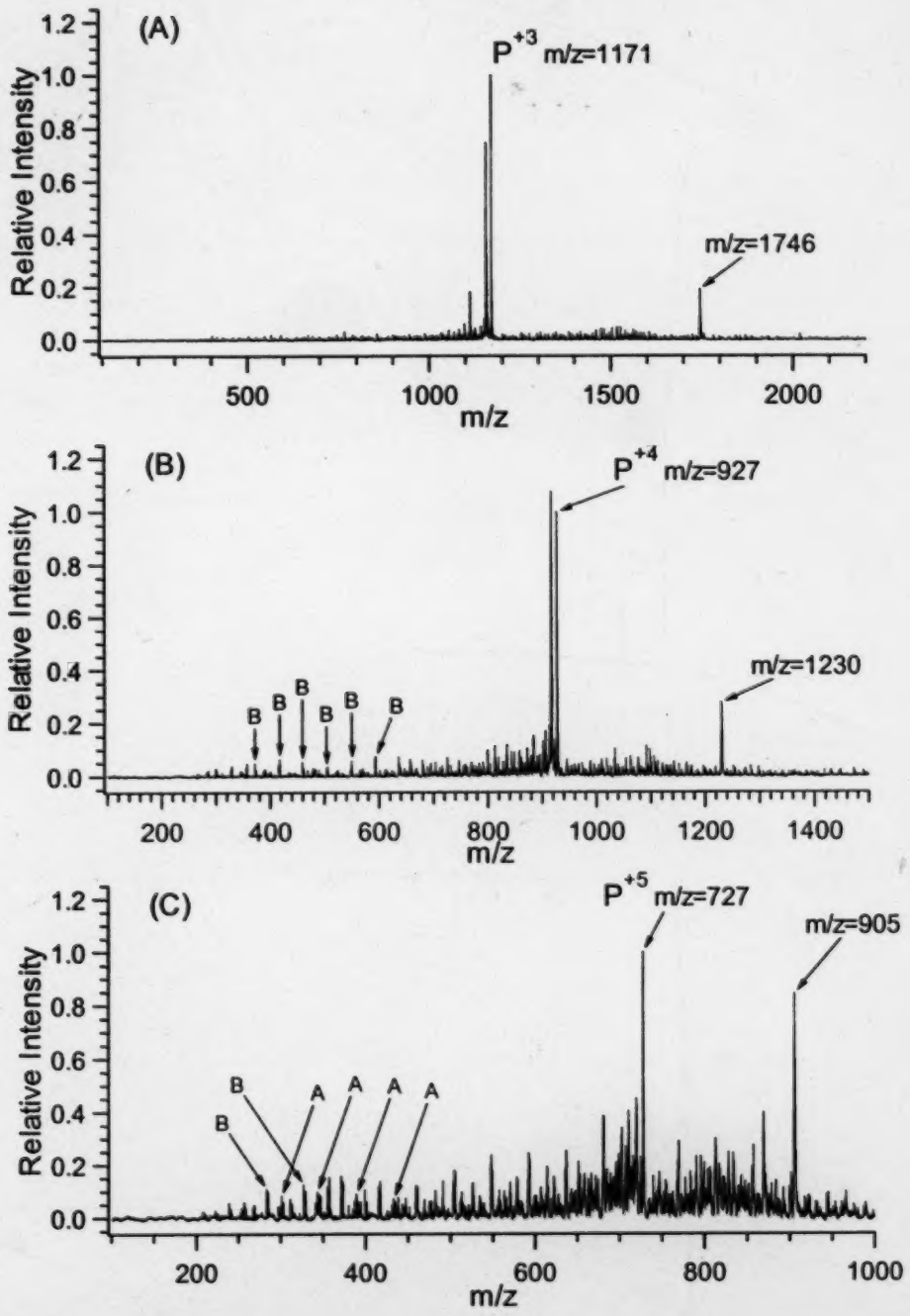

Figure 5.11. ESI MS/MS spectra of PEG 3350 with Ag^+ as the cationization reagent: (A) from +3 ion at m/z=1746, (B) from +4 ion at m/z=927, and (C) from +5 ion at m/z=727.

5.3.6 Copolymer analysis by ESI MS/MS

5.3.6.1 Introduction

Sequencing monomer distributions, determining composition of copolymers, and relating them to material properties are among the most common demands posed to polymer analysts. Because synthetic copolymers are such complex mixtures of oligomers with varying chain lengths and monomer arrangements, only an average sequence length can be defined [66].

In conjunction with chain statistics, both NMR [67] and MS [66, 68] can provide accesses to determine copolymer sequence by associating peak intensities to chain statistics quantities reflecting co-monomer composition and arrangement. Various models corresponding to various copolymerization methods have been developed with varying extent of success. Briefly, a Bernoullian distribution describes a complete random copolymer where all the co-monomers enjoy the same probability of being added to the growing chain; and a Markoffian distribution describes block or segmented copolymers where the probability of being added to the growing chain is in favor of one of the co-monomers.

Of particular interest are two MS based methods that are frequently used for copolymer sequence determination. The "statistics" approach is essentially accomplished by fitting experimental spectra with those derived from different distribution models. This approach requires information from synthesis *a priori* to select valid models, and as such, tends to be problematic when dealing with unknown samples. In the "composition estimates" approach, one calculates co-monomer ratio, and observes its variation with chain size to determine copolymer homogeneity (e.g., block *vs.* random). One key step in

this approach is to identify an individual copolymer constituent by mass fitting. The commonly employed mathematical practice is error-prone, when the copolymer under investigation possesses more than one type of end group. Different combinations of co-monomers, as well as end groups, could result in the same nominal mass value. Obviously, a complementary method to confirm the mass assignment is therefore necessary in order to generate an unambiguous peak table.

To demonstrate the utility of the previously described method to generate low energy CID spectra in an ion trap mass spectrometer, two applications in the area of copolymer analysis are presented in the following section. In the first application, it is demonstrated that copolymer with similar structure but different homogeneity (block vs. random) can be easily differentiated by a simple MS/MS experiment, therefore providing valuable information for subsequent sequence analysis without knowledge *a priori*. The second application deals with *de novo* sequencing of a model block copolymer. Note that the term sequencing adheres to its conventional definition as to decode the co-monomer arrangement for one specific copolymer chain, rather than its average sense often referred to in copolymer analysis. However, the information generated therein provides essential composition information required in the "composition estimate" approach with enhanced confidence.

5.3.6.2 Copolymer Differentiation: Block *vs.* Random.

Figure 5.12 and 5.13 are the mass spectra of a block copolymer and a random copolymer with similar average molecular mass, respectively. The ESI mass spectra of two samples bear great resemblance. One repeat pattern of peaks (Figure 5.12B and

5.13B) of each sample is comprised of four major peaks, representing different EO and PO compositions. No additional structural information can be derived from these spectra.

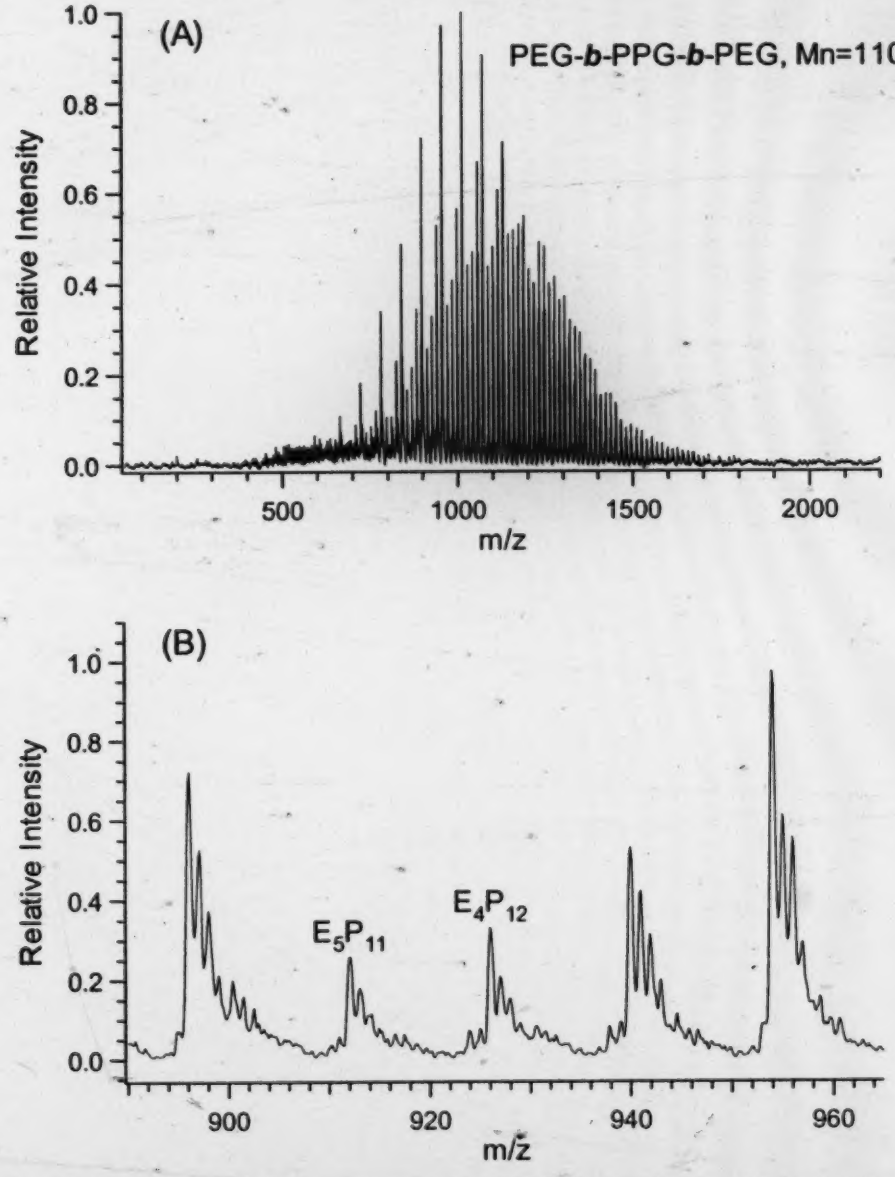

Figure 5.12. (A) ESI mass spectrum of a tri-block copolymer obtained using Li^+ as cationization reagent. (B) Expanded spectrum of (A) showing a repeat pattern of peaks with corresponding peak assignments.

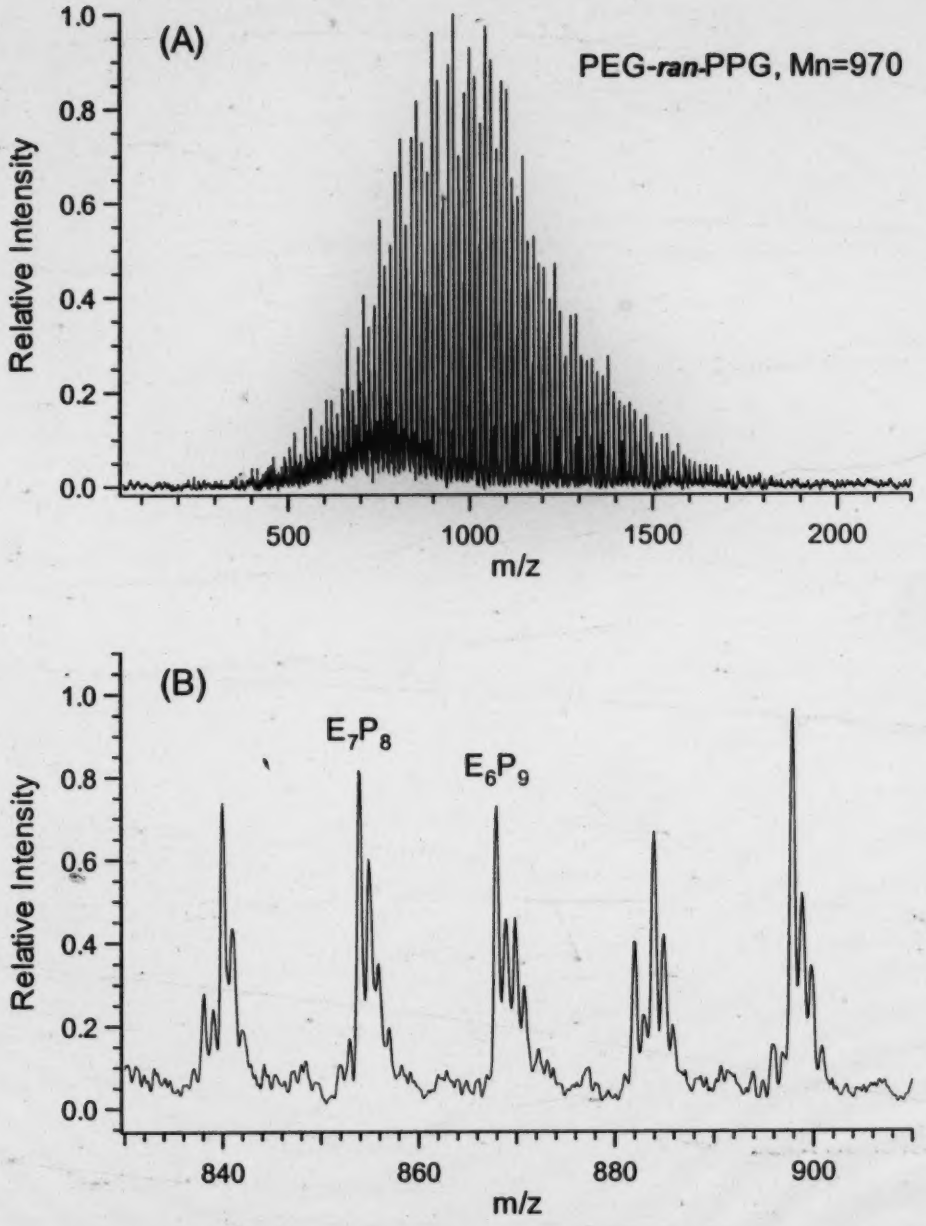

Figure 5.13. (A) ESI mass spectrum of a random copolymer obtained using Li^+ as cationization reagent. (B) Expanded spectrum of (A) showing a repeat pattern of peaks with corresponding peak assignments.

Figure 5.14 shows the MS/MS spectra of the block and random copolymers obtained using Li^+ as the cationization reagent. MS/MS of the block copolymer (Figure 5.14A) generates a simple spectrum with dominant **A** series ions. In sharp contrast, MS/MS of the random copolymer (Figure 5.14B) results in a much more complicated spectrum. This difference in spectral appearance can be related to the homogeneity difference between two copolymers. For the block copolymer, one peak in the mass spectrum only represents one type of copolymer chain with defined EO/PO composition and arrangement, whereas one peak for a random copolymer could represent multiple isobaric species, i.e., those with same EO/PO composition but different spatial arrangement. For example, a totally random copolymer with nominal formula E_2P_2 could have as many as 4 types of spatial arrangements, EEPP, EPEP, EPPE, and PEEP. Under low energy CID conditions, each individual chain with identical m/z will undergo fragmentation, and contributes to the ensuing MS/MS spectrum collectively. The superimposition of different fragmentation spectra results in a complicated MS/MS spectrum. The interpretation of such MS/MS spectrum is not trivial. Nonetheless, the above results clearly exemplify that low energy CID spectra generated by using Li^+ can be used to rapidly and unequivocally differentiate random and block copolymers that are indistinguishable by many traditional methods. Such information can be used as *a priori* knowledge for further composition and sequence analysis by MS. This is especially advantageous for sequence and composition analysis of unknown copolymers.

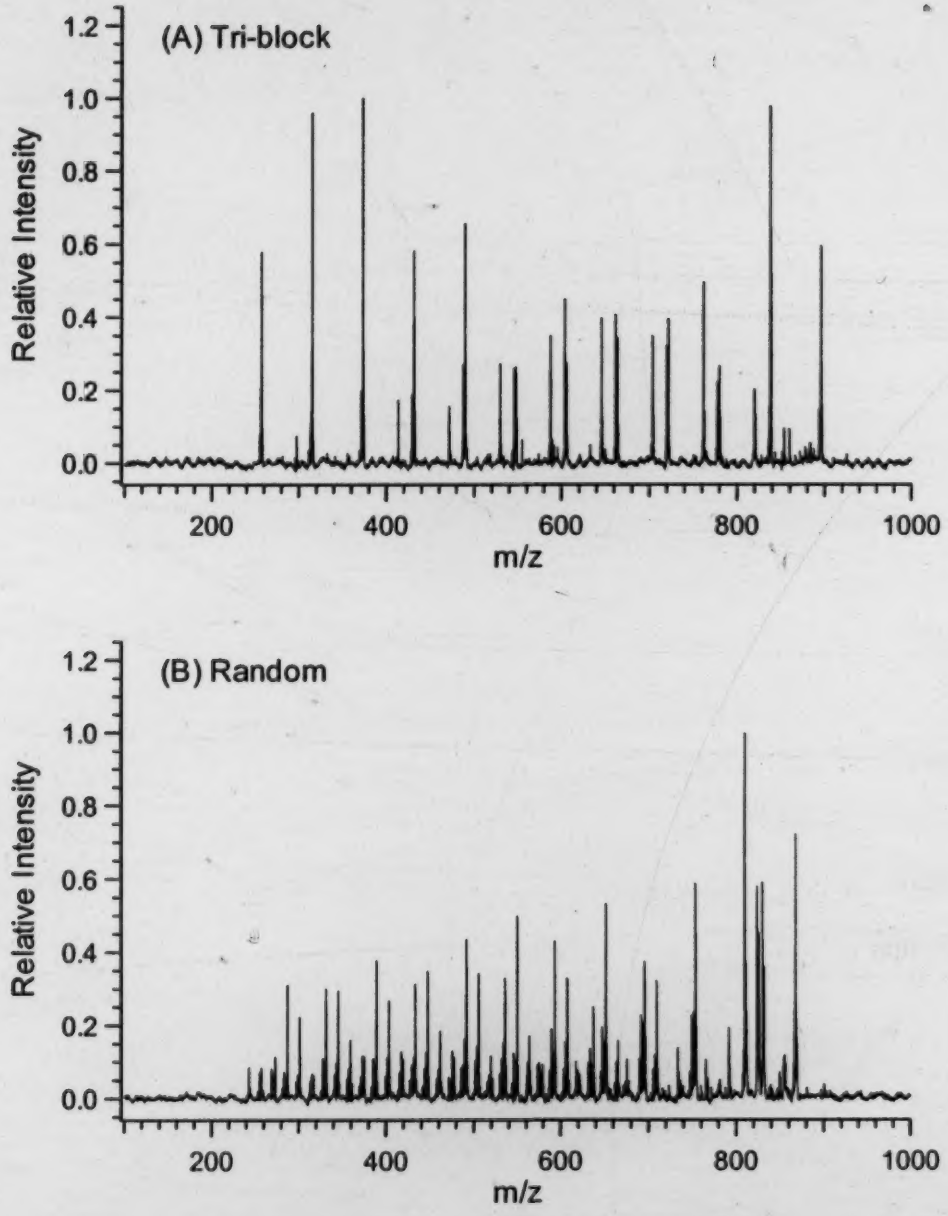

Figure 5.14. ESI MS/MS spectra of (A) block and (B) random EO/PO copolymers obtained using Li^+ as the cationization reagent.

5.3.6.3 Sequencing of EO/PO Copolymers: A Model System.

Figure 5.15 is the ESI mass spectrum of tri-propylene oxide methyl ether ethoxylates (TPM) obtained using Li^+ as the cationization reagent. The spectrum displays the typical PEG mass distributions with adjacent peaks separated by 44 Da, corresponding to the mass of the EO unit. The minor distribution, 16 Da apart from the main one, is the result of sodium attachment.

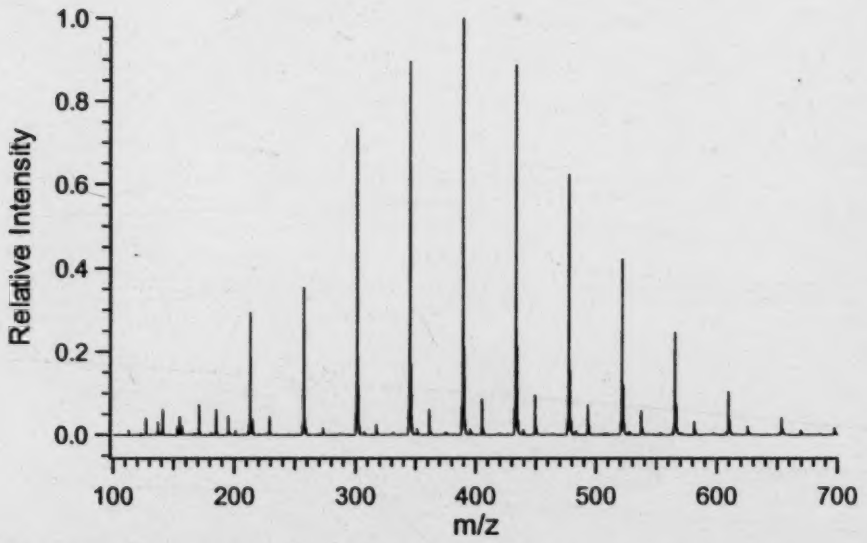

Figure 5.15. ESI MS spectrum of block copolymer TPM from Dow Chemical Canada obtained using Li^+ as the cationization reagent.

It is established from sections 5.3.1 and 5.3.2 that, Li^+ along with many transition metal ions, enable low energy CID of polyglycols. Among which, Li^+ and Co^{2+} were selected for the sequencing study. Both selected cation have relatively high ionization efficiency that ensures the generation of high quality MS/MS spectra. Moreover, the ensuing MS/MS spectra are relatively simple and easy to interpret without sacrificing

sequence coverage, as shown in Figure 5.16 and 5.17. Lithiated PEG ions almost exclusively generates A_H type ions, and PEG cobalt adduct ions preferentially generates A ions.

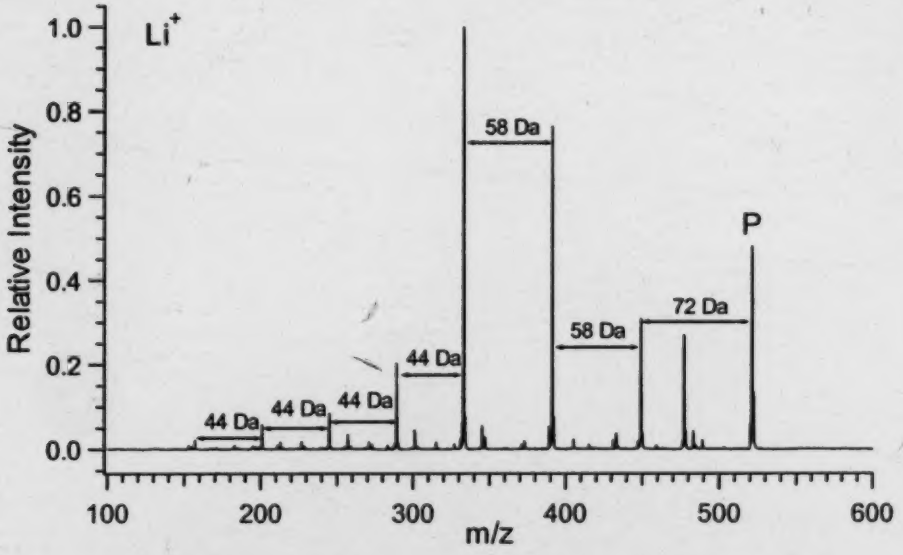

Figure 5.16. ESI MS/MS spectrum of one lithiated TPM oligomer.

Figure 5.16 is the ESI MS/MS spectrum of lithiated oligomer $CH_3O\text{-}PO_3\text{-}EO_7\text{-}H$. The dominant product ions are the A_H series with one intense A_{ME} peak at m/z=477, meaning principal fragmentations are initiated from the PO end of the oligomer. Part of the fragmentation pathway is illustrated in Scheme 5.8.

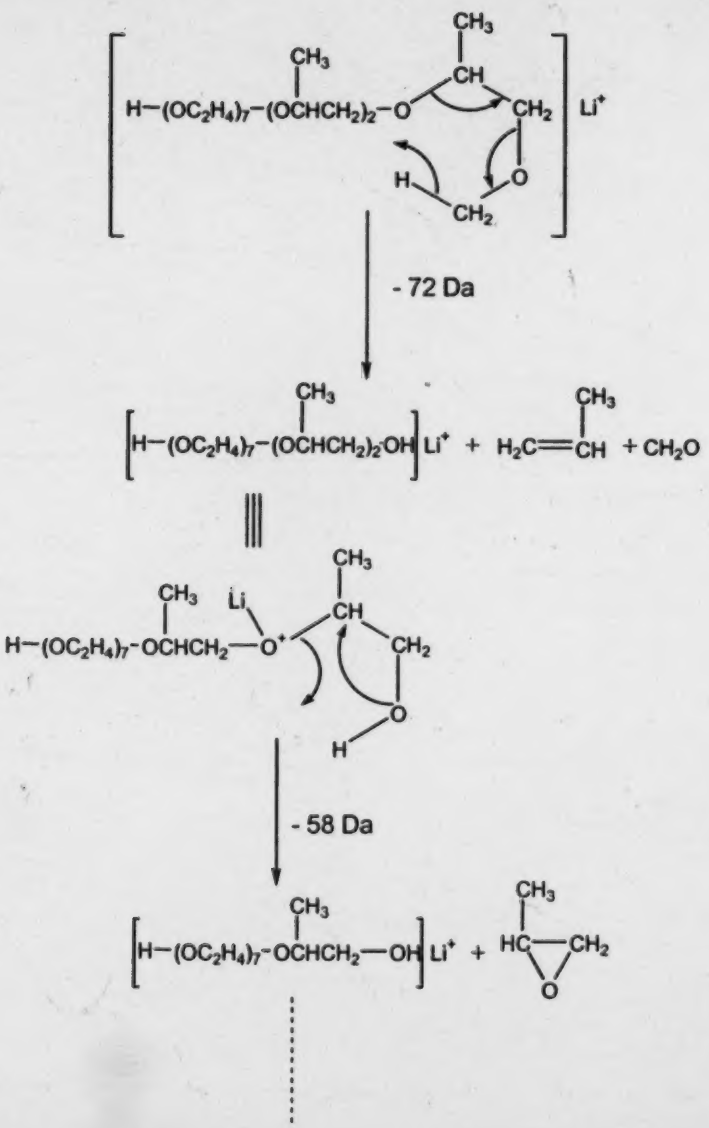

Scheme 5.8. Partial fragmentation pathway for the lithiated CH_3O-PO_3-EO_7-H oligomer.

A partial sequence, with 3 EO units still missing, can be derived from Figure 5.16. The lack of low mass fragments (m/z below ~150) is commonly encountered in low energy CID due to its low energy nature. One solution is to use heavy metal ions, such as Ag^+, to shift the product ions to higher mass. The trade-off of this approach in this

particular case is that resulting spectrum is too complicated to interpret, because silver adduct ions generates all four series of product ions (Chapter 5.3.4). Another solution is to generate product ions from both ends of the polymer chain, as in the case of using Co^{2+} as the cationization reagent (Figure 5.17). For clarity, Figure 5.17A and B are the same spectrum, but with different labels to demonstrate two different fragment ion series. Series α is A_{ME} type of ions, initiated from hydroxyl end (EO end); and series ω are A_H type of ions, initiated from the methoxyl end (PO end). Both α and ω series generate partial sequences starting from different ends and have a great extent of overlapping in the middle segment, as shown below. Thus, a complete sequence of the copolymer is obtained.

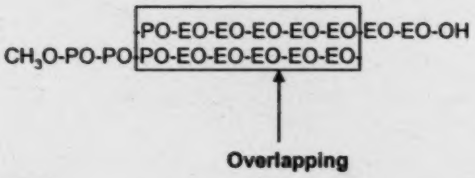

It is interesting to note that the fragmentation behavior of model copolymer TPM is somewhat different than that from its homopolymer counterpart, PEGME. For PEGME, using Li^+ generates both A_H and A_{ME} ions and using Co^{2+} mainly generates A_{ME} ions. For TPM, the trend is totally the opposite. Whether it is coincidence or it is caused by the increased heterogeneity due to the addition of 3 PO units requires more investigation. Nevertheless, it is shown that with proper choice of cations, the fragmentation can be maneuvered towards a desired pathway, from which complete sequence information can be retrieved. The methodology demonstrated herein should have general applicability in tackling similar problems.

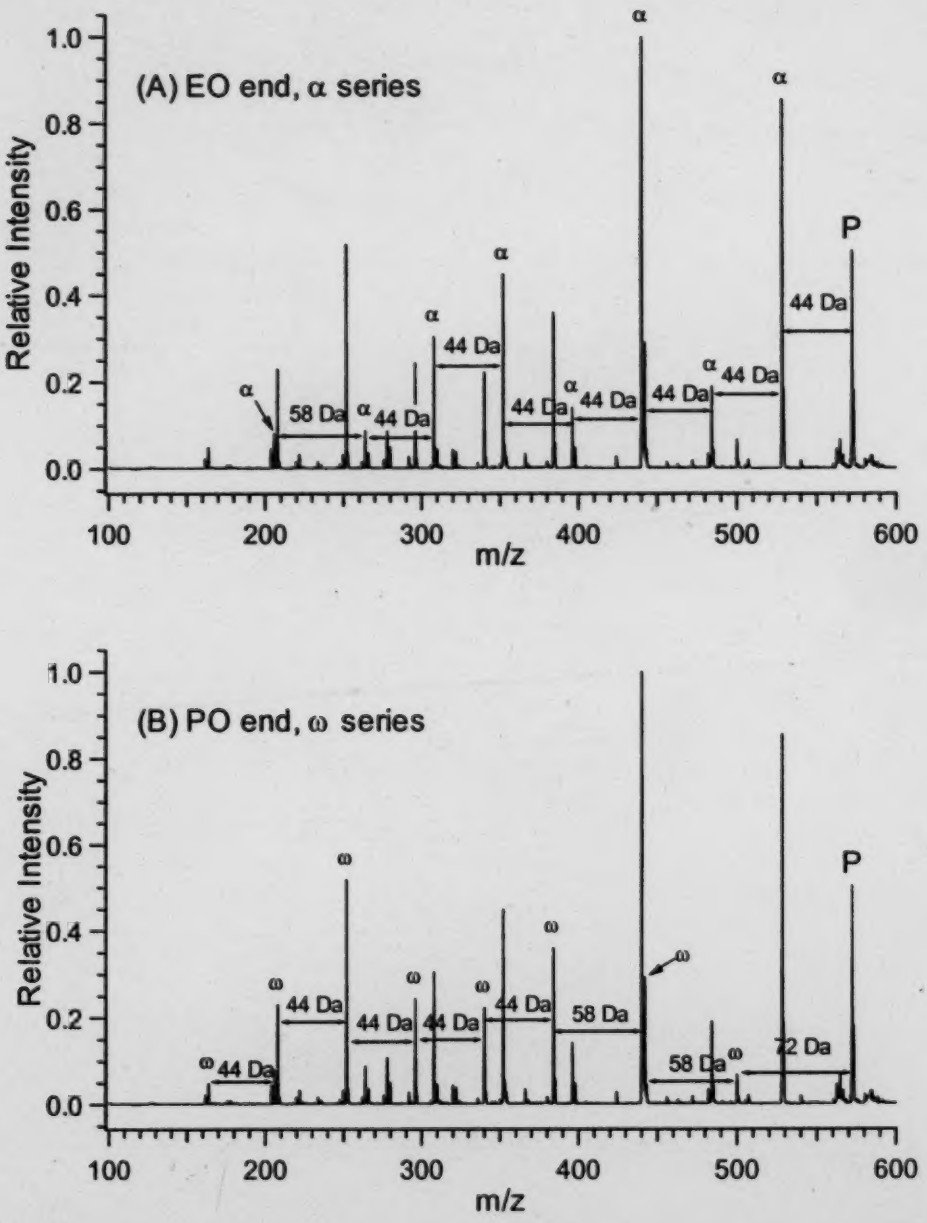

Figure 5.17. ESI MS/MS spectrum of the same oligomer shown in Figure 5.16 obtained by using Co^{2+} as the cationization reagent. Peaks labeled as α (A) are the product ions from the cleavages initiated from EO end, and ω (B) are from the PO end.

5.4 Summary

Electrospray ionization tandem mass spectrometry has the potential to be widely used as a tool for polymer structural characterization. However, the backbones or molecular chains of many industrial polymers including functional polyglycols are often difficult to dissociate in tandem mass spectrometers using low energy collision-induced dissociation (CID). A method that uses Li^+ and transition metal ions such as Ag^+ as the cationization reagents to generate low energy CID spectra of polyglycols in an ion trap mass spectrometer is presented. It is shown that lithium and transition metal polyglycol adduct ions can be readily fragmented with low energy CID. Comparative results from different cationization reagents and their abilities to produce both MS spectra and CID spectra are shown. In conjunction with H/D exchange, a fragmentation mechanism can be deduced. It is also found that when using divalent transition metal ions such as Co^{2+}, the counter ions play an active role in the ionization as well as the subsequent fragmentation. Finally, the utility of the methodology is demonstrated in the copolymer analysis. It is shown that a random copolymer and block copolymer can be easily differentiated using their low energy CID spectra. In another application, it is demonstrated that with proper choice of cations, a complete sequence of a block copolymer can be obtained. This method will offer the possibility of using conventional and readily available low energy CID tandem MS to study polyglycol structures.

5.5 Literatures Cited

1. Busch, K. L.; Glish, G. L.; McLuckey, S. A. *Mass Spectrometry/Mass Spectrometry*, VCH Publishers: New York, **1988**.
2. Tou, J. C.; Zakett, D.; Caldecourt, V. J. *Tandem Mass Spectrometry*, McLafferty, F. W. Ed. Wiley, New York, **1984**.
3. Lyon, P. A.; Stebbings, W. L.; Crow, F. W.; Tomer, K. B.; Lippstreu, D. L.; Gross, M. L. *Anal. Chem.* **1984**, 56, 8.
4. Lyon, P. A.; Crow, F. W.; Tomer, K. B.; Gross, M. L. *Anal. Chem.* **1984**, 56, 2278.
5. Catlow, D. A.; Johnson, M.; Monaghan, J. J.; Porter, C.; Scrivens, J. H. *J. Chromatogr.* **1985**, 328, 167.
6. Craig, A. G.; Derrick, P. J. *J. Chem. Soc., Chem. Commun.* **1985**, 891.
7. Craig, A. G.; Derrick, P. J. *J. Am. Chem. Soc.* **1985**, 107, 6707.
8. Ballistreri, A.; Garozzo, D.; Giuffrida, M.; Montaudo, G.; Filippi, A.; Guaita, C.; Manaresi, P.; Pilati, F. *Macromolecules* **1987**, 20, 1029.
9. Kiplinger, J. P.; Bursey, M. M. *Org. Mass Spectrom.* **1988**, 23, 342.
10. Lattimer, R. P.; Munster, H.; Budzikiewicz, H. *Int. J. Mass Spectrom. Ion Proc.* **1989**, *90*, 119.
11. Ventura, F.; Fraisse, D.; Caixach, J.; Rivera, J. *Anal. Chem.* **1991**, 63, 2095.
12. Maleknia, S.; Liou, C. C.; Brodbelt, J. *Org. Mass Spectrom.* **1991**, 26, 997.
13. Kalinoski, H. T.; Hargiss, L. O. *J. Am. Soc. Mass Spectrom.* **1992**, 3, 150.
14. Lattimer, R. P. *J. Am. Soc. Mass Spectrom.* **1992**, 3, 225.
15. Lattimer, R. P. *Int. J. Mass Spectrom. Ion Proc.* **1992**, 116, 24.

16. Lattimer, R. P. *J. Am. Soc. Mass Spectrom.* **1994**, 5, 1072.

17. Selby, T. L.; Wesdemiotis, C.; Lattimer, R. P. *J. Am. Soc. Mass Spectrom.* **1994**, 5, 1081.

18. Jackson, A. T.; Yates, H. T.; Scrivens, J. H.; Critchley, G.; Brown, J.; Green, M. R.; Bateman, R. H. *Rapid Commun. Mass Spectrom.* **1996**, 10, 1668.

19. Jackson, A. T.; Yates, H. T.; MacDonald, W. A.; Scrivens, J. H.; Critchley, G.; Brown, J.; Deery, M. J.; Jennings, K. R.; Brookes, C. *J. Am. Soc. Mass Spectrom.* **1997**, 8, 132.

20. Scrivens, J. H.; Jackson, A. T.; Yates, H. T.; Green, M. R.; Critchley, G.; Brown, J.; Bateman, R. H.; Bowers, M. T.; Gidden, J. *Int. J. Mass Spectrom. Ion Proc.* **1997**, 165/166, 364.

21. Bottrill, A. R.; Giannakopulos, A. E.; Waterson, C.; Haddleton, D. M.; Lee, K. S.; Derrick, P. J. *Anal. Chem.* **1999**, 71, 3637.

22. Pastor, S. J.; Wilkins, C. L. *Int. J. Mass Spectrom. Ion Proc.* **1998**, 175, 81.

23. Hunt, S. M.; Binns, M. S.; Sheil, M. M. *J. Appl. Polym. Sci.* **1995**, 56, 1589.

24. McEwen, C. N.; Simonsick, W. J., Jr.; Larsen, B. S.; Ute, K.; Hatada, K. *J. Am. Soc. Mass Spectrom.* **1995**, 6, 906.

25. Mahon, A.; Kemp, T. J.; Buzy, A.; Jennings, K. R. *Polymer*, **1996**, 37, 531.

26. Hunt, S. M.; Sheil, M. M.; Belov, M.; Derrick, P. J. *Anal. Chem.* **1998**, 70, 1812.

27. Yalcin, T.; Gabryelski, W.; Li, L. *Proceedings of the 46th ASMS Conference on Mass Spectrometry and Allied Topics*, Orlando, FL, May 31-June 4, **1998**; p1054.

28. Yalcin, T.; Gabryelski, W.; Li, L. *Anal. Chem.* **2000**, 72, 3847.

29. Adamus, G.; Kowalczuk, M. *Rapid Commun. Mass Spectrom.* **2000**, 14, 195.

30. Mowat, I. A.; Donovan, R. J.; Maier, R. R. J. *Rapid Commun. Mass Spectrom.* **1997**, 11, 89.

31. Varney J. E.; Derrick, P. J.; Szilagyi, Z.; Vekey, K. *Proceedings of the 45th ASMS Conference on Mass Spectrometry and Allied Topics,* Palm Spring, CA, June 1-5, **1997**; p317.

32. Kowalski, P.; Guttman, C.; Wallace, W. *Proceedings of the 46th ASMS Conference on Mass Spectrometry and Allied Topics,* Orlando, FL, May 31-June 4, **1998**; p1060.

33. Puapaiboon, U.; Taylor, R. T.; Jai-nhuknan, J. *Rapid Commun. Mass Spectrom.* **1999**, 13, 516.

34. *Poly(ethylene glycol) Chemistry: Biotechnical and Biomedical Applications:* Harris, J.M., Ed.; Plenum Press: New York, **1992**.

35. Roberts, M.; Scholes, D. F.; Karsa, D. R. *Chemical Aspects of Drug Delivery Systems*. Stephenson, R. A. Eds.; The Royal Society of Chemistry: Cambridge, **1996**; p89.

36. Fenn, J. B.; Mann, M.; Meng, C. K.; Wong, S. F.; Whitehouse, C. M. *Science* **1989**, 24, 64.

37. Smith, R. D.; Loo, J. A.; Orgorzalek-Loo, R. R.; Busman, M.; Udseth, H. R. *Mass Spectrom. Rev.* **1991**, 10, 359.

38. Nohmi, T.; Fenn, J. B. *J. Am. Chem. Soc.* **1992**, 114, 3241.

39. Kallos, G. J., Tomalia, D. A.; Hedstrand, D. M.; Lewis, S.; Zhou, J. *Rapid Commun. Mass Spectrom.* **1991**, 5, 384.

40. Prokai, L.; Simonsick, W. J., Jr. *Rapid Commun. Mass Spectrom.* **1993**, 7, 854.

41. Sherrard, K. B.; Marriott, P. J.; McCormick, M. J.; Colton, R.; Smith, G. *Anal. Chem.* **1994**, 66, 3394.

42. Hunt, S. M.; Binns, M. S.; Sheil, M. M. *J. Appl. Polym. Sci.* **1995**, 56, 1589.

43. O'Connor, P. B.; McLafferty, F. W. *J. Am. Chem. Soc.* **1995**, 117, 12826.

44. Crescenzi, C.; Di Corcia, A.; Samperi, R.; Marcomini, A. *Anal. Chem.* **1995**, 67, 1797.

45. Ogura, I.; DuVal, D. L.; Kawakami, S.; Miyajima, K. *J. Am. Oil Chem. Soc.* **1996**, 73, 137.

46. Mahon, A.; Kemp, T. J.; Buzy, A.; Jennings, K. R. *Polymer* **1996**, 37, 531.

47. Cumme, G. A.; Blume, E.; Bublitz, R.; Hoppe, H.; Horn, A. *J. Chromatogr. A* **1997**, 791, 245.

48. Crowther, M. W.; O'Connell, T. R.; Carter, S. P. *J Am. Oil Chem. Soc.* **1998**, 75, 1867.

49. Parees, D. M.; Hanton, S. D.; Cornelio Clark, P. A.; Willcox, D. A. *J. Am. Soc. Mass Spectrom.* **1998**, 9, 282.

50. Van Rooij, G. J.; Duursma, M. C.; de Koster, C. G.; Heeren, R. M. A.; Boon, J. J.; Wijnand Schuyl, P. J.; van der Hage, E. R. E. *Anal. Chem.* **1998**, 70, 844.

51. Willetts, M.; Clench, M. R.; Greenwood, R.; Mills, G.; Carolan, V. *Rapid Commun. Mass Spectrom.* **1999**, 13, 251.

52. Stolarzewicz, A.; Neugebauer, D.; Silberring, J. *Rapid Commun. Mass Spectrom.* **1999**, 13, 2469.

53. Castillo, M.; Alonso, M. C.; Riu, J.; Barcelo, D. *Environ. Sci. Technol.* **1999**, 33, 1300.

54. Nielen, M. W.; Buijtenhuijs, F. A. *Anal. Chem.* **1999**, 71, 1809.

55. von Helden, G.; Wyttenbach, T.; Bowers, M. T. *Science* **1995**, 267, 1484.

56. von Helden, G.; Wyttenbach, T.; Bowers, M. T. *Int. J. Mass Spectrom. Ion Proc.* **1995**, 146/147, 349.

57. Wyttenbach, T.; von Helden, G.; Bowers, M. T. *Int. J. Mass Spectrom. Ion Proc.* **1997**, 165/166, 377.

58. Adams, J.; Gross, M. L. *J. Am. Chem. Soc.* **1986**, 108, 6915.

59. Adams, J. *Mass Spectrom. Rev.* **1990**, 9, 141.

60. Leary, J. A.; Zhou, Z.; Ogden, S. A.; Williams, T. D. *J. Am. Soc. Mass Spectrom.* **1990**, 1, 474.

61. Zenobi, R.; Knochenmuss, R. *Mass Spectrom. Rev.* **1998**, 17, 337.

62. Deery, M. J.; Jennings, K. R.; Jasieczek, C. B.; Haddleton, D. M.; Jackson, A. T.; Yates, H. T.; Scrivens, J. H. *Rapid Commun. Mass Spectrom.* **1997**, 11, 57.

63. Vachet, R. W.; Callahan, J. H. *J. Mass Spectrom.* **2000**, 35, 311.

64. Colton, R.; D'Agstino, A.; Traeger J. C. *Mass Spectrom. Rev.* **1995**, 14, 79.

65. Jasieczek, C. B.; Buzy, A.; Haddleton, D. M.; Jennings, K. R. *Rapid Commun. Mass Spectrom.* **1996**, 10, 509.

66. Montaudo, G.; Lattimer, R. P. *Mass Spectrometry of Polymers*, CRC Press LLC: New York, **2002**.

67. Randall, J. C. *Polymer Sequences Determination*, Academic Press: New York, **1977**.

68. Montaudo, M. S. *Macromol. Symp.* **1999**, 141, 95.

69. Fenn, J. B.; Mann, M.; Meng, C. K.; Wong, S. F. *Mass Spectrom. Rev.* **1990**, 9, 37.

70. Hoberg, A-M.; Haddeleton, D. M.; Derrick, P. J. *Proc. 46th ASMS Conf. Mass Spectrom. Allied Topics*, Orlando, FL. **1998**, p1075.

Chapter 6. Characterization of Poly(Ethylene Glycol) Esters Using Low Energy Collision-Induced Dissociation in Electrospray Ionization Mass Spectrometry

As part of a continuous effort on developing MS/MS based structure characterization strategy for functional polyglycols, this chapter deals with another class of industrially important polyglycols, namely, polyglycol esters. These results are summarized into a separate chapter since the fragmentation behavior of polyglycol esters was found to be substantially different from that of polyglycol ethers (Chapter 5). In the case of polyglycol ethers, fragmentation mostly takes place along the polymer chain due to the similar chemical nature of the linkages between end-group and repeating units and those between adjacent repeating units (i.e., all ethereal bonds). In the case of polyglycol esters, however, the end group moiety is linked to the polymer chain via a much weaker ester bond, which allows much of the fragmentation to take place at the vicinity of the end group moiety. It is found that the fragmentation pattern of an ionic polyglycol ester oligomer generated by low-energy collision-induced dissociation is strongly dependent on the type of cation used for ionization. It is shown that structural information for the polymer chain and end-groups is best obtained by examining the fragment ion spectra of oligomers ionized by ammonium, alkali, and transition metal ions.

A form of this chapter has been accepted for publication:
R. Chen, X. Yu, and L. Li, "Characterization of poly(ethylene glycol) esters using low energy collision-induced dissociation in electrospray ionization mass spectrometry", *J. Am. Soc. Mass Spectrom.* **2002.**

6.1 Introduction

Tandem mass spectrometry using either matrix-assisted laser desorption ionization (MALDI) or electrospray ionization (ESI) is being developed as a tool for polymer structural characterization [1-16]. This research group has been particularly interested in characterizing functional polyglycols, including poly(ethylene glycol) (PEG), poly(propylene glycol) (PPG) and their copolymers [12-19]. Structural characterization of this type of polymer is important, because polyglycols are widely used in industry and their properties strongly depending on not only average molecular masses, but also on their structure and composition. Recently, polyglycols have also been increasingly used in biotechnical and biomedical applications such as the development of slow releasing drugs [20,21]. Traditionally, polyglycols were thought to be difficult to fragment in low-energy CID tandem MS. In Chapter 5, it was demonstrated that lithium and transition metal ions form adduct ions with polyglycol in ESI process, and these adduct ions readily undergo fragmentation. The resulting fragment ion spectra were very informative for the structural characterization of polyglycols. Chapter 5 focused on alcohol ethoxylates whose end-groups are linked to polyglycol chains via ether-type C-O bonds (i.e., polyglycol ethers). The results generated therein were compared to earlier studies by Latimer and coworkers [22-25] of the same type of polyglycols employing fast atom bombardment (FAB) MS/MS.

Poly(ethylene glycol) ester, especially fatty acid methyl ester ethoxylate (FAMEE), is another class of polyglycol, which can be used as an alternative to alcohol ethoxylates in many industrial applications. With varying alkyl chain lengths in the fatty acid moiety, a wide range of hydrophilic lipophilic balance (HLB) values can be achieved

to suit different applications [14]. FAMEE are extensively used as non-ionic bases for cosmetics and pharmaceuticals, non-ionic emulsifiers for vegetable and mineral oils, thickening agents for creams, anti-static agents for plastics, and non-ionic surfactants. Despite active MS study on alcohol ethoxylates [12-15, 17-19, 22-62], current literature on ester ethoxylates is scarce [5,16].

In this chapter, a method of generating low energy CID mass spectra of PEG esters for structural characterization is described. It is demonstrated that, with the proper choice of cationization reagents in ESI, the fragmentation behavior of these polymer ions can be altered to produce the desirable information. For example, the end group moieties can be lost as neutral species during fragmentation, providing mass information of the end groups. Under a different experimental condition, FAMEE can form product ions, offering the possibility for further tandem mass spectrometric analysis for direct structural elucidation. In addition, it is shown that in-source fragmentation can be purposely introduced to improve the quality of subsequent MS/MS spectra. Finally, the ESI CID MS/MS method is demonstrated to be useful for characterizing two fatty acid methyl ester ethoxylates.

6.2 Experimental

6.2.1 Materials and Reagents. Poly(ethylene glycol) methyl ether (PEG-ME) (Mn *ca.* 550), poly(ethylene glycol) dibenzoate (PEG-DBZ) (Mn *ca.* 410), and poly(ethylene glycol) monooleate (PEG-MOL) (Mn *ca.* 460) were from Aldrich Chemical Co. (Milwaukee, WI). Poly(ethylene glycol) distearate (PEG-DS) (Mn *ca.* 930) was obtained

from an industrial research partner. The structures of these samples are shown in Scheme 6.1.

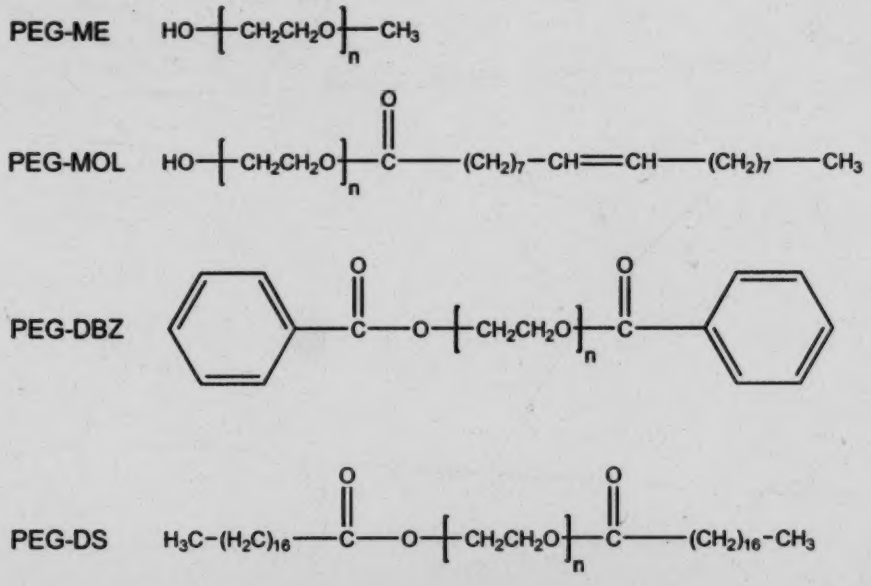

Scheme 6.1. Abbreviations and chemical structures of the PEGs used in this study.

All samples were analyzed without purification. Ammonium acetate, sodium chloride, lithium chloride, silver nitrate, cobalt chloride, and cupric nitrate were obtained from either Aldrich or Fisher and used as received. High performance liquid chromatograph (HPLC) grade methanol was obtained from Sigma (Milwaukee, WI). Distilled water was from a Milli-Q UV plus ultra-pure system (Millipore, Missussauga, ON).

6.2.2 ESI MS and MS/MS. All salts were dissolved in water at a concentration of 0.1 M. The analyte solution was prepared by mixing PEG stock solution, 10% (v/v) cationization reagent solution and appropriate amount of water/methanol (volume ratio 1:1) mixture to make the final PEG ester concentration about 100 μM.

All MS experiments were carried out in a Bruker/Agilent Esquire-LC Ion Trap LC/MS^n system. Sample solution was infused into the electrospray interface by a syringe pump (Cole-Parmer Instrument Co., IL) at a flow rate of 10 μl/min. Mass spectra were acquired over the mass range m/z 50-2200. Each spectrum was the result of an integration of the raw data for at least 1 minute to ensure the correct isotope patterns were reflected. All data were reprocessed using the Igor Pro Software package (WaveMetrics, Lake Oswego, OR) without background subtraction.

6.3 Results and Discussion

6.3.1 Differentiation of PEG Ethers and PEG Esters by ESI MS/MS.

Figure 6.1 displays the ESI mass spectra of PEG-ME and PEG-MOL, obtained by using Li^+ as the cationization reagent. Despite the evident end group difference between the two samples, both spectra show the typical PEG mass distributions with adjacent peaks separated by 44 Da, corresponding to the mass of the repeating unit. In addition, PEG-MOL appears to have a lower nominal average mass and narrower mass distribution. However, the MS/MS spectra (Figure 6.2) depict totally different scenarios for the two samples. Figure 6.2A displays the characteristic fragmentation pattern of PEG ethers [15]. Briefly, consecutive losses of repeating units form the major product ion series. Whereas in the case of PEG-MOL (Figure 6.2B), as will be illustrated in detail in section 6.3.2, the major fragments are the result of the loss of the end group and their derivatives. Figure 6.2 illustrates that PEG ethers and PEG esters behave differently under low energy CID conditions. Thus, these two classes of PEGs can be readily differentiated by a simple MS/MS experiment.

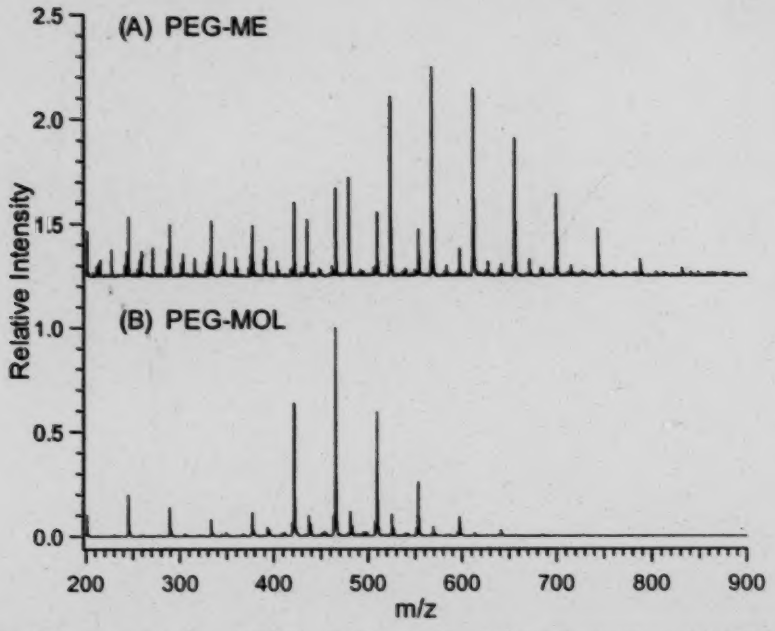

Figure 6.1. ESI mass spectra of PEGs obtained using Li^+ for ionization: (A) PEG-ME, and (B) PEG-MOL.

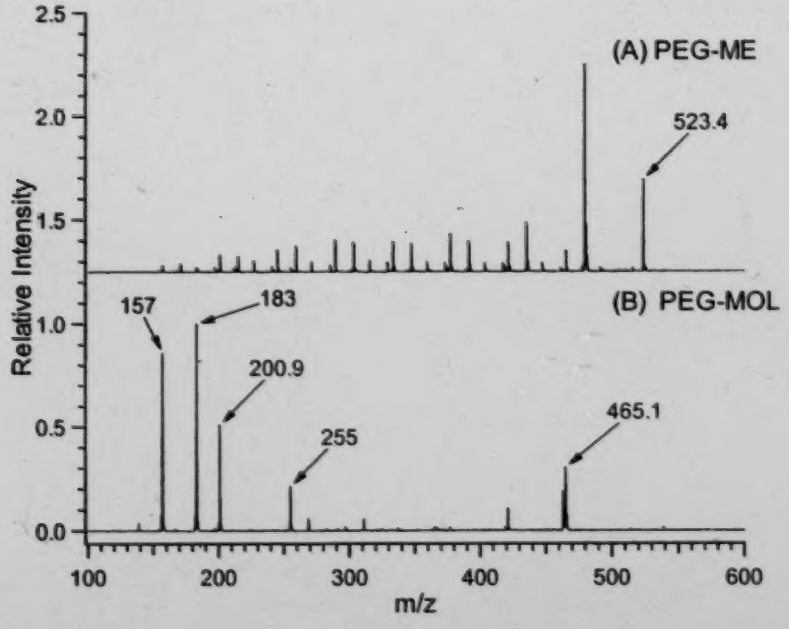

Figure 6.2. ESI MS/MS spectra of PEGs with Li^+: (A) PEG-ME, and (B) PEG-MOL.

6.3.2 End Group Elucidation for PEG Dibenzoate and Related Issues.

Figure 6.3 shows the ESI mass spectra of PEG-DBZ obtained using different cationization reagents, including Na^+, Li^+, NH_4^+, Ag^+, Co^{2+} and Cu^{2+}. The trend of ionization efficiency with these cations, judged by the signal-to-noise (S/N) ratios, agrees with that observed in the case of PEG-ME (Chapter 5). In short, Li^+ and Na^+ provide the most efficient ionization without in-source fragmentation. NH_4^+ and Ag^+ also generate clear spectra, but with slightly lower S/N ratios. Both divalent metal ions, Co^{2+} and Cu^{2+}, provide complex and somewhat different spectra. As labeled in Figure 6.3E, both $[\alpha\text{-}EO_n\text{-}\omega]CoCl^+$ and $[\alpha\text{-}EO_n\text{-}Co]^+$ (EO represents ethylene oxide, and α=ω=benzoyl group) were identified. The backbone of PEG serves as a strong coordinating ligand with oxygen atoms providing electron pairs. These electron pairs can be accommodated by the empty *s* and *p* orbitals of the center transition metal ions. By eliminating one counter ion Cl^- alone, or followed by an expulsion of stable benzoic chloride, $[\alpha\text{-}EO_n\text{-}\omega]CoCl^+$ and $[\alpha\text{-}EO_n\text{-}Co]^+$ are formed, respectively. In both cases, the oxidation state of Co remains +2.

It is interesting to note that, in Figure 6.3F, the oxidation state of copper is +1 in $[\alpha\text{-}EO_n\text{-}\omega]Cu^+$, although $Cu(II)(NO_3)_2$ was used in ESI. Results obtained under the same experimental condition with a high resolution ESI TOF instrument (results not shown) confirmed that the observed species is not the result of deprotonation (i.e. $[M\text{-}H+Cu(II)]^+$). Apparently, the Cu(II) from $Cu(NO_3)_2$ is reduced to Cu(I) in $[\alpha\text{-}EO_n\text{-}\omega]Cu^+$ during ESI. Redox reactions have been reported to occur in ESI and an ESI source is considered as "an electrolytic cell of a somewhat special kind" [63]. Depending on the polarity applied to the ESI capillary, electrochemical oxidation or reduction can be

observed in positive or negative mode. The current observation is somewhat surprising considering the fact that in a positive ESI mode, an oxidation rather than a reduction is expected. However, in the process of transferring ions from solution to the gas phase, additional changes and rearrangements can also occur since ions are transferred into a very different environment. For example, multiply charged ions often undergo gas phase charge reduction via proton transfer or charge separation, resulting in ions different than one would observe in solution. Gianelli *et al.* [64] also showed that Cu(II)→Cu(I) reduction could take place by Cu(II)-ligand complex transferring an electron to solvent methanol in the gas phase [64]. A better understanding of this rather unusual ion formation is required, which will aid in a better experimental design such as the choice of metal ion and solvent system.

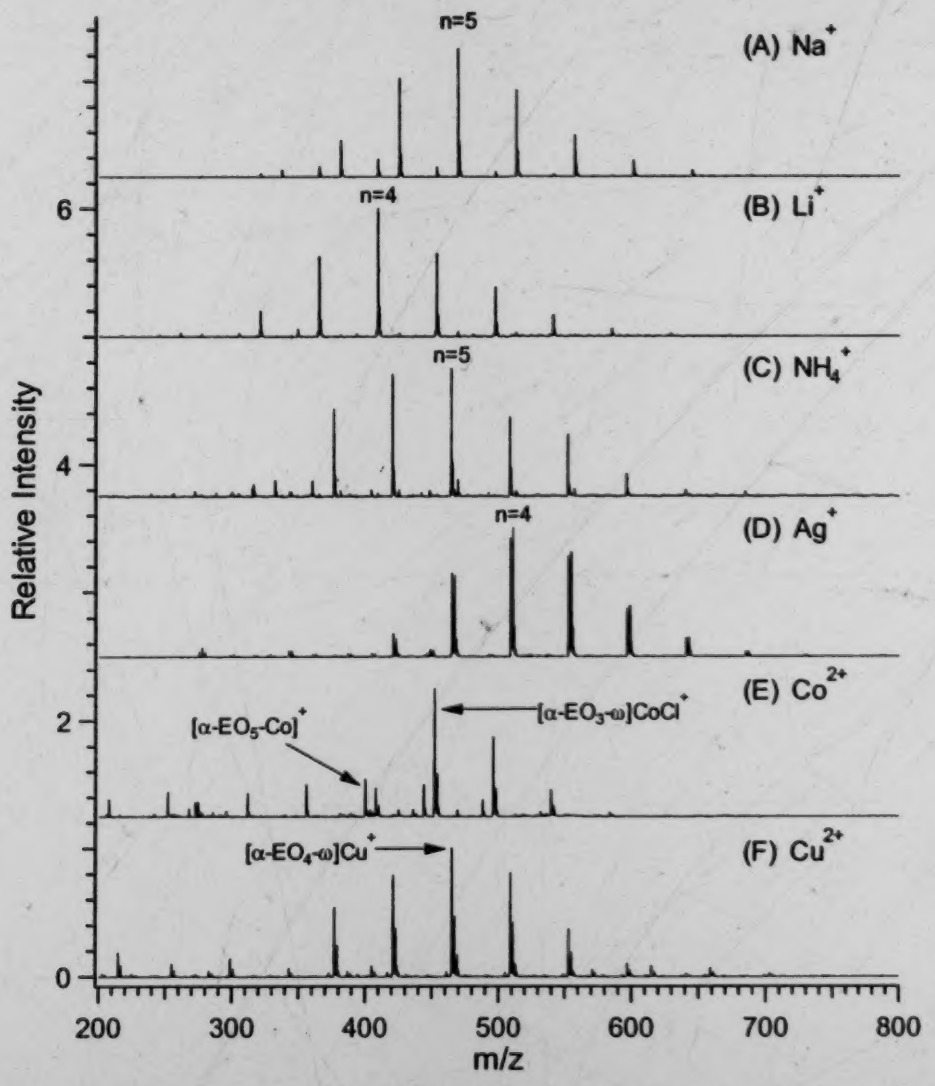

Figure 6.3. ESI mass spectra of PEG-DBZ obtained using different cations for ionization: (A) Na^+, (B) Li^+, (C) NH_4^+, (D) Ag^+, (E) Co^{2+}, and (F) Cu^{2+}. The *n* denotes the number of the repeating units of the most intense peaks.

Figure 6.4 shows the MS^2 and MS^3 spectra of sodiated PEG-DBZ. The annotations of the peaks are shown in Scheme 6.2. In both spectra, neutral loss of 122 Da results in the main product ions, namely, m/z=347.2 in Figure 6.4A and m/z=225.1 in Figure 6.4B. This neutral loss is attributed to the end group, benzoic acid. In early study

on PEG-ME, no MS/MS spectra were obtained for sodiated species (Chapter 5). This was ascribed to the weak electrostatic PEG-Na^+ interaction. The applied collision energy was dissipated preferentially by breaking up this interaction, rather than the PEG backbones. The results on sodiated PEG-DBZ ions shown here suggest that the energy requirement for the rearrangement involving ester linkage (Scheme 5.2) is less than that for the direct PEG-Na^+ breakage. These ester linkages provide a new energy release channel, hence, a new fragmentation pathway.

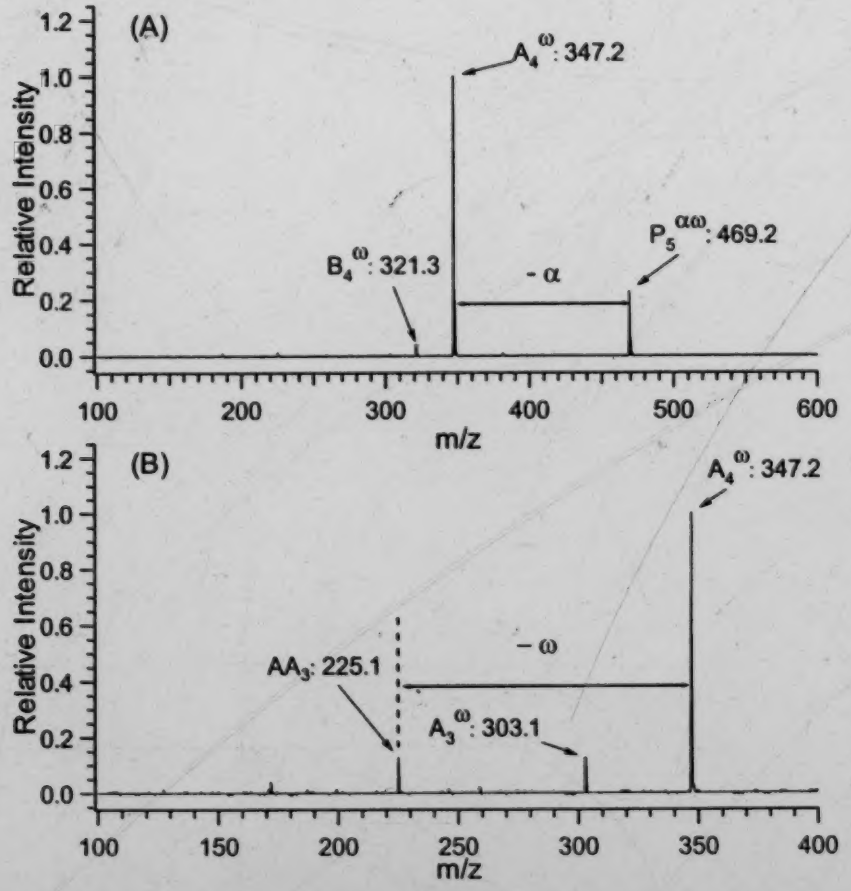

Figure 6.4. (A) ESI MS/MS spectrum of PEG-DBZ pentamer with Na^+ at m/z=469.2. (B) ESI MS^3 spectrum of the product ions at m/z=347.2 from Figure 6.4 (A).

Another relevant comparison is the different fragmentation behavior of sodiated PEG-DBZ under high- and low-energy CID conditions. The high energy CID spectrum of PEG-DBZ of Bottrill *et al.* consists of peaks originating from both end groups and repeating units [5]. That is, the end group fragments appear concurrently with those from the internal breakage of repeating units in the low mass region due to the applied high energy (~ 8 keV). To distinguish these two types of product ions requires careful interpretation. This lack of specificity imposes challenges in the identification of unknown samples. In the case of low energy CID, a much simpler and more straightforward fragmentation spectrum is generated (Figure 6.4). However, the information obtained from such spectra is very limited. Only the end group mass can be obtained in the current case of using sodium ion as the cationization reagent.

In light of the early study using Li^+ and transition metal ions to enable fragmentation of PEG ethers, a series of experiments using different cations have been performed with a hope that the resulting MS/MS spectra can provide enriched information for end groups as well as repeat units. Figure 6.5 shows the MS^2 and MS^3 spectra of lithiated PEG-DBZ. As can be seen, Figure 6.5A resembles Figure 6.4A, in which neutral losses of benzoic acid (mass 122 Da) and ethylene benzoate (mass 148 Da) result in the primary product ions. However, peaks resulting from consecutive losses of repeating units (i.e., A_n^{ω} series, m/z 331, 287, 243, 199, 155) were observed in Figure 6.5B, which were not found in Figure 6.4B.

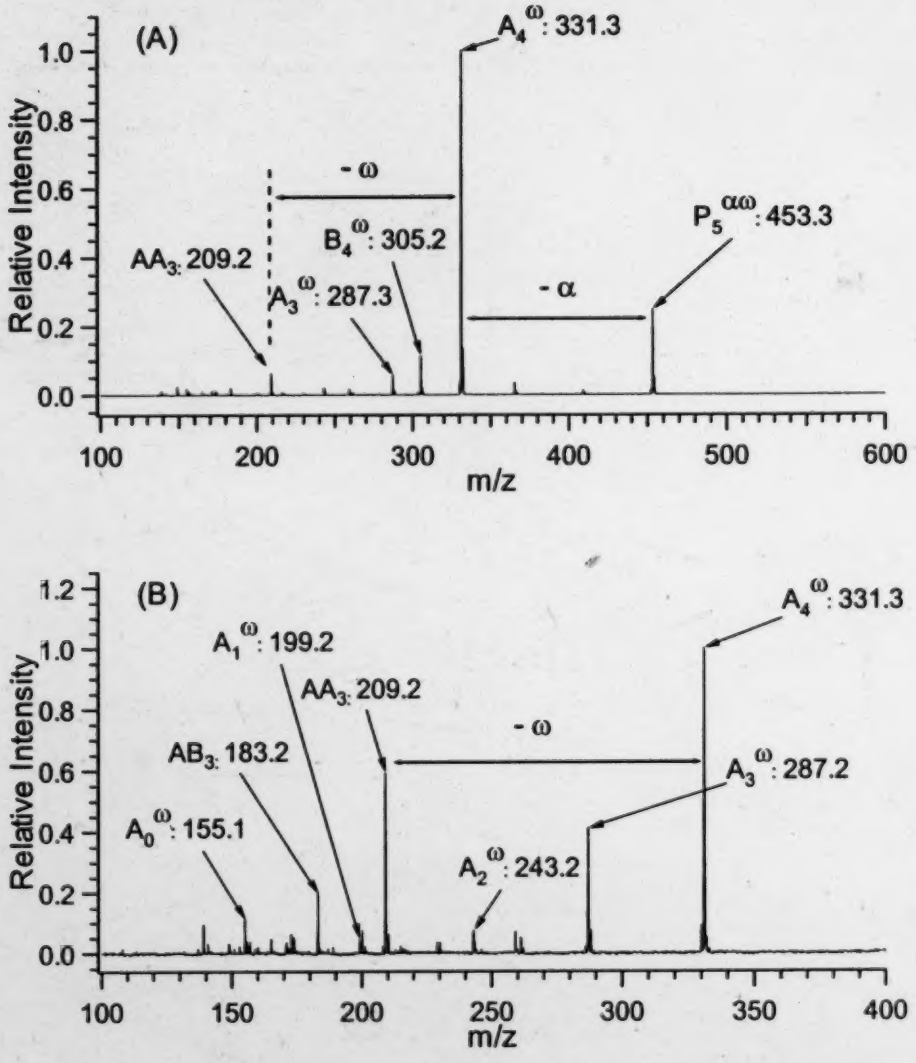

Figure 6.5. (A) ESI MS/MS spectrum of PEG-DBZ pentamer with Li^+ at m/z=453.3. (B) ESI MS^3 spectrum of the product ions at m/z=331.3 from Figure 6.5 (A).

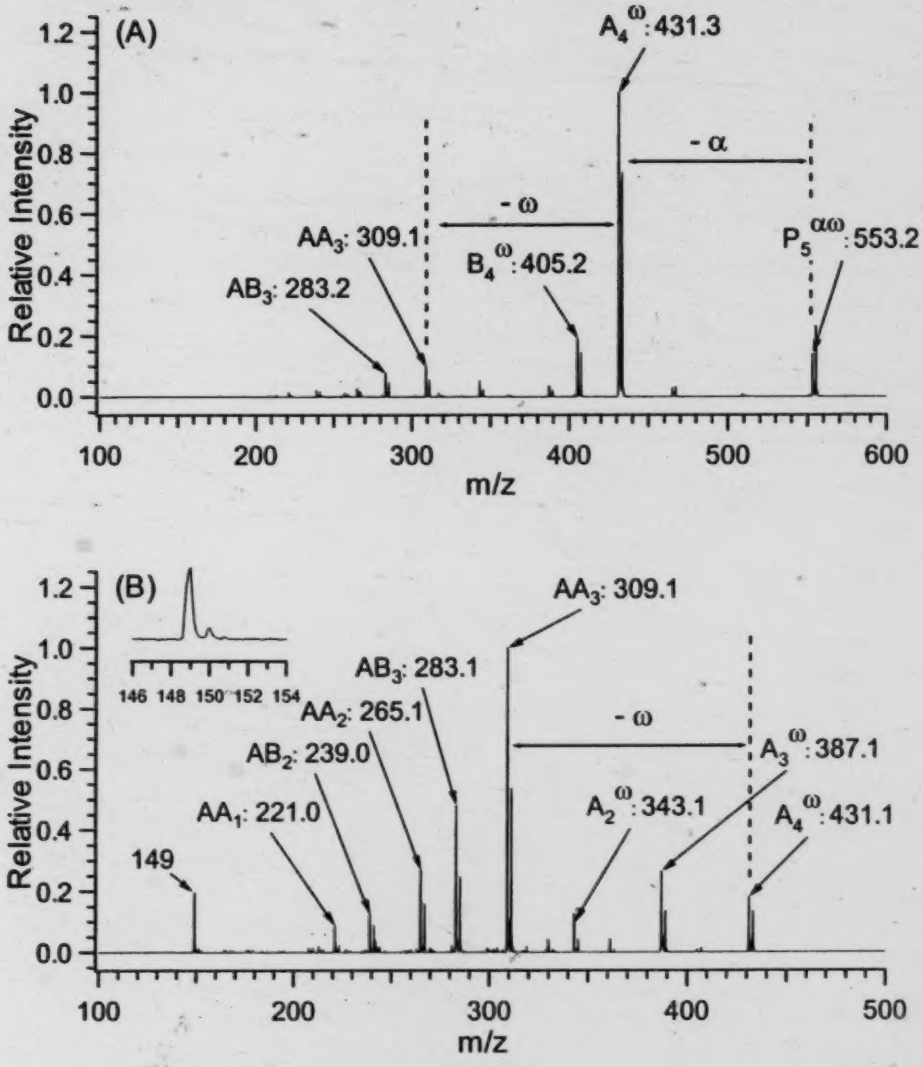

Figure 6.6. (A) ESI MS/MS spectrum of PEG-DBZ pentamer with Ag^+ at m/z=553.2. (B) ESI MS^3 spectrum of the product ions at m/z=431.1 from Figure 6.6 (A).

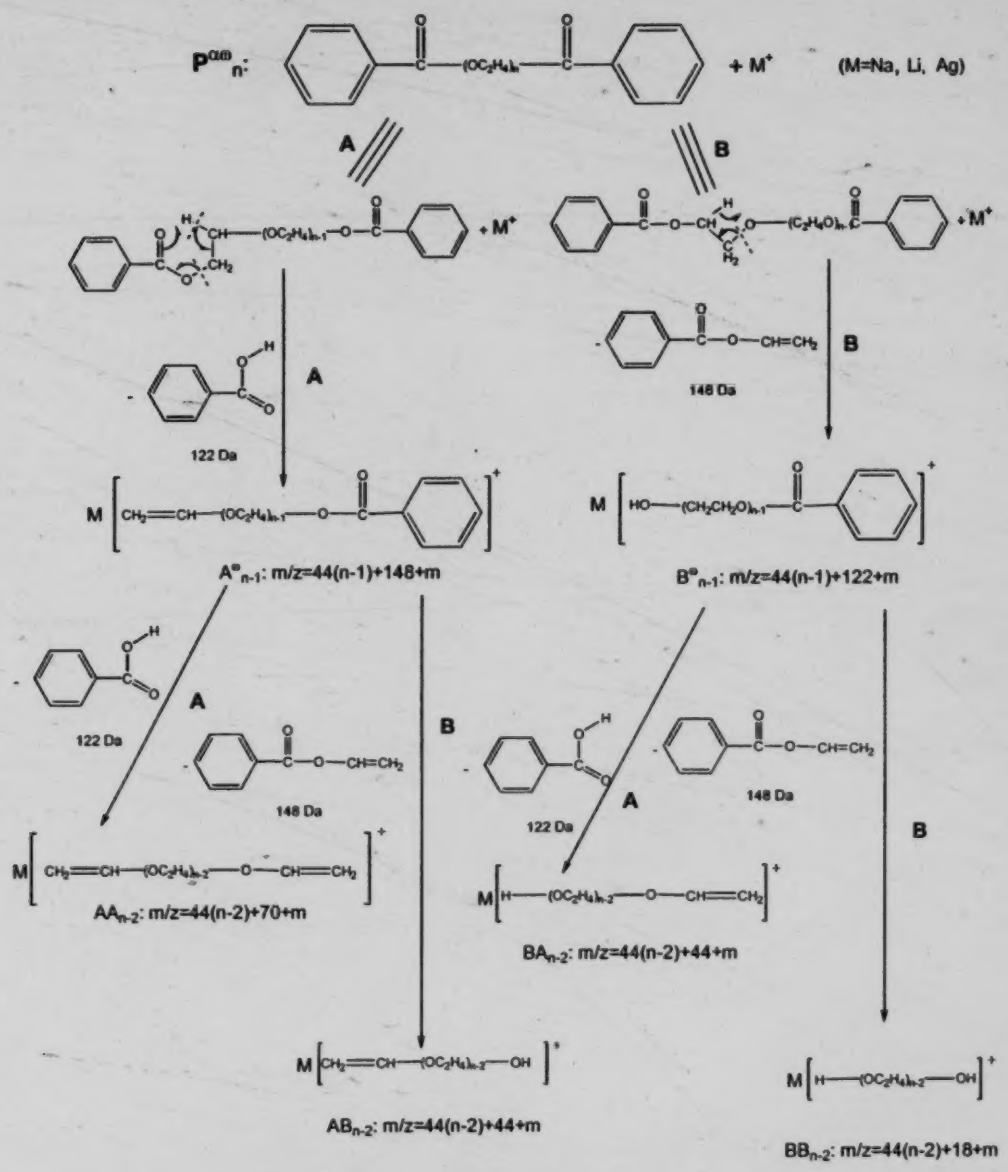

Scheme 6.2. Proposed fragmentation pathways for PEG-DBZ with different metal ions.

Similar spectra were obtained by using Ag^+ (Figure 6.6). In addition to the improved information content, there are at least two additional advantages of using Ag^+ as the cationization reagent. Firstly, the fragmentation products are shifted towards higher mass. This is advantageous as peaks below m/z 100 are often difficult to obtain in

low energy CID in the ion trap mass spectrometer due to its low-mass cut-off point. The second advantage is that the unique isotope pattern of silver will aid in data interpretation. For example, there is a peak at m/z 149 in Figure 6.6B. Unlike all the other product ions present in the spectrum, this peak does not contain silver, judged by its isotope pattern (see inset of Figure 6.6B), indicating that this peak is very likely from an internal fragmentation, as shown in Scheme 6.3. The implication of this product ion will be discussed in more detail.

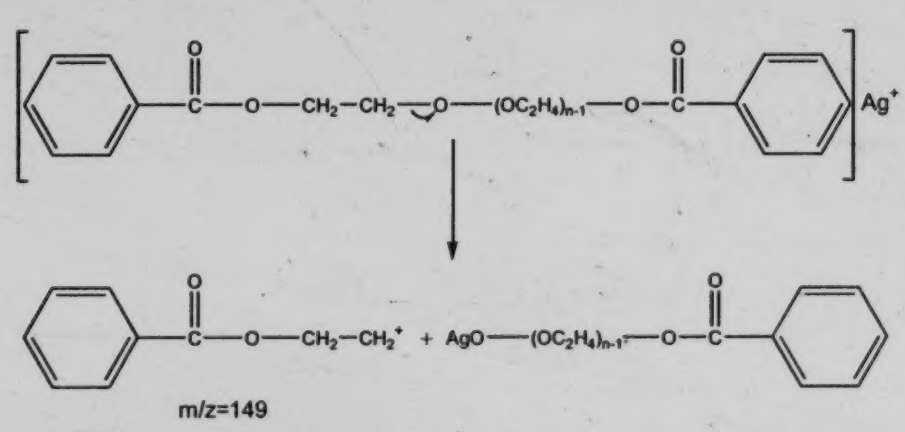

Scheme 6.3. Schematic illustration of the formation of the ions at m/z=149 in the case of using Ag^+ as the cationization reagent.

Scheme 6.2 shows the fragmentation pathways for $[PEG\text{-}DBZ]M^+$ (M=Na, Li, and Ag). A brief description of the nomenclature and mechanism is as follows. α and ω represent the two end groups. In the case of PEG-DBZ, α=ω=benzoyl group. Pathway **A** is a McLafferty rearrangement with neutral loss of benzoic acid (mass 122 Da). Pathway **B** involves the neutral loss of ethylene benzoate (mass 148 Da) via a four-member ring intermediate. The product ions resulting from pathways **A** and **B** are identified as **A** and **B** series, respectively. Similarly, ions identified as **AB** series are resulting from pathways

A and **B** in a tandem manner. The subscripted number denotes the number of the remaining repeating units in the structure, and the superscripted Greek letter signifies the remaining end group. In the mass calculation, ***m*** represents the mass of the involved metal ion, and isotopic mass is used.

Based on Scheme 6.2, the observation of the losses of repeating units by using Li^+ and Ag^+, but not Na^+, can be readily explained within the context of the early studies on PEG ethers [15]. The parent ions in all MS^3 spectra (Figures 6.3B, 6.4B, 6.5B) are PEGs containing both ester- and ether-linked end groups (i.e., $\mathbf{A}_n^{\omega}$ series). The subsequent fragmentation is still dominated by pathways **A** and **B** from the ester end. However, the PEG-lithium or -silver, but not -sodium, adducts also dissociate from the ether end, in a manner similar to the PEG-ME metal ion adducts, resulting in the observed repeating unit cleavages.

Thus far, product ions resulting from the neutral loss of end groups have been analyzed, but not from ions containing end groups. Obviously, this is not sufficient for the end group structure elucidation. Recall that in Figure 6.6B, the peak at m/z 149 is postulated to contain the end group moiety due to internal fragmentation. If, indeed, this ion has the proposed structure, fragmentation of this ion will generate direct end group structural information. Unfortunately, the signal intensity of this ion in the MS/MS spectrum is low. No meaningful MS^3 spectrum could be obtained.

This actually exemplifies one common problem encountered in MS^n studies using the ion trap. In a conventional ion trap system, the ions of interest are accumulated concomitantly with all other ions including interfering ions, if any, from the preceding MS/MS stage. If the ions of interest are present at low yield, very frequently they cannot

be accumulated to a sufficient number, without exceeding the space limit of the ion teap due to other more abundant ions, to endure the next isolation/dissociation stage. Thus an ion trap MS, in principle, has the capability of multiple MS/MS (i.e. MS^n); but in practice, high order MS/MS experiment can be quite difficult. It is noted that an interesting instrument design that uses a linear quadrupole as an ion storage and guiding device preceding the ion trap [65] might be able to exclude some interfering ions by physically separating different MS stages, but the applicability and robustness of this design remains to be determined.

To circumvent this problem, experiments have been carried out from the following two aspects: 1) to exclude the interfering ions by chemical means, and 2) to increase the ion yield from the previous stage by using a different mode of operation. Figure 6.7A illustrates the use of NH_4^+ to enable fragmentation of the ions at m/z 149. Unlike all the metal ions used, employing NH_4^+ generates a rather simple MS/MS spectrum with only two product peaks. The peak at m/z 447 corresponds to the loss of NH_3, and the peak at m/z 149 is the same ion as present in Figure 6.6B. The exclusive formation of the ions at m/z 149 is presumably due to the high affinity of H^+ towards the carbonyl oxygen atom in the end group. The ions at m/z 447 then undergo charge-driven dissociation to form the product ion. The product ions at m/z 149 can be further stabilized by the resonance involving a highly conjugated structure, or charge de-localization. Note that the spectrum shown in Figure 6.7A was obtained using a mild dissociation condition to demonstrate the presence of protonated PEG (m/z 447). In practice, by increasing the collision energy, peaks at m/z 447 can be completely eliminated and ion counts of m/z 149 can be further increased.

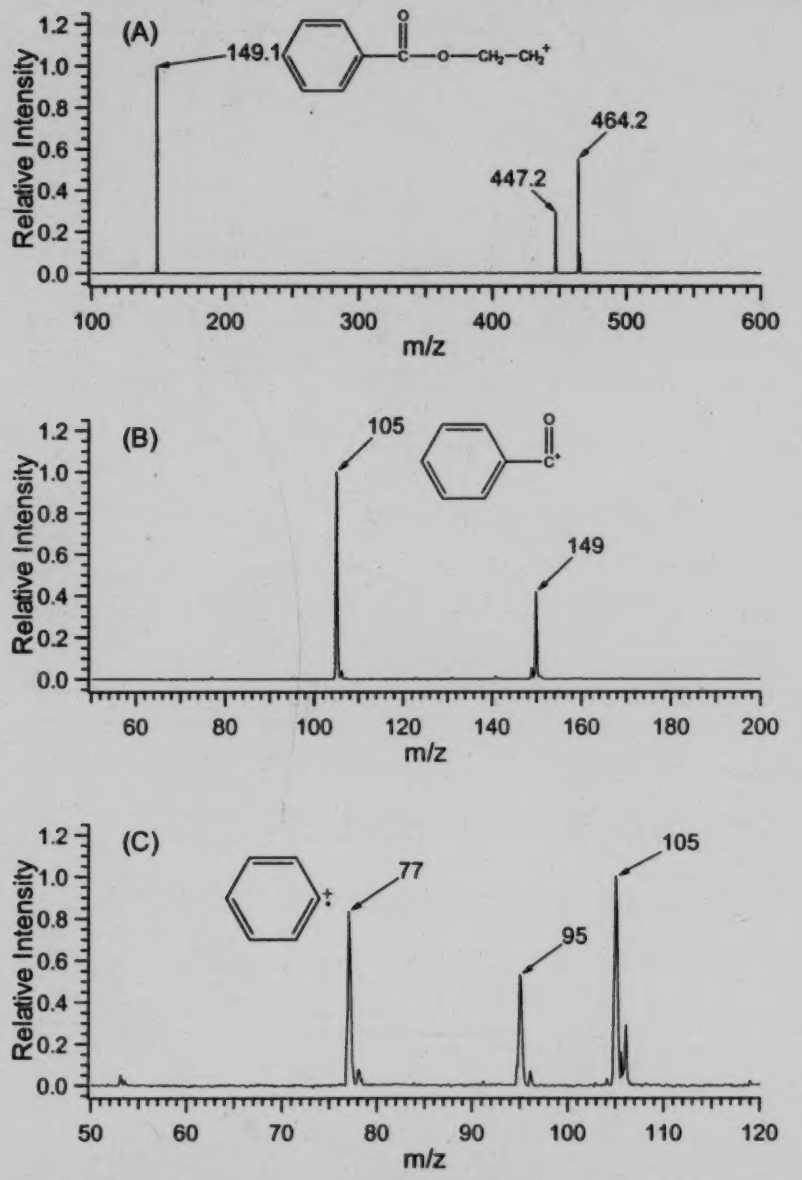

Figure 6.7. (A) ESI MS/MS spectrum of PEG-DBZ pentamer with NH_4^+ at m/z=465.2. (B) ESI MS^3 spectrum of the product ions at m/z=149 from Figure 6.7 (A). (C) ESI MS^4 spectrum of the product ions at m/z=105 from Figure 6.7 (B).

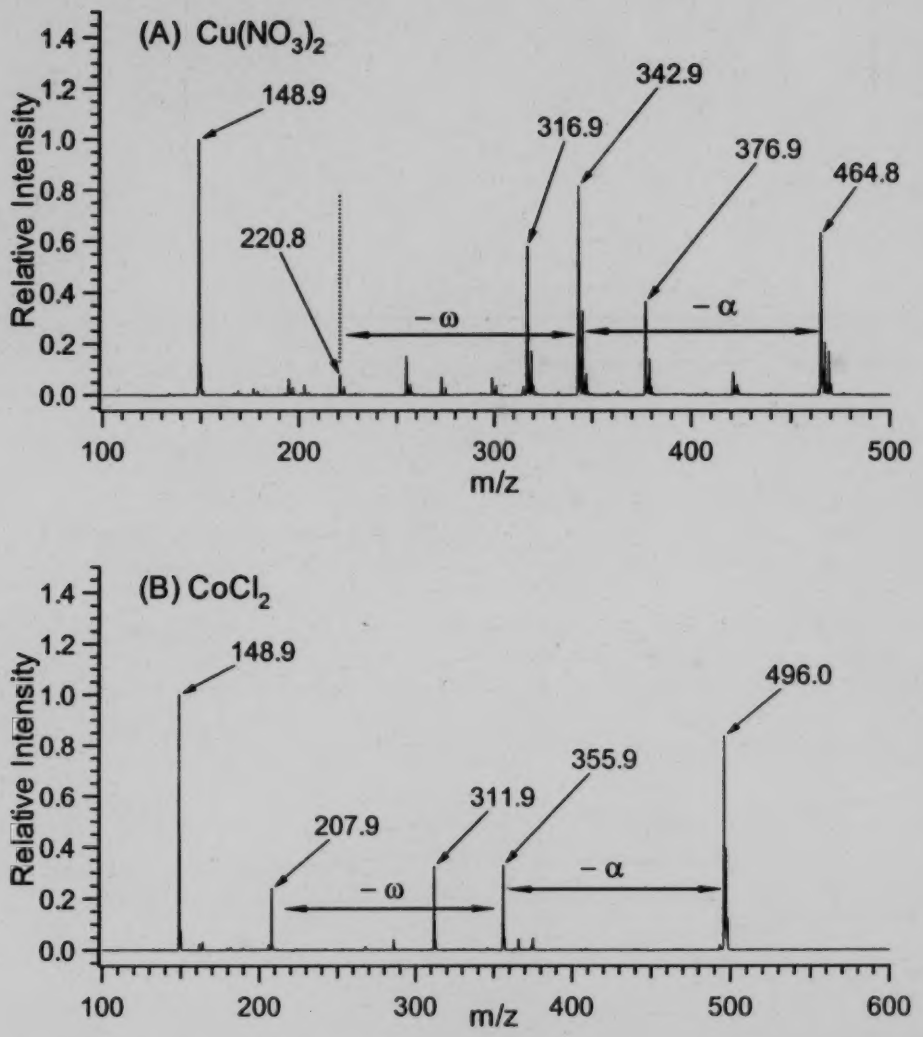

Figure 6.8. (A) ESI MS/MS spectrum of PEG-DBZ quadrimer at m/z=465.8 obtained using $Cu(NO_3)_2$. (B) ESI MS/MS spectrum of PEG-DBZ quadrimer at m/z=496.0 obtained using $CoCl_2$.

With increased ion counts and decreased interference, further isolation and fragmentation on m/z 149 was performed. MS^3 on m/z 149 followed by MS^4 on its product ions at m/z 105 are shown in Figure 6.7B and 6.7C, respectively, with proposed

structures labeled next to each major peak. The identity of the peak at m/z 95 remains uncertain. Possibly, this is due to ion/molecule reaction between benzene radical ions and water molecules in the trap. Nevertheless, a complete depiction of the end group structure was obtained.

Another way to improve the quality of tandem mass spectra is to increase the precursor ion yield in the preceding stage. Figure 6.8 shows the MS^2 spectra obtained by using divalent metal ions Co^{2+} and Cu^{2+}. The spectrum obtained using $Cu(NO_3)_2$ (Figure 6.8A) bears the similar fragmentation characteristics as those using Ag^+, but with greatly increased signal intensity of the peak at m/z 149. This similarity can be ascribed to the fact that both metals, Ag and Cu, belong to the same IB group, and both ions (+1) have a similar d^{10} electronic configuration. The empty ***s*** and ***p*** orbitals can well accommodate the electron pairs from adjacent oxygen atoms and form complex. However, the ionic radius of Cu^+ is smaller than that of Ag^+ (96 pm *vs.* 126 pm). As a consequence, Cu^+ is more easily coordinated by the surrounding PEG repeating units, giving rise to a stronger complex. Using Co^{2+} (Figure 6.8B) as the cation results in a somewhat different situation. The parent ion m/z 496 was selected from the $[\alpha\text{-}EO_n\text{-}\omega]CoCl^+$ series (see label on Figure 6.3E). The anion Cl^- participates in the formation of the neutral product, benzoyl chloride. Afterwards, the Co^{2+} ions are linked to the PEG chains via covalent bonding. This bonding is much stronger than those interactions of electrostatic nature. The increment of the interactions between the metal ions and PEG chains, by means of stronger complex formation or covalent bonding, will promote the likelihood of internal fragmentation to generate ions at m/z 149. In both cases, further fragmentation was enabled and identical spectra to Figures 6.7B and 6.7C were obtained (data not shown).

It was also found that using in-source fragmentation to generate end group moiety ions (i.e., m/z 149 for PEG-DBZ) in the first MS stage would considerably improve the quality of subsequent tandem MS spectra. The reason is rather straightforward. If the ions are generated by a MS/MS experiment, only those isolated PEGs with one nominal mass will undergo the dissociation and lead to the ions of interest. On the other hand, if the ions are generated by in-source fragmentation in the first MS stage, all PEGs with the same structure but different chain lengths will collectively contribute to the ion formation. Consequently, ion counts are considerably increased. This is particularly helpful when low-efficiency ionization reagents are used in the first MS stage. For example, NH_4^+ ionization of PEG often suffers from low efficiency, especially for real world samples containing large amounts of salt. In this case, tandem mass spectrometry does not have sufficient parent ions to begin with under normal operation mode, and to go through $MS \rightarrow MS^2 \rightarrow MS^3$ will not generate satisfactory results. Moreover, skipping one isolation/fragmentation cycle will also alleviate the ion loss during isolation and fragmentation.

Based on the above results and discussion, a MS-based approach tailored for a complete PEG ester characterization is summarized in the flow chart shown in Figure 6.9. With two (or more, if necessary) cationization reagents, information with regards to average molecular mass, repeating unit, and end group structure, can be readily obtained by a conventional ion trap mass spectrometer within a short experimental time frame.

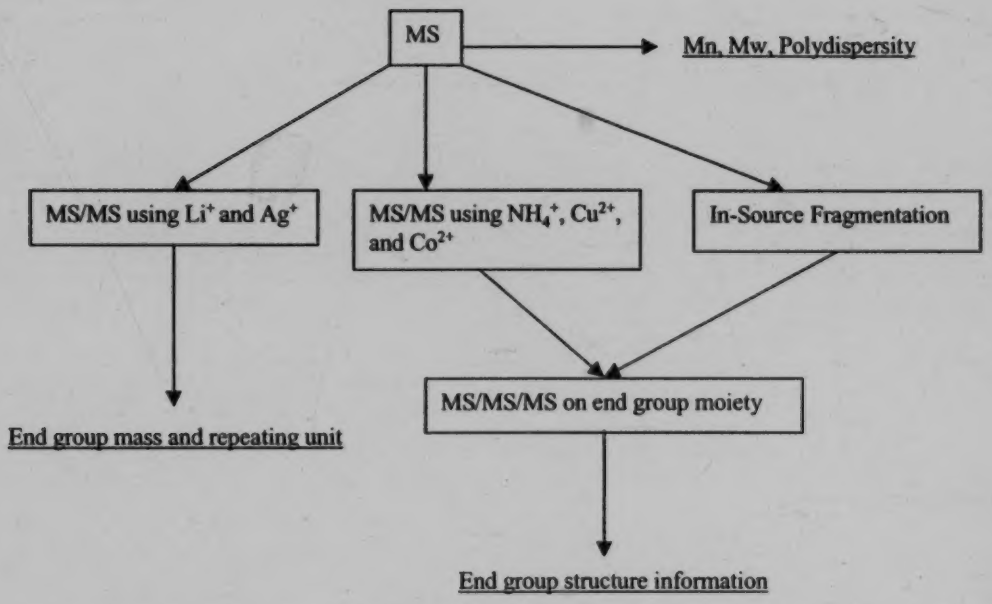
MS
Mn, Mw, Polydispersity
MS/MS using Li^+ and Ag^+
MS/MS using NH_4^+, Cu^{2+}, and Co^{2+}
In-Source Fragmentation
MS/MS/MS on end group moiety
End group mass and repeating unit
End group structure information

Figure 6.9. Schematic illustration of the MS-based protocol for PEG ester characterization.

6.3.3 Fatty Acid Methyl Ester Ethoxylates (FAMEE).

To demonstrate the general applicability of the protocol shown in Figure 6.9, two fatty acid methyl ester ethoxylates were studied. Representative MS^n spectra of these PEG esters obtained by using Li^+ and NH_4^+ along with the rationale to infer the structure information of these PEG esters are presented.

Figure 6.1B and Figure 6.10A show the ESI spectrum of PEG-MOL obtained using Li^+ and NH_4^+ as the cationization reagents, respectively. The MS/MS spectrum of PEG-MOL obtained using Li^+ is shown in Figure 6.2B. As depicted in Scheme 6.2, the major products should result from the loss of the end group moiety, via pathway **A** and **B**, respectively. Ensuing products are supposedly separated by 26 Da. Among four major product peaks present in Figure 6.2B, peak pairs at m/z 183 and 157 fit the profile. Therefore, the mass difference between parent ion m/z 465 and product ion m/z 183 can be tentatively assigned to the end group acid with nominal mass 282 Da. This was further confirmed by the MS/MS spectrum obtained using NH_4^+ (Figure 6.10C). In Figure 6.10C, the only product ions besides the loss of NH_3 are the end-group acid ethylene esters at m/z 309 (282-1+28=309), similar to the case of PEG-DBZ (Figure 6.7). These ions were also generated by in-source fragmentation (Figure 6.10B). Figure 6.10A is the ESI mass spectrum obtained under normal operation mode to reflect the correct mass distribution. By increasing the voltage drops between capillary exit and skimmer 1, skimmer 1 and 2, abundant fragment ions at m/z 309 are generated to enable the further fragmentation.

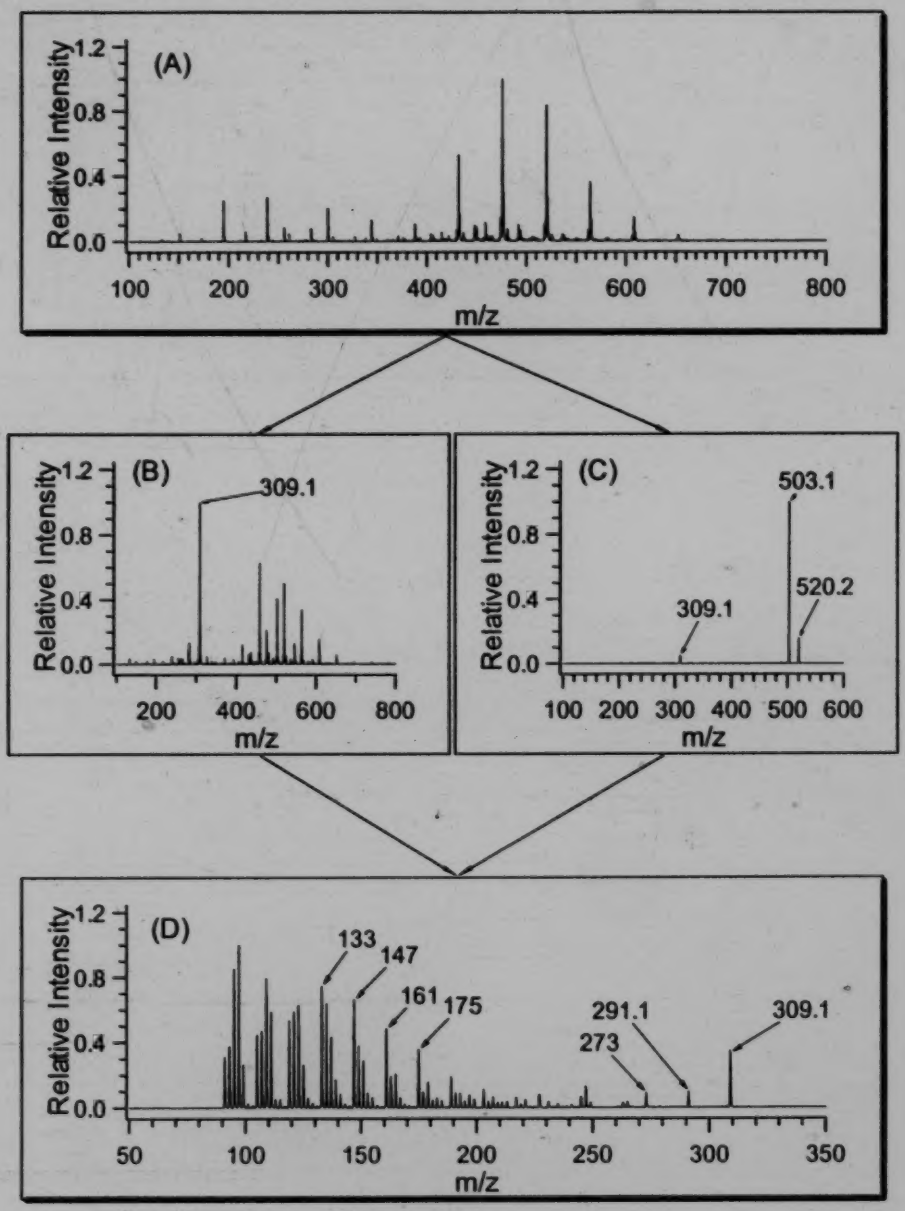

Figure 6.10. **(A) ESI mass spectrum of PEG-MOL obtained using NH_4^+ under normal operation mode. (B) ESI mass spectrum of PEG-MOL obtained using NH_4^+ with in-source fragmentation. (C) ESI MS/MS spectrum of PEG-MOL pentamer at m/z=520.2 with NH_4^+. (D) Fragmentation spectrum of product ions at m/z=309.1 from both Figure 6.10 (B) and (C).**

The fragmentation spectrum of m/z 309 is shown in Figure 6.10D. The foremost products are the carbocations below m/z 200 with major peaks separated by 14 Da, reflecting the alkyl nature of the fatty acid. However, it seems impossible to pinpoint the double bond position in the end group moiety within the current experimental frame. The loss of H_2O (peak at m/z 291) and formic acid, typical for the dissociation of fatty acids and their derivatives, will move the charge onto the alkyl chain and give rise to the observed carbocations. Carbocations are notorious for their ability to isomerize before fragmentation and lead to a complicated spectrum that is difficult to interpret. The well-established approach to solve this problem is via high-energy charge-remote fragmentation [66-77]. For example, Davoli *et al.* [64] showed that using alkaline earth metal ions, especially barium, in a FAB high-energy CID MS/MS experiment, the mass defect in the MS/MS spectrum can be related to the double bond position for unsaturated fatty acids and their derivatives. The facility of the charge remote fragmentation is ascribed to the formation of $[M-H+Cat.]^+$ species whose charge is tightly localized. Nevertheless, the resulting spectrum from our approach still contains information from alkyl chain as well as acid proximity. Moreover, in industrial practices, only a limited number of fatty acids, such as oleic acid, stearic acid, and palmitic acid, are commonly used for PEG ester manufacture. It is envisioned that compiling a reference MS/MS spectrum library could be useful for unambiguous end group identification.

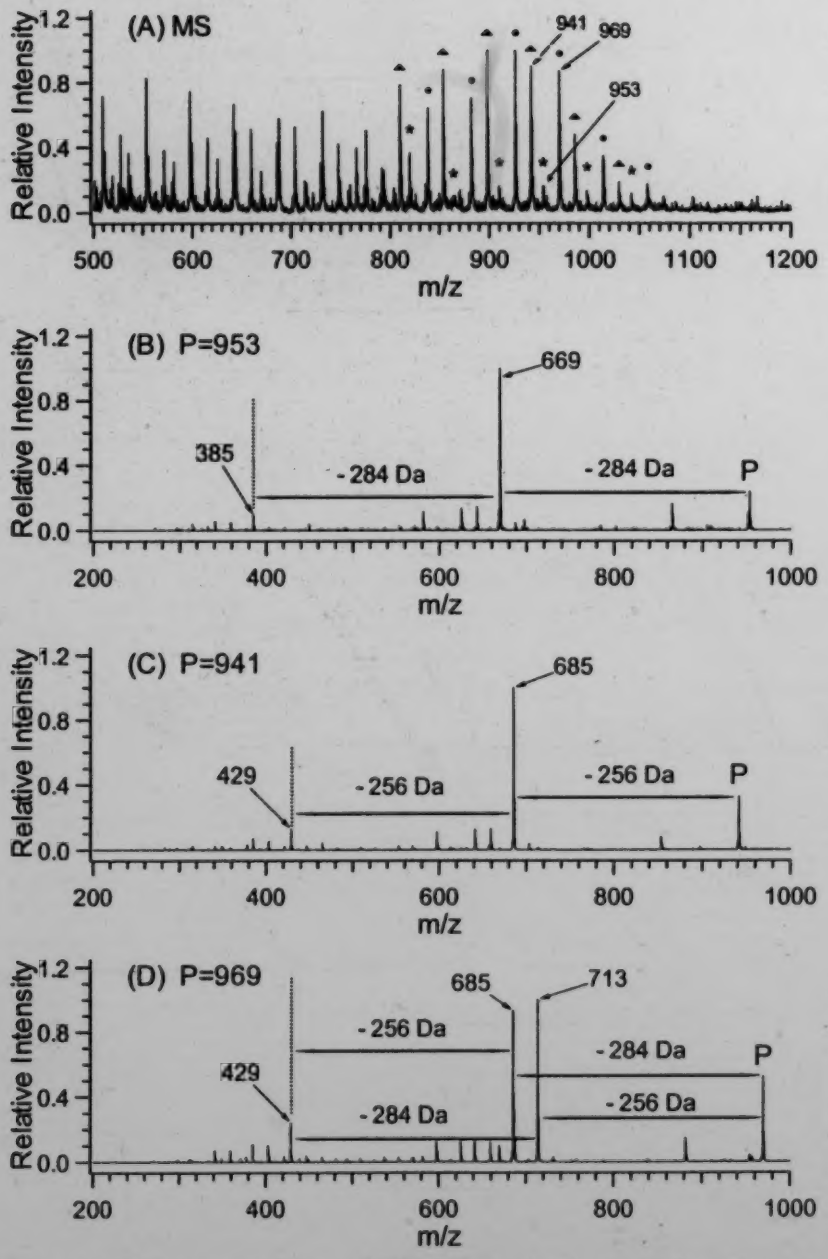

Figure 6.11. (A) ESI mass spectrum of PEG-DS obtained using Li^+ as the cationization reagent. The peaks labeled with ▲, *, and • indicate they are from different product series. (B) ESI MS/MS spectrum of ions at m/z=953 with Li^+. (C) ESI MS/MS spectrum of ions at m/z=941 with Li^+. (D) ESI MS/MS spectrum of ions at m/z=969 with Li^+. In Figures (B), (C), and (D), P denotes the parent ions of each spectrum.

Figure 6.11A shows an ESI mass spectrum of sample PEG-DS, obtained using Li^+ as the cationization reagent. The spectrum is surprisingly complicated with at least three identifiable distributions. The intended product (i.e., m/z 953 series, labeled as * in Figure 6.11A) is present in the lowest abundance. MS/MS spectra of ions from three series are shown in Figure 6.11B, C and D. Figure 6.11B reveals the presence of the expected stearic acid end groups with a nominal mass of 284 Da. However, Figure 6.11C suggests that this series of products (labeled as ▲ in Figure 6.11A) have two identical end group acids with a nominal mass of 256 Da, probably palmitic acid ($CH_3(CH_2)_{14}COOH$) in lieu of stearic acid. Fragmentation spectrum of the ions at m/z 969 (Figure 6.11D) reveals that, the major product ions at m/z 685 and 713 are from the loss of stearic acid and palmitic acid, respectively. This indicates that this series of PEGs contain stearic acid at one end, and palmitic acid at the other. Further evidence includes the similar signal intensities of the peaks at m/z 685 and 713, and their common product at m/z 429.

End group moieties from all three series of PEGs were further "isolated" using NH_4^+ and fragmented, with the results shown in Figure 6.12. Both spectra display similar fragmentation patterns, i.e., both spectra consist of peaks from the loss of formic acid (mass 46 Da) and carbocations, indicating their structural similarity.

The above results clearly suggest that the starting material, stearic acid, was contaminated by palmitic acid, hence, resulting in a complicated mixture with three different structures. It is worthy to mention that the carbocations resulting from the fragmentation of unsaturated fatty acid ester (i.e., oleic acid ester, Figure 6.10D) are slightly different from those from saturated fatty acid esters (i.e., stearic acid and palmitic

acid esters, Figure 6.12). Thus a library spectral comparison approach whould be useful for unambiguous end group identification.

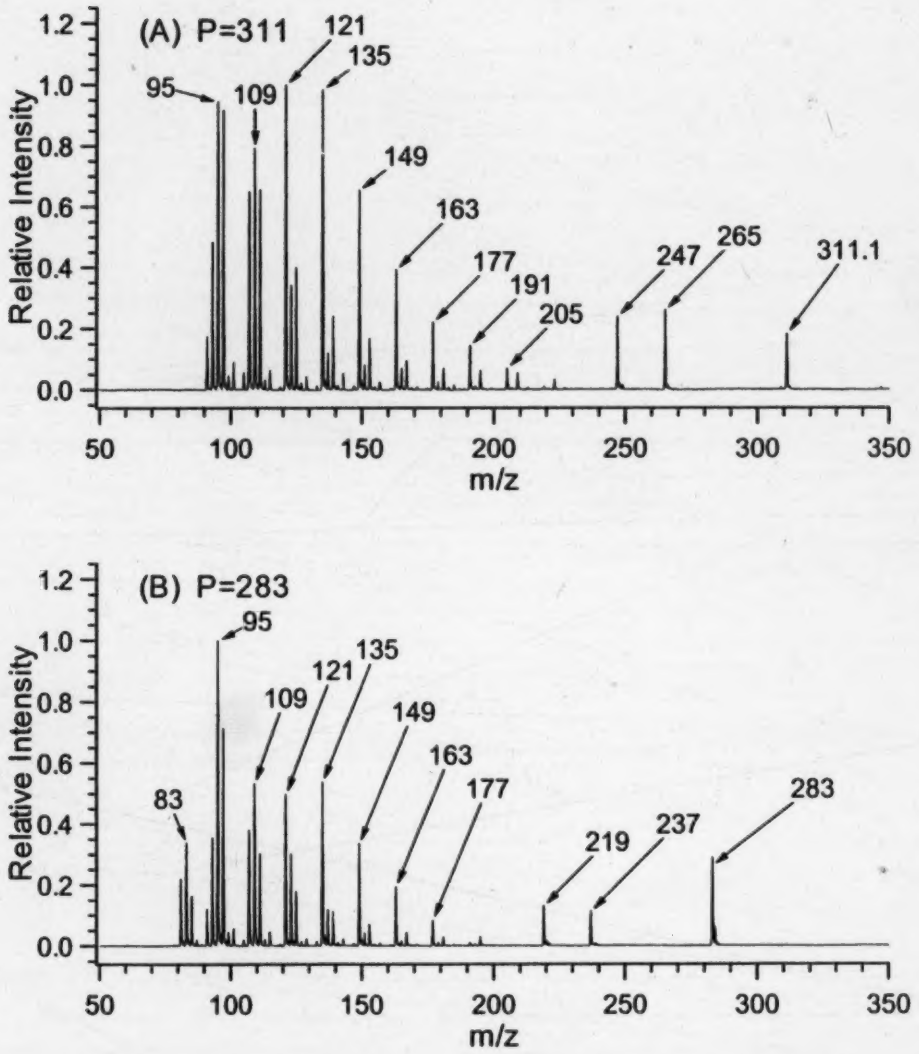

Figure 6.12. Fragmentation spectra of product ions at (A) m/z=311, and (B) m/z=283. In both cases, product ions were generated by in-source fragmentation of PEG-DS with NH_4^+.

6.4 Summary

In summary, it is shown that low energy dissociation of PEG esters strongly depends upon the cations involved. PEG ester-sodium adducts can undergo fragmentation, but provide limited information. The information content can be improved by the use of Li^+, Ag^+, and other transition metal ions. End group containing ions can be generated by using NH_4^+. Fragmentation on these ions leads to end group structural information. It is also demonstrated that ion-source fragmentation can improve the quality of ensuing MS/MS spectra of the end group containing ions. Based on these results, an integrated MS approach for PEG ester characterization is proposed. With the proper choice of cationization reagent and instrumental operation mode, a wealth of structure information can be obtained. Since the approach presented is based on the use of a low-energy CID tandem mass spectrometer that is widely available, it should be able to be adapted by others for problem solving in the area related to polyglycol structural characterization. For analytical method development, further effort should focus on extending this approach to the analysis of higher mass polyglycols.

6.5 Literatures Cited

1. Busch, K. L.; Glish, G. L.; McLuckey, S. A. *Mass Spectrometry/Mass Spectrometry*, VCH Publishers: New York, **1988**.
2. Jackson, A. T.; Yates, H. T.; Scrivens, J. H.; Critchley, G.; Brown, J.; Green, M. R.; Bateman, R. H. *Rapid Commun. Mass Spectrom.* **1996**, 10, 1668.
3. Jackson, A. T.; Yates, H. T.; MacDonald, W. A.; Scrivens, J. H.; Critchley, G.; Brown, J.; Deery, M. J.; Jennings, K. R.; Brookes, C. *J. Am. Soc. Mass Spectrom.* **1997**, 8, 132.
4. Scrivens, J. H.; Jackson, A. T.; Yates, H. T.; Green, M. R.; Critchley, G.; Brown, J.; Bateman, R. H.; Bowers, M. T.; Gidden, J. *Int. J. Mass Spectrom. Ion Proc.* **1997**, 165/166, 363.
5. Bottrill, A. R.; Giannakopulos, A. E.; Waterson, C.; Haddleton, D. M.; Lee, K. S.; Derrick, P. J. *Anal. Chem.* **1999**, 71, 3637.
6. Pastor, S. J.; Wilkins, C. L. *Int. J. Mass Spectrom. Ion Proc.* **1998**, 175, 81.
7. Hunt, S. M.; Binns, M. S.; Sheil, M. M. *J. Appl. Polym. Sci.* **1995**, 56, 1589.
8. McEwen, C. N.; Simonsick, W. J., Jr.; Larsen, B. S.; Ute, K.; Hatada, K. *J. Am. Soc. Mass Spectrom.* **1995**, 6, 906.
9. Mahon, A.; Kemp, T. J.; Buzy, A.; Jennings, K. R. *Polymer* **1996**, 37, 531.
10. Hunt, S. M.; Sheil, M. M.; Belov, M.; Derrick, P. J. *Anal. Chem.* **1998**, 70, 1812.
11. Adamus, G.; Kowalczuk, M. *Rapid Commun. Mass Spectrom.* **2000**, 14, 195.
12. Yalcin, T.; Gabryelski, W.; Li, L. *Proceedings of the 46th ASMS Conference on Mass Spectrometry and Allied Topics*, Orlando, FL, May 31-June 4, **1998**, p1053.
13. Yalcin, T.; Gabryelski, W.; Li, L. *Anal. Chem.* **2000**, 72, 3847.

14. Chen, R.; Tseng A. T., Uhing M., L. Li, *J. Am. Soc. Mass Spectrom.* **2001**, 12, 55.

15. Chen, R.; Li, L. *J. Am. Soc. Mass Spectrom.* **2001**, 12, 832.

16. Botrill A. R.; Giannakopulos, A. E.; Millichope A.; Lee, K. S.; Derrick, P. J.; *Eur. J. Mass Spectrom.* **2000**, 6, 225.

17. Whittal, R. M.; Li, L.; Lee, S.; Winnik, M. A. *Macromol. Rapid Commun.* **1996**, 17, 59.

18. Lee, S.; Winnik, M. A.; Whittal, R. M.; Li, L. *Macromolecules,* **1996**, 29, 3060.

19. Whittal, R. M.; Schriemer, D. C.; Li, L. *Anal. Chem.* **1997**, 69, 2735.

20. *Poly(ethylene glycol) Chemistry: Biotechnical and Biomedical Applications:* Harris, J.M., Ed.; Plenum Press: New York, **1992**.

21. Roberts, M.; Scholes, D. F. in *Chemical Aspects of Drug Delivery Systems:* Karsa, D.R., Stephenson, R.A., Eds. The Royal Society of Chemistry: Cambridge, **1996**; p89.

22. Lattimer, R. P.; Munster, H.; Budzikiewicz, H. *Int. J. Mass Spectrom. Ion Proc.* **1989**, 90, 119.

23. Lattimer, R. P. *J. Am. Soc. Mass Spectrom.* **1992**, 3, 225.

24. Lattimer, R. P. *Int. J. Mass Spectrom. Ion Proc.* **1992**, 116, 23.

25. Lattimer, R. P. *J. Am. Soc. Mass Spectrom.* **1994**, 5, 1072.

26. Selby, T. L.; Wesdemiotis, C.; Lattimer, R. P. *J. Am. Soc. Mass Spectrom.* **1994**, 5, 1081.

27. Bahr, U.; Deppe, A.; Karas, M.; Hillenkamp, F.; Giessman, U. *Anal. Chem.* **1992**, 64, 2866.

28. Danis, P. O.; Karr, D. E.; Mayer, F.; Holle, A.; Watson, C. H. *Org. Mass Spectrom.* **1992**, 27, 843.

29. Danis, P. O.; Karr, D. E. *Org. Mass Spectrom.* **1993**, 28, 923.

30. Juhasz, P.; Costello, C. E. *Rapid Commun. Mass Spectrom.* **1993**, 7, 343.

31. Prokai, L.; Simonsick, Jr. W. J. *Rapid Commun. Mass Spectrom.* **1993**, 7, 853.

32. Montaudo, G.; Montaudo, M. S.; Puglisi, C.; Samperi, F. *Macromolecules* **1995**, 28, 4562.

33. Dey, M.; Castoro, J. A.; Wilkins, C. L. *Anal. Chem.* **1995**, 67, 1575.

34. Blais, J. C.; Tessier, M.; Bolbach, G.; Remaud, B.; Rozes, L.; Guittard, J.; Brunot, A.; Marechal, E.; Talet, J. C. *Int. J. Mass Spectrom. Ion Proc.* **1995**, 144, 131.

35. Weidner, S.; Kuhn, G.; Just, U. *Rapid Commun. Mass Spectrom.* **1995**, 9, 697.

36. Fei, X.; Murray, K. K. *Anal. Chem.* **1996**, 68, 3555.

37. O'Connor, P. B.; Duursma, M. C.; van Rooij, G. J.; Heeren, R. M. A.; Boon, J. J. *Anal. Chem.* **1997**, 69, 2751.

38. Hensel, R. R.; King, R. C.; Owens, K. G. *Rapid Commun. Mass Spectrom.* **1997**, 11, 1785.

39. Parees, D. M.; Hanton, S. D.; Cornelio Clark, P. A.; Willcox, D. A. *J. Am. Soc. Mass Spectrom.* **1998**, 9, 282.

40. Pastor, S. J.; Wilkins, C. L. *Int. J. Mass Spectrom. Ion Proc.* **1998**, 175, 81.

41. Pasch, H. *Phys. Chem. Chem. Phys.* **1999**, 1, 3879.

42. Rashidzadeh, H.; Wang, Y.; Guo, B. C. *Rapid Commun. Mass Spectrom.* **2000**, 14, 439.

43. Wong, S. F.; Meng, C.K.; Fenn, J. B. *J. Phys. Chem.* **1988**, 92, 546.

44. Takashi, N.; Fenn, J. B. *J. Am. Chem. Soc.* **1992**, 114, 3241.

45. O'Connor, P. B.; McLafferty, F. W. *J. Am. Chem. Soc.* **1995**, 117, 12826.

46. Maziarz, E. P.; Baker, G. A.; Lorenz, S. A.; Wood, T. D. *J. Am. Soc. Mass Spectrom.* **1999**, 10, 1298.

47. Guo, X. H.; Fokkens, R. H.; Peeters, H. J. W.; Nibbering, N. M. M.; de Koster, C. G. *Rapid Commun. Mass Spectrom.* **1999**, 13, 2223.

48. Watson, E.; Shah, B.; DePrince, R.; Hendren, R. W.; Nelson, R. *BioTechnique* **1994**, 16, 278.

49. Weidner, S.; Kuhn, G. *Rapid Commun. Mass Spectrom.* **1996**, 10, 942.

50. Bullock, J.; Chowdhury, S.; Johnston, D. *Anal. Chem.* **1996**, 68, 3258.

51. Barry, J. P.; Carton, W. J.; Pesci, K. M.; Anselmo, R. T.; Radtke, D. R.; Evans, J. V. *Rapid Commun. Mass Spectrom.* **1997**, 11, 437.

52. Sauvagnat, B.; Enjalbal, C.; Lamaty, F.; Lazaro, R.; Martinez, J.; Aubagnac, J. -L. *Rapid Commun. Mass Spectrom.* **1998**, 12, 1035.

53. Enjalbal, C.; Sauvagnat, B.; Lamaty, F.; Lazaro, R.; Martinez, J.; Mouchet, P.; Roux, F.; Aubagnac, J. -L. *Rapid Commun. Mass Spectrom.* **1999**, 13, 1775.

54. Barton, Z.; Kemp, T. J.; Buzy, A.; Jennings, K. R. *Polymer* **1995**, 36, 4927.

55. Sherrard, K. B.; Marrlott, P. J.; McCormick, M. J.; Colton, R.; Smith, G. *Anal. Chem.* **1994**, 66, 3395.

56. Crescenzi, C.; Di Corcia, A.; Samperi, R.; Marcomini, A. *Anal. Chem.* **1995**, 67, 1797.

57. Ogura, I.; DuVal, D. L.; Kawakami, S.; Miyajima, K. *J. Am. Oil Chem. Soc.* **1996**, 73, 137.

58. Cumme, G. A.; Blume, E.; Bublitz, R.; Hoppe, H.; Horn, A. *J. Chromatogr. A* **1997**, 791, 245.

59. Crowther, M. W.; O'Connell, T. R.; Carter, S.P. *J. Am. Oil Chem. Soc.* **1998**, 75, 1867.

60. Van Rooij, G. J.; Duursma, M. C.; de Koster, C. G.; Heeren, R. M. A.; Boon, J. J.; Wijnand Schuyl, P. J.; van der Hage, E. R. E. *Anal. Chem.* **1998**, 70, 843.

61. Willetts, M.; Clench, M. R.; Greenwood, R.; Mills, G.; Carolan, V. *Rapid Commun. Mass Spectrom.* **1999**, 13, 251.

62. Castillo, M.; Alonso, M. C.; Riu, J.; Barcelo, D. *Environ. Sci. Technol.* **1999**, 33, 1300.

63. van Berkel, G. B.; McLuckey, S. A.; Glish, G. L. *Anal. Chem.* **1992**, 64, 1586.

64. Gianelli, L.; Amendola, V.; Fabbrizzi, L.; Pallavicini, P.; Mellerio, G. G. *Rapid Commun. Mass Spectrom.* **2001**, 15, 2347.

65. Cha, B.; Blades, M.; Douglas, D. J. *Anal. Chem.* **2000**, 72, 5647.

66. Davoli, E.; Gross, M. L. *J. Am. Soc. Mass Spectrom.* **1990**, 1, 320.

67. Gross, M. L. *Int. J. Mass Spectrom.* **2000**, 200, 611.

68. Cheng, C.; Gross, M. L. *Mass Spectrom. Rev.* **2000**, 19, 398.

69. Deterding, L. J.; Gross, M. L. *Anal. Chim. Acta* **1987**, 200, 431.

70. Deterding, L. J.; Gross, M. L. *Org. Mass Spectrom.* **1988**, 23, 169.

71. Crockett, J. S.; Gross, M. L.; Christie, W. M.; Holman, R. T. *J. Am. Soc. Mass Spectrom.* **1990**, 1, 183.

72. Cordero, M. M.; Wesdemiotis, C. *Anal. Chem.* **1994**, 66, 861.

73. Whalen, K.; Grossert, J. S.; Boyd, R. K. *Rapid Commun. Mass Spectrom.* **1995**, 9,1366.

74. Claeys, M.; Nizigiyimana, L.; van den Heuvel, H.; Derrick, P. J. *Rapid Commun. Mass Spectrom.* **1996**, 10, 770.

75. Nizigiyimana, L.; van den Heuval, H.; Claeys, M. *J. Mass Spectrom.* **1997**, 32, 277.

76. Huysmans, L.; Nizigiyimana, L.; van den Heuvel, H.; Claeys, M. *Int. J. Mass Spectrom.* **1999**, 188, 39.

77. Denekamp, C.; Heuvel, H. V.; Voinov, V. G.; Claeys, M.; Seto, C.; Grossert, J. S.; Waddell, D. S; Curtis, J. M.; Boyd, R. K. *Rapid Commun. Mass Spectrom.* **2000**, 14, 1035.

Chapter 7. Composition Analysis of Ethylene Oxide/Propylene Oxide Copolymer by MALDI MS

Matrix-assisted laser desorption ionization (MALDI) mass spectrometry has become an important tool for polymer characterization. This technique has been successfully applied to such areas as molecular mass determination, structure and end group identification, monitoring molecular association and degradation, and copolymer sequence and composition analysis [1-3]. This chapter focuses on copolymer composition analysis by MALDI.

The analysis of copolymers is generally more complicated compared to the analysis of homopolymers. For a simple A_mB_n type copolymer, in addition to the determination of average molecular mass, average molecular mass distribution, structure of repeat units and end-groups, a complete characterization should at least also include the average molar ratio of A and B, the number average length of A and B blocks.

Currently, NMR and MS are two commonly used techniques for copolymer composition analysis. Both techniques heavily rely on the statistical models for oligomer distribution in a copolymer. In short, Bernoullian distribution depicts the scenario where all co-monomers have equal probability to be added to a growing chain; hence, it deals with random copolymers. In a Markoffian distribution, one monomer is favorably added to the growing chain than is the other monomer; therefore, it is suitable for block or segmented copolymers [4-5].

A form of this chapter is published as:
R. Chen, N. Zhang, A. M. Tseng, and L. Li, "Effects of MALDI experimental conditions on quantitative composition analysis of ethylene oxide/propylene oxide copolymer", *Rapid Commun. Mass Spectrom.* **2000**, 14, 2175-2181.

In conjunction with the statistical models, NMR is a powerful tool for copolymer sequence and composition analysis by relating peak intensities to sequence probabilities. A detailed account can be found in references 6-8, and is beyond the intended scope of current work. However, for the EO/PO copolymers studied in this work, a large discrepancy was found between the composition results from NMR and that from feed ratio provided by the manufacturer, as indicated in Table 7.1. The most obvious difference is in standard #1, where no EO units were added during the synthesis, yet NMR gives a significant weight percentage of EO. One possible explanation is that this sample was contaminated by a small amount of ethoxylates that is not an intended part of the product. This demonstrates a common problem associated with NMR approach for copolymer composition analysis. It operates in a "blindfold" manner. Only average information can be obtained, sometimes at the expense of structural details. Mass spectrometry, on the other hand, is able to offer a direct vision of the polymer at an individual chain level. For the above case, such ethoxylate interference can be easily identified and excluded from the composition analysis.

Table 7.1. Comparison of composition results from NMR and feed ratio.

Sample Identity	Feed Ratio (wt% EO)	NMR (wt% EO)
Standard #1	0	4
Standard #2	14	20
Standard #3	29	35
Standard #4	46	51

MALDI MS has been applied to the composition analysis of a number of copolymer systems. Among others, Montaudo and co-workers have contributed a significant number of publications in this research area [9, and the literature cited therein]. Briefly, they investigated two methods suitable for composition calculation. The first method is the chain statistics approach [10-11], which compares the experimental mass spectra intensities with those derived from a specific model. The second method is to employ a combination of peak intensities to compute the average copolymer composition, termed the composition estimates (C_A), using the following equation [10, 12-13]:

$$C_A = \frac{\sum\sum mI(A_mB_n)}{\sum\sum (m+n)I(A_mB_n)} \qquad \textbf{Equation 7.1}$$

in which, the summations are over monomer repeat unit number m and n, and $I(A_mB_n)$ is the spectral intensity. An intuitive description of this equation is that the molar ratio of the co-monomers in each copolymer chain is calculated by mass assignment, and then averaged by molar number (reflected by peak intensity) over the entire mass region, much similar to the number average mass calculation (Equation 1.4). This equation will be adapted for the composition calculation in this chapter.

One underlying assumption for both MS methods is that peak intensity truly reflects the constituent quantity. However, this is not necessarily the case in polymer MALDI MS. Mass discrimination, i.e., certain species are misrepresented with peak intensity disproportional to their true quantity, could result from sample preparation, desorption/ionization, transmission, detection, as well as sample functionality [1, 14-20]. Overlooking this factor will jeopardize the foundation of these methods.

The main focus of the work presented in this chapter is to investigate the effect of experimental conditions on composition determination. It is demonstrated that experimental conditions can significantly change the spectral appearance (i.e. peak intensity). For the copolymer system studied, an alternative approach based on average molecular mass (M_n) is proposed and validated for composition computation.

7.1 Introduction

Matrix-assisted laser desorption ionization (MALDI) mass spectrometry has been demonstrated to be a powerful tool for providing accurate average molecular masses of many polymers with narrow polydispersity [1,2]. For number average (M_n) and weight average (M_w) molecular mass calculations of a polymer, MALDI mass spectra are first normalized and the relative peak intensities of oligomer ions are used to represent relative abundances of oligomer molecules in the polymer. Although there are potentially a number of experimental parameters that can affect the appearance of a mass spectrum, and hence the M_n and M_w results, many of these parameters can be controlled [1,14-15]. For example, the type of solvent can influence the mass spectral data [16-20]. But so long as the use of nonsolvents (i.e., those solvents that do not dissolve the analyte well) in sample preparation is avoided, reproducible mass spectra and reliable M_n and M_w can be obtained [19]. The possibility of obtaining accurate M_n and M_w data suggests that oligomers with minor chain length variations within a narrow mass range should have a similar overall analytical response. In a quantitative sense, each individual oligomer in a narrow polydispersity homopolymer can play the role of an internal standard for relative quantification of the other oligomers. This is not surprising in light of the fact that oligomers have the same backbone structures with only minor variation in number of

repeat units. Of course, for a polymer with broad polydispersity, there is a large variation in the number of repeat units over a broad mass range. Mass discrimination can take place, resulting in poor representation of the actual oligomer distribution in a MALDI spectrum [14-15].

One of the great strengths of MALDI is its ability to generate compositional information on a polymeric material. Determination of copolymer composition represents an important area of application that capitalizes on this unique strength [9-13, 21-44]. However, the requirement for quantitative composition analysis of a copolymer by mass spectrometry is much more stringent than average molecular mass determination. A copolymer is composed of different building blocks that may give different overall detection responses [31]. Thus relative peak intensities from different building blocks in a mass spectrum may not reflect the true copolymer composition.

Quantitative analysis of copolymer composition by MALDI has been demonstrated in a limited number of systems with varying degrees of success. For example, Abate *et al.* demonstrated that the relative amounts of hydroxybutyrate and hydroxyvalerate in a random copolymer, poly(β-hydroxybutyrate-co-β-hydroxyvalerate), determined by MALDI, agreed with those expected from theory [22]. Wilczek-Vera *et al.* have shown that, for diblock copolymers of poly(α-methylstyrene)-b-polystyrene, the mole fraction of poly(α-methylstyrene) determined by MALDI is similar to that obtained by NMR and GPC, as well as from reagent ratio calculation [28]. The assumption of uniform response from structurally very similar polystyrene and polymethylstyrene seems to be valid in this case. On the other hand, for copolymers with greater monomer structural differences, composition analysis by MALDI can be problematic. For example, for diblock copolymers of poly(α-methylstyrene)-b-poly(4-vinylpyridine), the molar

fraction of poly(α-methylstyrene) determined by MALDI can be quite different from that obtained by other methods [42]. A bias in MALDI data was also reported for composition analysis of copolymers of methyl methacrylate and n-butyl methacrylate [29]. Servaty and coworkers demonstrated that quantitative compositional interpretation could be difficult with MALDI data alone for poly(dimethylsiloxane)-co-poly(hydromethysiloxane) [40]. In addition, they noted that the laser power could affect the relative peak intensities in the MALDI spectrum of the copolymer [40].

The objective of this study is to develop a mass spectrometric approach that would provide rapid and accurate quantitative composition information on copolymers. Of particular interest is composition analysis of ethylene oxide (EO)/propylene oxide (PO) copolymers [45]. The structurally similar EO and PO polymers are expected to have very similar detection responses. For example, a mixture of well-blended poly(ethylene glycol) and poly(propylene glycol) homopolymers of similar molecular weights shows similar detection efficiencies. However, it is found that experimental conditions in MALDI can significantly influence the mass spectral appearance of EO/PO copolymer. This work has implications for the practice of using MALDI as a tool for deducing quantitative composition information on EO/PO copolymers, and likely other types of copolymers as well.

7.2 Experimental

7.2.1 Materials and Reagents. The EO/PO copolymers were from Nalco Chemical (Naperville, IL). NMR results indicate that the sample used in the first study (section7.3.1) contains 4 wt% EO and 96 wt% PO, and the series used in the second study (section 7.3.2) contain varying weight percentages of EO, as shown in Table 7.1. *All-trans* retinoic acid (RA), dithranol and 2-(4-hydroxyphenylazo)-benzoic acid (HABA)

were purchased from Aldrich Chemical Co (Milwaukee, WI). HPLC grade acetone, methanol and tetrahydrofuran (THF) were from Fisher (Mississauga, ON). All chemicals were used without purification.

7.2.2 MALDI TOF MS. A dried-droplet method was employed in all sample preparation. Briefly, sample solution was mixed with 0.1 M matrix/THF solution at different ratios. Thereafter, a 0.5 µl aliquot was deposited onto a stainless-steel sample target. Unless specified, a matrix solution of 0.1 M RA in THF was used in all experiments. The laser power was adjusted slightly above the threshold of the desorption/ionization process except in the laser effect study, in which laser power was varied and indicated by laser index (LI).

MALDI experiments were carried out using an Applied Biosystems Voyager laser desorption/ionization time-of-flight (TOF) mass spectrometer (Framingham, MA) equipped with a 337-nm pulsed nitrogen laser. Ions were detected by the reflectron TOF. All spectra were the results of signal averaging of between 100 and 200 shots and calibrated externally using peptide mixtures. All data were reprocessed using the Igor Pro Software package (WaveMetrics, Lake Oswego, OR) and no background subtraction was performed.

7.3 Results and Discussion

7.3.1 Effects of MALDI Experimental Conditions on Quantitative Composition Analysis of Ethylene Oxide/Propylene Oxide Copolymer.

Figure 7.1A shows the mass spectrum of the EO/PO copolymer studied in this work. The expanded spectrum in a mass range that covers one repeat pattern of peaks is shown in Figure 7.1B. A repeat pattern consists of four clusters of peaks that arise from

several series of distributions representing different PO and EO compositions as well as different end-groups. This EO/PO copolymer was initiated with a mixture of long-chain alcohols, $C_{18}H_{37}OH$ (C18) and $C_{16}H_{33}OH$ (C16). The general formula is as follows:

$$C18 \text{ or } C16\text{-}[CH_2\text{-}CH(CH_3)\text{-}O]_n\text{-}[CH_2\text{-}CH_2\text{-}O]_m\text{-}H$$

where n and m correspond to the PO and EO numbers in the structural formula, respectively. All peaks detected in MALDI spectra are Na^+ adduct peaks. This is confirmed by adding KCl to the sample preparation and observing the mass shift resulted from the replacement of Na^+ by K^+. The addition of 1% (v/v) 0.1 M NaCl to the sample aliquot did not alter the mass spectrum shown in Figure 7.1, indicating that the sample itself contains a large amount of sodium salt. The effects of different type of metal ions on the mass spectral appearance are not studied in this work.

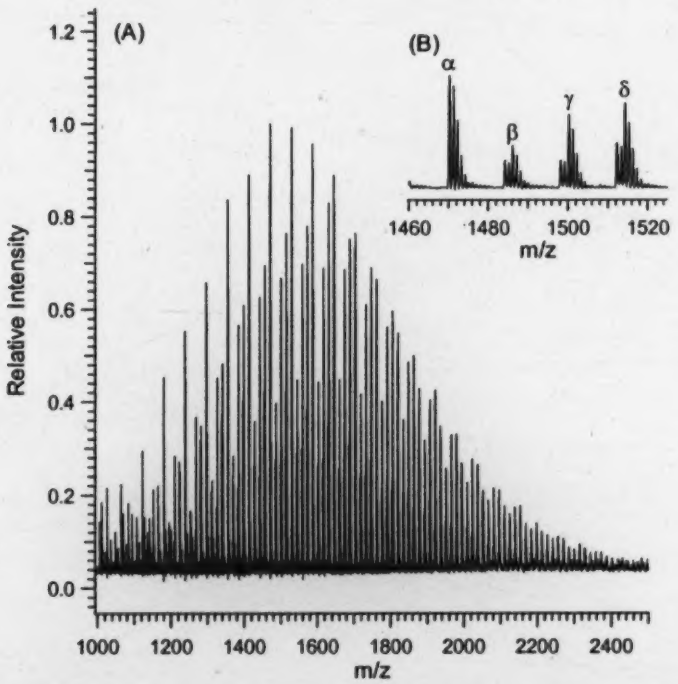

Figure 7.1. (A) MALDI-TOF mass spectrum and (B) expanded spectrum of an EO/PO copolymer. *All-trans* retinoic acid was used as the matrix.

Table 7.2 lists the peak assignments for the ^{12}C isotope peaks shown in Figure 7.1B. Peak cluster α consists of two isobaric oligomers. Since they have the same ostensible formula, there is only one isotope pattern displaying at least five discernable peaks. Cluster β is from four oligomers, with a 2 Da mass difference between two pairs of possible formulae, and shows seven major peaks from these two overlapping isotope patterns. Clusters γ or δ are also from two overlapping isotope patterns, displaying seven peaks.

Table 7.2. Assignment of major peaks shown in Figure 7.1B.

Peak Cluster	Experimental Mass	Formula	Calculated Mass
α	1470.2	18PO+3EO+C18	1470.1
		20PO+1EO+C16	
β	1484.3	19PO+2EO+C18	1484.1
		21PO+C16	
	1486.1	16PO+6EO+C18	1486.1
		18PO+4EO+C16	
γ	1498.2	20PO+1EO+C18	1498.1
	1500.2	17PO+5EO+C18	1500.1
		19PO+3EO+C16	
δ	1512.2	21PO+C18	1512.2
	1514.3	18PO+4EO+C18	1514.1
		20PO+2EO+C16	

Since the relative amounts of all these oligomers can affect the properties of this copolymer, quantitative information on the copolymer composition would be very useful for studies of the relationship between the structure/composition and polymer activity [45]. MALDI can potentially provide the quantitative information. A fundamental requirement for generating quantitative results is that the MALDI spectra must reflect the actual composition of a copolymer. Before one can establish a relation between composition and relative peak intensities in MALDI spectra, it is crucial to ensure that the MALDI spectra can be reproducibly obtained. Understanding how spectra can be affected by the experimental conditions is clearly the first step in developing a mass spectrometric approach for compositional quantification. For this EO/PO sample, the type of matrix and solvent used for sample preparation, the analyte and matrix ratio and the laser power can have a significant effect on mass spectral appearance, as demonstrated below.

Figure 7.2 shows the effect of matrix on MALDI spectra of the EO/PO copolymer. The peak intensities are normalized to cluster α. The peak intensities are normalized to cluster α. Table 7.3 lists the relative peak intensities of these clusters. The experimental variation among repeat experiments under a specific matrix condition is generally less than 2% RSD. The large variation among matrices (Table 7.3) is clearly statistically significant, indicating that the type of matrix used can affect the relative intensities of these oligomers. In addition, the extent of this peak intensity variation is mass dependent. The relative intensity changes are smaller as masses of the oligomers increase. This can be seen by comparing the spectra shown in Figure 7.2A and Figure 7.2B. This observation suggests that, as the polymer chain length increases, the MALDI responses from different components become more uniform. In an earlier work by

Whittal *et al.* with poly(ethylene glycol), it is shown that the type of matrix can affect the MALDI mass resolution and sensitivity [46]. The relative peak intensity changes in the copolymer spectra are likely due to the different degrees of sensitivity variation responding to the change of matrix.

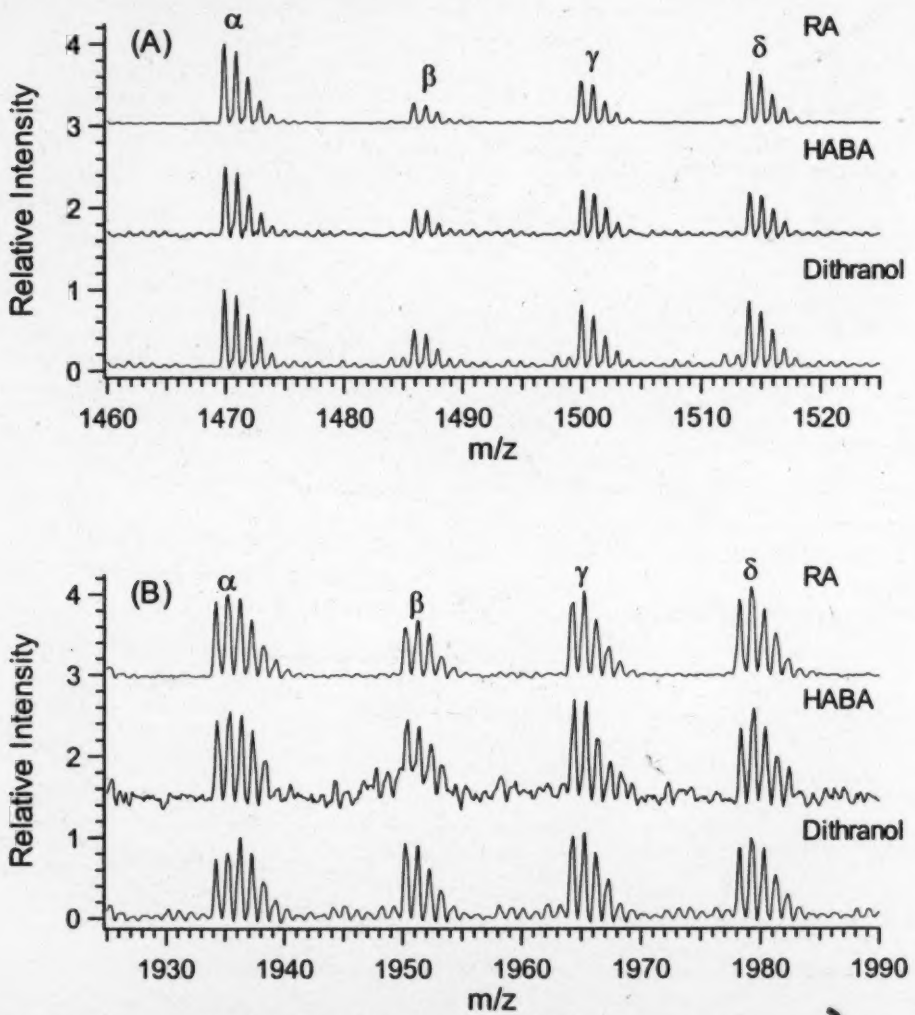

Figure 7.2. Expanded MALDI-TOF mass spectra obtained by using different matrices: (A) low mass and (B) high mass region of the copolymer distribution. The copolymer sample was mixed with 0.1 M matrix/THF solution in 1:10 volume ratio. The laser power used was at the desorption/ionization threshold (LI = ~1750).

Table 7.3. Relative peak ratios among the ^{12}C peaks from different clusters obtained by using different matrices.

	α/α	β/α	γ/α	δ/α
RA	1	0.26	0.54	0.65
HABA	1	0.38	0.64	0.62
Dithranol	1	0.50	0.80	0.85
RSD	0	31.5%	20.0%	17.7%

The effect of solvent on mass spectral patterns is shown in Figure 7.3. Using RA as the matrix and various solvents for sample preparation, the mass spectral variation is quite significant. For example, when methanol is used the oligomers with lower numbers of EO units (see peaks labeled as L in Figure 7.3ii) are detected with much higher relative intensities, compared to those using THF as the solvent (Figure 7.3iii). The extent of the solvent effect is also mass dependent (see Figure 7.3A and Figure 7.3B). Acetone, methanol and THF are all good solvents for the copolymer. Polymer precipitation prior to matrix crystallization is not expected. However, the morphology of matrix crystals formed is dependent on the type of solvent(s) used [19]. It is known that analyte distribution can be affected by the crystal morphology [47]. Thus the solvent effect observed in this copolymer analysis is likely due to the difference in polymer incorporation and distribution in the matrix crystals. Other more uniform sample preparation methods such as electrospray [48,49] may overcome this solvent effect.

It is interesting to note that there seems to be a correlation between the polarity of solvent and relative signal intensities of peak L. The order of polarity is methanol > acetone > THF. The spectra of the copolymer obtained by using methanol as the solvent

show a more intense peak L than those obtained with acetone (see Figure 7.3). The use of THF generates the spectra with very low intensity for peak L. Among all the "good" solvents, polarity match between analyte and solvent might play an important role in the final spectral appearance. The generality of this observation, and any possible correlation between the properties of solvent and analyte, should be investigated in the future.

The most significant peak intensity variation is shown in Figure 7.4 where the analyte to matrix ratio is changed. Low analyte concentration favors the detection of peaks labeled as L. Mass dependence of this concentration effect is shown by comparing Figure 7.4A with Figure 7.4B. The exact cause of the concentration effect is difficult to ascertain. It is plausible that ion suppression is reduced as analyte concentration decreases, resulting in the increase in signal intensities of the minor components (i.e., peaks L). It is noted that the minor components are completely suppressed throughout the entire mass region studied for the sample prepared at the ratio of 1:10.

Finally, Figure 7.5 shows the laser dependence of mass spectral patterns for the copolymer. Some variations in relative intensity are observed but the magnitude of the variation is not as great as those due to the effects of matrix, solvent and analyte concentration. In the high mass region, the relative intensity changes are barely noticeable. Note that the use of excessively high laser power should always be avoided in MALDI analysis of a polymer to avoid detector saturation. In the case of analysis of a copolymer, detector saturation will result in under-determination of the major components, since the signals from the major components will become saturated first.

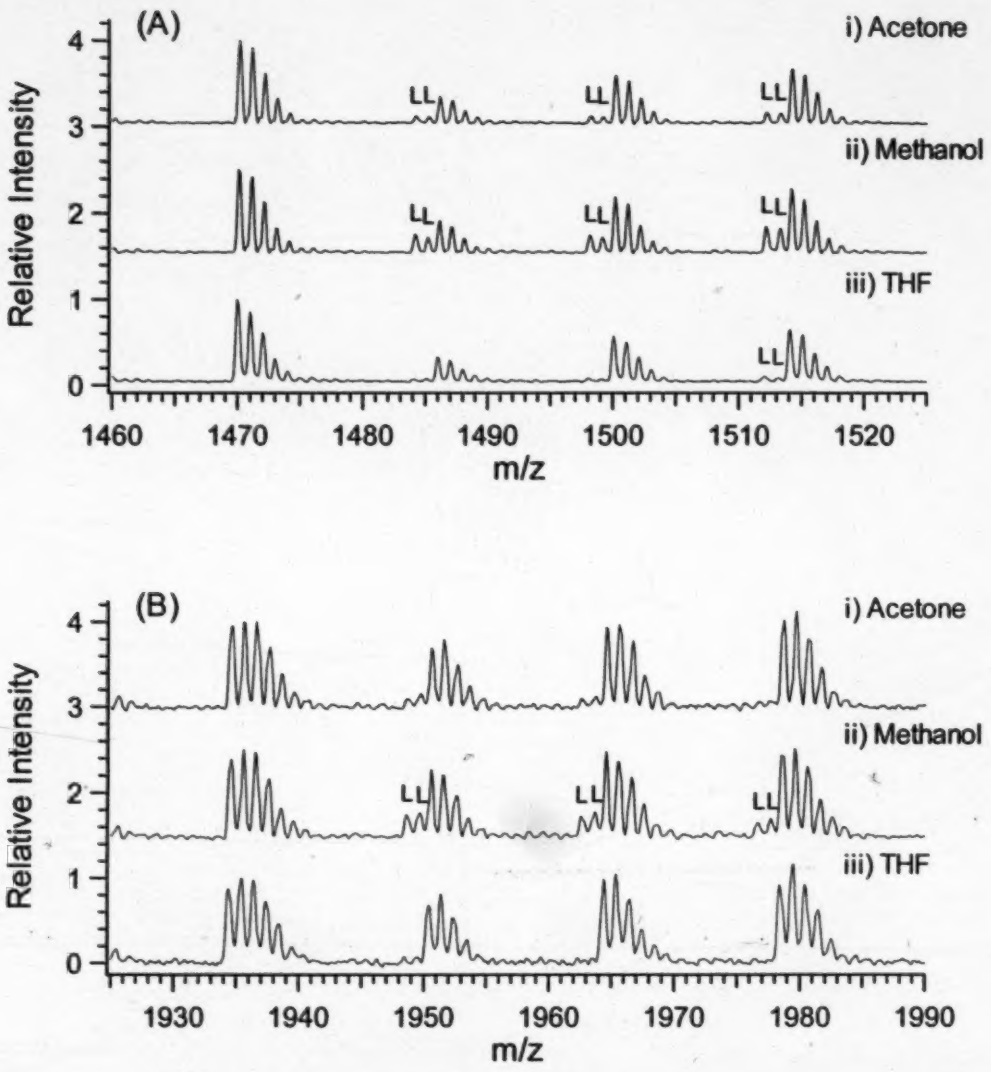

Figure 7.3. Expanded MALDI-TOF mass spectra obtained by using different solvents: (A) low mass and (B) high mass region of the copolymer distribution. *All-trans* retinoic acid was used as the matrix. The copolymer sample was mixed with 0.1 M matrix solution in different solvents in 1:15 volume ratio. The laser power used was at the desorption/ionization threshold (LI = ~1750).

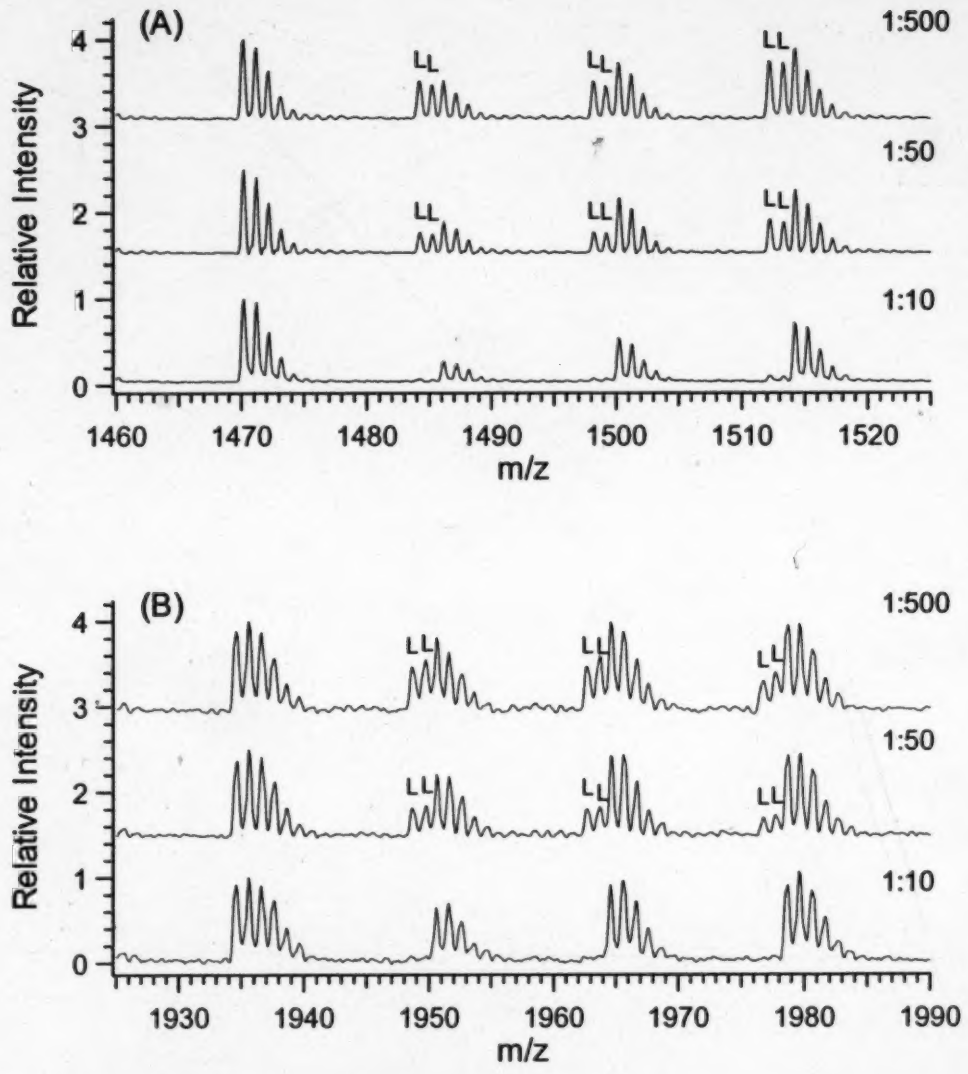

Figure 7.4. Expanded MALDI-TOF mass spectra obtained by using different analyte concentrations: (A) low mass and (B) high mass region of the copolymer distribution. *All-trans* retinoic acid was used as the matrix. The number shown refers to the volume ratio of the copolymer sample and 0.1 M matrix/THF solution. The laser power used was at the desorption/ionization threshold (LI = ~1750).

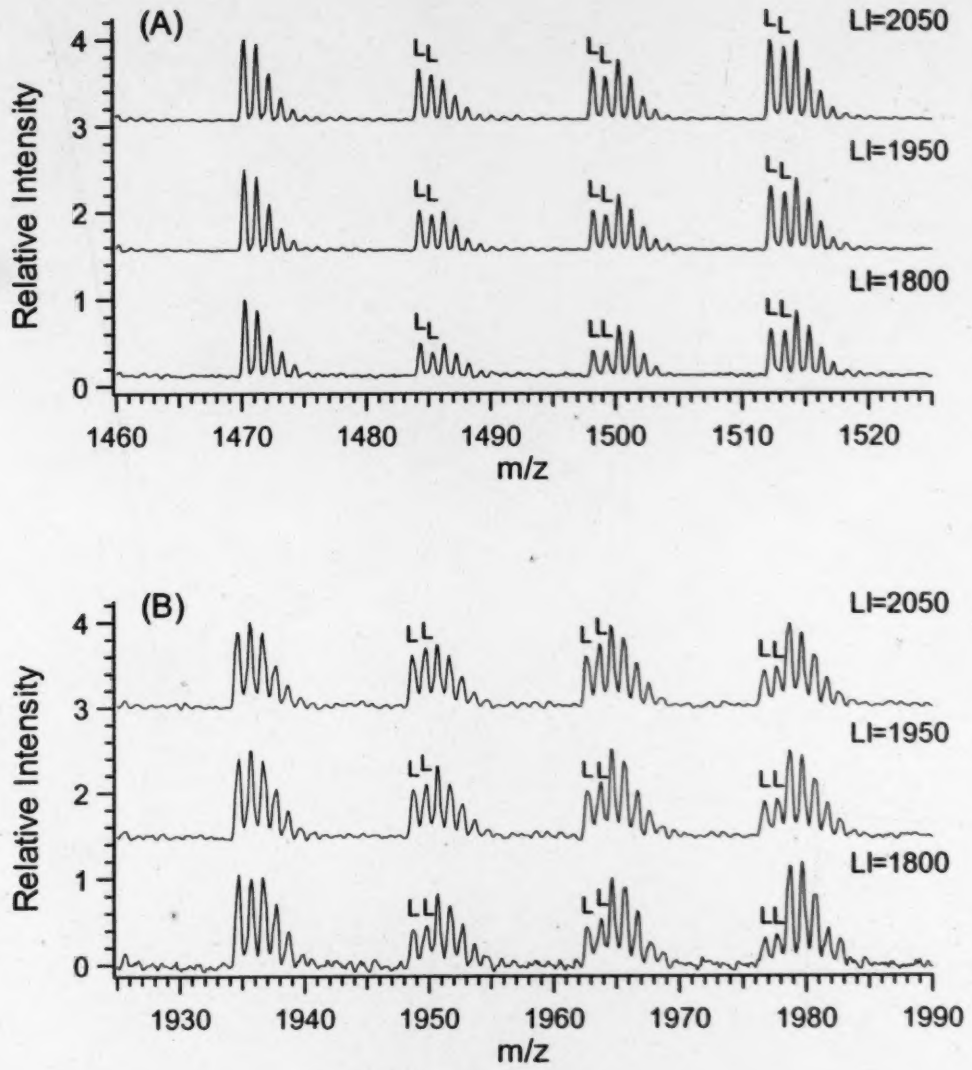

Figure 7.5. Expanded MALDI-TOF mass spectra obtained by using different laser power: (A) low mass and (B) high mass region of the copolymer distribution. *All-trans* retinoic acid was used as the matrix. The copolymer sample was mixed with 0.1 M matrix/THF solution in a volume ratio of 1:100. Note that, the desorption/ionization threshold is LI=~1750.

7.3.2 A Statistical View: Compositional Estimate *vs.* Average Molecular Mass.

In the previous section, it was demonstrated that the type of matrix, solvent, analyte/matrix ratio, and laser power all influence the copolymer composition analysis, but in a much intuitive manner by observing the spectral appearance. The matter is further pursued in this section via the means of statistics to examine to what extent these experimental conditions will affect the outcome of composition calculations. The type of solvent, type of matrix, and analyte/matrix ratio are all considered in the study.

A series of EO/PO copolymers were analyzed. The copolymers were synthesized at Nalco Chemical Co. (Naperville, IL) in such a manner that the EO/PO ratios were systematically varied. The reactions were initiated by $C_{16}H_{33}OH$ under basic conditions. Propylene oxide was then added and polymerized to certain chain lengths. Afterwards, differing amounts of ethylene oxide were added. The reactions were finally terminated at the desired molecular mass by the addition of acid solution. The resulting copolymers have the following general formula, and number average molecular masses (M_n) ranging from ~1000 Da to ~2500 Da.

$$C_{16}H_{33}O\text{-}(C_3H_6O)_m\text{-}(C_2H_4O)_n\text{-}H$$

MALDI spectra on these polymers were obtained under various experimental conditions. Figure 7.6 shows the representative MALDI mass spectra of five EO/PO copolymers under the experimental conditions listed in the figure caption. When the EO percentage increases (A to D), the oligomer distribution shifts towards high mass accordingly. The number of peaks increases as well, and the spectrum becomes formidably complex for sample Standard #4. It has been pointed out that, for an AB type copolymer, the number of peaks increases linearly with the chain size [3]. Consequently, high resolution is generally required to detect separated peaks. In the current case, an

oligomer resolution or better (depending on sample complexity) was achieved for all samples studied, enabling subsequent computations. Note that all peaks detected are sodium-adduct peaks, and as such, a 23 Da deduction should be included in any average mass calculation.

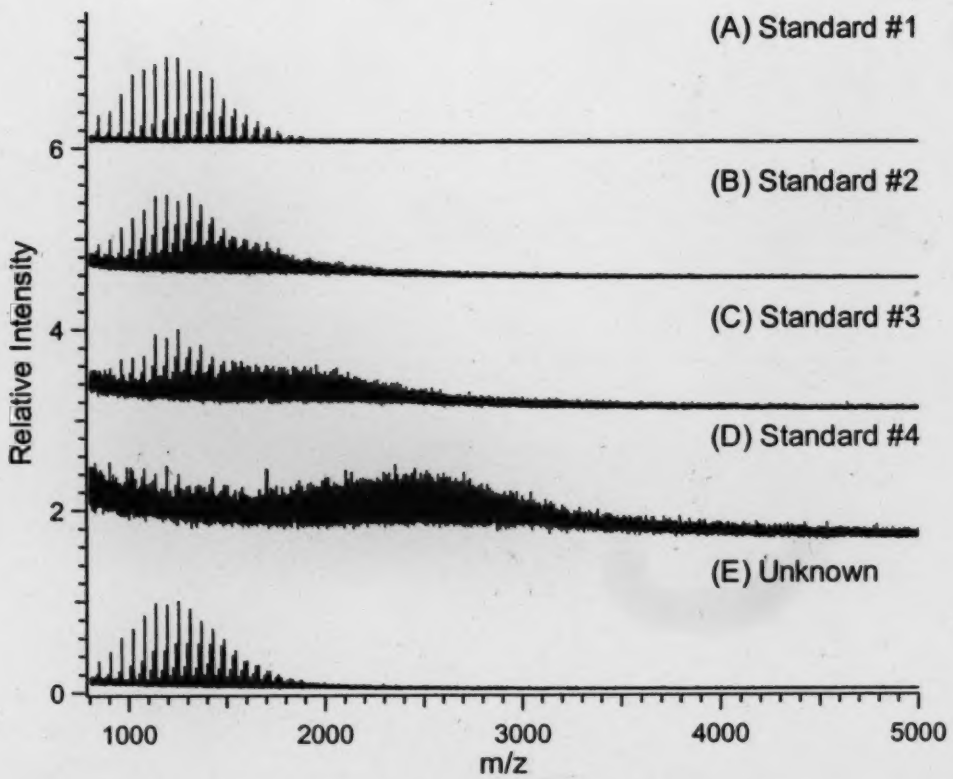

Figure 7.6. MALDI mass spectra of four standards and one unknown sample. All samples were dissolved in THF and RA was used as the matrix. Analyte/Matrix=1:10 (v/v).

For each spectrum, the EO/PO ratio and average molecular mass (M_n) were calculated using Equations 7.2 and 7.3.

$$EO/PO = \frac{\sum I(n/m)}{\sum I} \qquad \textbf{Equation 7.2}$$

$$Mn = \frac{\sum IM}{\sum I} \qquad \textbf{Equation 7.3}$$

Equation 7.2 is a varied form of Equation 7.1, in which *I* is the peak intensity and *m* and *n* are the numbers of repeat units of propylene oxide and ethylene oxide, respectively. This calculation will be referred to as the "composition estimate" approach. *M* in Equation 7.3 denotes the nominal mass of each individual peak. Under each chosen experimental condition, five replicate experiments were performed. For EO/PO and M_n, their average and standard deviation within one set of replicate experiments and among different sets of experiments were calculated. Representative results are listed in Tables 7.4-7.6.

A computer *C* program (see appendix) was developed and used to expedite the composition calculation. The basic algorithm is described in the flowchart in Figure 7.7. All variables were selected, tested, optimized, and kept constant for the sample under investigation to ensure a valid statistical analysis, but might differ from sample to sample due to the deterioration of spectral quality as average mass increases (Figure 7.6).

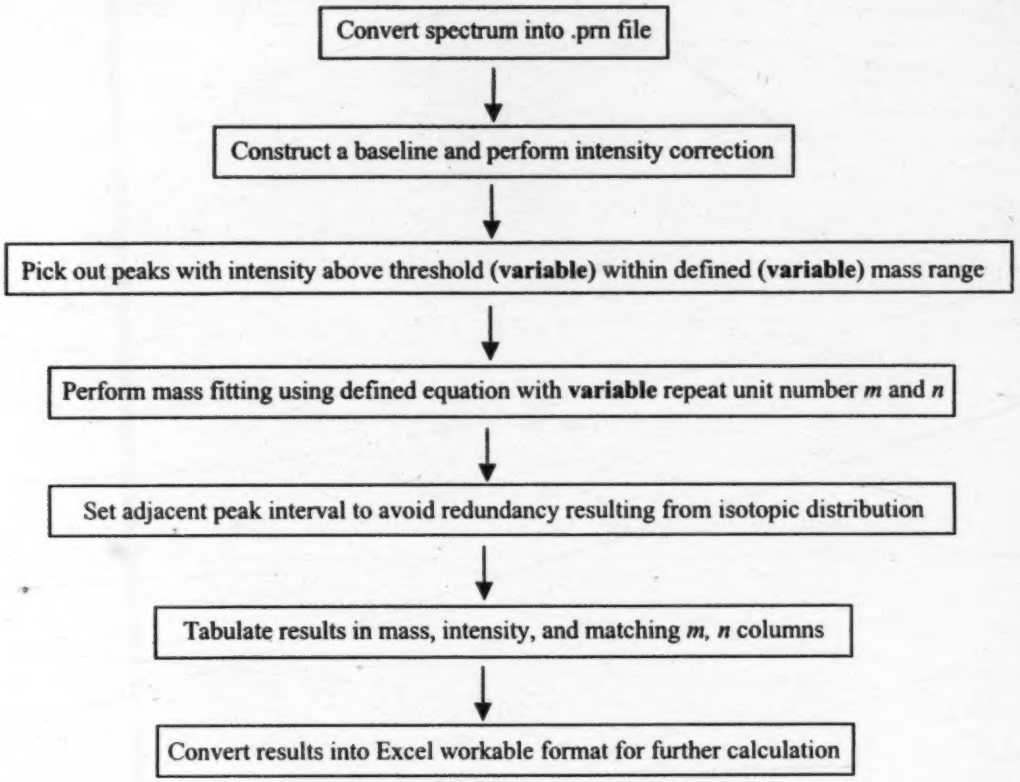
Convert spectrum into .prn file
Construct a baseline and perform intensity correction
Pick out peaks with intensity above threshold (variable) within defined (variable) mass range
Perform mass fitting using defined equation with variable repeat unit number m and n
Set adjacent peak interval to avoid redundancy resulting from isotopic distribution
Tabulate results in mass, intensity, and matching m, n columns
Convert results into Excel workable format for further calculation

Figure 7.7. Flow chart of computer *C* program "PeakPick".

Table 7.4 shows the solvent effect on EO/PO and M_n calculations for sample Standard #2. The result displays a surprisingly high discrepancy in EO/PO among three sets of replicate experiments. Even within one set of replicate experiments, the relative standard deviation (RSD) could be as high as 9.7% (in the case of methanol). More revealing information was obtained by performing a two-tailed *t*-test using the following equation [50]:

$$t = \frac{\left|\overline{X_1} - \overline{X_2}\right|}{\sqrt{\frac{\sigma_1^2}{n_1} + \frac{\sigma_2^2}{n_2}}}$$ **Equations 7.4**

in which, $\overline{X}$ is the average, σ^2 is the variance, and n is the number of replicate experiments. For example, taking data sets from acetone and methanol experiments, the experimental t is calculated to be 10.3, well above the critical t value 1.96 at 0.05 level of significance, meaning that these two averages are significantly different with 95% confidence. The question is therefore raised as to what condition should be considered as the "right" condition for composition analysis. This is especially problematic for unknown samples where no *a priori* information or reference is available. This result clearly suggests that great caution should be taken when interpreting composition result from "composition estimate" approach.

Table 7.4. Solvent effect on EO/PO and Mn calculation.

Solvent	Acetone		Methanol		THF	
	EO/PO	Mn	EO/PO	Mn	EO/PO	Mn
	0.152	1387	0.0980	1345	0.0980	1367
	0.173	1368	0.0843	1339	0.100	1357
	0.146	1389	0.0850	1358	0.0897	1351
	0.165	1397	0.105	1332	0.0930	1342
	0.161	1416	0.0987	1378	0.105	1350
Average	0.159	1391	0.0942	1350	0.0972	1353
RSD %	6.7	1.3	9.7	1.3	6.1	0.70
			EO/PO		Mn	
Overall Average (n=15)			0.117		1366	
Overall RSD % (n=15)			28		1.7	

Table 7.5. Analyte/Matrix (A/M) ratio effect on EO/PO and Mn calculation.

A/M	1:5		1:10		1:50	
	EO/PO	Mn	EO/PO	Mn	EO/PO	Mn
	0.302	1250	0.0980	1345	0.0732	1339
	0.233	1287	0.0843	1339	0.0886	1362
	0.256	1277	0.0897	1358	0.0711	1347
	0.308	1254	0.0930	1332	0.0725	1352
	0.299	1264	0.105	1378	0.0739	1337
Average	0.279	1266	0.0972	1353	0.0759	1347
RSD %	12	1.2	6.1	0.70	9.5	0.77
			EO/PO		Mn	
Overall Average (n=15)			0.151		1322	
Overall RSD % (n=15)			64		3.2	

Table 7.6. Matrix effect on EO/PO and Mn calculation.

Matrix	Dithranol		HABA		RA	
	EO/PO	Mn	EO/PO	Mn	EO/PO	Mn
	0.123	1443	0.107	1417	0.0980	1345
	0.151	1431	0.156	1358	0.0843	1339
	0.143	1440	0.146	1334	0.0897	1358
	0.123	1446	0.151	1341	0.0930	1332
	0.168	1417	0.102	1397	0.105	1378
Average	0.142	1436	0.132	1369	0.0972	1353
RSD %	13.8	0.81	19.4	2.6	6.1	0.70
			EO/PO		Mn	
Overall Average (n=15)			0.127		1388	
Overall RSD % (n=15)			20		3.1	

Similar observations were also found in the studies using different analyte/matrix ratios and different types of matrix, as shown in Tables 7.5 and 7.6. It is noted that when a low analyte/matrix ratio (1:5) were employed, the resulting EO/PO ratio of 0.279 is drastically higher than those from all other experiments. Apparently, in this case, the species with high EO/PO ratio were much preferentially ionized and overly represented in the MALDI spectra. Very irregular sample/matrix crystal formation was observed during the sample preparation in this case. It is hard to discern the exact cause for such an observation. One speculation is that when less than sufficient matrix is used, the polymer is not evenly spread over the sample target. Instead, high mass (hence, high EO/PO ratio) species along with most of the matrix quickly precipitate into the middle of target, hence, are preferentially desorbed and ionized. The matrix is then quickly depleted to prevent proportional amount of low mass species at the edge being ionized and detected.

Overall, the RSDs for EO/PO from the composition estimate approach among 15 experiments were 20% or greater. The largest deviation (64% RSD) results from the set of experiments where the analyte/matrix ratio was changed. This result indicates that when composition is analyzed, additional care should be taken with regard to the analyte/matrix ratio during the sample preparation. A series of experiments with varying ratios is recommended to establish a "dynamic range" over which no significant deviations should be observed.

On the other hand, all M_n calculations show a great extent of agreement, with RSD ranging from 0.7% to 2.6% (Tables 7.4-7.6). The overall RSD over 45 analyses are 3.4% (*vs.* 46% for EO/PO). MALDI MS has been well established as a powerful tool to generate reliable and reproducible average molecular masses and their distributions for polymers with narrow polydispersity (<1.2), providing a suitable experimental protocol is

followed [1,2, 14-20]. The National Institute of Standard and Technology (NIST) has recently conducted a round-robin experiment among 18 laboratories to investigate the accuracy of MALDI MS for polymer average mass measurement [51]. The low uncertainty in the molecular mass result shows good reproducibility from lab to lab. The results shown here also suggest that experimental condition variation has much less effect on the average molecular mass determination than that on the molar ratio determination by composition estimate approach.

In summary, for the copolymers studied, the composition estimate approach fails to generate reproducible EO/PO ratios when experimental conditions are varied. On the other hand, M_n is much less affected by these experimental condition variations. In this particular case, M_n increases along with the EO content increase (Figure 7.6). It seems natural that using M_n to determine EO/PO would be a more sensible approach, IF, a linear relationship between EO/PO and M_n can be established.

7.3.3 EO/PO Determination by Average Molecular Mass Measured by MALDI MS.

To test the above hypothesis, another series of MALDI experiments were carried out. All samples and matrix, *all-trans* retinoic acid, were dissolved in THF at concentrations of 1 mM and 0.1 M. The analyte solution was then mixed with the matrix solution at a volume ratio 1:10. As evidenced by the statistical analysis described in the previous section, this combination of experimental parameters will generate M_n results with the least variance. Each datum is generated by an average of 15 replicate measurements. M_n results were calculated using the built-in software provided by the instrument manufacturer to test if this methodology can be applied in a real world situation where no program such as "PeakPick" is available. This will provide a good

estimate of the robustness of the proposed methodology. Feed ratios (wt% EO) for the standards are listed in Table 7.1.

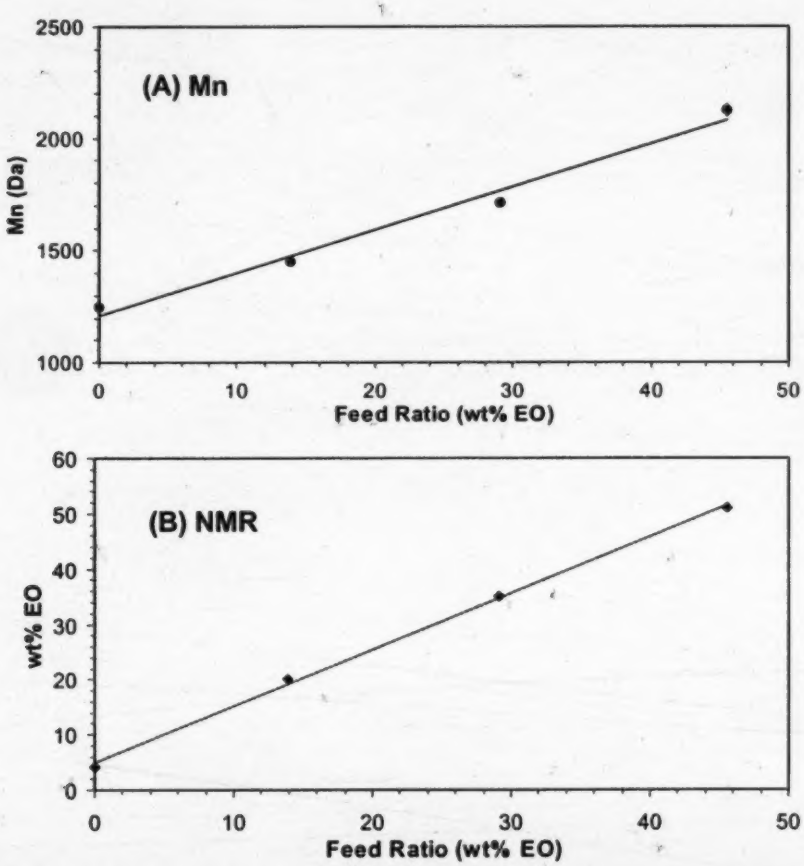

Figure 7.8. Calibration curves. (A) From the Mn data vs. wt% EO determined by the feed ratio and the error bar shows the standard deviation, and (B) from the NMR data vs. wt% EO determined by the feed ratio.

Figure 7.8A shows a plot of M_n data against the feed ratio for this series of standards. A linear calibration curve with correlation coefficient R^2=0.983 is established. The wt% EO determined by NMR is shown in Figure 7.8B for comparison. The NMR data also displays a linear response as in the case of using MALDI. The response

agreement between the NMR and MALDI data indicates that the use of M_n results from MALDI to determine copolymer composition in this particular case is a valid method. Moreover, the results shown in Figure 7.8B indicates that NMR, being an absolute method, does not necessarily give correct composition information. NMR overestimates the wt% EO (see for example, data point 1, where no EO is present). This overestimation results from both statistical modeling and interference from low mass components in the copolymer sample.

Once a calibration curve such as that shown in Figure 7.8A has been established, the EO/PO ratio of an unknown sample of similar nature can be determined. In the current case, one sample with 4.7 wt% EO feed ratio was analyzed by MALDI. The number average molecular mass was determined to be 1302.4±8.7 Da from an average of 15 measurements. From the calibration curve shown in Figure 7.8A, the EO content is determined to be 4.9 wt% EO, whereas direct NMR measurement gives 9.0 wt% EO for this sample. It must be realized that the feed ratio only serves as a reference value for method validation, and it does not necessarily reflect the actual copolymer composition. Nevertheless, the MALDI result is more reliable, since it excludes the interference from other EO and PO components, other than the principal distribution.

Compared to the composition estimate method, this M_n approach is more reliable because of the good reproducibility in M_n determination. In addition, this approach has the advantage of being able to analyze copolymers with reasonably high molecular mass with the condition that these polymers have low polydispersity to enable accurate M_n determination. In contrast, the composition estimate approach is limited to those copolymers whose spectra are oligomer resolved. Even for a MALDI reflectron TOF instrument equipped with time-lag focusing such as the one used in this study, the upper

limit to achieve an oligomer-resolved spectrum can be only as high as ~5000 Da due to the inherent complexity of copolymers.

However, it should be pointed out that the proposed M_n approach does require the availability of a set of calibration standards with different copolymer component ratios, and the general applicability is therefore limited.

7.4 Summary

MALDI mass spectrometry has the potential to become a valuable tool for composition analysis of copolymers. For a copolymer composed of structurally very similar building blocks with minor chain length changes, one would expect the relative peak intensities observed in the MALDI mass spectra to reflect its composition, at least within a narrow mass range. However, it is shown that variations in experimental conditions in MALDI can have a significant effect on the mass spectral appearance of a copolymer. The effects of concentration, laser power, type of matrices and solvents on mass spectra of an ethylene oxide/propylene oxide copolymer are illustrated. Since quantitative composition analysis of a copolymer relies on the use of relative peak intensities, the mass spectral pattern variation can certainly alter the composition results. The EO/PO copolymer examined in this work is composed of structurally similar monomers. For other types of copolymer with greater variability in monomer structures, even larger spectral variations are expected. It is evident that a better understanding of how experimental parameters affect the mass spectral pattern will facilitate the search for conditions under which reproducible results can be obtained. Once reproducible spectra can be obtained, one can then explore the use of other techniques such as NMR to correlate the relative peak intensities in MALDI mass spectra with actual copolymer

composition. A validated MALDI method would provide a means of accurate and rapid analysis of copolymer composition. These somewhat surprising results show that great care needs to be exercised in interpreting copolymer spectra for compositional analysis, even for copolymers with structurally similar monomers. Further studies are needed to better understand and optimize spectral acquisition conditions for reliable copolymer compositional analysis by MALDI. By statistical analysis, it is further demonstrated that average molecular mass is considerably less affected by the experimental condition variation. In the case where a series of copolymers synthesized from the same route, such as the practices in many manufacturing sites, M_n obtained from MALDI MS can be used for a rapid and accurate composition determination. These results suggest that M_n should be seriously considered as an integral part of MS based composition analysis where applicable.

7.5 Literatures Cited

1. Nielen, M. W. F. *Mass Spectrom. Rev.* **1999**, 18, 309.
2. Hanton, S. D. *Chem. Rev.* **2001**, 101, 527.
3. Montaudo, G.; Lattimer, R. P. *Mass Spectrometry of Polymers*, CRC Press LLC, New York, **2002**.
4. Odian, G. *Principles of Polymerization*, McGraw-Hill, New York, **1970**.
5. Elias, H. G. *Macromolecules*, Plenum Press, New York, **1984**.
6. Bovey, F. *High Resolution NMR of Macromolecules*, Academic Press, New York, **1972.**
7. Randall, H. *Polymer Sequence Determination (the ^{13}C Method),* Academic Press, New York, **1977.**
8. Tonelli, A. E. *NMR Spectroscopy and Polymer Microstructure*, VCH Publishers, New York, **1989**.
9. Montaudo, M. S. *Macromol. Symp.* **1999**, 141, 96.
10. Montaudo, M. S.; Montaudo, G. *Macromolecules* **1992**, 25, 4264.
11. Montaudo, M. S.; Puglisi, C.; Samperi, F.; Montaudo, G. *Macromolecules* **1998**, 31, 8666.
12. Montaudo, G.; Montaudo, M. S.; Scamporrino E.; Vitalini, D. *Macromolecules* **1992**, 25, 5099.
13. Nuwaysir, L. M.; Wilkins, C. L.; Simonsick, W. J. *J. Am. Soc. Mass Spectrom.* **1990**, 1, 66.
14. Schriemer, D. C.; Li, L. *Anal. Chem.* **1997**, 69, 4169.
15. Schriemer, D. C.; Li, L. *Anal. Chem.* **1997**, 69, 4176.
16. Schriemer, D. C.; Li, L. *Anal. Chem.* **1996**, 68, 2721.

17. Dogruel, D.; Nelson, R. W.; Williams, P. *Rapid Commun. Mass Spectrom.* **1996**, 10, 801.

18. Chen, H. R.; Guo, B. C. *Anal. Chem.* **1997**, 69, 4399.

19. Yalcin, T.; Dai, Y. Q.; Li, L. *J. Am. Soc. Mass Spectrom.* **1998**, 9, 1303.

20. Hanton, S. D.; Cornelio Clark, P. A.; Owens, K. G. *J Am. Soc. Mass Spectrom.* **1999**, 10, 104.

21. Danis, P. O.; Karr, D. E. *Org. Mass Spectrom.* **1993**, 28, 923.

22. Abate, R.; Ballistreri, A.; Montaudo, G.; Garozzo, D.; Impallomeni, G.; Critchley, G.; Tanaka, K. *Rapid Commun. Mass Spectrom.* **1993**, 7, 1033.

23. Montaudo, G.; Garozzo, D.; Montaudo, M. S.; Puglisi, C.; Samperi, F. *Macromolecules* **1995**, 28, 7983.

24. Pasch, H.; Rode, K. *J. Chromatogr. A*, **1995**, 699, 21.

25. Kalinoski, H. T.; Hargiss, L. O.; Shay, B. J.; Schuyl, P. J. W. *Proceedings of the 43rd ASMS Conference on Mass Spectrometry and Allied Topics*, Atlanta, GA. **1995**, p 756.

26. Schaer, M. *Proceedings of the 43rd ASMS Conference on Mass Spectrometry and Allied Topics*, Atlanta, GA. **1995**, p 948.

27. Vitalini, D.; Mineo, P.; Bella, S.D.; Fragala, I.; Maravigna, P.; Scamporrino, E. *Macromolecules* **1996**, 29, 4478.

28. Wilczek-Vera, G.; Danis, P. O.; Eisenberg, A. *Macromolecules* **1996**, 29, 4036.

29. Suddaby, K. G.; Hunt, K. H.; Haddleton, D. M. *Macromolecules* **1996**, 29, 8642.

30. Lacey, M. P.; Keough, T.; Pan, Y.; Armstrong, M. P.; Fritz, M. D. *Proceedings of the 44th ASMS Conference on Mass Spectrometry and Allied Topics*, Portland, OR. **1996**, p 908.

31. Schriemer, D. C.; Whittal, R. M.; Li, L. *Macromolecules* **1997**, 30, 1996.

32. Wang, Y. F.; Paventi, M.; Hay, A. S. *Polymer* **1997**, 38, 469.

33. Haddleton, D. M.; Maloney, D. R.; Suddaby, K. G.; Clarke, A.; Richards, S. N. *Polymer* **1997**, 38, 6207.

34. Goldschmidt R. J.; Owen, K. G.; Hanton, S. D. *Proceedings of the 45th ASMS Conference on Mass Spectrometry and Allied Topics*, Palm Spring, CA. **1997**, p 1106

35. Guttman, C. M.; Blair, W. R.; Danis, P. O. *J. Polymer Sci. Part B: Polymer Phys.* **1997**, 35, 2409.

36. Scrivens, J.; Jackson, T.; Quinn, S.; Carter, J.; Critchley, G.; Brown, J. *Proceedings of the 46th ASMS Conference on Mass Spectrometry and Allied Topics*, Orlando, FL. **1998**, p 1189.

37. Yoshida, S.; Yamamoto, S.; Takamatsu, T. *Rapid Commun. Mass Spectrom.* **1998**, 12, 536.

38. Van Rooij, G. J.; Duursma, M. C.; de Koster, C. G.; Heeren, R. M. A.; Boon, J. J.; Schuyl, P. J. W.; van der Hage, E. R. E. *Anal. Chem.* **1998**, 70, 843.

39. Francke, V.; Rader, H. J.; Geerts, Y.; Mullen, K. *Macromol. Rapid Commun.* **1998**, 19, 276.

40. Servaty, S.; Kohler, W.; Meyer, W.H.; Rosenauer, C.; Spickermann, J.; Rader, H. J.; Wegner, G.; Weier, A. *Macromolecules* **1998**, 31, 2468.

41. Wallace, W. E.; Guttman, C. M.; Antonucci, J. M. *J. Am. Soc. Mass Spectrom.* **1999**, 10, 224.

42. Wilczek-Vera, G.; Yu, Y. S.; Waddell, K.; Danis, P. O.; Eisenberg, A. *Rapid Commun. Mass Spectrom.* **1999**, 13, 764.

43. Allgaier, J.; Martin, K.; Rader, H. J.; Mullen, K. *Macromolecules* **1999**, 32, 3190.

44. Yu, D.; Vladimirov, N.; Frechet, J. M. J. *Macromolecules* **1999**, 32, 5186.

45. Nace, V. M., Ed. *Nonionic Surfactants Polyoxyalkylene Block Copolymers*; Macrcel Dekker: New York, **1996**.

46. Whittal, R. M.; Schriemer, D. C.; Li, L. *Anal. Chem.* **1997**, 69, 2734.

47. Dai, Y. Q.; Whittal, R. M.; Li, L. *Anal. Chem.* **1996**, 68, 2494.

48. Hensel, R. R.; King, R.; Owens, K. G. *Proceedings of the 43rd ASMS Conference on Mass Spectrometry and Allied Topics*, Atlanta, GA. **1995**, p 947.

49. Axelsson, J.; Hoberg, A. M.; Waterson, C.; Myatt, P.; Shield, G. L.; Varney, J.; Haddleton, D. M.; Derrick, P. J. *Rapid Commun. Mass Spectrom.* **1997**, 11, 209.

50. Anderson, R. L. *Practical Statistics for Analytical Chemists*, VNR Inc. New York, **1987**.

51. Guttman, C. M.; Wetzel, S. J.; Blair, W. R.; Fanconi, B. M. Girard, J. E.; Goldschmidt, R. J.; Wallace, W. E.; VanderHart, D. L. *Anal. Chem.* **2001**, 73, 1252.

7.6 Appendix

Program "PeakPick" for Copolymer Mass Assignment

By Rui Chen and Haiyan Zhang

```
#include <stdio.h>
#include <string.h>
#include <stdlib.h>
#include <ctype.h>
#include <math.h>

static void findpeak(float *, int *, int, int, float,float);
static void pickone();
static void check_noise();
static void calmn();
char outfile[54];
char finalfile[60];
float noi, tol;

/* The main program of PeakPick  */
main()
{
  FILE *fpin;
  char line[256],**filename;
  float *mass;
  int max, number, fileno, i=0, base=1000, *intensity;
  int maxpeak, begin, end,j;
  float data1, data2;

  printf("\nPlease input the number of files you want to
          analyze:");
  scanf("%d",&fileno);

  filename=(char **) malloc(fileno*sizeof (char *));
  for(i=0;i<fileno;i++)
   {
     filename[i]=(char *) malloc (50*sizeof(char));
     printf("Please input the mass data file %d (<50
             characters):", i+1);
     scanf("%s",filename[i]);
     fpin= fopen(filename[i],"r");
     if(fpin==NULL)
      { printf("Invalid file name. Continue......\n");
        free(filename[i]);
        i--;
      }
```

```
 }

printf("Please input mass starting point (m=):");
scanf("%d", &begin);
printf("Please input mass ending point (m=):");
scanf("%d", &end);

printf("Please input the percentage of highest value as
          noise level(0-1):");
scanf("%f",&noi);
printf("Please input tolerance value:");
scanf("%f",&tol);

for(j=0;j<fileno;j++)
{
  sprintf(outfile,"%s.out",filename[j]);
  sprintf(finalfile,"%s.final",filename[j]);
  mass=(float *)malloc(1000*sizeof(float));
  intensity=(int *)malloc(1000*sizeof(int));
  max=1000;
  i=0;maxpeak=0;
  fpin= fopen(filename[j],"r");
  while(1)
    {
     if(fgets(line,256,fpin)!=NULL)
       {
         if(isdigit(line[0]))
          {
            if(i==max)
             {
              mass=(float *)realloc((float *) mass,
                        (max+base) * sizeof(float));
              intensity=(int *)realloc((int *) intensity,
                        (max+base) * sizeof(int));
                   max+=base;
             }
            sscanf(line,"%f %d",&mass[i], &intensity[i]);
            if(mass[i]>begin&&mass[i]<end){
               if(intensity[i]>0) {
                   if(intensity[i]>maxpeak)
                       maxpeak=intensity[i];
                        i++;
               }
            }
          }
       }
    else break;
```

```
      }
    fclose(fpin);
    number=i;
    check_noise(&data1,&data2,intensity,number);
    printf("baseline at %8.2f =%8.2f, baseline at %8.2f =
            %8.2f \n",mass[0],data1, mass[i-1],data2);
    findpeak(mass,intensity,number,maxpeak,data1,data2);
    free(mass);
    mass=NULL;
    free(intensity);
    intensity=NULL;
  }
} /* End of main program */

/* function of find peaks   */
void findpeak(float *mass, int *intensity, int number,int
              maxpeak,float data1, float data2)
{
  FILE *fpout;
  int i, j, max, *peak, base=1000, peaknum;
  float a, b, noise;

  peak=(int*)malloc(1000*sizeof(int));
  max=1000;

  a = (logf(data1)*logf(2500)-logf(700) * logf(data2)) /
       (logf(2500) - logf(700));
  a = expf(a);
  b = (logf(data1)-logf(data2))/(logf(700)-logf(2500));
  noise=noi*maxpeak;
  printf("noise level=%f\n",noise);
  j=0;
  for(i=0;i<number-1;i++)
   {
     if((intensity[i+1]-intensity[i])>0){
        while((intensity[i+1]-intensity[i])>0)
           { peak[j]=i+1; i++;}
             intensity[i]-=a*pow(mass[i],b);
             if(intensity[i]>noise)
              {
                j++;
                if( j == max)
                 {  peak=(int *) realloc ((int*)peak,
                                  (max+base)*sizeof(int));
                    max+=base;
                 }
              }
```

```
            }
        }
        peaknum=j;
        fpout=fopen(outfile,"w");
        for(i=0;i<peaknum;i++)
        fprintf(fpout,"%8.2f %8d\n", mass[peak[i]],
                                    intensity[peak[i]]);
        fclose(fpout);
        printf("The raw results saved as file %s\n",outfile);
        pickone(peak,peaknum,mass, intensity);
    } /* End of findpeak() */

    /* pick the highest intensity for the peak */
    void pickone(int *peak,int number,float *mass, int
                        *intensity )
    {
        FILE *fpout;
        int i, j, In[10], m[10], n[10], k, write;

        fpout=fopen(finalfile,"w");

        i=0;  write=0; In[0]=0;
        for(k=1;k<number;k++)
          {
            if((mass[peak[k]]-mass[peak[k-1]]<2) &&
                   (intensity[peak[k]]-intensity[peak[k-1]]<0))
             {
               In[i++]=k; continue;
             }

            for(j=0;j<10;j++)
             {  m[j]=0;  n[j]=0;  }

            calmn(m,n,mass, peak, In[0]);
            if(!(m[0]==0 && n[0]==0))
              {
                if((mass[peak[In[0]]]-mass[peak[write]]>2) ||
                  (mass[peak[In[0]]]-mass[peak[write]]==2 &&
                   intensity[peak[In[0]]]>intensity[peak[write]])
                   ||k==1)
                  {
                    fprintf(fpout, "%8.2f %8d ",
                      mass[peak[In[0]]], intensity[peak[In[0]]]);
                    for(j=0;j<10;j++)
                     {  if(!(m[j]==0&&n[j]==0))
                            fprintf(fpout,"%4d %4d",m[j],n[j]);
                     }
```

```
                fprintf(fpout, "\n");

                write=In[0];
            }
        }
       i=0;
       In[i++]=k;
       }
    fclose(fpout);
    printf("The final results saved as file %s\n",finalfile);
} /* End of pickone() */

/* calculate the mass and the number  */
void calmn(int M[10], int N[10], float *mass, int *peak,
              int I)
{
  int count,m,n;
  float s;

  M[0]=0;N[0]=0;count=0;
  for(m=0;m<(int)(mass[peak[I]]-265)/44+1;m++)
    {
       for(n=0;n<(int)(mass[peak[I]]-265)/58+1;n++)
       {
         s=44.0258*m+58.0414*n+266.2496;
         if(fabs(s-mass[peak[I]])<tol)
            { M[count]=m; N[count]=n; count++; }
        }
    }
}/* End of calmn() */

/* calculate the noise base line */
void check_noise(float *data1, float *data2,int *intensity,
                    int number)
{
  int i,t1=0,t2=0;
  float mean1,sum1=0,sum2=0, mean2;

  *data1=0; *data2=0;
  for(i=0;i<100;i++)
    {
      sum1+=intensity[i];
      sum2+=intensity[number-i-1];
    }
  mean1=sum1/100;
  mean2=sum2/100;
```

```
  for(i=0;i<100;i++)
   {
     *data1+=pow((mean1-intensity[i]),2);
     *data2+=pow((mean2-intensity[number-i-1]),2);
   }
  *data1/=100;
  *data2/=100;
  *data1=sqrt(*data1);
  *data2=sqrt(*data2);
  for(i=0;i<100;i++)
   {
     if(fabs(intensity[i]-mean1)/3>*data1)
      {
       sum1-=intensity[i]; t1++;
      }
     if(fabs(intensity[number-i-1]-mean2)/3>*data2)
      {
      sum2-=intensity[number-i-1];t2++;
      }
   }
  *data1=sum1/(100-t1);
  *data2=sum2/(100-t2);
} /* End of check_noise */

/* End of PeakPick program */
```

Chapter 8. Conclusions and Future Work

The main objective of the research presented in this thesis is to develop enabling MS methods for polymer structure and composition characterization. I have completed several projects in three areas of research.

1. Better understanding of gas phase reactions between atomic transition metal ions with long chain alkyl, which led to the development of a MALDI MS method for polyethylene (PE) analysis (Chapters 2 and 3).
2. Developing structural characterization strategies based on ESI tandem mass spectrometry (or MS^n), and applying these methods for polyol analysis (Chapters 4, 5, and 6).
3. Investigating the experimental effects of the commonly used MS approach on copolymer composition analysis, and developing a more robust, alternative method for such a purpose (Chapter 7).

In Chapter 2, it is demonstrated that laser desorption ionization time-of-flight mass spectrometry can be used to study transition-metal ion interactions with relatively nonvolatile, long-chain alkanes. The observed product distribution as well as the reactivity of Cr^+, Mn^+, Cu^+ and Ag^+ is different from those with small alkane systems. The difference is attributed to the large initial thermal energy of a more polarizable long-chain alkane that can be converted into excess energy, when a more rigid metal-ion alkane complex is formed. The results also suggest that many transition-metal ions can potentially be useful as the cationization reagent for polyethylene analysis. Among all,

the LDI spectra of long chain alkanes obtained by using silver ionization display the least amount of fragmentation. Therefore, the silver ion is perhaps the most suitable transition-metal ion studied for molecule mass analysis of polyethylene. The fragmentation patterns of long chain alkanes studied in this work should be very useful in interpreting LDI spectra of polyethylene.

With the groundwork laid in Chapter 2, a study of ionization behavior of several polyethylene samples with molecular masses up to 4000 Da is presented in Chapter 3. Polyethylene's inert nature and difficulty to dissolve in conventional solvents at room temperature present special problems for sample preparation and ionization in mass spectrometric analysis. It is shown that LDI mass spectra of low molecular mass polyethylene with narrow polydispersity can be obtained in conventional time-of-flight mass spectrometers equipped with a nitrogen laser. It is also demonstrated unambiguously that silver or copper ion attachment to saturated polyethylene can occur in the gas phase during the UV LDI process, but the method is not suitable for molecular mass analysis of polyethylene with broad polydispersity. In LDI spectra of polyethylene with molecular masses above ~1000 Da, low mass ions corresponding to metal-alkene structures are observed in addition to the principal distribution. By interrogating a well-characterized polyethylene sample and a long chain alkane, $C_{94}H_{190}$, these low mass ions are unequivocally determined to be the fragmentation products of the intact metal-polyethylene adduct ions. It is further illustrated that while addition of commonly used polymer matrices such as *all-trans* retinoic acid and dithranol to the sample preparation assists in enhancing signal intensity and/or reducing the extent of fragmentation, fragmentation cannot be totally eliminated with the current sample preparation method in

a conventional MALDI-TOF mass spectrometer equipped with a nitrogen laser. Fragmentation is likely a major obstacle that needs to be overcome in order to extend the LDI or MALDI method to analyzing higher molecular mass polyethylene.

Future study should focus on a better understanding of the LDI process related to polyethylene analysis, and improving sample preparation conditions, such as choice of matrix and sample deposition method, that would significantly reduce or eliminate fragmentation.

Polyols are being used in a wide range of industrial applications including surfactants and precursors for grafted polymers. Characterization of polyols is of significance in correlating compositions and structures with their properties. In Chapter 4, it is illustrated by two real world examples that traditional analytical methods including GPC and NMR failed to reveal compositional differences, but the combination of MALDI-TOF, ESI MS and MS/MS can produce compositional information required for problem solving. The first example involves failure analysis of four ethylene oxide and propylene oxide (EO/PO) copolymer products. The results from the MS analysis demonstrate that one of the samples has small variation in copolymer composition, leading to its abnormal activity. The second example is in the area of deformulation of complex polyol mixtures. Two samples displaying similar properties and activities are found to be two different polyol blends. One of the samples is a more cost-effective product. These examples demonstrate that MALDI, ESI MS and MS/MS should be seriously considered as an integrated component of an overall polyol characterization

program in product failure analysis and de-formulation. The second application also demonstrates the demand for developing MS/MS method in polymer structural characterization.

Chapters 5 and 6 describe the method development for polyglycol structural characterization by tandem MS in a readily accessible ESI ion trap mass spectrometer. The backbones or molecular chains of many industrial polymers including functional polyglycols are often difficult to dissociate in tandem mass spectrometers using low energy CID. A method that uses Li^+ and transition metal ions such as Ag^+ as the cationization reagents to generate low energy CID spectra of polyglycol ethers is presented in Chapter 5. It is shown that lithium and transition metal polyglycol adduct ions can be readily fragmented with low energy CID. Comparative results from different cationization reagents in their abilities of producing both MS spectra and CID spectra are shown. It is also shown that when using divalent transition metal ions such as Co^{2+}, the often-overlooked counterion could affect ionization efficiency as well as subsequent fragmentation of the adducts. A H/D exchange approach to deduce fragmentation mechanism is also described. The methodology was further examined by two applications in the area of copolymer analysis. It is shown that a block and a random copolymer could be readily differentiated from their low energy CID spectra. The other application deals with copolymer sequencing. It is demonstrated that with proper choice of cations, a complete sequence of a block EO/PO copolymer can be obtained with relative ease. The work presented in this chapter is the first ESI low energy CID study on polymeric systems. The method described therein opens the possibility of using

conventional and readily available low energy CID tandem MS to study polymer structures.

Chapter 6 mainly focuses on another class of polyol, namely, polyglycol ester. It is shown that low energy CID behavior of PEG esters is substantially different than that of PEG ethers, and strongly dependent upon the involved cations. PEG ester-sodium adducts can undergo fragmentation, but provide limited information. This can be improved by the use of Li^+, Ag^+, and other transition metal ions. End group containing ions can be generated by using NH_4^+. Based on the results, an integrated MS approach for PEG ester characterization is presented. With the proper choice of cationization reagent and instrumental operation mode, wealthy structural information can be obtained. The described approach should be able to be adapted by others for problem solving in the area related to polyglycol structural characterization.

For analytical method development, future effort should focus on extending this approach to analyze higher mass polyglycols. As well, a study to better understand the roles of transition metal ions in ionization/fragmentation should be carried out for a better ESI MS/MS experimental design. ESI using some unconventional solvent systems better suited for a variety of polymers should also be studied to extend the general applicability of ESI MS and MS/MS for polymer structural characterization.

MALDI mass spectrometry has been widely used for composition analysis of copolymers. For a copolymer composed of structurally very similar building blocks with minor chain length changes, it is usually assumed that the relative peak intensities

observed in the MALDI mass spectra truly reflect its composition, at least within a narrow mass range. However, it is shown in Chapter 7 that variations in experimental conditions in MALDI can have a significant effect on the mass spectral appearance of a copolymer. The effects of concentration, laser power, type of matrices and solvents on mass spectra of an ethylene oxide/propylene oxide copolymer are illustrated. Since quantitative composition analysis of a copolymer relies on the use of relative peak intensities, the mass spectral pattern variation can certainly alter the composition results. The EO/PO copolymer examined in this work is composed of structurally similar monomers. For other types of copolymer with greater variability in monomer structures, even larger spectral variations are expected. It is evident that a better understanding of how experimental parameters affect the mass spectral pattern will facilitate the search for conditions under which reproducible results can be obtained. Once reproducible spectra can be obtained, one can then explore the use of other techniques such as NMR to correlate the relative peak intensities in MALDI mass spectra with actual copolymer composition. A validated MALDI method would provide a means of accurate and rapid analysis of copolymer composition. These somewhat surprising results show that great care needs to be exercised in interpreting copolymer spectra for compositional analysis, even for copolymers with structurally similar monomers. It is further demonstrated by a statistical analysis that average molecular mass is considerably less affected by the experimental condition variation than direct EO/PO ratio from 'composition estimate" approach. For a series of EO/PO copolymers with varying EO/PO ratio, M_n obtained from MALDI MS was used for the composition determination. A linear response between M_n and EO/PO was established. This M_n approach was validated by analyzing a

sample with an unknown EO/PO ratio. The result from M_n approach shows good agreement with that from feed ratio. Although this M_n approach is circumstantial, the result suggests that Mn should be seriously considered as an integral part of MS based composition analysis where applicable.

Future studies should focus on better understanding and optimizing spectral acquisition conditions for reliable and reproducible copolymer compositional analysis by MALDI.